THE ROLE OF SIMULATION IN
PACE TECHNOLOGY PART B

VIRGINIA POLYTECHNIC INSTITUTE

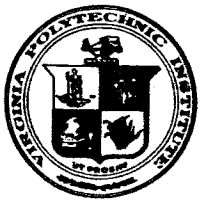

ENGINEERING EXTENSION SERIES CIRCULAR No. 4
(In four parts: A,B,C,D)

PART B

PROCEEDINGS OF THE CONFERENCE ON

The Role of Simulation in Space Technology

AUGUST 17-21, 1964

Supported by grants from the National Aeronautics and Space Administration and the National Science Foundation; assisted in planning and presentation by the NASA Langley Research Center.

TABLE OF CONTENTS

PART B

HYPERSONIC FLIGHT SIMULATION

Hypersonic Flight Simulation: Aerodynamics - J. Leith Potter VI

Convective and Radiative Heat Transfer During Reentry and Advanced Techniques for Their Simulation - Thomas N. Canning VII

Evaluation of Materials in Entry Heating Simulation - William A. Brooks, Jr. VIII

Detection of, and Communication with Space Vehicles During Atmospheric Entry; Problems in Simulation - S. C. Lin IX

Flight Reentry Experiments - Herbert A. Wilson, Jr. and Robert L. Wright X

REAL-TIME DYNAMIC SIMULATION

Background of Piloted Simulator Development - C. B. Westbrook XI

HYPERSONIC FLIGHT SIMULATION: AERODYNAMICS

by

J. Leith Potter

von Karman Gas Dynamics Facility

ARO, Inc.

INTRODUCTION

In this lecture an attempt is made to partially assess the current status and direction of laboratory simulation of the aerodynamics of full-scale, hypersonic flight. Problems of simulation related to establishing satisfactory flow fields and the determination of the basic aerodynamic quantities consisting of pressures, forces, and moments, on scale models in these laboratory environments are discussed. In addition, some questions arising in extending scale-model data to full-scale are noted. Other important hypersonic simulation problems are the subjects of later lecturers.

The Role of Aerodynamic Simulation

Inasmuch as the role of simulation in hypersonic aerodynamics has always seemed rather clearly established, it was a temptation to give that aspect of the subject only little attention. After all, the

Wright brothers used a wind tunnel such as the replica shown in Fig. 1. However, opinions recently have been voiced which imply that hypersonics as a research subject is rapidly losing its importance. At the risk of assuming excessive authority, the speaker will venture to place those remarks in which he believes to be the proper context.

More specifically, it does seem true that many of the problems faced by designers of aerospace vehicles once again lie between the subsonic and low-supersonic speed regimes. Examples may be found in the landing of lifting bodies returning from space, drag reduction of supersonic transports, inlet design for air breathing engines, and transonic and supersonic aero-thermo-elastic problems, to name only a few. There is now reasonably adequate understanding, though not necessarily a design solution or precise method of calculation, of most of the well-known hypersonic flow phenomena, e.g., low lift-to-drag ratios and high heating rates. This circumstance exists, in part, because of the degree of Mach number independence and the strong-shock simplifications in hypersonic flow, the essentially perfect-gas behavior which may be assumed in a large range of hypersonic aerodynamic problems, and a formidable effort involving skilled manpower and experimental facilities. Thus, it is not unreasonable to conclude, as others have done, that the unsolved problems in subsonic, transonic, and supersonic flow regimes deserve renewed attention. Furthermore, simulation facilities for these regimes are few in number and sometimes inadequate when tests of unusual new configurations are desired, e.g., V/STOL craft. On the contrary, if one overlooks several

significant points, it may seem that hypersonic wind tunnels providing Mach numbers of 5 to 25 are available in adequate numbers. The significant points alluded to in the last sentence refer to the rather general failure of these current hypersonic tunnels to provide real-gas simulation and the full-scale free-flight range of highest and lowest Reynolds numbers.

Clearly, it may be said that certain by-passed aerodynamic problems related to lower-speed flight indeed deserve renewed attention at the possible expense of effort in hypersonic areas. Also, except for conditions of extreme Reynolds numbers, perfect-gas laboratory simulation facilities seem adequate. Development of facilities substantially simulating real-gas effects of super-orbital speeds and permitting collection of all needed data represents a great difficulty, and much remains to be done. Following from these statements, the need for construction of new hypersonic aerodynamic simulation facilities appears diminished in the category of facilities which provide Mach number but not extreme Reynolds number or real-gas simulation. On the other hand, the role of newer facilities having the capability to simulate less well explored areas of hypersonic aerodynamics cannot beooverlooked when we know that the first craft planned to return to Earth from lunar and interplanetary flights must be very conservatively designed and inefficient owing to lack of precise aerodynamic data. For example the severe requirements pertaining to guidance accuracy for shallow-angle entry and aerodynamic braking in planetary atmospheres may be relieved by further improvements in lift-to-drag ratios

of hypersonic bodies. Also, there now exists roughly a $\pm$ 40 percent scatter in heat transfer rates measured at velocities above 20,000 fps. As in the past, it is expected that simulation, more often only partial simulation, in aerodynamic laboratories will provide a large share of the necessary knowledge.

Of course, it is obvious that ground based laboratories alone cannot enable the accomplishment of every investigation. For example, composition and properties of planetary atmospheres are better established by flight of survey vehicles. Also, as long as ground facilities are deficient in speed generated, or in simulation of any other important parameter, certain free-flight experiments are needed. A most interesting example is the use of recorded meteor luminosity and trajectory data to deduce heating rates as described by H. J. Allen in Ref. 1, pp. 1-41.

It may be assumed that the foregoing statements too strongly reflect one individual's personal beliefs. The lecturer is fortunate in being able to refer to a written account of a panel discussion which dealt largely with the role of simulation facilities (Ref. 1, pp. 745-778). Study of that source is recommended. Some of the strong and weak points of laboratory simulation vis-a-vis full-scale free-flight are brought out, and the substantial role of aerodynamic simulation in future developments is clearly indicated in the discussion which is reported in Ref. 1.

No single type of experimental facility stands above all others. Certain types of simulation devices have earned roles that will remain well established although their further development seems of limited

importance. Attention is here confined to facilities not now abundantly represented in the family and which are needed to support hypersonic flight of aerospace vehicle.

FLOW FIELDS

This section is devoted to discussing some of the problems of creating in a laboratory the types of flow fields necessary for adequately simulating the aerodynamics of hypersonic flight. As a prelude to this task, it is obvious that the flow-field conditions expected in full-scale free-flight must be established as accurately as possible. In a fine display of foresight, the organizers of this Conference laid the groundwork for this year's meeting, beginning with the 1961 Conference on Physics of the Solar System and Reentry Dynamics (Ref. 2).

References 1-10*, including the work of many authors, represent a few of the more general or documentary sources of information on characteristics of flow fields and aerodynamic problems relevant to hypersonic flight. Many more references are listed therein. Although not all of the included papers pertain to flow fields under hypersonic conditions, knowledge useful in regard to low-density aerodynamic simulation also may be found in Refs. 11-14, which concern the past

*Here, as in other parts of these notes, no pretense of an exhaustive reference list is intended. Where possible, only more recent publications are indicated.

four Symposia on Rarefied Gas Dynamics.

The remainder of this section is devoted to discussion of some selected problems which arise in trying to produce laboratory flow fields for simulating real-gas and either high- or low-Reynolds number phenomena under hypersonic conditions. Actually, many of the comments apply to general aerodynamic laboratory experimentation. Because so much has been written lately concerning simulation of real-gas effects, the problems of simulation related to extremes in Reynolds number, particularly low Reynolds number, will receive most attention. This arrangement recognizes not only the areas of discussion wherein the lecturer is afforded an opportunity to mention his own work, but also the close connection between real-gas phenomena and the topics of later lecturers. References are cited for more extensive and detailed information.

Real-Gas Effects in Aerodynamic Simulation

Although not proposed to be discussed at any length in the present lecture, it is impossible to ignore real-gas effects which are related to other questions to be addressed at this time. Those not familiar with the general subject of real-gas and nonequilibrium processes in gas dynamics simulation will find numerous earlier sources of information, e.g., the papers in the sections entitled "Experimental Techniques" in Ref. 3 (particularly the paper by Hertzberg, et al.) or in Refs. 1, 4, 5, and 11-19. The paper by Lordi and Mates, listed but

not included in Ref. 16, is of much interest. It has been published as Ref. 20. Subsequent lecturers will, no doubt, add to these references.

Real-gas effects often would not be such a problem to aerodynamicists if thermo-chemical nonequilibrium of the gas medium were not encountered. Because the degree of nonequilibrium is a function of the number of collisions allowed among gas particles in a flow field, both density and scale are important. Thus, the possibility of nonequilibrium forces us to consider duplicating free-flight flow fields to an extent not previously necessary. Figure 2 shows the altitude-velocity regime of nonequilibrium chemical-kinetics for conditions representative of a blunt-nose stagnation region in the Earth's atmosphere. The lecturer knows of no complete scaling for nonequilibrium flow. Then, to produce the free-flight flow fields for cases falling within the nonequilibrium regions, the laboratory facility must essentially duplicate not only the flow-field conditions but also the flow-field dimensions! While it may be shown that certain conditions sometimes permit relaxation of this extreme stand in regard to simulation, the general situation is as difficult as the previous statement implies. Figure 3, prepared by C. H. Lewis of ARO, Inc., shows the map of isentropic stagnation pressures and temperatures corresponding to flight in part of the regimes covered in Fig. 2. Comparison of these figures leads to the immediate conclusion that the conditions required for duplicating the higher free-flight speeds become impossible for conventional wind tunnels wherein a high-pressure, high-temperature gas is expanded from a reservoir to hypersonic speeds.

This is demonstrated by Fig. 4, which is representative of current technology insofar as one of the major problems in wind tunnel design is concerned. Even the impulse-type tunnels cannot achieve the levels of total pressure and temperature desired. There is one type of facility that can far exceed others in this respect, namely the aero-ballistic range. However, difficulty of measureing local flow quantities on the model or in its flow field greatly reduces the utility of aero-ballistic ranges. Actually, another type of facility should be included in this category; the counterflow system where a gun fires a model upstream in the expanded flow of a shock tunnel has many of the advantages and handicaps of an aero-ballistic range. Since none of these devices satisfy all requirements and each possesses certain advantages and disadvantages when compared with others, there is need to use all types. It is not necessary to dwell on the economic aspects of construction of large or long-running wind tunnels capable of high pressures, temperatures, and Mach numbers simultaneously.

Even if it is accepted that full matching of flow-field conditions is not now feasible when the more extreme speeds are of concern, much trouble remains in producing wind tunnel conditions that legitimately qualify as "hypervelocity." If we consider that term to denote speeds great enough to create significant real-gas effects, say dissociation in the shock layer of a model, it is likely that dissociation and vibrational excitation must exist in the setting section of the wind tunnel. Under such circumstances, it may often be found the recombination or

even the speedier relaxation of vibration does not keep pace with the decrease in translational and rotational temperatures as the gas expands down a hypersonic nozzle of reasonable length.

When one tests under conditions wherein nonequilibrium may be a factor, calibration of the nozzle flow is more difficult and requires far more work by the aerodynamicist. Some examples of calibration procedures used may be found in Refs. 16, 21 - 23. Low densities and high Mach numbers further complicate the diagnosis of real-gas flows because they make certain measurements difficult.

High reservoir pressures are the best medicine for nonequilibrium troubles in wind tunnel flows, but there are practical limits. Figure 5, available through the courtesy of J. D. Whitfield of ARO, Inc., shows how the required wind tunnel reservoir pressure increases with test section velocity if nonequilibrium is avoided or minimized. The assumed gas is air and only oxygen dissociation is considered. α_{fo} represents the mass fraction of oxygen dissociation. The method of calculation is that of Bray (Ref. 24) and is based on the approximation of a sudden freezing process in the noxxle.

A way was suggested in Ref. 25 to account for the influence of ambient dissociation of a simple diatomic gas, as might exist in a wind tunnel using nitrogen as the test medium. This method consists of subtracting the ambient degree of dissociation from the free-flight shock-layer dissociation under similar flow conditions. Another scheme advanced to help the experimenter is the binary-scaling method of Ref. 26.

Analysis of nonequilibrium, high-enthalpy flows is complicated by the necessity to take into account simultaneously the many reaction processes and their interdependence. It has been suggested (Ref. 26) that a scaling law for simulation of flows with coupled chemical reactions is represented by the produce $\rho_\infty L$ = const. when U_∞ = const., if all chemical reactions occur through two-body, or binary, collisions, In this case, L represents body scale (e.g., nose radius), ρ_∞ = freestream density, and U_∞ = freestream velocity. This procedure is said to automatically scale the corresponding inviscid, afterbody flows correctly at a given Mach number if either the latter are frozen or else the three-body recombination remains unimportant. Also, the afterbody boundary-layer flow is correctly scaled by the same process if atom diffusion dominates over recombination, correct surface conditions are maintained, and velocity and Mach number are duplicated.

The foregoing examples show the large part of the operating map of aerospace vehicles wherein nonequilibrium, real-gas influences may exist, and the difficulty of duplicating flight conditions in laboratory facilities. The next task is the evaluation of the importance of these matters in the determination of aerodynamic performance of full-scale free-flight vehicles on the basis of laboratory experiments, i.e., is only partial simulation adequate? Fortunately, the answer to this question often is a qualified yes, particularly in regard to rarefied flows, which receive the most attention in this lecture.

SIMULATION OF RAREFIED FLOW FIELDS

It is the purpose of this section to offer some remarks on aerodynamic simulation in the particular case of low-density, hypersonic flows. Considering the scarcity of flight data, one can only partially assess the validity of laboratory data at this time. Quite possibly, we are on the verge of developments which could provide data in abundance. But, in view of the continuing deficiency in detailed full-scale, free-flight results suitable for critical comparison with tunnel and range data, one should not anticipate any such sudden change in circumstances. Comments pertaining to some aspects of the subject follow, but first the present interpretations of the terms "low-density" and "hypersonic" require a few words.

Here, and in other parts of this lecture, "hypersonic" is taken to mean freestream numbers, M_∞, sufficient in regard to any particular problem to approximate closely the conditions of $M_\infty > 20$. It is well known that this requirement may sometimes be met when $M_\infty \approx 4$ and in other cases it is necessary that $M_\infty > 20$. The lecturer wishes to suggest that a reasonable criterion for "low-density" is

$$\lambda \simeq 1.49\, M_\infty/(Re_\infty/\text{in}) = 0\,(0.02\ \text{in.}).$$

where

λ_∞ = mean free path in freestream

M_∞ = Mach number

R_∞ = Reynolds number

Note that the Knudsen number, $\lambda_\infty/L \sim M_\infty/Re_\infty$.
Other definitions, including those not involving dimensions, may be proposed. However, note that unless a dimension is used in the definition, any wind tunnel may be called a low-density tunnel because of the evident possibility of using very small models to achieve very low Reynolds numbers regardless of test section conditions.

To further examine the low-density criterion advanced here, note that λ_∞ = 0.02 in. when the altitude in the Earth's atmosphere is approximately 220,000 ft. If, at that altitude, the velocity is 20,000 fps, then $Re_\infty \approx 20{,}000/ft$ and $M_\infty/\sqrt{Re_\infty/ft} \approx 0.14$. Neither blunt nor sharp-nosed, full-scale bodies of typical size will experience pronounced second-order effects of rarefied flow under these conditions, but increasing altitude will bring on rapidly growing effects.

Unfortunately, the suggested criterion is not really as precise as one would wish. The problem is much the same as that of defining hypersonic flow, because a low-density flow need only be as rarefied as the particular experiment requires. It is obvious that, by this standard, only the indivdiual experimenter can decide if his is effectively a low-density flow.

One additional remark concerning the flow regimes should be made. Namely, because almost all cases of practical interest are characterized by the "cold-wall" condition, it is very desirable that low-density wind tunnel tests simulate situations where wall temperature is well below adiabatic recovery temperature.

Real-Gas and Nonequilibrium Effects in Rarefied Flow

Thermo-chemical nonequilibrium more often becomes a factor when low-density conditions exist. But a compensating feature in this connection is that freezing of vibratory and dissociative energies occurs more readily at low densities, making most of the rarefied-flow regimes also essentially perfect-gas regimes. In the latter case, much may be accomplished with wind tunnels and aeroballistic ranges producing approximate Mach and Reynolds number simulation without duplicating stagnation conditions or body dimensions. In particular, pressures, forces, and moments, as well as heat transfer rates, in many cases are little affected by real-gas phenomena. This state of affairs is more understandable when the factors determining heating rates and pressures are reviewed.

Heat Transfer Rate - A very large percentage of the total enthalpy may be represented by a few percent dissociation. Heat transfer rates are determined by the difference between the generalized recovery enthalpy and the thermal enthalpy corresponding to surface temperature. To be more specific, consider the laminar, axisymmetric, stagnation-point, boundary-layer flow discussed by Rosner in Ref. 27, among others. He shows that the heat transfer rate at the stagnation point is:

$$\dot{q} = 0.763 \left(\frac{\rho_w \mu_w}{\rho_e \mu_e}\right)^{0.1} (\beta \rho_e \mu_e)^{0.5} (Pr_{\lambda,f})^{-0.6} \Delta h \left\{1 + \phi \left[(Le_f)^{0.6} - 1\right] \Delta h_{chem,\,eq}/\Delta h\right\}$$

The definitions of particular importance at this point are

$$\Delta h = (h_e - h_{f,w}) - (1 - \phi)\, \Delta h_{\text{chem, eq}}$$

$$\phi = (\alpha_e - \alpha_w) / \alpha_e = \Delta h_{\text{chem}} / \Delta h_{\text{chem, eq}}$$

h_e = total enthalpy at edge of boundary layer, including chemical contributions

$h_{f,w}$ = chemically frozen enthalpy at the wall, i.e., thermal enthalpy based on wall temperature

Δh_{chem} = change in chemical energy content across boundary layer

$\Delta h_{\text{chem, eg}}$ = equilibrium value of Δh_{chem}

It follows that the major influence of chemical processes on $\dot{q}$ is represented by

$$\Delta h = (h_e + h_{\text{chem, e}} - h_{\text{chem, eq,e}}) - (h_{f,w} + h_{\text{chem, w}} - h_{\text{chem, eq, w}})$$

and

$$\Delta h_{\text{chem}} = h_{\text{chem, e}} - h_{\text{chem, w}}$$

In otherwise equivalent cases, if recombination is completed to the same degree and if Δh is equal, these results imply that $\dot{q}$ will be equal regardless of whether recombination occurs in the boundary layer or on the wall.

The importance of surface catalylicity in connection with dissociated freestream flows should not be overlooked. Boundary layers, even at stagnation points, are expected to be essentially frozen

throughout practically all of the low-density regime defined earlier in these remarks, cf Refs. 6 and 27-30, but surface recombination may remain effective. Thus, even if low densities do not permit appreciable vibratory excitation or dissociation behind shock waves, portions or all of any energy content of the freestream related to vibration and dissociation may be transferred to the body surface. Therefore, if such energies are frozen in the expansion of flows from tunnel settling chambers, they must be accounted for in the interpretation of test data.

An example of the effect of frozen dissociation energy in the expanding nozzle flow may be of interest. As an exploratory experiment, W. H. Carden and J. T. Miller, colleagues of the lecturer, have measured the results given in Table 1. These data represent heat transfer rates to hemispherical noses of electrical cooper in a heated, slightly dissociated nitrogen stream. Non-catalytic coatings of orthophosphoric acid were applied to the cooper model as a viscous liquid and allowed to cure in the tunnel flow until a thin, solid coating remained. This was soft enough to be removable by wiping with emery paper. The $\dot{q}$ measured is the heat transfer rate for the entire hemisphere. Lees' distribution (ref. 31) is assumed in conjunction with Fay-Riddell theory (Ref. 32).

Table 1

Heat Transfer Rates in Dissociated Flow Experiment

	Run 1	Run 2
$\frac{\dot{q}_{\text{meas., clean surface}}}{\dot{q}_{\text{Fay-Riddell, 100\% recomb.}}}$ =	0.99	0.96
$\frac{\dot{q}_{\text{meas., coated surface}}}{\dot{q}_{\text{Fay-Riddell, 100\% recomb.}}}$ =	0.67	0.63
$\frac{\dot{q}_{\text{Fay-Riddell, 0\% recomb.}}}{\dot{q}_{\text{Fay-Riddell, 100\% recomb.}}}$ =	0.54	0.54

To see if the heating was reduced by mass transfer from the coating rather than reduced recombination, we conducted the same test at equal total enthalpy, though somewhat lower impact pressure, in a flow known from our measurements to have essentially no dissociation in the nozzle flow. In that case coating the nose had no influence on heat transfer. Thus, we believe mass-transfer effects were negligible after the coating was "cured." Prior to curing, there was a measurable variation of heat transfer rate with time.

We have data from calorimeters which provide the value of total

entalpy and can compute the active or equilibrium enthalpy from known reservoir and nozzle throat conditions and the nitrogen Mollier chart. Normally, the tunnel is operated at higher reservoir pressures and no evidence of dissociated flow in the nozzle exists.

Pressure - It is easily demonstrated that nonequilibrium thermochemical processes will affect pressures and, therefore, forces and moments on aerodynamic bodies. However, evidence of this is hard to find in experimental data, and it is interesting to consider why this is so.

First, regardless of optimistic predictions of performance, most hypersonic wind tunnels are essentially perfect-gas tunnels. Secondly, only a few percent dissociation exists in the flow over slender, sharp bodies in free-flight or tunnel flows. Therefore, the number of places where one may find relatively strong, aerodynamic evidence of dissociation is greatly reduced. One such place would seem to be the stagnation regions of blunt-nosed bodies in flight at high speeds and at altitudes low enough to permit dissociation to occur in the shock layer. However, in the stagnation regions of bodies at hypersonic speeds, pressures are mainly determined by the product $\rho_\infty U_\infty^2$, where ρ_∞ = freestream density and U_∞ = freestream velocity. Thus, presence or absence of dissociation in the shock layer will not greatly affect this pressure.

If the expansion around a blunt body with appreciable dissociation in the stagnation region is a frozen expansion, under suitable conditions

pressures will differ widely from those corresponding to an equilibrium expansion (cf Ref. 30). It appears that this is the model to investigate if one wants to see nonequilibrium effects on pressures. However, based on the definition of low-density flow given earlier, it is implied that blunt-nosed flows with appreciable dissociation in the shock layer are not likely to be a prominent type of low-density flow because, except at the lower part of the altitude range, densities may be too low to enable dissociation to occur in the shock layer. What does occur presumably will remain largely frozen thereafter (cf Refs. 28 and 33).

From the foregoing, it appears that flight under hypersonic, low-desnity conditions should be relatively free of real-gas effects because thermo-chemical processes will most often be frozen. This means that perfect-gas tunnels simulating Mach and Reynolds numbers with cold-wall test conditions are suitable for most work.

Aeroballistic ranges appear to have some utility for investigation of real-gas influences because they offer a means of producing high speeds in low-density gases of known, controlled composition and the binary scaling rule can be applied. The obvious handicap resulting from having no direct, data-transmitting connection to the model and difficulty of launching complex models at high speed, of course, greatly reduces the advantage that would otherwise be gained by use of ranges for study of real-gas effects.

Some Typical Problems of Low-Density Flow

The last section certainly falls short of a complete analysis of nonequilibrium effects, and the present section must be equally incomplete. Insofar as validity of test data or degree of simulation is concerned, if one assumes that necessary molecular speed ratios and Knudsen numbers are achieved, there remain questions such as those concerning molecular speed distribution, gas-surface interactions, and the techniques of accurate measurements in high-speed, possibly non-continuum flows. These topics are sometimes so related that they can be demonstrated in one example. The thermal transpiration phenomenon is somewhat of this nature (see e.g., Ref 34).

Thermomelecular Flow in Tubes - This phenomenon has received relatively little attention in aeronautics. It may become important in such tasks as the measurement of very low pressures by means of a typical setup whereby the orifice at the point where knowledge of the pressure is desired is connected to the measuring instrument by a tube of small diameter. If Knudsen number is sufficiently large and there is an appreciable temperature gradient along the tube, the condition of zero mass flux along the tube does not correspond to equality of pressure along the tube. Thus, the measurement is in error. The most recent research on this subject has been reported by Arney and Bailey (Ref. 34). A typical example of the results of their investigation is given in Fig. 6.

Figure 6 represents a case where pressure at the cold end of a tube is three-fourths the pressure at the hot end when the Knudsen number is 10 and the temperatures differ by a factor of 1.955. In the course of these experiments, four weeks' time was allowed for outgassing the apparatus which was maintained under vacuum at elevated temperature during this period. Approximately $\pm$ 5 percent scatter is indicated by the data at higher Knudsen numbers, but it is noteworthy that this experimental scatter corresponds to only about $\pm$ 0.5 micron Hg. Based on data such as these, charts for use in estimating the thermomolecular flow correction have been prepared (Ref. 33).

Gas Surface Interaction - The lecturer believes that the problems of simulation and measurements in noncontinuum flows go deeper than the mere production of high-speed, very-low-density streams. There are questions related to surface cleanliness which affects accommodation coefficients (Refs. 12 and 35). All tests in wind tunnels thus far involved models with "engineering surfaces" -- a term believed to have been coined by physicists to denote unclean surfaces. It may be added that the origin of the term is no more obscure than the specific definition of such a surface. However, a considerable difference may exist between, say, heat transfer rates to bodies cleansed of all foreign gases and other matter and the usual type of wind tunnel model in noncontinuum flows. Obviously, accommodation coefficient may vary with time of exposure of the surface to low-pressure environment.

Other peculiarities of rarefied flow may be mentioned. For example, at sufficiently high speeds, the recoil forces of ablating body material may be significant. Pressures along the axes of orifices may be variable even in the absence of temperature gradients in the orifice walls if temperature gradients exist in the gas at the orifice entrance. This latter phenomenon is discussed in a recent paper (Ref. 36).

Orifice Effect - A problem may arise when it is attempted to measure pressures on a solid surface in rarefied flow by the usual method involving an orifice in the surface connected to a pressure transducer. The pressure at the surface and that in the orifice cavity will be equal, only if there is no heat or momentum transfer, or other net fluxes to or from the surface at the orifice. By utilizing a two-stream Maxwellian velocity distribution, a relation between measured pressure, p_i, true pressure on the surface, p_{io}, and heat transfer rate, $\dot{q}$, was derived in Ref. 36 for a case where only heat transfer was considered to contribute to the orifice effect. The theoretical analysis was limited to very large Knudsen numbers, i.e.,

$$\lambda_w/d \gg 1$$

where

λ_w = mean free path based on wall temperature

d = Orifice diameter

An experiment was devised to extend the investigation to low Knudsen numbers, thereby enabling the drawing of curves to be used in correcting experimental data. A typical result of applying the data of Ref. 36 is illustrated in Fig. 7.

Several points of interest are apparent in Fig. 7. First, it may be observed that measured static pressures increased roughly 30 percent as orifice size increased in these examples. Further, it is inferred that much larger orifices would be necessary to avoid the orifice effect. Also, the predicted curves are in close agreement with the experimental data.

Nozzle Design - Although it is not the only design problem connected with low-density, hypersonic (LDH) wind tunnels, nozzle design is important and interesting. If we consider that the model LDH tunnel should have heated flow, then there is not only the problem of calculating boundary-layer thicknesses but also that of throat heat transfer rate.

Some high-enthalpy wind tunnels, not necessarily LDH type, incorporate conical nozzles, which are cheaper to build and less sensitive to off-design operating conditions. However, conical nozzles normally have undesirable axial gradients in flow properties through the test section. Such gradients often are not prohibitive if blunt-nosed, short (bluff) bodies are being tested, but appreciable errors may be incurred if slender bodies are tested, cf Ref. 37. Figure 8 taken from Ref. 37, shows an example of the error incurred. More recently, C. H. Lewis of ARO, Inc., has calculated the pressure distribution on cones in both parallel and diverging flow by the method of characteristics. The results of these more refined calculations also indicate large errors when long bodies are tested in conical nozzle flows with axial gradients (Ref. 38).

The method used to design contoured nozzles for the arc-heated, continuous type LDH Tunnel (L) in the von Karman Facility* combines an "inviscid core" calculated by the method of characteristics and a boundary-layer correction whereby the displacement thickness, δ^*, is added to the core radii, r_{ec}, to yield nozzle wall radii. Although it is somewhat surprising that the simple addition of displacement thickness suffices when $\delta^* > r_{ec}$, excellent results have been obtained thus far. Nozzles for Tunnel L look almost conical because of the large boundary-layer corrections, as illustrated in Fig. 9. Calibration results for the nozzle of Fig. 9 have shown that computed and measured displacement thicknesses are in very good agreement. There is no axial gradient in the test section of this nozzle, and radial uniformity in the inviscid core is also excellent.

Pumping Systems - It is not intended to discuss the engineering of pumping systems, although they are of utmost concern in connection with larger LDH tunnels. Rather, the opportunity is taken to emphasize the important benefits of diffusers, which were considered to offer little pressure recovery in low-density flow until it was shown (Ref. 3, pp. 599 - 624 and Ref. 39) that sufficient recovery could be attained to enable large savings in pumping system cost to be realized. Figure 10 illustrates the variation of diffuser efficiency with Reynolds number. Coupling diffusers with use of overexpanded nozzles (Refs. 39 and 40)

* von Karman Gas Dynamics Facility (VKF), Arnold Engineering Development Center (AEDC), Air Force Systems Command (AFSC).

allows pressure at the entrance of the pumping system to be 15 to 20 times greater than static pressure in the test section of the nozzle. Dr. Ray Chuan of Celestial Research Corporation has privately communicated to the lecturer the information that cryopumping, i.e., boundary-layer freezing, in diffusers further enhances their performance.

Other problems which arise in work with LDH facilities will be apparent in the following section. Some of these are due to small model size and low aerodynamic loads in existing, pilot facilities.

Some Results from the AEDC - VKF Low-Density Hypersonic Tunnel

To illustrate some of the practical reasons for studying LDH flows, a few results are presented.

Heat Transfer - Total heating rates of various blunt-nosed shapes have been measured in Tunnel L (Ref. 41). Total heat flux (Btu/sec) to the entire nose was measured and converted to average heat transfer rate per unit area by dividing the total heat flux by the wetted area of the nose. Results for the hemispherical shape are shown in Fig. 11. The data in Fig. 11 are normalized by dividing the measured rates by those calculated from a theory for flows corresponding to higher Reynolds numbers. In the calculation, the theory of Fay and Riddell (Ref. 32) was used to obtain heating rate at the stagnation point, and the theory of Lees (Ref. 31) was used to obtain the distribution of heating rates around the hemisphere. The data in Fig. 11 clearly show the effects of reduced Reynolds numbers.

The results of three theories (Refs. 42, 43, and 44) applicable for low Reynolds numbers are shown in Fig. 11 for comparison. Qualitative agreement is evident, but some difference in actual values exists. It should be noted that the theories only yield the stagnation-point heating rate. Lees' distribution was assumed in converting these theoretical, stagnation-point values to average values. Thus, the comparison is possibly slightly qualitative for that reason. There are data for low Reynolds numbers showing Lees' distribution to be close to the experimental.

Drag - Both sharp- and blunt-nosed cones have been tested to determine drag under low-desnity conditions. A water-cooled, sting-type balance capable of resolving drag forces on the order of 0.001 lb was used. The marked effects of combined low Reynolds number and high Mach number are illustrated by the data presented in Fig. 12. It may be seen there that the drag coefficient at $M_\infty/\sqrt{Re_\infty} \approx 0.3$ is roughly three times the value when $M_\infty/\sqrt{Re_\infty} \approx 0$ for the more bluff body and 12 times greater for the more slender body. For a 15-ft body at orbital velocity, this condition of $M_\infty/\sqrt{Re_\infty} \approx 0.3$ would exist at approximately 300,000-ft altitude. More slender bodies, such as delta wings, tested in Tunnel L have yielded drag coefficients nearly 20 times greater than their essentially inviscid values.

Through use of the low-density, hypersonic wind tunnel of the von Karman Gas Dynamics Facility, drag of spheres has been measured under hypersonic, cold-wall, support-free conditions in a nonreacting flow in which molecular vibration was frozen (Ref. 45). Data were obtained

for a nominal freestream Mach number of 11 and for Reynolds numbers from 1 to 10 based on conditions immediately downstream of an assumed Rankine-Hugoniot type of normal shock and sphere diameter. Photographs were taken of the tracks of small spheres falling through the test section of Tunnel L and being deflected by the drag force, which was calculated by knowledge of the mass of the sphere, time interval, and distance between the images on the photo. These data were supplemented by measurements at a nominal Mach number of 10 where a conventional balance was used, and Reynolds numbers downstream of the shock as high as 10^4 were investigated in the cold-wall condition.

The experimental results have been analyzed both from the point of view of continuum flow with second-order viscous effects and from the standpoint of a noncontinuum concept, taking account of first collisions between re-emitted and freestream molecules. Results are shown in Fig. 13.

Shock Waves - An experimental investigation has been made to determine the pressure distribution, shock shape, detachment distance, and wave thickness for spheres, and the latter three characteristics for flat-bodies in heated argon where Mach number was from 4 to 14, stagnation temperature was from 1900 to 4100°K, and Reynolds number downstream of the normal shock waves was 25 to 225 based on radius (Ref. 46). The purposes of this investigation were to determine the validity of the various theories available for predicting the above properties in the low- flow regime and to extend available data to lower Reynolds numbers.

When argon is used as the working gas, at the nozzle exit and some distance downstream there is a clearly visible, light-blue jet surrounded in most cases by a pink glow. This natural glow, thought to be caused by radiation from relaxing metastable atoms, enabled this study of the shock properties in front of spheres and flat-faced bodies to be made by simply photographing the flow field, wherein the brightness was proportional to the number density of radiating atoms.

Photographs of the shocks generated by the spheres and flat-faced bodies were analyzed with a photo-densitometer to determine the shock shape, detachment distance, and wave thickness.

In Fig. 14 the results of the measurement of shock detachment distance for spheres at different wall-to-stagnation temperature ratios is shown. It will be noted that the shock detachment distance is a function of Mach number, Reynolds number, wall temperature, and body shape. A study of the magnitude of the shock-wave and boundary-layer thicknesses indicates that in these tests these layers were incipiently or fully merged. As the Reynolds number decreases, the shock detachment distance increases to values more than double the "inviscid" values. Also, for the bodies where the wall-to-stagnation temperature ratio is 0.1, there is evidence to confirm the decrease in shock detachment distance to a value less than the inviscid value, as predicted by Ho and Probstein (Ref. 47), before the increase as mentioned above for the lower Reynolds numbers.

Three-Component Measurements - The effect of rarefied flow on drag of representative bodies has been illustrated in Figs. 12 and 13. Other

aerodynamic forces and moments also are affected, and it is desirable to determine these on the basis of experiments because the theoretical computation is not yet sufficiently reliable.

Figure 15 relates the viscous interaction parameter, $M_\infty \sqrt{C_\infty/Re_\infty}$, to vehicle size and altitude above Earth for a typical gliding atmospheric entry trajectory from orbital or lunar excursions. At altitudes of roughly 300,000 ft, forces may be roughly 1/50 their values at 200,000 ft, but considerations of stability and lift-to-drag ratios are none the less important in some cases. Therefore, designers have need for aerodynamic data of the type forthcoming from more common wind tunnel tests. To explore the problem and with the hope of gaining a capability for measuring lift, drag, and pitching moment, colleagues of the author have developed the balance described in Ref. 48. A photograph of this remarkable device is shown in Fig, 16, and a sample of data obtained from a short, blunt conical model is shown in Fig. 17. This model is of interest as a possible Mars probe or Earth satellite. Because the forces and moment measured are more indicative of the balance performance, Fig. 17 gives those data instead of the usual coefficients. In this experiment, based on matching Reynolds numbers, n altitude of 316,000 ft. was simulated under hypersonic, cold-wall conditions.

Viscous Interaction - The hotshot and shock tunnel, impulse-type wind tunnels, and the continuous-type, LDH Tunnel L have been used to investigate pressure distribution on sharp-edged flat plates under

conditions of pronounced viscous interaction. Examples of data from the VKF hotshot and LDH tunnels, as well as data from other sources soon will be published by J. D. Whitfield and H. E. Deskins, ARO, Inc. A preliminary example is shown in Fig. 18. It may be noted that these data, which extend into the region of appreciable slip flow, did not display such relatively good agreement until the method of Ref. 36 was applied to correct for orifice effect. This correction removed discrepancies of up to 45 percent in pressure coefficients.

SIMULATING CONDITIONS OF HIGH REYNOLDS NUMBERS

Much less is included in this section than in the preceding ones which concerned phenomena and simulation problems related to low Reynolds numbers. Really serious efforts to produce large Reynolds numbers under hypersonic conditions seem to have taken second place, in most laboratories, to efforts toward higher Mach numbers and velocities. Lately some indications of renewed interest in facilities providing high Reynolds numbers have seen manifest. Special tests in impulse-type tunnels recently have been arranged so that high Mach number is sacrificed in return for higher Reynolds number. However, the higher Reynolds numbers have been achieved with $5<M_\infty<15$, so the Mach numbers are comparable to large continuous-type tunnels where $M_\infty \leq 10$ and typical maximum $Re_\infty/in. \doteq 2 \times 10^5$. Figure 19 represents an attempt to summarize the current Reynolds and Mach number relationship with regard to hypersonic wind tunnels using air or nitrogen gases. The tunnel described by Perry (Ref. 16, pp. 395-422) is said to be

capable of Re_∞/in. = 1.5 x 10^5 at M_∞ = 18 for run times of two to perhaps ten milliseconds. On rare occasions hotshot-type tunnels have produced Re_∞/in. = 0.85 x 10^5 at $M_\infty \approx 19$.

Viewing Fig. 20 and comparing the typical trajectories shown in Fig. 2, it is evident that very high Reynolds numbers may characterize flows on relatively low-drag, heavy bodies during important portions of their descent. For example, a body moving at 18,000 fps at 100,000 ft altitude has a freestream unit Reynolds number of 1.6 x 10^5 per in. Corresponding, Mach and Reynolds numbers attained at the edge of the boundary layer on a 10-deg half-angle cone would be approximately 9.2 and 3.6 x 10^5 per in., respectively. These two cone surface flow conditions are not impossible to simulate in present laboratory facilities but it is necessary to examine the other requirements for natural boundary-layer transition and turbulent flow under the influence of factors present in high-speed flight. For example, the ratio of wall temperature to adiabatic recovery temperature, T_w/T_{aw}, usually is considered a significant parameter in such studies, and, in the free-flight example cited, it would be approximately 0.1. However, by far the largest obstacle to creating these conditions in a wind tunnel exists because of the tendency for Reynolds number of boundary-layer transition, Re_t, to increase markedly as Mach number increases, whether $T_w \ll T_{aw}$ or not. For the case $T_w \approx T_{aw}$, this is shown by Fig. 21, which is taken from Ref. 50. Supporting data from various sources may be seen in Ref. 51. Actually, comparisons of this type are highly qualitative, for reasons too numerous to discuss here (see, e.g., Refs. 52 and 53), but Fig. 21

serves present purposes. Data, for the case $T_w << T_{aw}$ are less plentiful, but Ref. 51 provides an indication that the ratio T_w/T_{aw} may not be an extremely important factor when local Mach number exceeds, say 5 or 6. In the absence of more plentiful data for the hypersonic case, the latter may be regarded as a conservative assumption in the present context, i.e., Re_t for a cooled wall normally exceeds Re_t for an adiabatic wall. Then, returning to Fig. 21 and assuming Re_t to represent the "end" of transition, one would estimate that $Re_t \geq 5 \times 10^7$ under conditions described earlier for the sharp cone.* Therefore, using the value of unit Reynolds number of 3.6×10^5 in.$^{-1}$, the distance from the apex of the cone to the end of transition, i.e., fully developed turbulent boundary-layer flow would be at least 140 in. or nearly 12 ft. Few hypersonic wind tunnels are large enough to accept such a large model. From Fig 21, note that transition would begin at about one-seventh of this length or a little less than 2 ft from the nose of the cone. Thus, nearly the entire cone would be covered by a transitional boundary layer. As pointed out in Ref. 54, this is typical of hypersonic flows and it adds to the experimenter's woes. To quickly understand some of the reasons why it is difficult to build wind tunnels which simultaneously produce high Mach and Reynolds number conditions, a few of the problems are briefly outlined.

---

* In Refs. 50 and 54 it is shown that Re_t on a sharp cone at $M_\infty \approx 3$ is more nearly 3 times the value of Re_t on a flat plate or hollow cylinder. However, this factor has not been considered here, partly because its omission is consistent with the estimate of a lower possible value of Re_t and partly because it is not certain that it applies under the conditions being discussed.

Mach and Reynolds numbers in the nozzle of a tunnel are related to reservoir pressure, p_o, and temperature, T_o, such that, for fixed reservoir conditions, increasing M_∞ lowers Re_∞. Fox fixed p_o and M_∞, increasing T_o lowers Re_∞. Now the minimum T_o is established by the need to avoid liquefaction of the gas medium when it expands to low temperature and high M_∞. For a perfect gas, the static temperature at M_∞ is

$$T_\infty = T_o / [1 + (\gamma-1) M_\infty^2/2]$$

where γ= ratio of specific heats

Thus, when $M_\infty >> 1$, $T_\infty \sim T_o/M_\infty^2$, and it is evident that high M_∞ requires high T_o if T_∞ is not to fall below the liquefaction line. Recently there seems to be growing acceptance of the feasibility of allowing T_∞ to be well below the conventional limit, as indicated in Fig. 22 from Ref. 16, p. 335. In other words, the liquefaction rate seems slow enough to effectively displace the change-of-phase boundary in hypersonic nozzle flows. Nevertheless, the requirement to avoid liquefaction presents an obstacle to the combining of high reservoir pressures with low reservoir temperatures to achieve a higher Reynolds number at a given Mach number. Of course, it also should be noted that the throat heat transfer problem influences the relation between p_o and T_o, and the lack of adequate data on viscosity and other properties of air at low temperatures discourages acceptance of very low T_∞ for aerodynamic work.

The hypersonic wind tunnel using helium as the working fluid has

been developed because the low liquefaction temperature of helium largely remove the liquefaction barrier just discussed. (See, e.g., the paper by Henderson in Ref. 1, pp. 163-190.) However, the fluid properties are considerably different from air, making it questionable if inviscid and viscous fluid flow effects can be simulated simultaneously when using helium to test configurations with complicated flow fields involving strong shocks, separated flows, and shock-boundary layer interference. Simpler measurements of, say, friction drag on slender, sharp-nosed bodies may be carried out with air closely simulated.

Aeroballistic ranges wherein a model may be launched at very high velocity into relatively dense air offer possibilities for study of boundary-layer transition under hypersonic, cold-wall conditions. (See, e.g., the paper by Charters and Curtis in Ref. 1, pp. 371-404, and Refs. 55 and 56). The range is attractive because of high attainable Reynolds numbers (see Fig. 19), low ambient air turbulence, the possibility to achieve high Mach numbers, and the cold-wall condition of the model. Disadvantages are rather obvious, e.g., the model may pitch and yaw, optical methods must be relied on for transition detection, under some conditions the model may ablate, and it is difficult to launch and separate sabots from complex models. The range is almost essential for studies of wakes far downstream of bodies, regardless of Reynolds numbers of interest.

Counterflow, range-plus-tunnel, facilities offer some of the same advantages as ranges, but they also suffer most of the same disadvantages as the range in addition to those pertaining to impulse-type

tunnels. Very high relative velocities have been proved feasible and unit Reynolds numbers up to 5×10^6 in $^{-1}$ at 35,000 fps are attainable according to Ref. 57. Seiff, in Ref. 57, suggests that relative velocities as high as 50,000 to 60,000 fps may be reached in the next five years. This performance is an indication of the reason why counterflow facilities are intersting.

PLANETARY ATMOSPHERES

Because of contemplated exploration of other planets, aerodynamic simulation of the atmospheres of these planets has become a concern of the aerodynamicist. Some studies of lift, drag, and stability have been accomplished, e.g., Refs. 58-60. In Ref. 58, a blunt-nosed, axisymmetric cylinder with a flared afterbody is shown to yield different static-stability derivatives in different, unmixed gases, the static stability increasing as ratio of specific heats, γ, increases. One infers from these data that γ is the dominant variable, because it appears that the results were the same in argon and helium.

Reference 60 reports tesys of two blunt, conical bodies in air and in gases composed of varying amounts of nitrogen and carbon dioxide, mixed to simulate atmospheres of Mars and Venus. Both a very blunt cone of 10-deg half-angle and a moderately blunt(nose radius = 0.5 base radius) cone of 15-deg half-angle were tested. It was concluded that drag coefficients of these bodies were not perceptibly affected, even when comparing data where $N_2 > 97\%$ with data where $CO_2 > 78\%$. The very bluff body experienced a slight decrease in stability in the

medium with the percentage of CO_2 large (≈85%), i.e., the trend was in qualitative agreement with results of Ref. 58 described above. However, the moderately blunt cone appeared to become slightly more stable in the case where CO_2 was the major constituent (>78%). Stability of both models seemed little different when CO_2 = 14% and N_2 = 86% and when N_2>97% or when the gas was air. Seiff (Ref. 4, p. 29) has suggested that configurations which generate embedded flow fields (i.e., fields containing secondary shock waves) are more sensitive to gas composition.

CLOSING REMARKS

Although not intending to undertake to catalog all known means for hypersonic aerodynamic simulation, the lecturer wishes to close this discussion with a few remarks on certain particularly relevant types of facilities. In doing this, examples are drawn from the AEDC-VKF complex.

Continuous - or Intermittent-Type Wind Tunnel

The continuous-or intermittent-type hypersonic tunnel employing a resistance-type electric heater or a storage heater and capable of $8<M_\infty<14$ must be accorded a full share of the credit forour present knowledge of hypersonic aerodynamics. A good representative of this class is AEDC-VKF Tunnel C, shown in Fig. 23. Capable of M_∞ = 10 (later 12) and having a 50-in.-diam. test section, this tunnel has

been used in the development of almost every aerospace system involving hypersonic aerodynamics. One of the noteworthy features of this tunnel is its "bomb bay" doors opening from the test section to a cabin below. The model support system withdraws the model into this cabin for cooling and/or adjustments while the tunnel compressor plant continues to run. At the chosen time, the model and its supports are injected into the tunnel flow. This method has proved very advantageous for measurements of heating rates, data being obtained more rapidly and economically. Further description may be found in Ref. 61.

Impulse-Type, High-Enthalpy Wind Tunnel

The large, impulse-type tunnel of either the shock tunnel or hotshot variety also has provided a major share of the support of hypersonic flight. Typically these are operated with $M_\infty \geq 20$ and with total temperatures which place them in the border region of perfect-gas and real-gas regimes. Hotshot-type Tunnel F of the AEDC is shown in Fig. 24 as a representative of this class. Numerous tests have been conducted in connection with the development of aerospace vehicles and also research on fluid mechanics. Papers by Lukasiewicz, Whitfield, and Jackson in Ref. 3, pp. 473-511, and Ref. 1, pp. 323-356, give further information on the hotshot type of wind tunnel. At the present time, studies of advanced shock tunnel designs are being conducted because of the apparent potential for improved performance offered by the shock-heating process. Consideration is being given to the augmentation of the shock tunnel driver by magnetogasdynamic acceleration.

Low-Density, Hypersonic (LDH) Wind Tunnel

A major part of this lecture is devoted to descriptions of low-density flow research. While the wind tunnel used for this work cannot be called typical, it is, none the less, mentioned here because of its prominent role in aerodynamic studies of LDH flows. The present AEDC Tunnel L, now four years old, is quite small. Typically, the usable, uniform core of flow in the test section is 1- to 2-in. diam. However, experience with this little, prototype facility once again teaches us how much can be learned from such a modest monetary investment.

Because this type of tunnel is not yet widely represented in the world's laboratories but is beginning to appear in increasing numbers, a sketch showing the main features of an idealized, typical LDH tunnel is included as Fig. 25. It should be pointed out that various arc-heated tunnels were used for heating studies preceding the advent of the LDH-type "aerodynamic" wind tunnel. Flow quality and calibration procedures were not of so much concern in these earlier facilities, but high enthalpy was the main concern. For aerodynamic work, the potential of the arc heater for high enthalpy has been subordinated to achieve more steady, uniform flow of lower total enthalpy closer to thermochemical equilibrium. Figure 26 is a photograph of AEDC-VKF Tunnel L. More details may be found in Ref. 62. The possibility of combining magnetogasdynamic acceleration with arc-heated tunnels is receiving serious consideration at several laboratories.

Aeroballistic Range and Counterflow Facility

These two types of experimental facilities are related to such an extent that both are combined in the few remarks made here. To better illustrate each type, Fig. 27 is included. The very great length of these facilities makes it difficult to obtain photographs clearly showing their main features. Figure 27 is divided into three parts, the top part showing a shock tube, the middle showing nozzle, test section and dump tanks, and the lower part showing a launcher or gun. Combining the top two components of Fig. 27 gives a shock tunnel. Combining the bottom component with the middle part, excluding the nozzle, gives an aeroballistic range. Putting all together, of course, yields the counterflow facility.

Although very high muzzle velocities may be produced by modern aeroballistic launchers, the peak launch accelerations (up to 10^6 - 10^7 g's) are so great that model and sabot structural problems arise. In fact, if it were not for this obstacle, we might be telemetering aerodynamic data from models in flight. Figure 28 is offered as a summary of the current ability to launch models in ranges. Areas to the lower left of the three boundaries represent achieved launches. One can see why the aeroballistic range or the combined shock tunnel and gun is attractive to aerodynamicists seeking closer simulation of orbital and super-orbital flight. Practical problems of great difficulty also are apparent, but further development seems to be worthwhile. Figures 29a and 29b show gun and shock tunnel components of the pilot counterflow facility at AEDC-VKF. References pertaining to

these devices have been mentioned earlier, e.g., Refs. 1, 15, 16, 56, and 57. One may also find more information on guns in Refs. 63-65.

Various, less-well-developed but interesting types of facilities could be mentioned, e.g., expansion tubes, high intensity molecular beams, and any of several devices wherein acceleration of ionized gases plays a key role. However, these latter are still in developmental stages and have not yet played important parts in aerodynamic simulation work. Free-flight research using rocket booster models may be regarded as simulation in a broader sense, but it is beyond the scope of this discussion. It is understood that a later lecture will deal with this subject.

ACKNOWLEDGMENTS

The lecturer owes thanks to all of his colleagues in ARO, Inc., and the Arnold Engineering Development Center, Air Force Systems Command, USAF, for their cooperation during the preparation of this material. In addition to those employes of ARO cited in the references, particular acknowledgments are due G. W. Chumbley and Mrs. Maxine O'Dear.

REFERENCES

1. The High Temperature Aspects of Hypersonic Flow. (W. C. Nelson, ed.) Pergamon Press, Oxford, London, New York and Paris, 1964.

2. Reentry Dynamics, Proceedings of the Conference on Physics of the Solar System and Reentry Dynamics. Bulletin of the Virginia Polytechnic Institute, Engr. Exp. Sta. Series No. 150, Vol. LV, No. 10, August 1962.

3. Hypersonic Flow Research. (F. R. Riddell, ed.) Academic Press, New York and London, 1962.

4. Proceedings of the NASA - University Conference on Science and Technology of Space Exploration: Aerodynamics of Space Vehicles (NASA SP-23) and Gas Dynamics in Space Exploration (NASA SP-24). Chicago, December 1962.

5. "Aerospace Engineering: High Temperatures Issue." Aerospace Engineering, Vol. 22, No. 1, Institute of the Aerospace Sciences, January 1963.

6. Cheng, H. K. "Recent Advances in Hypersonic Flow Research." AIAA Jour., Vol. 1, No. 2, pp. 295-310, February 1963.

7. Symposium on Dynamics of Manned Lifting Planetary Entry. (S. M. Scala, A. C. Harrison and M. Rogers, eds.) John Wiley and Sons, New York and London, 1963.

8. Eggers, A. J. and Wong, T. J. "Motion and Heating of Lifting Vehicles During Atmosphere Entry." Paper presented at ARS Conference on Lifting Reentry Vehicles, April 4-6, 1961, in Palm Springs, California

9. "Physics of Entry into Planetary Atmospheres." AIAA Conference Cambridge, Massachusetts, Preprints 63-433 to 63-465, August 26-28, 1963.

10. "International Symposium on Fundamental Phenomena in Hypersonic Flow." Sponsored by Cornell Aeronautical Laboratory, Inc., June 25-26, 1964. Proceedings to be published by Cornell University Press.

11.- Rarefied Gas Dynamics. (Ed. by F. M. Devienne, 1959, Ref.
14. 11; L. Talbot, 1961, Ref. 12; J. A. Laurmann, 1964, Ref. 13; and J. H. deLeeuw, 1965, Ref. 14, to be published.) Academic Press, New York and London.

15. Advances in Hypervelocity Techniques: Proceedings of the Second Symposium on Hypervelocity Techniques. (A. M. Krill, ed) Plenum Press, New York, 1962.

16. Advanced Experimental Techniques for Study of Hypervelocity Flight: Third Hypervelocity Techniques Symposium. Co-sponsored by Denver Research Institute, University of Denver, and Arnold Engineering Development Center, ARO, Inc., 1964.

17. Hall, J. G. "Studies of Chemical Non-equilibrium in Hypersonic Nozzle Flows." Cornell Aero. Lab. Rept. 1118-A-6; AD 229131, November, 1959.

18. Ferri, A., "Hypersonic Flight Testing." International Science and Technology, No. 28, April 1964.

19. Henshall, B. D. "A Review of the Development of High Enthalpy Aerodynamic Test Facilities." Appl. Mech. Rev., Vol. 13, No. 6, June 1960

20. Lordi, J. A. and Mates, R. E. "Nonequilibrium Expansions of High-Enthalpy Airflows." Cornell Aero. Lab. Rept. No. AD-1716-A-3, March 1964.

21. Hurle, I. R., Russo, A. L. and Hall, J. G. "Spectroscopic Studies of Vibrational Nonequilibrium in Supersonic Nozzle Flows." Jour. of Chem. Physics, Vol. 40, No. 8, pp. 2076-2089, April 15, 1964

22. Potter, J. L., Arney, G. D., Jr., Kinslow, M., and Carden, W. H. "Gasdynamic Diagnosis of High-Speed Flows Expanded from Plasma States." IEEE International Symposium on Plasma Phenomena and Measurements, San Diego, California, October 29 - November 1, 1963.

23. Potter, J. L., Arney, G. D., Jr., Kinslow, M., and Carden, W. H. "Irreversible Flow in Reservoir and Throat Sections of Wind Tunnels with Constricted-Arc Heaters." Paper to be presented at AGARD Fluid Dynamics Panel Specialists Meeting, Rhode-Saint-Genese, Belgium, September 21-23, 1964.

24. Bray, K. N. C. "A Sudden-Freezing Analysis for Non-equilibrium Nozzle Flows." University of Southampton, AASU Rept. No. 161, December 1960.

25. Gibson, W. "The Effect of Ambient Dissociation and Species Diffusion on Non-equilibrium Shock Layers." Paper 63-70, presented at the 31st Annual IAS Meeting, New York, January 1963.

26. Hall, J. G., Eschenroeder, A. Q., and Marrone, P. V. "Blunt-nose Inviscid Airflows with Coupled Nenequilibrium Processes." J. Aerospace Sci., Vol. 29, No.9, September 1962, pp. 1038-1051.

27. Rosner, D. E. "Scale Effects and Correlations in Nonequilibrium Convective Heat Transfer." AIAA J., Vol. 1, No. 7, July 1963, pp. 1550-1555.

28. Chung, P. M. "Hypersonic Viscous Shock Layer of Nonequlibrium Dissociating Gas." NASA TR R-109, 1961.

29. Inger, G. R. "Nonequilibrium Hypersonic Flat-Plate Boundary-Layer Flow with a Strong Induced Pressure Field," AIAA J., Vol. 2, No. 3, March 1964, pp. 452-460.

30. Whalen, R. J. "Viscous and Inviscid Nonequilibrium Gas Flows." J. Aerospace Sci., Vol. 29, No. 10, October 1962, pp. 1222-1237.

31. Lees, L. "Laminar Heat Transfer over Blunt-Nosed Bodies at Hypersonic Flight Speeds." Jet Propulsion, Vol. 26, No. 4, April 1956, pp. 259-269.

32. Fay, J. A. and Riddell, F. R. "Theory of Stagnation Point Heat Transfer in Dissociated Air." Jour. of the Aero/Space Sciences, Vol. 25, No. 2, February 1958, pp. 73-85.

33. Talbot, L. "Survey of the Shock Structure Problem." ARS Jour., Vol. 32, No. 7, July 1962, pp. 1009-1016.

34. Arney, G. D. and Bailey, A. B. "The Effect of Temperature on Pressure Measurements." AIAA J., Vol. 1. No. 12, December 1963, pp. 2863-2864.

35. Wachman, H. Y. "The Thermal Accommodation Coefficient: A Critical Survey." ARS Jour., Vol 32, No. 1, January 1962, pp. 2-12.

36. Potter, J. L., Kinslow, M. and Boylan, D. E. "Influence of the Orifice on Measured Pressures in Rarefied Flow." Paper presented at the Fourth International Symposium on Rarefied Gas Dynamics, Toronto, 1964.

37. Whitfield, J. D. and Norfleet, G. D. "Source Flow Effects in Conical Hypervelocity Nozzles." AEDC-TDR-62-116, June 1962.

38. Lewis, C. H. Personal communication, July 1964.

39. Boylan, D. E. "An Experimental Study of Diffusers in an Open-Jet, Low-Density, Hypersonic Wind Tunnel." AEDC-TDR-64-47, April 1964.

40. Potter, J. L. and Boylan, D. E. "Experience with an Over-expanded Nozzle in a Low-Density, Hypervelocity Wind Tunnel." AEDC-TDR-62-85, April 1962.

41. Potter, J. L. and Miller, J. T. "Total Heating Load on Blunt, Axisymmetric Bodies in Low-Density Flow." AIAA Journal, Vol. 1, No. 2, February 1963, pp. 480-481.

42. Cheng, H. K. "Hypersonic Shock-Layer Theory of the Stagnation Region at Low Reynolds Number." Cornell Aero. Lab. Rept. No. AF-1285-A-7, April 1961.

43. Probstein, R. F. and Kemp, N. H. "Viscous Aerodynamic Characteristics in Hypersonic Rarefied Gas Flow." Journal of the Aero/Space Sciences, Vol. 27, No. 3, March 1960, pp. 174-192.

44. Van Dyke, M. "Second-Order Compressible Boundary-Layer Theory With Application to Blunt Bodies in Hypersonic Flow." AFOSR-TN-61, July 1961.

45. Kinslow, M. and Potter, J. L. "The Drag of Spheres in Rarefied, Hypervelocity Flow." AEDC-TDR-62-205, December 1962; AIAA Journal, Vol. 1, No. 11, November 1963, pp. 2467-2473.

46. Bailey, A. B. and Sims, W. H. "The Shock Shape and Shock Detachment Distance for Spheres and Flat-Faced Bodies in Low-Density, Hypervelocity Argon Flow." AEDC-TDR-63-21, January 1963

47. Ho, Hung-Ta and Probstein, R. F. "The Compressible Viscous Layer in Rarefied Hypersonic Flow." Brown University, ARL-TN-60-132, August 1960.

48. Arney, G. D., Jr., and Harter, W. T. "A Low-Load, 3-Component Force Balance for Measurements in a Low-Density Wind Tunnel." IEEE First International Congress on Instrumentation in Aero-Space Simulation Facilities, Paris, September 28-29, 1964.

49. Moore, F. K. "On Local Flat Plate Similarity intthe Hypersonic Boundary Layer." Vol. 28, No. 10, October 1961, pp. 753-762.

50. Potter, J. L. and Whitefield, J. D. "Effects of Slight Nose Bluntness and Roughness on Boundary-Layer Transition in Supersonic Flows." Jour. Fluid Mech., Vol. 12, Part 4, pp. 501-535, 1962.

51. Nagamatsu, H. T. and Sheer, R. E., Jr., "Boundary-Layer Transition on a Highly Cooled 10 deg Cone in Hypersonic Flows." General Electric Res. Lab. Rept. No. 64-RL-(3622C), March 1964.

52. Potter, J. L. and Whitfield, J. D. "Transition Measurements and the Correlation of Transition Sensitive Data." AEDC-TR-59-4, February 1959.

53. Laufer, J. and Verbalovich, T. "Stability and Transition of a Supersonic Boundary Layer." Jour. Fluid Mech. Vol. 9, Part 2, October 1960, pp. 257-299.

54. Potter, J. L. and Whitfield, J. D. "Effects of Unit Reynolds Number, Nose Bluntness, and Roughness on Boundary Layer Transition. AEDC-TR-60-5, March 1960.

55. Lyons, W. C., Jr., Brady, J. J. and Levensteins, Z. J. "Hypersonic Drag, Stability, and Wake Data for Cones and Spheres." AIAA Aerospace Sci. Meeting. Preprint No. 64-44, New York, January 20-22, 1964.

56. Lyons, W. C., Jr., "Application of the Ballistics Range for the Study of Aerodynamic Flow Phenomena About Free-Flight Bodies." AIAA Aerodynamic Testing Conference, Washington, D. C., March 9-10, 1964, pp. 225-238.

57. Seiff, A. "Ames Hypervelocity Free-Flight Research." Astronautics and Aerospace Engr., Vol. 1, No. 1, pp. 16-23, 1963.

58. James, C. S. and Smith, W. G. "Experimental Studies of Static Stability and Radiative Heating Associated with Mars and Venus Entry." Presented at IAS 31st Annual Meeting, New York, January 21-23, 1963.

59. Smith, W. G. and Peterson, W. P. "Free-Flight Measurements of Drag and Stability of a Blunt-Nosed Cylinder With a Flared After-Body in Air and Carbon Dioxide." NASA TM X-642, 1961.

60. Jaffe, P. "Hypersonic Ballistic Range Results of Two Planetary Entry Configurations in Air and Carbon Dioxide/Nitrogen Mixtures." Jet Propulsion Lab. Tech Rept No. 32-543, January 31, 1964.

61. Sivells, J. C. "Aerodynamic Design and Calibration of the VKF 50 in. Hypersonic Wind Tunnels." AEDC-TDR-62-230, March 1963.

62. Potter, J. L. "Low-Density, Hypersonic (LDH) Wind Tunnel L." von Karman Gas Dynamics Facility Technical Developments (J. Lukasiewicz, Ed.) 1964, pp. 61-63.

63. Stephenson, W. B. and Anderson, D. E. "Two-Stage, Light-Gas Model Launchers." Aerospace Engr., Vol. 21, No. 8, pp. 64ff., August 1962.

64. Charters, A. C. and Curtis, J. S. "How an Accelerated Reservoir Light-Gas Gun is Used in a Hypervelocity Free Flight Range." The Jour. of the Environmental Sci., December 1963, pp. 27-32.

65. Curtis, J. S. "An Accelerated Reservoir Light-Gas Gun." NASA TN D-1144, February 1962.

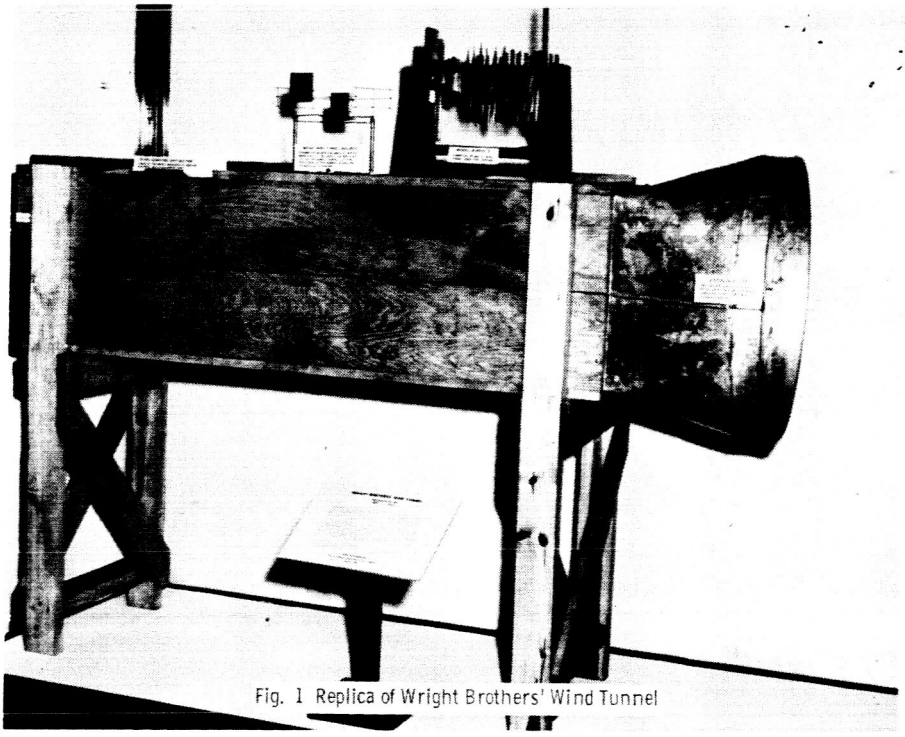

Fig. 1 Replica of Wright Brothers' Wind Tunnel

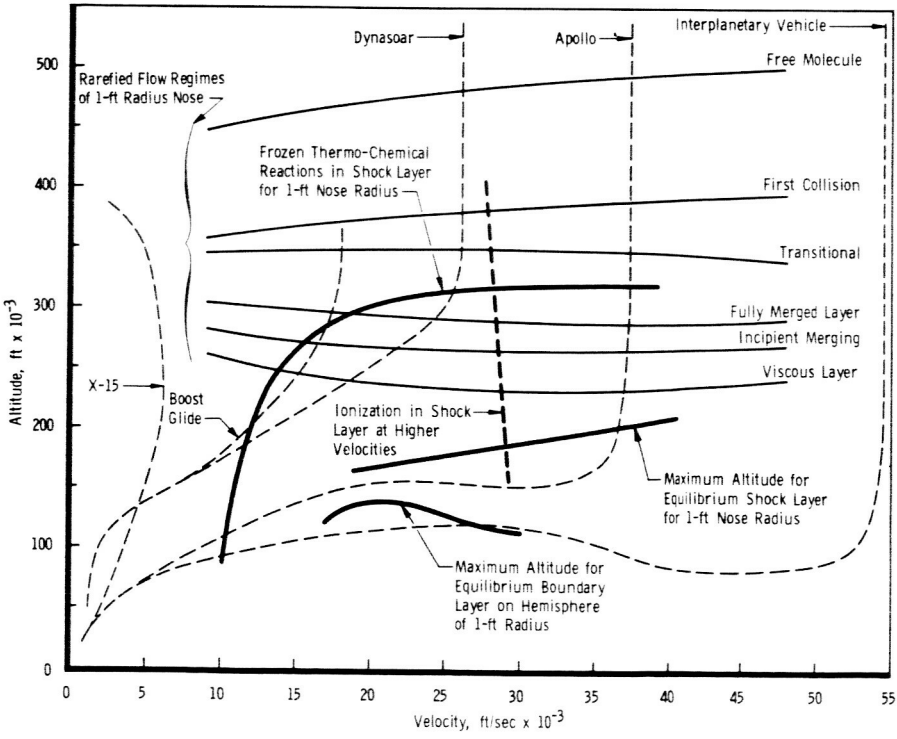

Fig. 2 Flow Regimes and Typical Trajectories in the Earth's Atmosphere (flow regimes apply to the stagnation region of a sphere of 1-ft radius.)

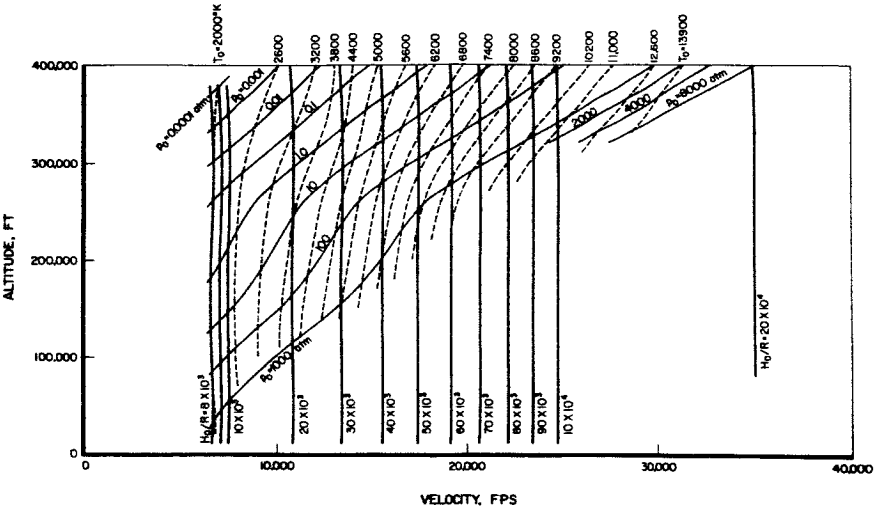

FIG 3 WIND TUNNEL RESERVOIR CONDITIONS CORRESPONDING TO FLIGHT IN THE EARTH'S ATMOSPHERE

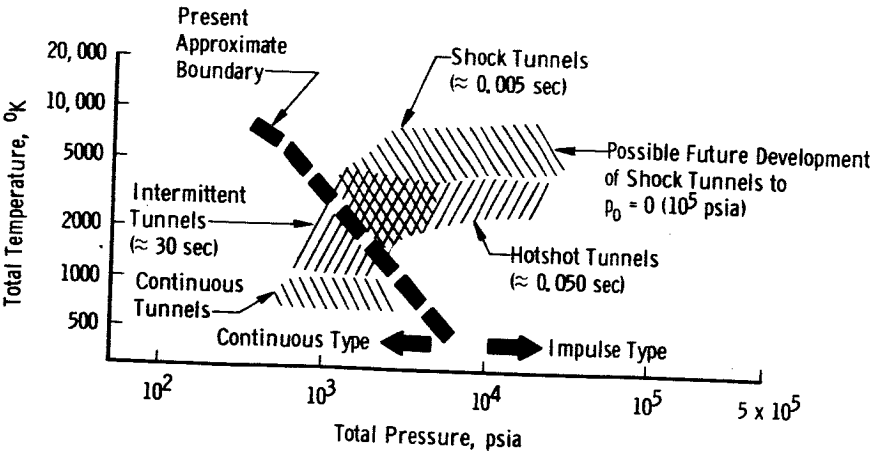

Fig. 4 Approximate Limits Imposed on Conventional Wind Tunnels by Throat Heating Alone

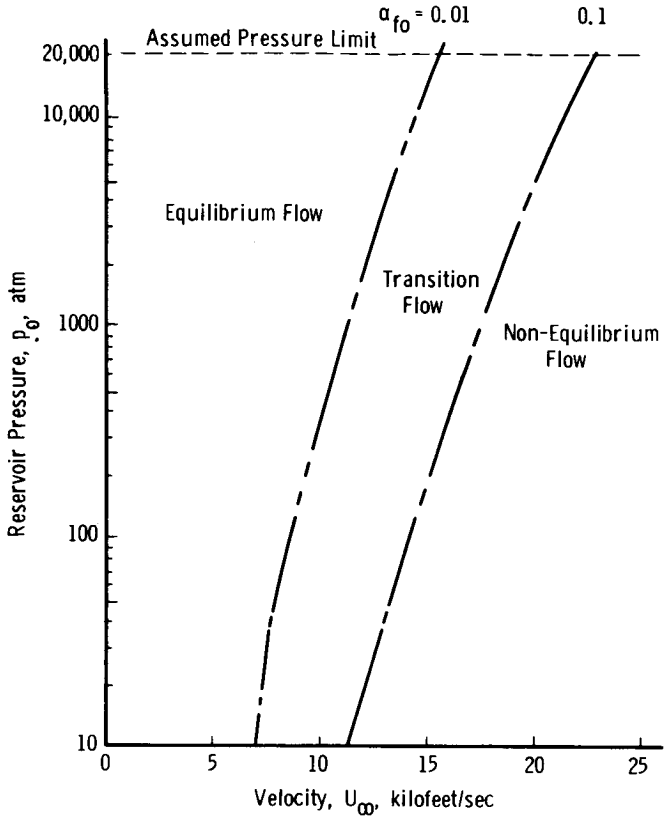

Fig. 5 Reservoir Pressure Required for Equilibrium Nozzle Flow of Air with Oxygen Dissociation

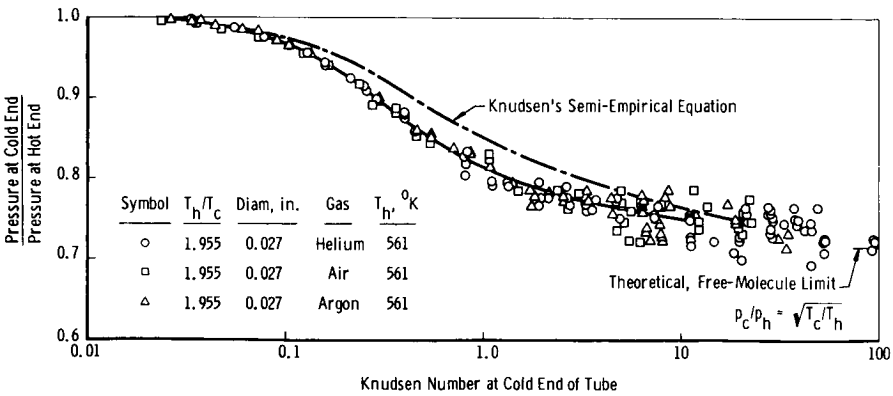

Fig. 6 Thermo-Molecular Flow Effect in Tubes (The symbols p and T represent pressure and temperature, respectively. Subscript c denotes cold end of the tube, and h denotes hot end.)

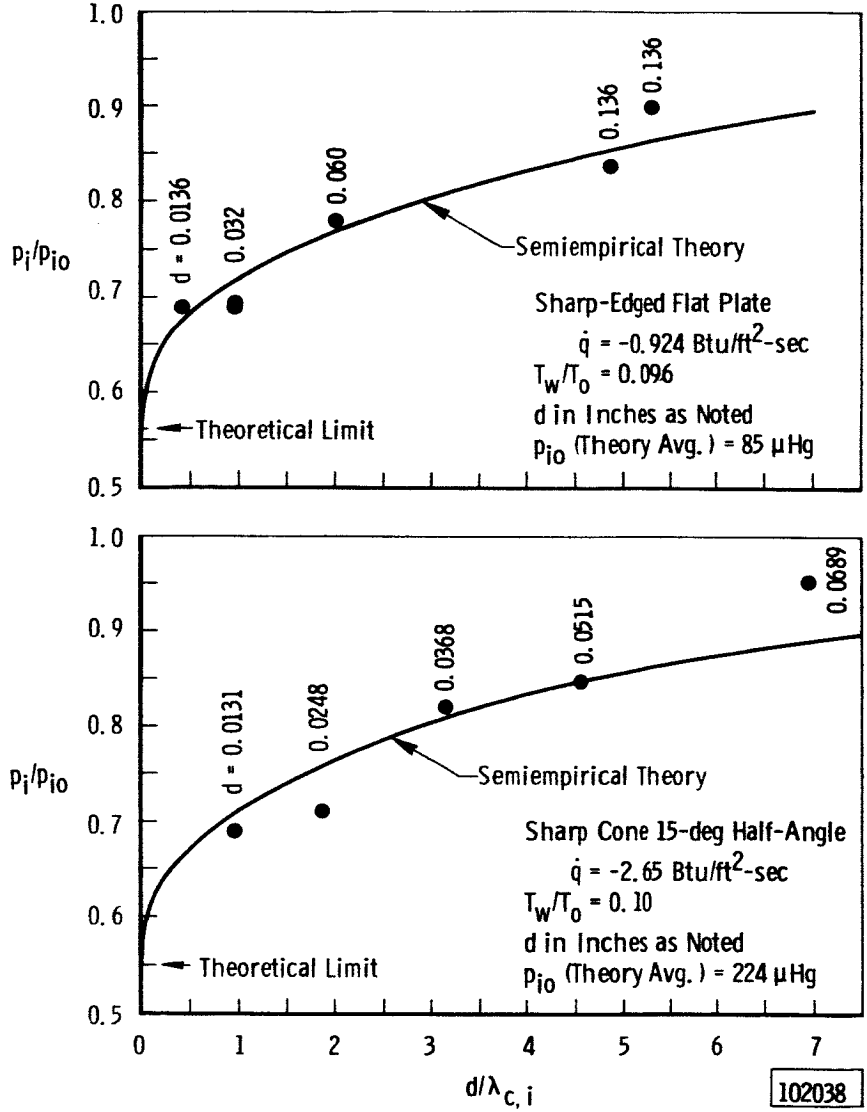

Fig. 7 Measured Static Pressure in Tunnel L (nitrogen gas, M_∞ = 10.15, T_0 = 5620°R, Re_∞ = 388/in., p_i = indicated pressure, p_{io} = true pressure, $\dot{q}$ = heat transfer rate, $\lambda_{c,i}$ = mean free path at p_i and T_c, d = orifice diameter, and T_w = wall temperature.)

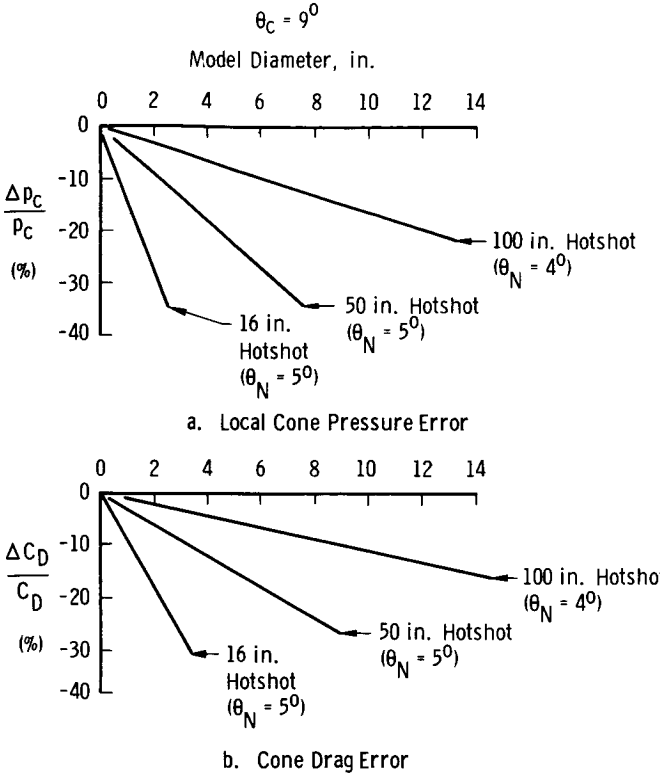

Fig. 8 Theoretical Errors in Cone Pressures and Drag Due to Source Flow over a 9-deg Half-Vertex Angle Cone (p_c = pressure on cone, C_D = drag coefficient, θ_N = nozzle effective expansion angle.)

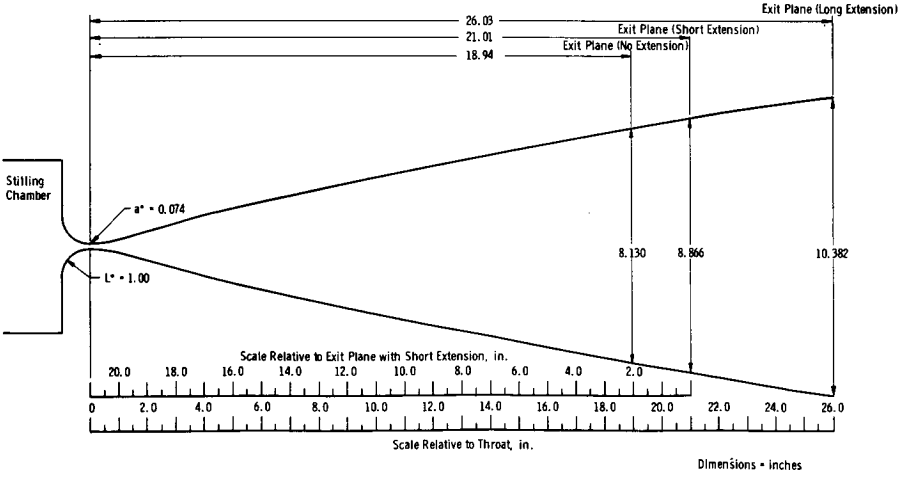

Fig. 9 Tunnel L Nozzle Contour

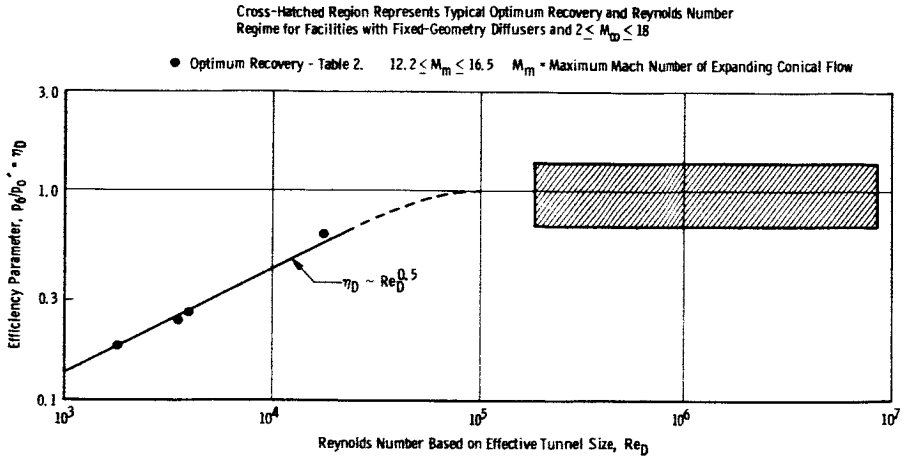

Fig. 10 Diffuser Efficiency as a Function of Reynolds Number (η_D = total pressure ratio across diffuser, Re_D based on stream conditions at M_m and effective diameter of stream expanded to M_m from nozzle throat diameter.)

DATA

○ Tunnel L, August 1962
$\epsilon = 0.175$
$\dot{q}$ = average to entire hemisphere

THEORIES

① Free-molecular flow, diffuse reflection, hypersonic speed, α = accommodation coefficient, normalized to Fay and Riddell.

② Theories of Probstein and Kemp and Van Dyke, normalized to Fay and Riddell for $Re_0 \geq 10^4$ and with Van Dyke's result restricted to $Re_0 \geq 50$. Both theories adjusted to apply to the case $\epsilon = \rho_\infty/\rho_2 = 0.175$.

③ Theory of Cheng, normalized to Cheng's limit for $Re_2 \to \infty$, for $\epsilon = 0.11$. Result of Cheng not strongly affected by ϵ.

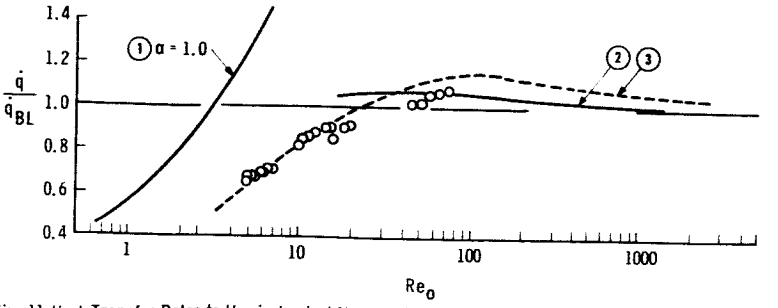

Fig. 11 Heat-Transfer Rates to Hemispherical Noses at Low Reynolds Numbers and Hypersonic Speeds ($\dot{q}$ = Btu/ft^2-sec. $Re_0 = U_\infty \rho_\infty R/\mu_0$ where U_∞ = free-stream velocity, ρ_∞ = free-stream density, R = hemisphere radius, and μ_0 = viscosity corresponding to total enthalpy; ϵ = density ratio across normal shock, subscript BL indicates value calculated by theory of Fay and Riddell.)

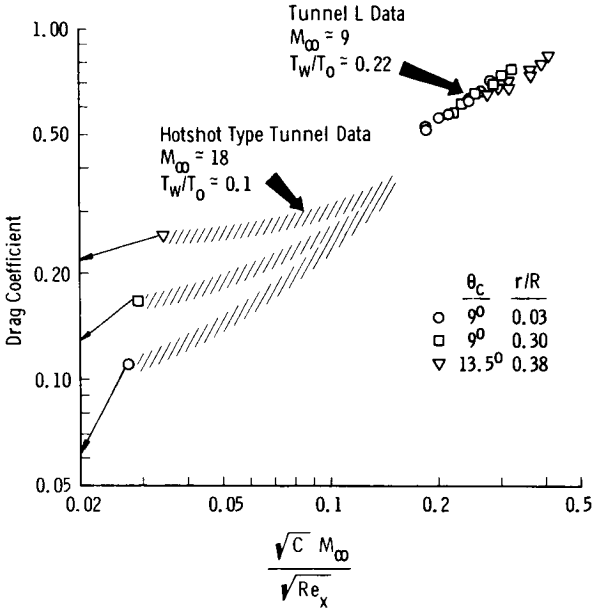

Fig. 12 Drag of Cones at Low Reynolds Number and Hypersonic Speed (Inviscid limits indicated by arrows to ordinate. The ratio of cone nose radius to base radius is denoted as r/R. θ_c = cone half-angle. C = coefficient in linear viscosity-temperature relation, M_∞ = free-stream Mach number, Re_x = Reynolds number based on free-stream conditions and axial length of body.)

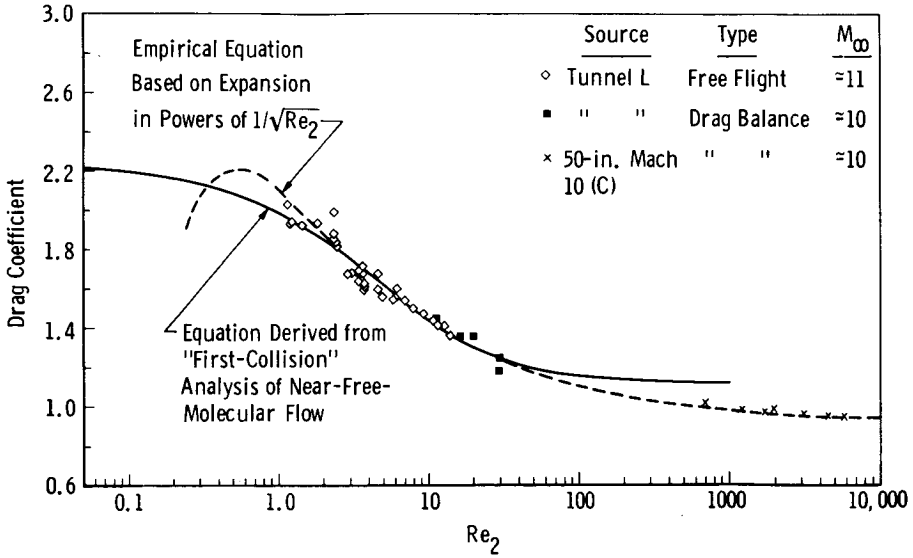

Fig. 13 Drag of Spheres at Low Reynolds Numbers and Hypersonic Speeds (Re_2 is Reynolds number based on conditions immediately downstream of normal shock and sphere diameter, assuming Rankine-Hugoniot shock.)

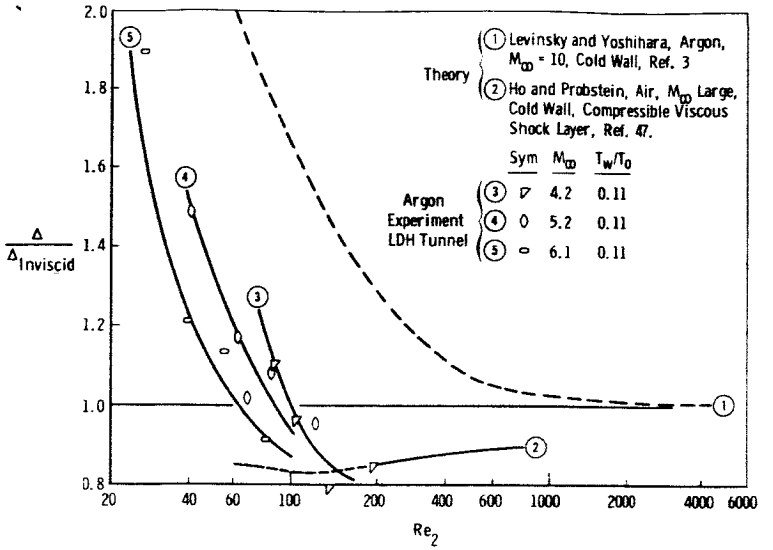

Fig. 14 A Comparison of Theoretical and Experimental Shock Detachment Distances for Hemispheres (Δ is the detachment distance or shock-layer thickness. Re_2 is a Reynolds number based on conditions immediately downstream of a normal shock wave and hemisphere diameter, assuming Rankine-Hugoniot shock.)

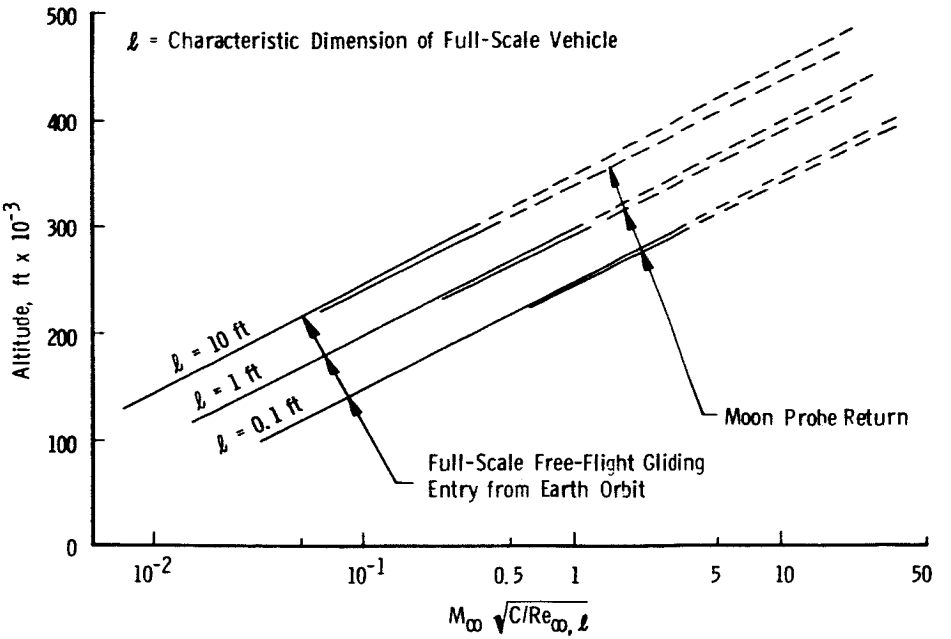

Fig. 15 Viscous Drag Parameter (trajectories of hypothetical, typical, gliding-entry vehicle designs.)

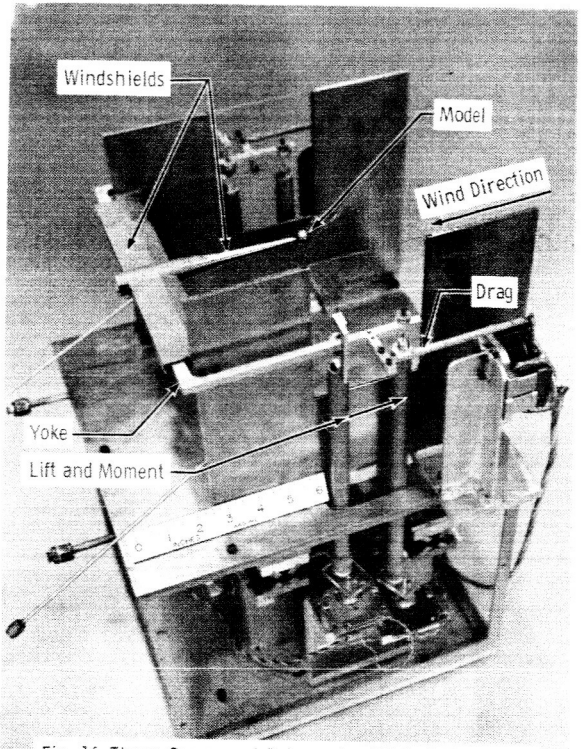

Fig. 16 Three-Component Balance for AEDC-VKF Tunnel L

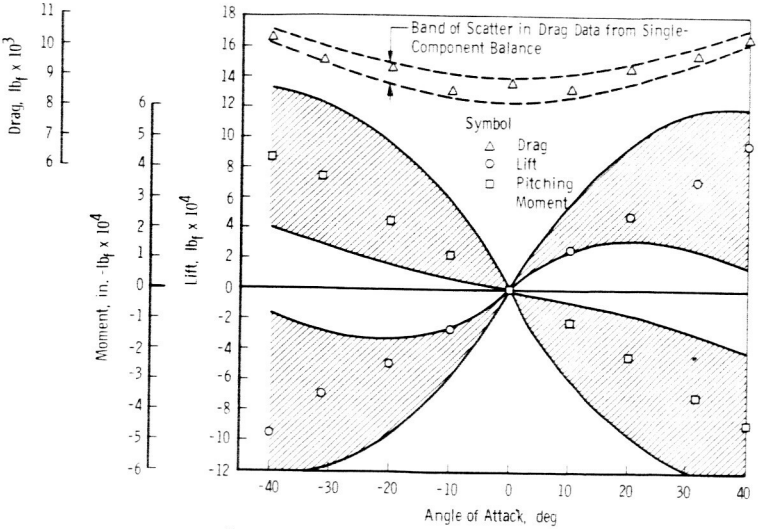

Fig. 17 Example Wind Tunnel Lift, Drag and Pitching Moment Measurements on Blunted Cone (Shaded Regions Lie between Extremes of Free Molecular and Newtonian Theories for Lift and Moment)

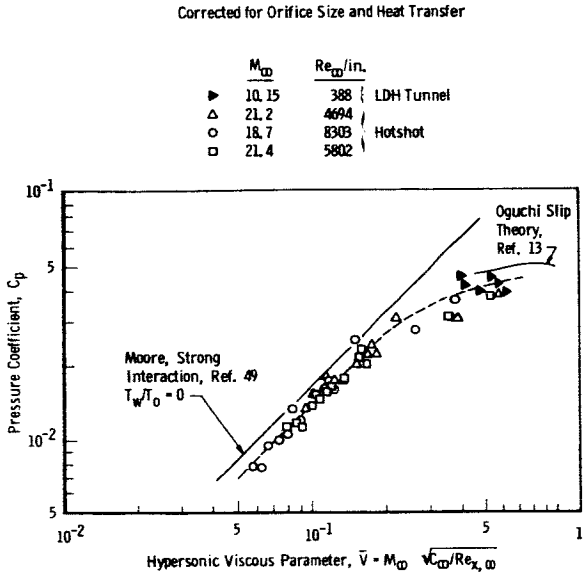

Fig. 18 Hypersonic Viscous Parameter, $\bar{V} = M_\infty \sqrt{C_\infty/Re_{x,\infty}}$ (C_∞ = coefficient in linear viscosity-temperature law, Re_x based on distance to orifice from plate leading edge.)

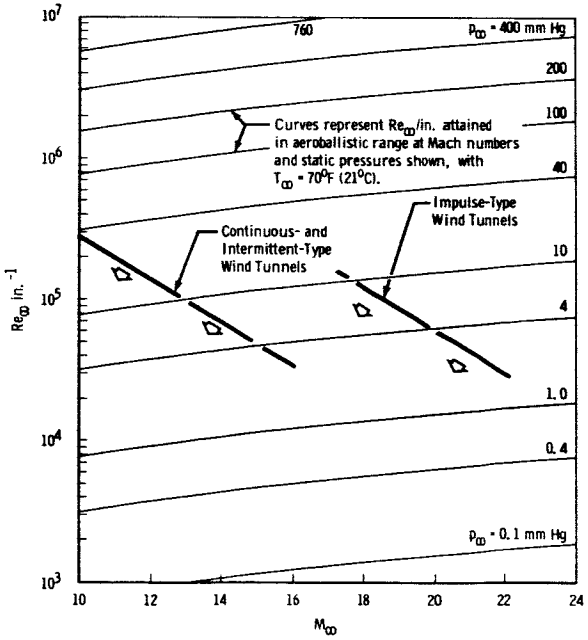

Fig. 19 Unit Reynolds Numbers Currently Available in Hypersonic Wind Tunnels Compared with Aeroballistic Ranges

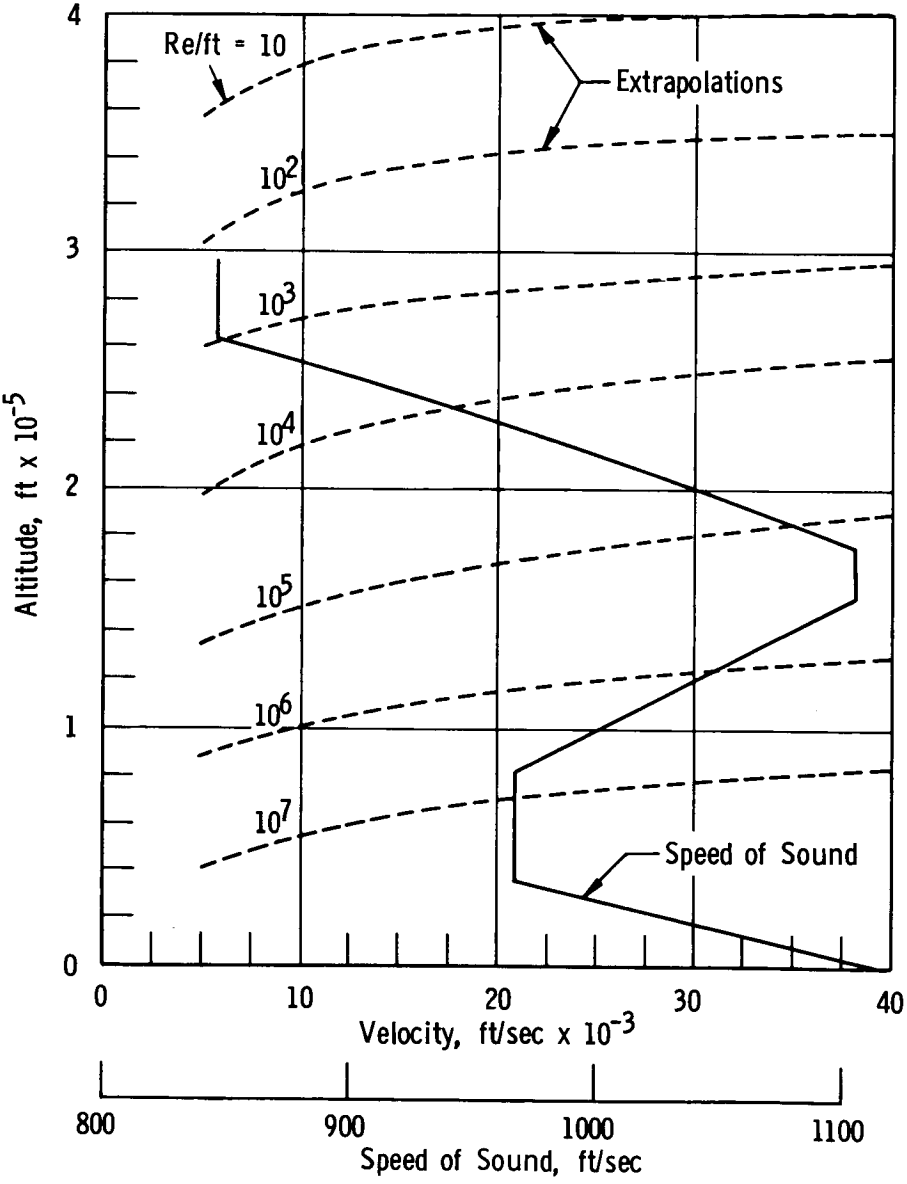

Fig. 20 Selected Data from 1959 ARDC Standard Atmosphere

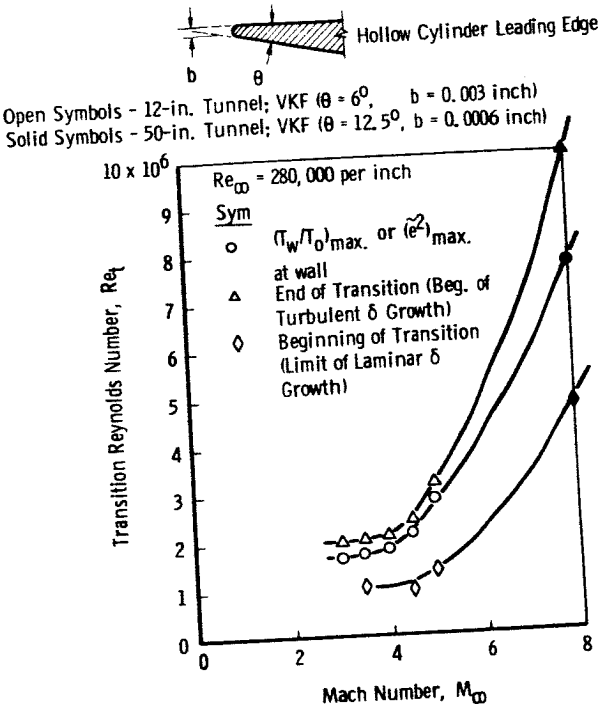

Fig. 21 Influence of Mach Number on Transition Reynolds Number on Exterior of a Hollow Cylinder Aligned with the Flow (T_w = wall temperature, $\tilde{e}^2$ = mean squared fluctuation energy.)

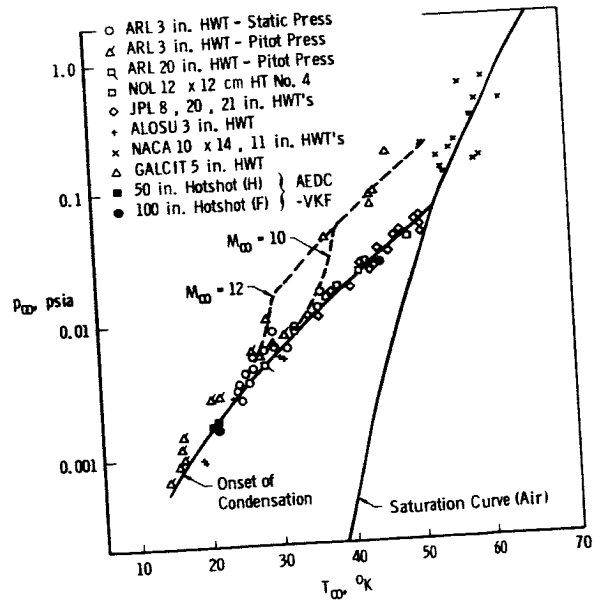

Fig. 22 Phase Diagram

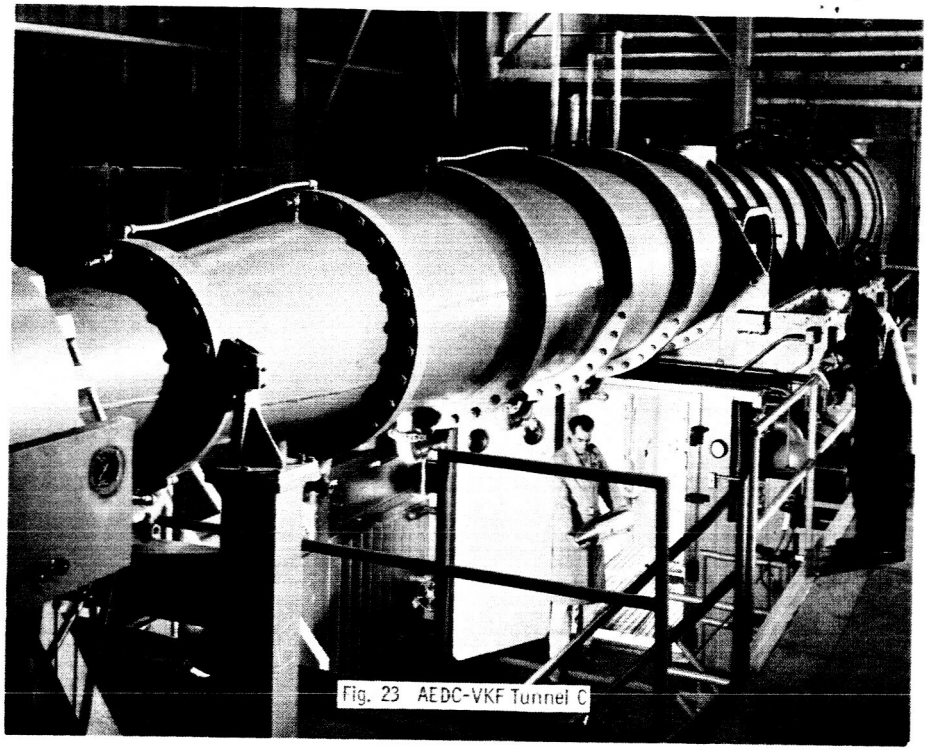

Fig. 23 AEDC-VKF Tunnel C

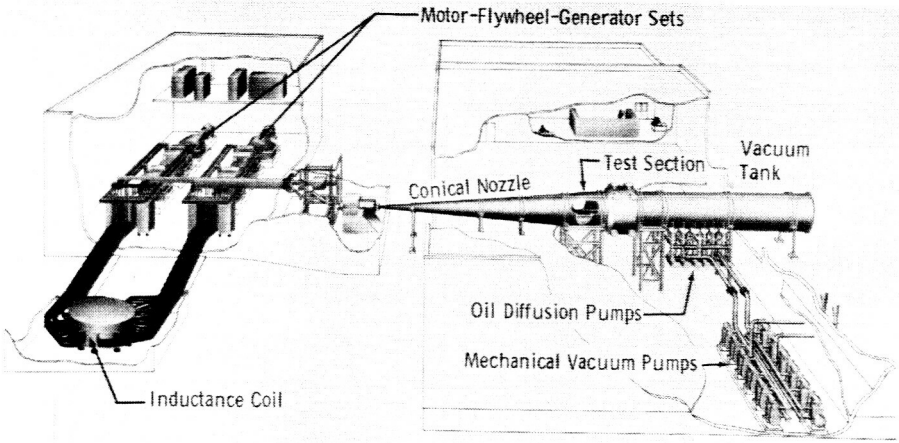

Fig. 24 AEDC-VKF Hotshot-Type Tunnel F

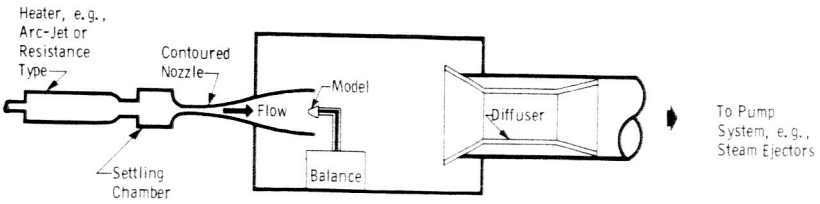

Fig. 25 Schematic of Low-Density, Hypersonic, Continuous-Type Wind Tunnel

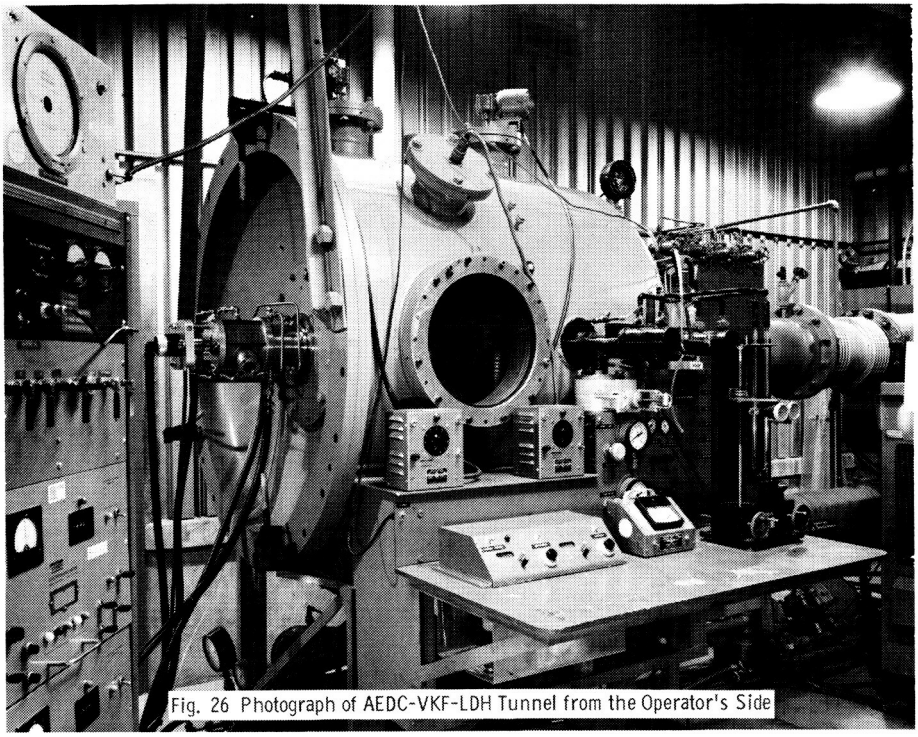

Fig. 26 Photograph of AEDC-VKF-LDH Tunnel from the Operator's Side

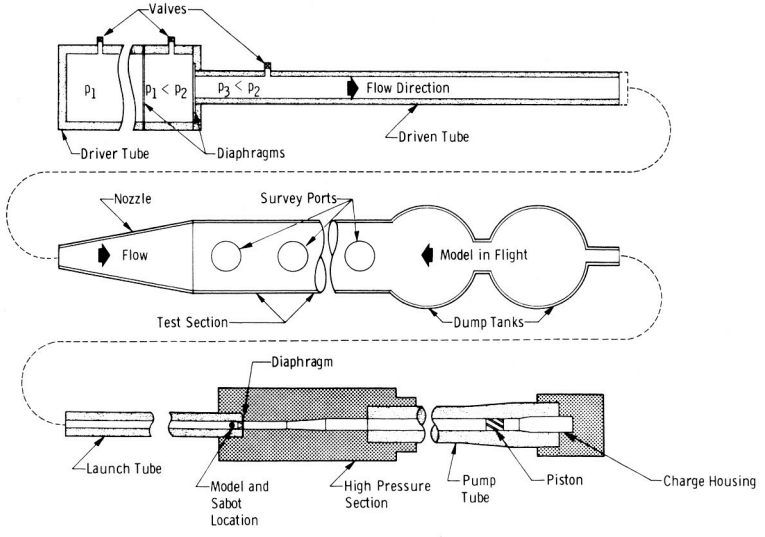

Fig. 27 Schematic of Counterflow Tunnel Components, Also Showing Shock Tube, Shock Tunnel, and Aeroballistic Gun

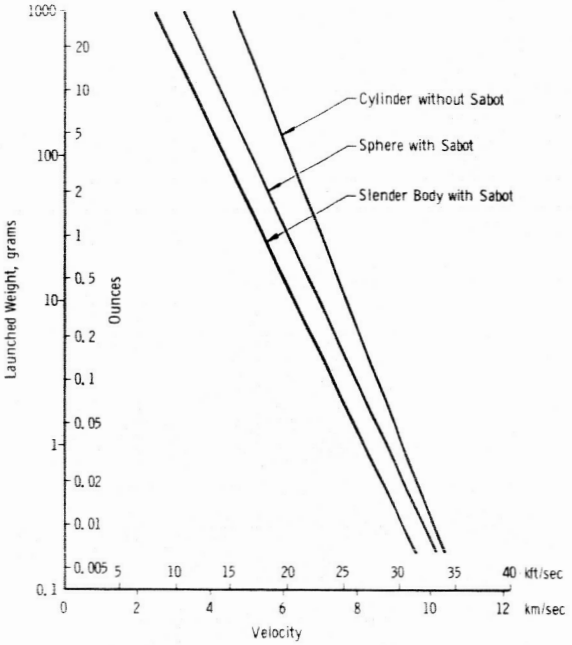

Fig. 28 Current (1964) Status of Aeroballistic Range Launcher Capability

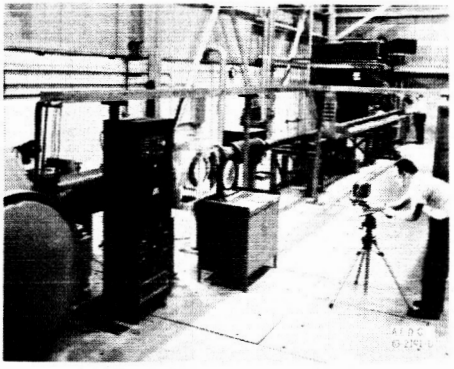

a. Shock Tunnel

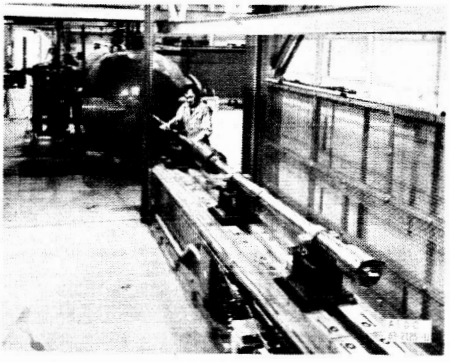

b. Model Launcher

Fig. 29 AEDC-VKF Counterflow Facility

CONVECTIVE AND RADIATIVE HEAT TRANSFER DURING REENTRY AND ADVANCED TECHNIQUES FOR THEIR SIMULATION

by

Thomas N. Canning

INTRODUCTION

Experimental engineering research has been largely devoted to simulation, in the laboratory, of phenomena and systems which are difficult, for one reason or another, to reproduce in full-scale tests. The success of these efforts at simulation in guaranteeing the final system performance has been in direct proportion to the success in choosing the proper parameters to be matched and to the exactness of scaling laws derived for use in projecting to full-scale behavior. In the best of all possible worlds one could always make his tests at the design conditions using the complete system under consideration. One example will suffice to show why this generally cannot be done.

The Apollo command module will enter the earth's atmosphere at about 11 km/sec and will have on board three people, whose value has been enhanced by recent experiences. If all of the bits and pieces as well as the subsystems necessary for the mission have not been checked thoroughly in the laboratory, the chances of the complete system operating are nil.

One bit of this system which - thanks to hundreds of fairly cheap laboratory tests and scores of careful theoretical studies - assumes a lessening threat to success is the heat-protection system. It is to this narrow part of the vast complex of technologies that the present discussion of simulation is devoted. Since Brooks[1] has discussed the study of material response, the present paper is further restricted to evaluation of expected heat loads.

These heat loads are conveniently divided into two components which can usually be treated separately, convection and radiation from the gas within the shock layer to the vehicle surface.

CONVECTIVE HEATING

The stagnation-point convective heat load on blunt hypervelocity bodies has been treated extensively by many investigators, for example, Lees[2] and Fay and Riddell[3] in the speed range up to 10 km/sec. Lees has also related the heating elsewhere on simple bodies to that at the stagnation point. Starting with the former problem we see, in Figure 1, that the heating rate normalized with respect to the body size and pitot pressure is nearly a linear function of the driving potential, that is, the difference between stagnation and wall enthalpy. As the flight speed increases above about 9 km/sec, the temperatures become high enough that partial ionization occurs. The influence of ionization on convective heating has been argued widely: the consensus of those theoreticians who have used the transport properties predicted by Hansen[4] for hot air is that the influence is fairly small; the controversy is essentially settled by results of actual measurements of heating rates in two types

of modern laboratory equipment. Figure 2 shows the experimentally determined heating and indicates that there is, at least, fair agreement among the experimenters.

Most of the data shown in Figure 2 were obtained by use of shock tubes; the remainder were collected from aeroballistic tests. The shock tube consists of a tube containing a sample of test gas, say, air, and a driver filled with gas at high pressure (Fig. 3). When the diaphragm which separates the chambers is ruptured, a shock moves through the test gas simulating the detached bow shock of a flying body. Instruments may be placed around the test area to study the physical and chemical changes wrought by the shock compression. The pertinent setup for the study of convection requires small aerodynamic models to be mounted within the tube to simulate the hypervelocity flow field. Thin-film resistance gages or thicker calorimeter gages are deposited on the models so that the history of surface temperature, and hence heating rate, can be determined.[5, 6, 7]

The two most popular shock-tube configurations in use today are illustrated in Figure 4. The simplest form (in the upper sketch) uses the flow just behind the incident wave as the airstream. This part of the gas flow is very hot so that, even though its speed may be high, its Mach number is low and the aerodynamics of the test flow must be analyzed accordingly. This disadvantage is not serious when only the stagnation point heat transfer is being measured or when the details of the flow field are well known. The other configurations will be discussed later. Only a fraction of available convective-heating data (obtained in simple shock tubes) are shown in Figure 2. As with most rapidly developing experimental techniques, the data scatter unacceptably at the higher enthalpy, that is, velocity, levels. Most but not all of the apparent discrepancies are at least partially understood.

If the researchers using shock tubes had been content to use only the simplest designs, the description of the research done by them might be made more nearly complete; because these people have been inventive, the emphasis is necessarily put on descriptions of other shock-tube designs.

Variants on Simple Shock Tubes

The fact that the Mach number in the flow behind the incident wave is low, even when the wave speed is very high, has prompted investigators to employ simple expansion nozzles to cool the air adiabatically as well as increase its speed. Both of these effects are desirable, but the already short test times, a few milliseconds at best, are further eroded by starting and stopping transients. As the shock and its following gas sample starts into the expanding tube, the expansion and compression waves necessary to make the air adjust to the new flow geometry develop. Until the flow has become steady, test results are of doubtful value.

The net effect of this loss of testing time has been greatly reduced by introduction of the reflected-shock hypersonic-nozzle configuration in wide use today (see Fig. 4).

In this facility full advantage may be taken of the fact that upon reflection of the initial wave from the shock-tube end wall (the convergent part of the nozzle), the hot gas is brought to rest and heated further. This gas in the stagnation chamber advances slowly towards the nozzle and is used at less than one-tenth of the rate it would be used were there no constriction. The small nozzle throat also makes feasible the construction of moderate-sized hypersonic nozzles having very large expansion ratios

(greater than 1000) to accelerate the flow to high speed and low static temperatures (hence high Mach number).

The thermodynamic state in the test region is somewhat less perfectly understood than that in the stagnation chamber because of possible non-isentropic flow through the nozzle. This disadvantage is offset by the great gain in steady flow duration. The testing done in these reflected-shock-tube hypersonic tunnels may be made more representative of real flight because the Mach number, and hence inviscid flow phenomena, may be more adequately imitated than in the simple, straight tube. The importance of this simulation has been demonstrated in references 8 and 9, where it was shown that the strong bow wave of a blunt-nosed slender body, such as that shown in Figure 5, may seriously impair the stabilization afforded by flares and fins. This effect arises from severe changes in static and dynamic pressure distributions; the correspondence between pressure and heat load shown by Lees leads one to expect similar complications here. It is safe to say that if we are to simulate the heat-load distribution, we must simulate pressure distribution. The utility of the reflected-shock, hypersonic tunnel is well recognized for this reason.

A new entry to the field is the so-called expansion tube.[10] In this device the steady expansion through the nozzle of the shock-tube wind tunnel is replaced by an unsteady expansion into a nearly completely evacuated tube. The stream velocity capability is approximately double that of the nozzle-type facility. The steady flow duration just ahead of the unsteady expansion, on the other hand, is far shorter. Since the exploitation of this concept is just starting, it is difficult to predict its success. It is anticipated that simple extensions of shock-tube technology will make it very useful.

Ballistic Facilities

The course of imitation taken in shock-tube testing, that is providing a fast-moving hot or cold airstream, is a natural extension of older conventional wind-tunnel technology. A completely different approach has arisen from recent evolution of ballistic-range techniques. Development of guns capable of firing test bodies at speeds up to 10 km/sec provides us with the opportunity of observing actual flying bodies in the laboratory. By suitable adjustment in test parameters it is possible to simulate in varying degree most of the important governing phenomena. These hypervelocity projectors are called light-gas guns because they commonly use hot compressed hydrogen as a propellant. Differences in detail inevitably exist, but the schematic in Figure 6 shows the essentials of the best guns.

A small charge of gun powder is used to propel a heavy piston through the pump tube, thereby compressing the hydrogen it contained to peak pressures estimated to exceed 20,000 atm. As the pressure rises past about 1,000 atm, a thick steel diaphragm separating the pump tube from the launch tube ruptures and opens in four petals; and the hydrogen propels the model at accelerations exceeding a million g's to velocities exceeding 10 km/sec. The piston is arrested in the conical transition between the two tubes. These guns can launch well-designed models of remarkable complexity without damage, as will be discussed later.

The principal uses in defining the convective-heating environment expected in hypervelocity flight have been by detection of the onset of ablation of metal models as a measure of local maximum total heating rate, by calorimeter measurements of the total heat transferred to models which do and do not ablate, and by measurement of the surface-temperature histories

of the models with on-board thermocouple circuits.

These techniques have been described in references 11 and 12 but will be outlined herein for completeness. In the first method the many shadowgraph pictures taken of the model during its flight are studied to determine the time at which melting of the surface first commenced (see Fig. 7). This melting permits material to flow into the wake, where it can cast a shadow in the pictures. The analysis of the data consists of finding the theoretical prediction of heating rate which predicts the observed phenomena. This method has been checked directly against heat-transfer measurements in shock tubes and other facilities and found to be reliable. Subsequently, tests have been performed at flight speeds above 11 km/sec (Fig. 2).

At launch speeds below about 6 km/sec the small models used in these studies do not begin to melt, but simply absorb the heat. The second method method of measurement uses a calorimeter, into which the model drops, to measure this heat input. The apparatus used is shown in Figures 8 and 9. The model, after leaving the light-gas gun, flies along the ballistic range until it decelerates to low speed and is caught in the laminated paper-model catcher. It then drops into a calorimeter, where the heat increment is measured. By combining measurements made at a variety of muzzle velocities the variation of total heating with speed is deduced.

The third method of convective-heat-transfer measurement is the use of telemetered signals from the model to antennae along the flight path. Active FM telemetry has been developed for this work, but has not been usable in the speed range of interest because the acceleration loads are too great. A passive system has been developed using the principles

indicated in Figures 10 and 11. In this case a model containing a complete thermocouple circuit, including a four-turn coil, is fired at high speed. The surface junction is heated and the resulting emf produces a magnetic field. This dipole field, passing through the pickup coils, produces signals which can be analyzed to determine the temperature history of the surface and hence heating rate. This technique has been used to measure stagnation-point and afterbody-heating rates on blunt bodies at speeds up to 5.6 km/sec.

RADIATIVE HEATING

As mentioned earlier, the heating environment also includes radiative transport of energy from the hot shock layer to the surface. Since the consequences of radiation are proportionately more severe than convection, in terms of material removal from the heat shield, it is necessary that we measure this source fairly well for high-speed flight. The radiation is a consequence of excitation of internal degree of freedom of the gas molecules and atoms; if de-excitation occurs spontaneously, rather than by virtue of collisions with other particles, radiation is emitted. At high speeds this radiation becomes an important, perhaps, dominant, heat load on large bodies.

The emission and absorption spectra of thermally excited gases have been studied intensively in recent years. Several papers specializing in thermal radiation from air[13, 14, 15] agree acceptably in the speed range where radiative heating is small. These same discrepancies become unacceptable when considering flight at 15 km/sec. Figure 12 summarizes results from some of the experimental and theoretical work based on

shock-tube and ballistic tests. A simple application of these data to flight of a bluff body, 1 meter in radius, at 10 km/sec at 60 km altitude, shows an expected radiative heat load of about 200 watts/sq cm. This is probably not too serious, but the precipitous increases with increasing speed impels us to pin down the answers more precisely. The chief experimental tools for this work are shock tubes and ballistic ranges. This is not to say that no other facility can supply a hot-gas sample for study; the chief justification advanced here is that the thermodynamic state of the gas in these two types of test is quite precisely known and relatable to full-scale flight; since the mode of heat addition to the gas is identical to that in flight, we have even more confidence. For these tests the shock tube was historically first and in some aspects the more versatile facility.

Returning to the shock tube, Figure 13, we see that, as the incident wave passes through the test section, it usually duplicates the normal shock ahead of a hypervelocity blunt body. The absolute spectral emission from the gas behind the wave front can be determined from groups of radiometers placed to look through the test volume. It has been found possible to survey with sufficient spatial resolution to unravel some of the chemical changes within the reaction zone behind the wave front. As these net reactions cease, on reaching equilibrium, the radiometer measurements yield the type of data on which Figure 12 is based. The reaction zone itself has attracted much interest as well because the higher-than-equilibrium temperatures result in radiation in excess of that which would have been emitted had equilibrium been achieved instantaneously.

The chief advantages of the shock tube lie in the near-perfect duplication of the essentially one-dimensional flow along the stagnation

streamline near the shock. Only at very low air densities do the tube walls interfere directly with the flow near the middle of the tube. On the other hand, all measurements of radiation are distorted by emission and absorption in the turbulent, nonuniform contaminated shock-tube boundary layer. It has proven very difficult to keep contamination at acceptable levels in many studies.

Much of the fundamental research on absolute emissive power of particular radiating species and the reaction rates in the flow just behind wave fronts has been done with shock tubes. Recently precise techniques have been devised for these studies in ballistic ranges. Radiation from complete three-dimensional flow fields is also measurable in these tests.

Essentially the hypervelocity ballistic test gives us a small object of known shape flying at known speed through a gas of selected properties. Within quite broad limits it is possible to simulate the physical, chemical, and thermodynamic properties of flows about full-scale vehicles.[16] The thermal radiation from these flows has been studied for several years at Ames Research Center. In these studies the absolute spectral emitted power is measured with radiometers mounted near the flight path of the model. The bandpasses of these devices are made narrow enough to make meaningful engineering measurements of heating rates but too wide to identify radiating species. An example of such data for flight at ballistic-missile speeds, taken from reference 17, is shown in Figure 14. The general verification of the predictions at short wavelengths is clear; the dependence of the infrared on model material is seen to be strong. This latter point is a whole field of study in itself and beyond the scope of this paper. The implications in the fields of radiative transport may be seen.

These measurements were made with assorted photomultiplier-filter combinations and are used to deduce the radiation per unit volume at the gas-cap stagnation conditions. These figures may then be applied point by point within the calculated shock layers of the full-scale body to estimate complete radiative heat loads.

Recently, as implied above, Reis has used the hot-stagnation-region gas on ballistic models as a radiation source and unusual measuring techniques to obtain the absolute band-system strengths of several molecular species.[18] The spectral resolution is sufficient in these tests to make accurate independent measurements of the transition probabilities, one of the fundamental properties necessary for rigorous prediction of absolute spectral emissive power at conditions different from those of the particular test.

It has proven to be possible to calculate theoretically the spectral distribution of relative intensity of remarkably complex band systems of molecular radiators. Recourse must be had to experiment if the absolute strengths are to be known. In practice the factor necessary to achieve agreement between theory and experiment is found. This factor may take the form of a transition probability or f-number.

The required spectra were obtained photoelectrically by means of a time-of-flight scanning spectrometer. This device is shown schematically in Figure 15. As the model flies by in the focal plane of the collecting mirror, the luminous gas cap acts as a moving entrance slit, sweeping out the spectrum of the shock-heated gas on the exit slit. (That the gas cap is the only source of radiation in the flow field and is indeed slit-like in form is shown in a typical image-converter photograph of a plastic model, Fig. 16.) The energy passing through the exit slit of the scanning

spectrometer is divided; 95 percent passes through a splitter plate and on to the cathode of an RCA 1P28 multiplier phototube. The output of this multiplier phototube is recorded on an oscilloscope and yields a continuously recorded spectrum over a wavelength range dictated mainly by the geometry of the system. For the tests reported in reference 18, the wavelength range was as a rule from 0.290 to 0.430μ. Figure 17 shows a typical oscillogram. The remaining 5 percent of the energy passes through a narrow-band interference filter (100 Å wide between the 50-percent response points) and onto a Dumont 6935 multiplier phototube. The output of this phototube is displayed on an oscilloscope which has been triggered so as to start sweeping simulataneously with the oscilloscope which records the spectrum. The auxiliary oscillogram thus allows a specific wavelength to be transposed to the oscillogram displaying the spectrum. Such wavelength transposition was found to be repeatable from shot to shot to $\pm$10 Å.

The time-of-flight scanning spectrometer was constructed by modifying a Farrand uv-vis f/3.5 grating monochromator. A large opening was cut in the monochromator housing in the region of the intended entrance slit and the standard collecting mirror was replaced by a spherical mirror which focused at the center of the test chamber. Further, the new collecting mirror was masked down to a rectangular slot to improve depth of field and to insure uniform illumination of the grating. The rise time of the complete system was 25 nanoseconds and was dictated by the oscilloscope.

Another instrument was devised in order to measure the spatial distribution of radiation over the faces of bluff models. These measurements were needed in order to substantiate calculations used in analyzing the above test results and also to describe more completely the real distribution.

The instrument in point required that a near head-on view of the model be imaged on a plate having tiny orifices opening onto a phototube (Fig. 18). The system effectively registers any light radiated from area sources along the optical axis. As the model flies by the optical axis, a scan of the shock layer occurs. Auxiliary equipment is used to determine where on the model the scan occurred. In this manner the actual distribution of radiative heat load can be measured. More recently head-on photographs (Fig. 19) have been taken successfully using image-converter and Kerr-cell-shutter cameras.

These photographs have been analyzed, using step-wedge filters for film calibration and microdensitometers for exposure measurements, to yield similar heat-load distributions. The agreement between the two systems is good. The advantage of the dissector is that it involves fewer experimental steps; the advantage of the photographic system is that is permits complete determination of the distribution rather than a few scans.

VELOCITY AUGMENTATION

Since tests at speeds above 7 or 8 km/sec are difficult in purely ballistic facilities, we have superposed a countercurrent airstream which can move as fast as 5 km/sec. This airstream is in a reflected-shock, hypersonic-wind-tunnel test section and the models are fired upstream (Fig. 20). Some data have been obtained in this manner at flight speeds above 13 km/sec.[19] The most reliable of these data, where the flow fields were known to be in equilibrium, extend above 12 km/sec (Fig. 12).

The chief advantages of this test facility lie in excellent simulation

of velocity, Mach number, Reynolds number, complete flow configuration, and degree of equilibration of all binary-scaled chemical and physical changes.

In still-air tests, it has proven possible to reduce contamination to negligible levels; also no stream boundary layer is present to distort the results. In air-on tests it appears simple to reduce contamination to acceptable levels. The drawbacks are that data extraction is not simple; much effort is required to advance the instruments and test techniques. The duration of observations is typically about a microsecond and the attitude and condition of the model must be accurately registered because it cannot be predicted. The thermodynamic simulation of the flow along streamlines can be quite nicely duplicated, but it has as yet been impractical to study individual stream tubes as has effectively been done in shock-tube flows.

CONCLUDING REMARKS

The use of shock tubes, ballistic ranges, and combinations thereof in simulation of convective and radiative heat loads has been described. The complementary nature and the highly independent techniques used in these facilities lend great strength to the research results where they agree. The shortcomings of these facilities are such that, if possible, both should be applied to important problems. When all-out performance is required, the combination of the two can clearly provide advantages. That these advantages are becoming more widely recognized is demonstrated by the construction of new facilities at Arnold Engineering Development

Center and Boeing Company, Seattle, similar to those in service at Ames Research Center since the late 1950's.

REFERENCES

1. Brooks' paper presented at same conference.

2. Lees, L.: Laminar Heat Transfer Over Blunt-Nosed Bodies at Hypersonic Flight Speeds. Jet Propulsion, vol. 26, no. 4, April 1956, pp. 259-269, 274.

3. Fay, J. A., and Riddell, F. R.: Theory of Stagnation Point Heat Transfer in Dissociated Air. Jour. Aero. Sci., vol. 25, no. 2, Feb. 1958, pp. 73-85, 121.

4. Hansen, C. Frederick: Approximations for the Thermodynamic and Transport Properties of High-Temperature Air. NASA TR R-50, 1959.

5. Rose, P. H., and Stark, W. I.: Stagnation Point Heat-Transfer Measurements in Dissociated Air. Jour. Aero. Sci., vol 25, no. 2, Feb. 1958, pp. 86-97.

6. Hoshizaki, H.: Heat Transfer in Planetary Atmospheres at Super-Satellite Speeds. ARS Journal, vol. 32, no. 10, Oct. 1962, pp. 1544-51.

7. Warren, W. R., Rogers, D. A., and Harris, C. J.: The Development of and Electrically Heated, Shock Driven Test Facility. Second Symposium on Hypervelocity Techniques, Denver, 1962.

8. Seiff, Alvin: Secondary Flow Fields Embedded in Hypersonic Shock Layers. NASA TN D-1304, 1962.

9. Terry, James E., and James, Carlton S.: A Parametric Study of Hypersonic Flow Fields About Blunt-Nosed Cylinders at Zero Angle of Attack. NASA TN D-2342, 1964.

10. Trimpi, R. L.: A Preliminary Theoretical Study of the Expansion Tube, A New Device for Producing High Enthalpy Short-Duration Hypersonic Gas Flows. NASA TR R-133, 1962.

11. Compton, Dale L., and Chapman, Gary T.: Two New Free-Flight Methods for Obtaining Convective-Heat-Transfer Data. Paper for AIAA Aerodynamic Testing Conference, March 9-10, 1964.

12. Yee, Layton, Bailey, Harry E., and Woodward, Henry T.: Ballistic Range Measurements of Stagnation-Point Heat Transfer in Air and in Carbon Dioxide at Velocities up to 18,000 Feet Per Second. NASA TN D-777, 1961.

13. Meyerott, R. E., Sokoloff, J., and Nicholls, R. W.: Absorption Coefficients of Air. LMSD 288052, Lockheed Aircraft Corp., 1959.

14. Kivel, B., and Bailey, K.: Tables of Radiation From High Temperature Air. Res. Rep. 21, AVCO-Everett Research Lab., 1957.

15. Breene, R. G., Nardone, Maria, Riethof, T. R., and Zeldin, Saydean: Radiance of Species in High Temperature Air. General Electric Space Sciences Lab., July 1962.

16. Gibson, W. E., and Marrone, P. V.: Nonequilibrium Scaling Criterion for Inviscid Hypersonic Airflows. QM-1626-A-8, Cornell Aero. Lab., 1962.

17. Page, William A., and Arnold, James O.: Shock-Layer Radiation of Blunt Bodies at Reentry Velocities. NASA TR R-193, 1964.

18. Reis, Victor H.: Oscillator Strength for the N_2 Second Positive and N_2^+ First Negative Systems From Observations of Shock Layers About Hypersonic Projectiles. Jour. of Quant. Spectrosc. and Radiat. Transfer, vol. 4, no. 6, 1964, p. 783.

19. Canning, Thomas N., and Page, William A.: Measurements of Radiation From the Flow Fields of Bodies Flying at Speeds Up to 13.4 Kilometers Per Second. Presented at the AGARD meeting, Brussels, Belgium, April 1962.

Figure 1. Theoretical laminar convective heating at stagnation point of hypervelocity spheres.

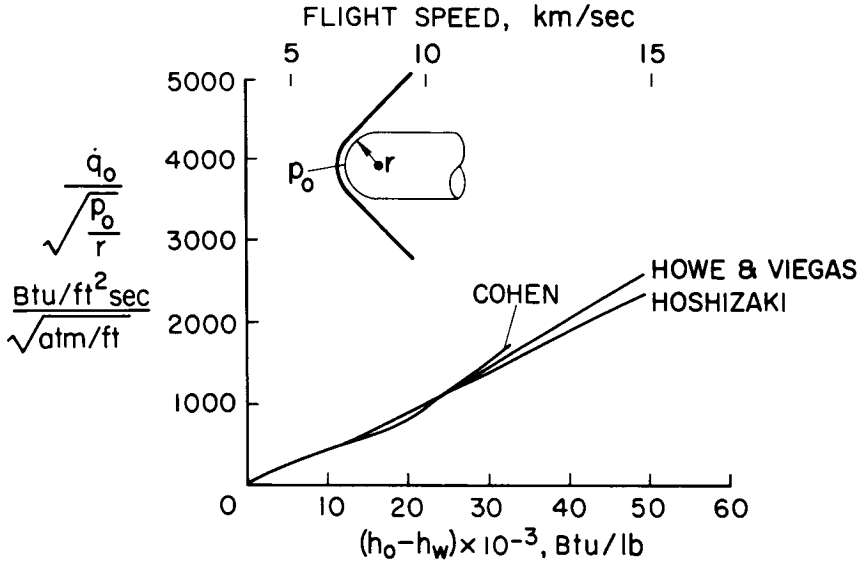

Figure 2. Experimental laminar convective heating at stagnation point of hypervelocity spheres.

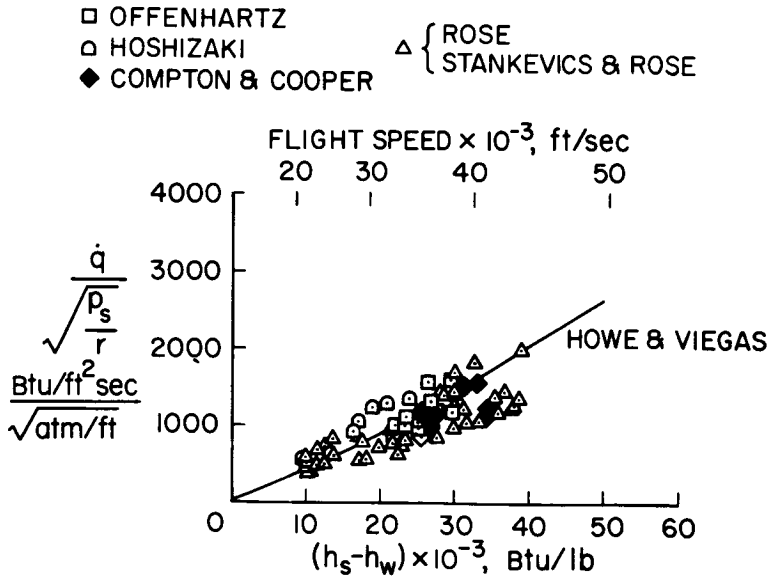

Figure 3. Simple shock tube.

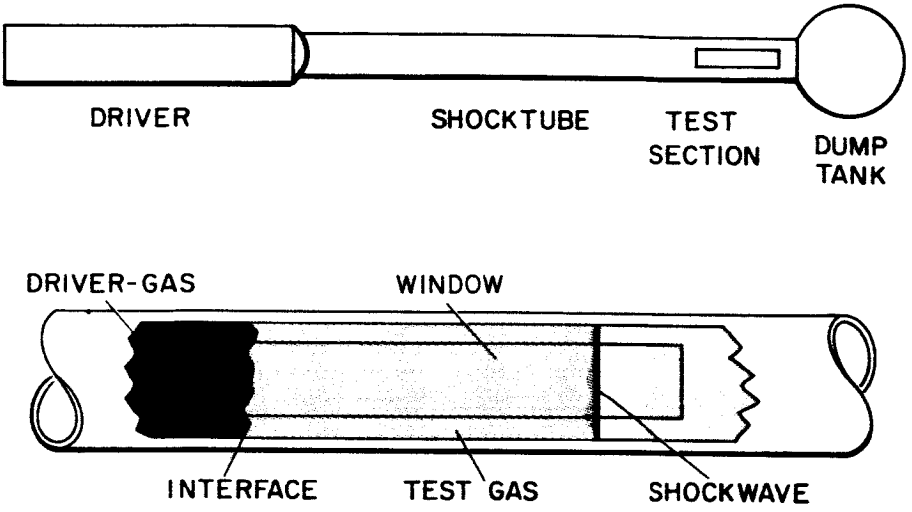

Figure 4. Popular modifications of simple shock tube.

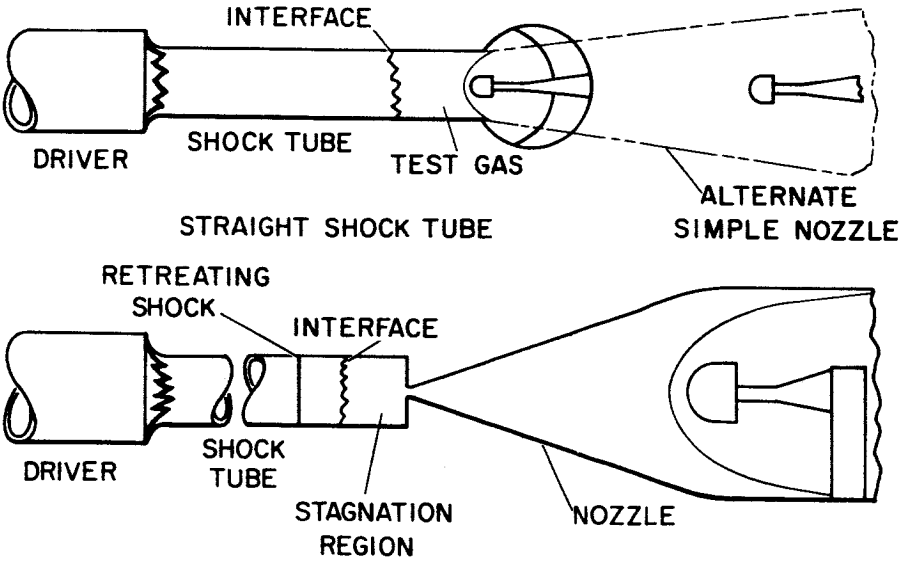

Figure 5. Shadowgraph of blunt-nosed cylinder showing embedded supersonic flow in hypersonic flow field.

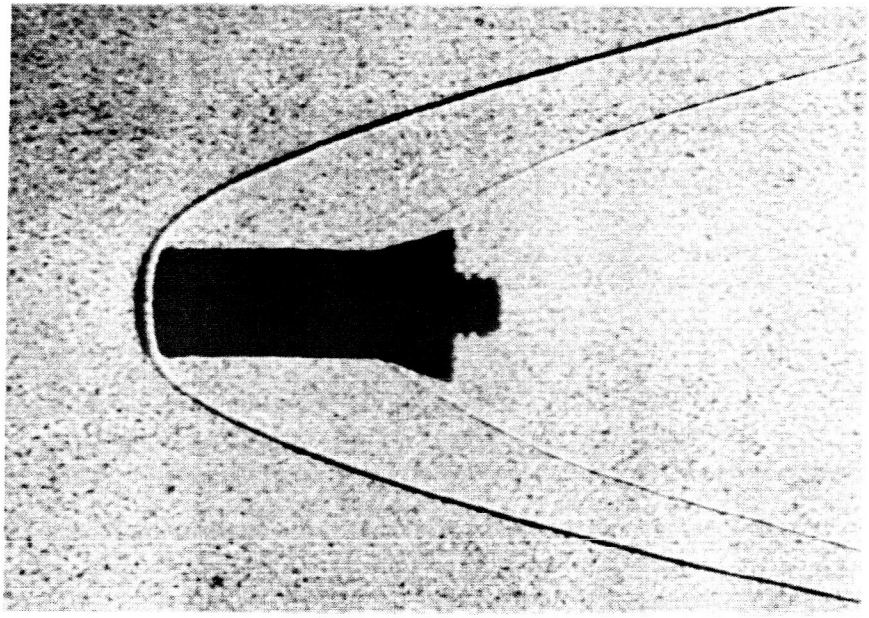

Figure 6. Deformable piston light-gas gun.

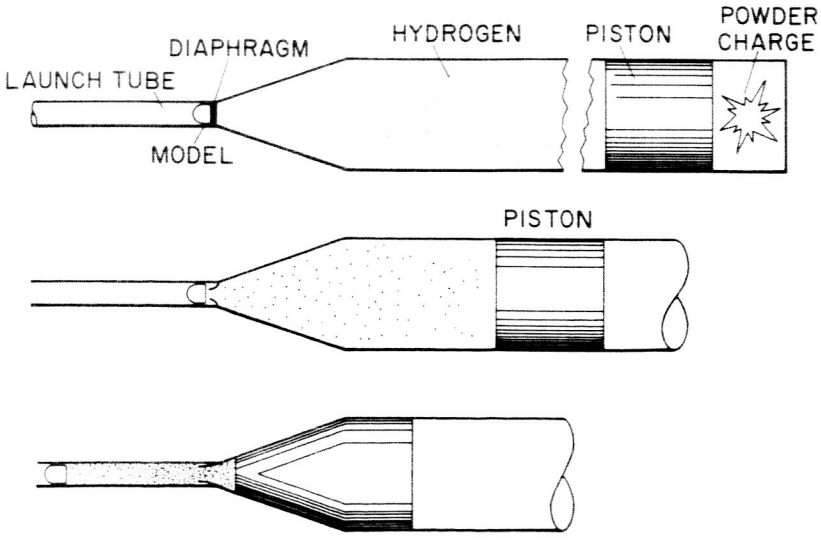

Figure 7. Shadowgraph sequence showing onset of ablation.

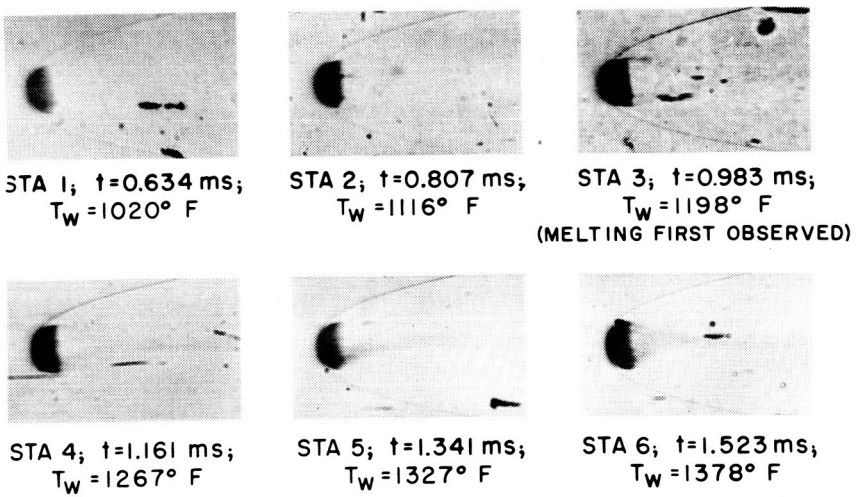

Figure 8. Ballistic range arrangement for calorimetry flights.

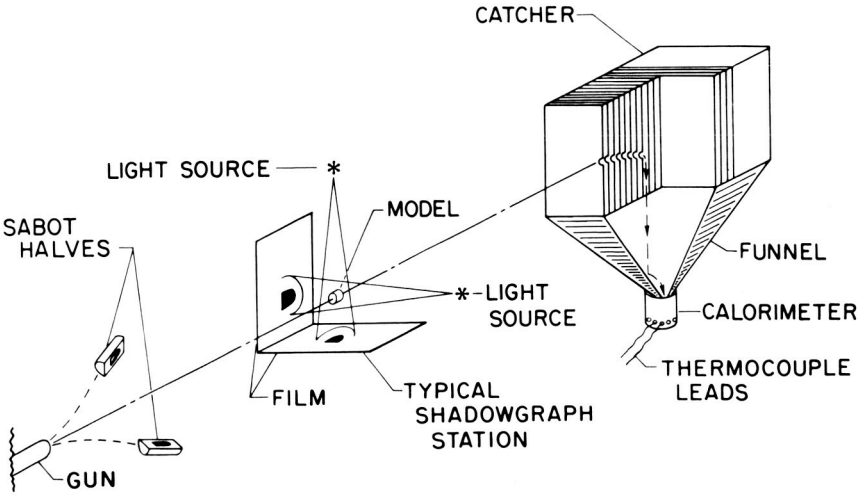

Figure 9. Calorimeter section.

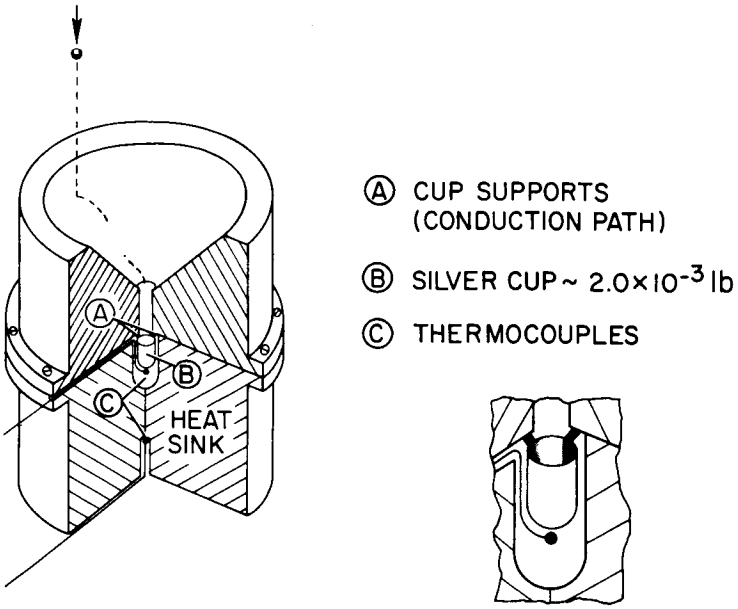

Figure 10. Thermocouple model for stagnation-point heating tests.

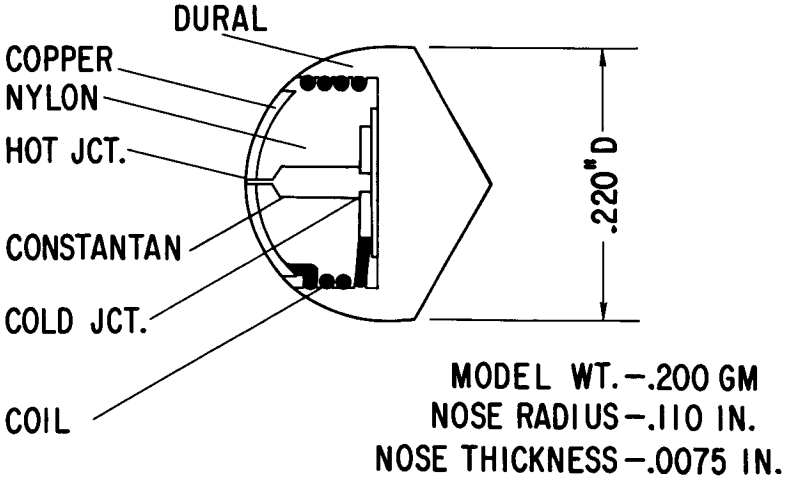

Figure 11. Ballistic range arrangement and antenna for thermocouple model flights.

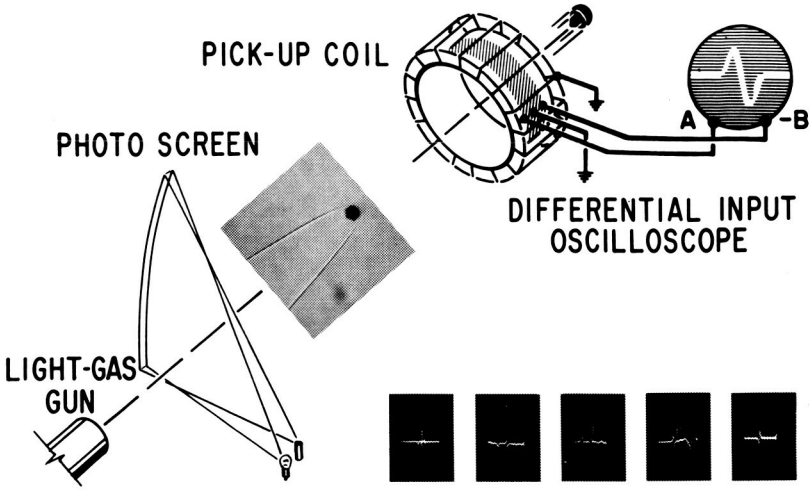

Figure 12. Variation with velocity of emissive power of air behind normal shock waves.

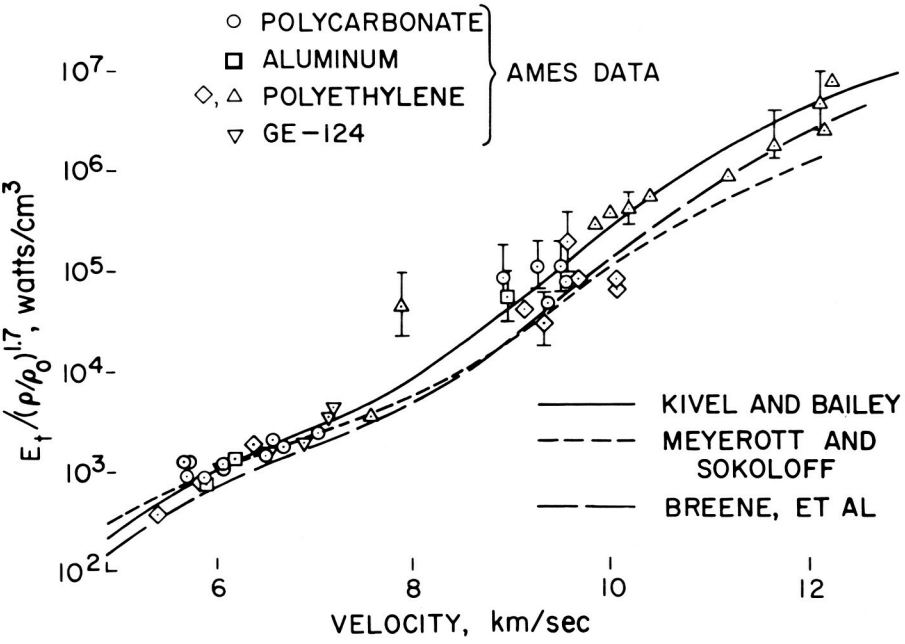

Figure 13. Nonequilibrium zone air radiation.

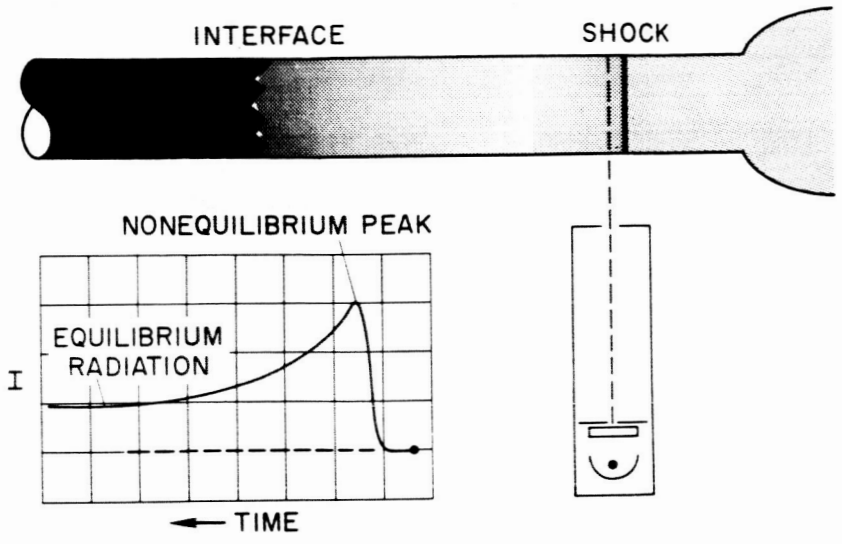

Figure 14. Absolute spectral emission from complete flow fields of bodies made of several materials.

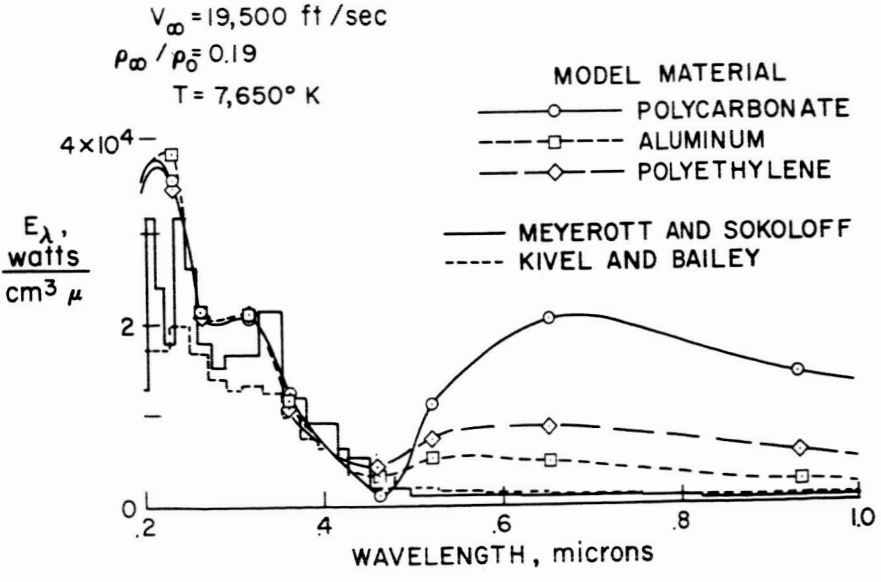

Figure 15. Time-of-flight scanning spectrometer.

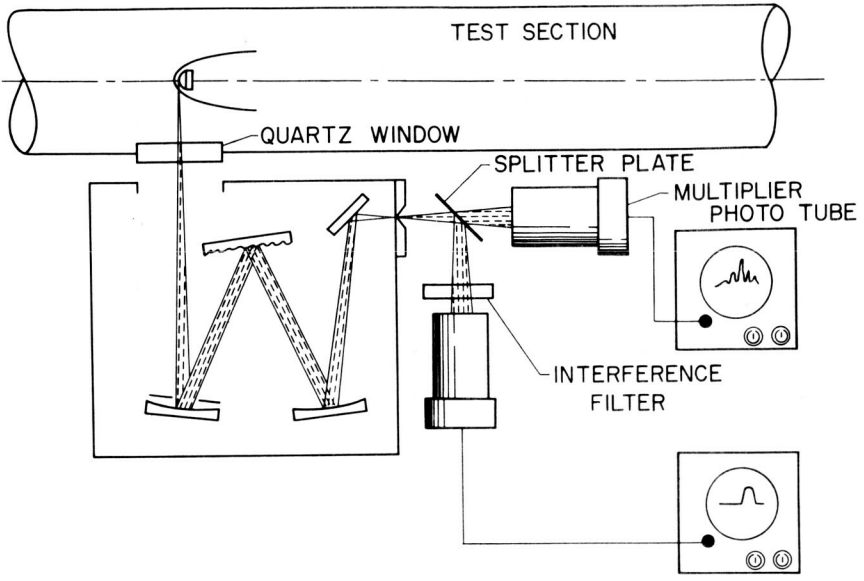

Figure 16. Image-converter photograph of polyformaldehyde model in flight at 5.5 km/sec; p_∞ = 60 mm Hg.

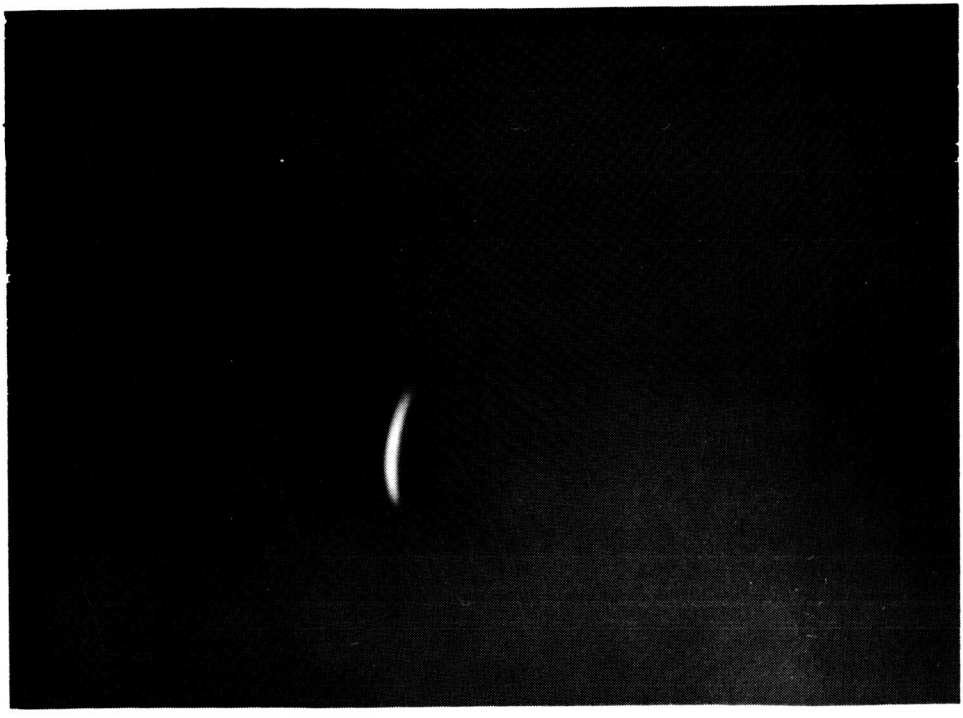

Figure 17. Oscillogram of near ultraviolet spectrum from time-of-flight scanning spectrometer.

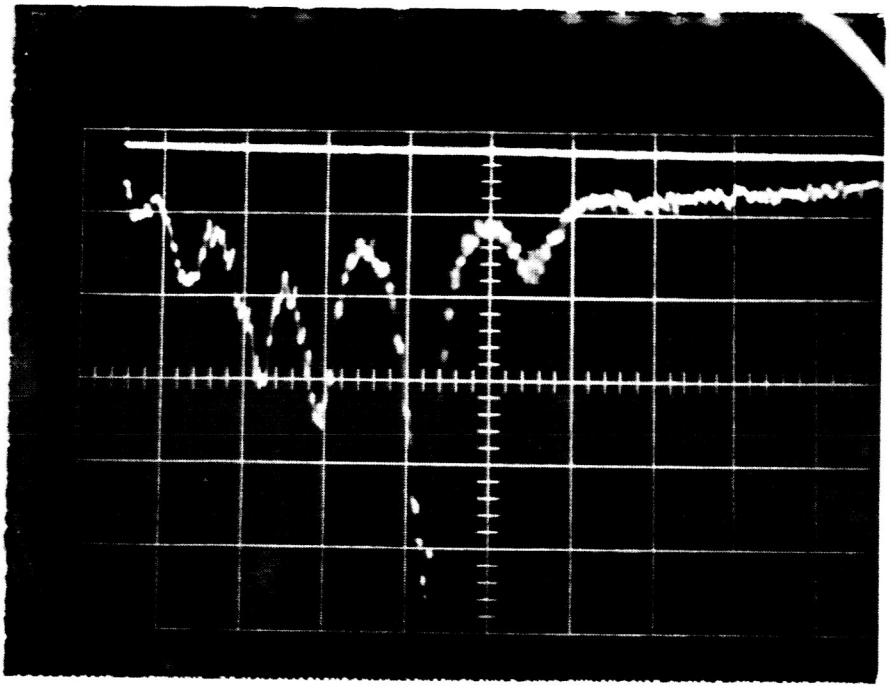

Figure 18. Image dissector scheme.

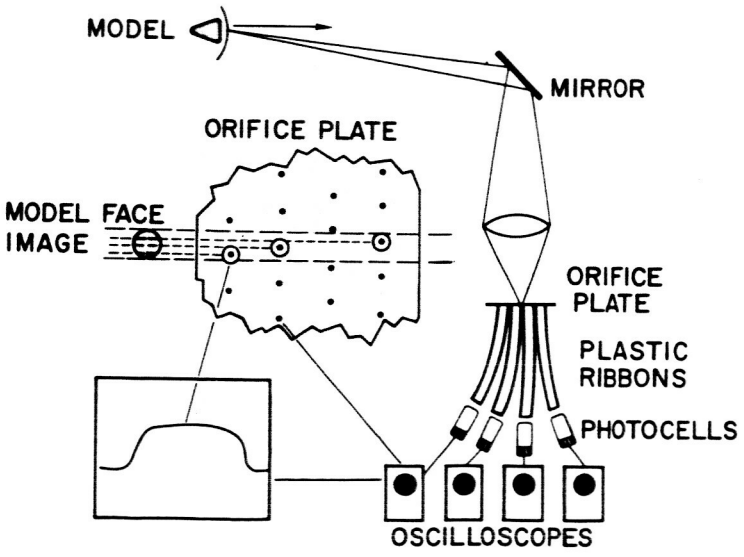

Figure 19. "Head-on" photograph of polycarbonate model flying through air at 6 km/sec; p_∞ = 60 mm Hg.

Figure 20. Schematic of counterflow facility.

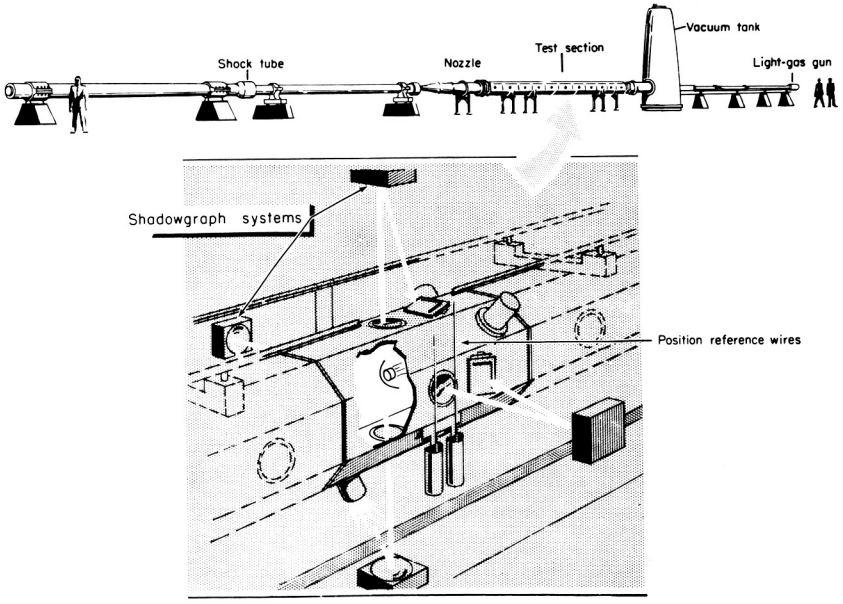

EVALUATION OF MATERIALS IN ENTRY HEATING SIMULATION

by

William A. Brooks, Jr.

NASA - Langley Research Center

INTRODUCTION

The basic objective in designing thermal protection systems is the provision of sufficient material to protect the vehicle structure and cargo from the severe heating encountered during entry into a planetary atmosphere. Conservative designs that may compromise the mission objective should be avoided. Ideally just enough material to ensure successful entry should be provided. The degree of success that is achieved by adhering to this philosophy is entirely dependent upon our knowledge of the entry environment and the manner in which the various materials respond to the environment.

The importance of avoiding excessive heat shield weight can be underscored by reference to figure 1 (ref. 1). Of course, the basic problem of reentry is the dissipation of a vehicle's energy in a controlled and acceptable fashion. This figure was prepared to qualitatively demonstrate the influence of thermal protection weight upon the useful payload capability.

The ordinate is energy in Btu/lb and the abscissa is velocity, covering the range of concern for manned vehicles and planetary probes. The solid line is the kinetic energy per pound of vehicle which must be

dissipated at each velocity. Fortunately, most of the energy is absorbed by the atmosphere which envelops the entering vehicle. At most, only a few percent of the kinetic energy is transferred to the vehicle in the form of heat. The lower cross-hatched band represents the total heat load per pound of vehicle. The lower edge of the band corresponds to less than 1 percent and is typical of the heat load for a ballistic reentry. The upper edge is about 3 percent of the kinetic energy which is typical for lifting entry vehicles. At the higher velocities, radiative heat transfer from the hot gas cap becomes significant and increases with velocity, resulting in large increases in heat load. The cross-hatched horizontal band represents the energy absorbing capability of thermal protection materials and ranges from 2,000 to 20,000 Btu/lb.

Now if the vehicle heat load is equal to the heat shield energy absorbing capability, that is, the two bands coincide, then the vehicle must be constructed entirely of thermal protection material in order to survive the heating. Therefore, the difference between the two bands indicates the amount of vehicle weight which can be devoted to functions other than thermal protection. As velocity increases, the useful payload capability becomes smaller, and the matter of excessive heat shield weight becomes more critical.

REQUIREMENTS FOR DUPLICATING THE ENTRY ENVIRONMENT

If it were possible to duplicate the reentry environment in ground facilities, the manner in which thermal protection materials respond could be more precisely determined and better heat shield designs would result. However this is not generally the case and usually one must resort to a partial simulation.

Figure 2 shows the flight regions of immediate concern in an altitude-velocity plane (ref. 2). Regions are shown for Apollo, ICBM's, Mercury, and Dynasoar. A slight broadening of the Dynasoar band will result in a region which is typical of hypersonic gliders. Future planetary exploration vehicles will result in a region whose lower bound may be as much as 50,000 feet below the Apollo region near escape velocity, extending off-scale to the right.

Figures 3, 4, and 5 show some of the wind-tunnel characteristics that would be required to produce exact flow duplication (ref. 2). First consider the chamber pressure required (fig. 3). Pressure curves have been superposed on the flight regions shown in figure 2. The technology of building pressure vessels of the size required by a wind tunnel and pumps probably provides a pressure limitation somewhere between 10^4 and 10^5 psi. In any event, the limitation is remotely removed from the point of maximum heating for Apollo which is about 32,000 fps.

Figure 4 shows the mass flow rate that would be required per square foot of test section. It can be seen that the required flow rate is not a strong function of entry velocity but is influenced by the simulated altitude. The small and moderate flow rate curves pass through the Apollo region. However, a very substantial flow rate is required for the ICBM region.

Figure 5 shows the heat energy required per square foot of test section to provide a duplication of enthalpy. It is to be noted that this is the energy in the air and that the energy supply must be 2 to 3 times as great because of the losses incurred during transfer to the air. At the higher altitudes where small and moderate mass flow rates are adequate, the energy requirment can be met without difficulty. However at the lower altitudes which require large mass flow rates, the power requirement is prohibitive.

At the NASA Langley Research Center with the existing power distribution system, it is possible to draw a maximum of 100 megawatts. Assuming about 50 percent efficiency, a device with 1 square foot of test section could be powered at an energy level that would approximately coincide with the lower bound of the Apollo region.

Exact duplication of the stagnation flow condition is out of the question, mainly because of the pressure requirements.

FACILITIES FOR SIMULATING CONVECTIVE HEATING

The type of facility most commonly used to evaluate thermal protection materials is that which utilizes an electric arc for adding energy to the gas stream. Figure 6 shows the capabilities of arc facilities presently being used. In this figure, the limitations of present facilities have been plotted in terms of arc chamber pressure and enthalpy, the two most important parameters in an arc-heated wind tunnel (ref. 3).

One of the principal factors that limits the capabilities of present facilities is the energy losses which result from thermal radiation from hot, high-pressure gases to the walls of the arc chamber. This problem area has not yet been well researched. Perhaps a more fundamental difficulty is the inability to sustain an arc in a moving gas stream at high pressures.

Another problem area results from the cooling requirements for the nozzles. The dashed line is an estimate of a practical limitation and approximately corresponds to nozzle heating of 10,000 Btu/ft^2-sec.

The stringent requirements of exact duplication of high-velocity entry is indicated for the altitude range of 100,000 to 300,000 feet and quite obviously will not be achieved with present techniques. If one is willing

to relax the Mach number requirement and settle for a partial simulation, the indicated shaded area results. Even this partial simulation of a low-altitude flight cannot presently be achieved for high-entry-velocity situations.

This point can be made more directly by superposing the exact and partial simulation capabilities of present facilities on the flight regions as shown by figure 7. Our attempts to simulate all the quantities of interest cover only a small portion of the flight regions.

As yet no mention has been made of size and it is pertinent to point out that certain of the entry effects such as heating rate, aerodynamic shear, etc., are dependent on the size and geometry of the specimen. Further complications result because the mass flow characteristic of presently available facilities greatly limits the size of the specimens.

So one is confronted with partial simulation of a few of the entry heating parameters in a given test, a scaled-down specimen, but generally with full-scale heat shield materials. It is not possible to model with a different material because of the dissimilarity of material response in a given environment. The heat shield material thickness is generally not scaled because a given heating environment requires a given thickness regardless of the specimen size.

The usual technique is to conduct a series of tests in each of which a few parameters are simulated. Then analysis or other test results are employed to indicate the degree that the interaction between the parameters influences material response.

Figure 8 shows the test stream configurations commonly employed for materials testing with arc air heaters (ref. 4). Free jets, which exit to the atmosphere, are used in both subsonic and supersonic arrangements. The pressure at the model is atmospheric pressure or greater. The splash

technique is the simplest and one of the more commonly used techniques. The heated stream and the specimen are sized so that the stream impinges on the specimen rather than enveloping it. This condition affords a simulation of stagnation-point heating conditions. Some attention must be devoted to preventing heat flow into the sides of the specimen if stagnation-point heating is to be realistically simulated. The splash technique is utilized in material screening and evaluation programs and in instrumentation studies.

The arc tunnel arrangement is utilized for the consideration of locations other than the stagnation point. The stream is expanded and discharged into an evacuated plenum chamber. Expansion of the stream results in the capability of enveloping rather large specimens with a hot gas stream. The pressure at the specimen can be less than atmospheric, thus simulating high altitudes.

The technique of shrouding the test model is utilized to produce subsonic flow ahead of the model. With a given mass flow, more of the hot gases can be brought into contact with the specimen. The result is that for a given flow situation larger specimens can be tested. This technique is employed to study the effects of pressure gradients and other phenomena associated with two-and three-dimensional stagnation areas.

The pipe flow technique consists of utilizing the test specimen in the form of a simple or internally contoured pipe through which the gas stream flows. This method of testing materials has been used to determine the effects of flow on the test material. The shape of the pipe and the flow parameters can be selected so that turbulent flow results. Thus the interaction between an ablation material and turbulent flow can be investigated.

FACILITIES FOR SIMULATING COMBINED RADIATIVE AND CONVECTIVE HEATING

Up until the present time, entry velocities have generally been sufficiently low that entry heating has been essentially a convection process. For entry near earth satellite speed, the radiative component is negligible - except for the ICBM's which plunge deep into the atmosphere. As the entry velocities become greater, the air in the bow shock layer becomes excited to the point where it becomes a powerful source of radiative heating. At escape velocity, radiative heat transfer is a significant part of the heating. For planetary exploration vehicles that reenter the earth's atmosphere at very high speeds - well above escape velocity - radiative heating can become the dominant mode.

At present, most of the experimental research on thermal protection materials is carried out in facilities that provide only convective heating. Arc image furnaces are used to provide radiative heating only. It is a generally accepted view that even in those cases where radiative heating is the dominant mode some convection at the heated surface is required for proper simulation. Only in a few instances have there been attempts to provide combined convective and radiative heating.

The next few figures show known existing devices for providing combined heat. Figure 11 shows a device used at Langley (ref. 5). A resistance heated graphite sleeve was placed in tandem with the output from an arc jet, providing radiative inputs to the specimen up to 200 Btu/ft^2-sec. This device is unsatisfactory because the jet stream consumes the graphite heater resulting in frequent replacement. In addition, because of the presence of large amounts of carbon in the stream, the chemistry at the surface of the

ablating specimen is not correct. Lastly, the radiative rates available are not high enough.

The Ames Research Center is using a device (ref. 6) which couples an arc image furnace to a small arc jet, producing the radiative rate shown in figure 12. The output from the carbon arc is refocused on the specimen by means of mirrors with the output being controlled by a shutter, screen, and filter arrangement. An advantage of this type of arrangement is that the radiative and convective heating are independently controlled. However, the radiative rate shown represents about the maximum that can be achieved with arc image furnaces.

Another device is shown in figure 13. This device is employed by the General Electric Company and is essentially a long constricted arc (ref. 7). The test gas is heated by the arc and expelled into the plenum chamber and through the nozzle. The model is positioned so that it receives radiative heating from the arc and the plenum chamber gases. The maximum radiative rate is obtained when the specimen completely blocks the flow and the bypass port is used to discharge the heated air. By selective positioning of the specimen and adjustment of the bypass port, various combinations of convective and radiative heating are obtained. The technique involves the use of the same arc to provide both radiative and convective heating. The disadvantages are the relatively low radiative rate and the coupled control of convective and radiative heating.

Figure 14 shows a device which reportedly affords a very high radiative heating rate. In this device the material specimen serves as the chamber that confines the arc which radiates directly to the test material. The radiative rates are calculated to be as shown. However, the only gases involved are those generated when the test material decomposes. These gases

exit around the electrodes as shown and reportedly produce a stagnation area type of flow at the center of the specimen. It is evident that the convective heating and the surface chemistry are not correct.

In another version of the technique of using the test material to confine the arc, the arc and test gases are passed through a cylinder of test material which confines the arc and the gas flow. The test material thus constitutes a portion of the constrictor.

There are shock tunnels both existing and proposed, modified in various ways, that produce good simulation of the high-speed thermal environment. However, testing is restricted to very small models and to test times measured in microseconds. Thus, although the shock tube facilities are extremely valuable in research on the physics and chemistry of air, they are of little value for testing materials. The one known exception is the Cornell Aeronautical Laboratory's Wave Superheater. The superheater which utilizes a sequential firing of many shock tubes provides good simulation up to about $M = 14$ with test times as great as 15 seconds.

RESPONSE OF ABLATIVE MATERIALS TO SIMULATED ENTRY ENVIRONMENTS

Research has shown that two of the important characteristics of a good heat shield material are the ability to sustain high surface temperatures so as to reject heat by reradiation and good insulative properties so as to delay heat penetration to the interior of the vehicle.

Charring Ablators

A class of materials which has been shown to have these characteristics

are the so-called charring ablators. Charring ablators function in a very complex manner. In addition to being related to each other, the basic processes and mechanisms which are brought into play are intimately related to the aero-thermal environment. Therefore the type of test simulation influences the material response.

Some of the details of a charring ablator are shown in figure 15 (from ref. 8). The charring composites, in general, consist of plastic resins - such as phenolic, epoxy, and silicone - filled with organic or inorganic materials in the form of powder, fibers, or cloth. On the left are typical layers which result during ablation. At the bottom is the structural substrate to which the virgin composite is bonded. Above the virgin material is the pyrolysis zone at which, due to the influence of heat, the virgin material decomposes into gases and a carbonaceous residue. As the decomposition proceeds, the carbonaceous layer, or char, reinforced by the filler materials builds up to an appreciable thickness. Finally, if glassy filler materials are used, a melt layer may exist.

On the right are some of the processes which take place during ablation. Pyrolysis takes place at the relatively low temperature. Thus the potential for heat conduction is not very large and if the diffusivity of the virgin material is sufficiently low the temperature response of the structure is slow. When pyrolysis takes place the degradation process serves as a heat sink. However the heat of degradation is generally small compared to the amount of heat that must be accommodated overall by the ablator. The pyrolysis gases percolate, or transpire, through the char picking up heat in the process. There is also a possibility that reactions may take place between the gases and the chars or between the various gaseous species. Within the char, conduction of heat toward the pyrolysis zone is partly

canceled by action of the transpiring gases. The gases are then injected into the boundary layer, thereby blocking convective heat transfer to the surface. As the char layer becomes thicker the surface temperature rises and a large amount of heat is rejected by reradiation to space. The char is then eroded by thermal, chemical, or mechanical means such as sublimation, oxidation, or removal by aerodynamic shear.

Basic equations governing the response of charring ablators are shown in figure 16. At the top, the surface energy balance, or boundary condition, is given. The convective heating is reduced by the hot wall correction and the blocking effect of the transpiring gases. Next is that portion of the radiative heating which is absorbed. For present materials, this is usually most of the radiative heating because the reflectivity of the charred surface is low. The next term is the heat input which results from the oxidation of the char. There might also be another term here which results when the pyrolysis gases undergo a homogeneous combustion reaction in the boundary layer. On the right side is the reradiative term which is very important for charring ablators, conduction into the interior of the heat shield, and a term to allow for the sublimation of the char which may take place if the temperature is sufficiently low. The effects of pressure and aerodynamic shear are not shown here - mainly because there is very little experimental evidence to indicate how these mechanisms must be treated. At present, they are usually treated with auxiliary equations which specify a maximum char thickness.

An energy balance on the degrading material produces the very general equation shown here. Except for the term which accounts for heat disposed of by convective transport, the equation is similar to the diffusion equation. This equation probably overly simplifies the mathematical formulation of the

problem as many auxiliary equations are required to account for all of the mechanisms.

Instrumentation of Ablators

One of the primary difficulties that is experienced with the experimental evaluation of charring ablators is that several effects take place simultaneously and what one sees when the test is completed is the combined, or overall, effect. During the course of the test, the receding char surface is usually obscured by the pyrolysis gases or the air stream and therefore motion pictures do not yield much quantitative information.

In the past, the principal type of instrumentation utilized in ablation tests has been thermocouples. However, even when thermocouples are used the utility of the data is limited and, in fact, sometimes erroneous. Figure 17 has been prepared to illustrate the latter point. There is shown a sectioned test specimen which was instrumented with complete disregard for the basic rules of thermometry. The thermocouples were positioned with the axes of the wire in the direction of the flow of heat. The thermocouples are much better conductors than the virgin plastic as is evidenced by the degradation of material along the wire. There can be not doubt that erroneous temperature readings were obtained in this test.

Figure 18 shows quantitatively the effect of thermocouple configuration. Configuration (1) consists of a grooved plug with a wire running down each side. The wire insulation is removed and replaced with ceramic tubing. At the end of the plug, the bare wires are joined at the center. Several diameters of the wires are perpendicular to the heat flow direction to minimize the conduct effects. Configuration (2) consists of a thermocouple potted

in a hole whose axis is parallel to the heat flow. In this case, the wire insulation is replaced with two-tube ceramic tubing. Configuration (3) is similar to configuration (2) with the exception that the resin-glass insulation is left on the thermocouple wire. The difference between the response of sensors (1) and (2) shows the effect of thermocouple configuration with the temperature difference being as much as 1500° F. The difference between the responses of sensors (2) and (3) results from the difference between the conductivities of the wire insulation and the ceramic tubing.

Even the use of correct thermocouple technique does not yield as much information on the performance of charring ablators as is desired. Among the items one would like to see recorded during a test are the surface recession and the char thickness. The Instrument Research Division at Langley has been studying instrumentation for ablators and has devised some rather promising sensors using simple techniques.

Figure 19 shows a make-wire gage. Make-wire gage techniques have been utilized before but with rather limited success. This version, which is intended to sense the interface between the virgin material and the char, shows considerable promise. Ten-mil platinum wires are positioned as shown in a split plug of the plastic material. Noble metal is used to prevent the formation of conductive oxides. It has been found essential to peen the ends of the wires to make good contact with the char. As the front of material degradation passes the ends of the wire the electrical conductivity of the material in contact with the ends increases and the circuit is completed through the char. Conditioning circuitry is used to provide a constant voltage step indicating the event.

A gage for sensing the surface recession is shown in figure 20. A

tungsten wire is attached to one leaf of a spring-loaded microswitch. The wire is threaded through a molybdenum tube and knotted in such a fashion that the switch is open. As the surface recedes toward the end of the sensor the temperature increases to the point where the tungsten melts and the switch is closed by the spring, giving a voltage indication of the event. Tungsten melts at about 4700° F so this is actually a temperature indicator. However, the temperature gradients are very steep near the surface and therefore the 4700° F isotherm corresponds very closely to the surface location. In principle, one would make the wire refractory enough to ensure the surface being reached but of small enough mass so that it would melt immediately upon exposure at the surface.

Another type of surface sensor is shown by figure 21. This is a light pipe sensor which consists of a sappire light pipe, an infrared filter, and a photo-resistive diode. The diode decreases in resistance with increasing light. The infrared filter is used to make the gage less sensitive and more capable of a sharp output. At 1000° F there is essentially no output from this gage. As the end of the light pipe approaches the surface due to the rapidly increasing temperature an output results.

Figure 22 shows the determination of char thickness with these gages. Recession of the char interface was sensed by the make-wire gage and recession of the surface by the light pipe sensor. The difference between the two readings gives the char thickness as a function of time. The magnitude and steady-state char thickness were verified by measurements of char thickness on sectioned specimens tested for 10, 20, and 30 seconds.

In addition to sensors such as these, research is being performed by several organizations on sensors which utilize radioactive elements. The

change in measured radioactivity is used as a means of locating the surface and the char interface.

The most careful simulation of entry heating on a charring ablator will not yield the detailed information regarding the ablation processes unless suitable ablation sensors are developed.

Effect of Radiative Heating

Unfortunately there is a dearth of useful experimental data from combined convective and radiative tests – principally because of the lack of adequate facilities. Figure 23 shows some results obtained by Langley using the resistance-heated graphite radiator previously described (ref. 5). The efficiencies of three materials - Teflon, Fluorogreen, and phenolic-nylon - are given as a function of the total cold-wall heating rate. Efficiency or effectiveness will be used in succeeding figures and is defined as the total cold-wall heat input which can be accommodated by a pound of material before reaching a specified back-surface temperature - which was 300° F in this case. Data are shown for radiative heating alone, convective heating alone, and combined convective and radiative heating. Briefly, when teflon experiences radiative heating alone or combined radiative and convective heating its efficiency drops considerably from the level that would have been obtained with convective heating only. This is attributed to the thermal transparency of teflon. Fluorogreen is essentially Teflon with additives that increase the opaqueness to thermal radiation. Although the result with convective heating alone is the same as for Teflon, radiative heating produces much less decrease in efficiency.

Finally, for the phenolic-nylon material, it is seen that over the test

range of heating rates about the same efficiency is obtained regardless of the type of heating. However these results are not believed to be indicative of what would happen in a flight situation. In these tests the enthalpy was quite low and therefore the ablation blocking mechanism was not very significant. Inasmuch as it is this blocking mechanism that is most affected by radiative heating, the simulation was not adequate.

Figure 24 shows some calculated results (ref. 11) which probably provide a clearer picture of the effect of radiative heating. The ordinate is dimensionless heat of ablation, which is a gage of material performance, and is defined by the equation where q_o is hot-wall convective heating rate to a nonablating body and q_r is the net radiative heating. The abscissa is the dimensionless enthalpy difference. The quantity q_r/q_o is the ratio of the net radiative heating - that is, the radiative input minus reradiation - to the hot wall convective rate. The curve marked for the zero value of the ratio is for convective heating only. As the ratio increases, the heat of ablation decreases by a substantial amount. This results because the gases that the ablating surface injects into the boundary layer generally do not block radiative heating. More mass is injected into the boundary layer than would be the case if all the heating were convective. Negative values of the ratio result when the reradiative rates are higher than the radiative input. In this instance, there is an increase in heat of ablation. Thus it can be seen that the effect of radiative heating depends critically upon the relative magnitudes of the radiative and convective heating and the enthalpy difference.

Another aspect of this problem is the effect of radiative heating in a situation where char oxidation is significant as it may be for charring ablator. At the higher temperatures, oxidation is a function of the rate of

diffusion of oxygen to the surface. In turn, the diffusion of oxygen is related to convective heating. Just as mass injection blocks convective heating, it also interferes with the diffusion of oxygen to the ablator surface. Therefore, the mass injection which results from the radiative component of heating will lessen the char oxidation. Combined radiative and convective heating should result in less severe oxidation than an equal amount of convective heating only.

Effect of Convective Heating

Heat shield efficiency changes greatly with variation of the entry environment and the various materials respond differently to these variations as shown by figure 25. In each of the four graphs, the change in thermal efficiency of two good heat shield materials is plotted as a function of changes in an important environmental; for example, an increase in velocity, or enthalpy, from orbital to escape speed, such as going from the Mercury to the Apollo mission. Also considered are changes in the heating rate, surface oxidation, and shear.

Figure 26 shows qualitatively the effect of oxidation on char erosion. The sectioned specimens shown here were tested in an arc jet condition that was not energetic enough to remove char by means of pressure or shear forces. In addition, the surface temperatures experienced by these specimens were not high enough to result in the sublimation of char. The principal means of char erosion was oxidation.

The specimens were made of the same material and were of the same shape and size. They were subjected to the same heating conditions for the same

period of time. The only differences in the tests were the oxygen percentages of the stream. The original specimen outlines are shown for reference purposes.

The specimen on the left was tested in a 100-percent nitrogen stream. This specimen, which shows a small change in size and practically no change in shape, lost about 47 percent of the original mass. The small change in size is believed to have resulted from shrinkage which occurs when this material pyrolyzes. The specimen in the middle was tested in a stream whose content by weight was 90-percent nitrogen and 10-percent oxygen. The change in size is more substantial and there is a significant change in shape. The total mass loss in this test was about 56 percent. Finally, the specimen on the right was tested in air. Here there is a drastic change in size and shape. The mass loss for this case was 68 percent. A closer examination also reveals that the char thickness is inversely related to the oxygen content with the thickest char being developed in the nitrogen stream.

Effects such as these have a marked influence on the efficiency of a material as can be seen in figure 27. Thermal effectiveness of a phenolic-nylon material is plotted as a function of cold-wall heating rate for tests in streams of four different compositions. For tests in air, the effectiveness is about 6000 Btu/lb and is a very weak function of heating rate. For tests in nitrogen, the effectiveness is from 2 to 3 times as great as obtained in the tests in air for the range of heating rates shown and is strongly influenced by heating rate.

Figure 28 shows a comparison of calculated and experimental oxidation effects. In this case, the material effectiveness is plotted as a function of stream oxygen content for a single heating rate. Calculated data are shown for enthalpies ranging from 3,000 to 25,000 Btu/lb - corresponding

to a low enthalpy test condition and the enthalpy associated with entry at escape velocity. Experimental data taken at 3,000 Btu/lb indicated fair agreement between experiment and theory. More important, however, is the conclusion that the major oxidation effects occur at the lower enthalpies.

If high enthalpy char oxidation is to be simulated in a low enthalpy facility, the stream oxygen content must be reduced. Tests in air would indicate a more deleterious effect than would be obtained in flight. This also emphasizes the attention which must be given to producing the proper surface chemistry when simulating heating.

The oxidation effect just shown for phenolic nylon might not appear when dealing with another material. Figure 29 shows the results of a similar series of tests on a silicone resin with glass fillers. Again effectiveness is plotted as a function of heating rate. The first thing to note here is that the stream composition generally speaking has a rather negligible effect on the performance of the material. However this material does show a heating rate effect. When this material ablates, a glassy layer is formed at the surface. As the heating rate, and in turn the surface temperature, increases, the glassy layer becomes less viscous and is rapidly removed by aerodynamic forces. The maximum efficiency is produced at about 150 Btu/ft^2-sec.

If one were considering this material and the previously discussed phenolic-nylon material for a flight application and made screening tests in air to determine which material was best, he might erroneously conclude that the silicone material was much better than the phenolic-nylon material. Actually, if proper consideration is given to the fact that the test of phenolic nylon in air is more severe than would be experienced in flight, one concludes that up to a heating rate of 150 Btu/ft^2-sec the efficiencies

would be about the same.

Figure 30 shows a comparison of calculated and experimental heating rate effects for the silicone material. The experimental data curve is the average of data taken at 3,000 Btu/lb. Calculations are shown for two enthalpies, 3,000 and 25,000 Btu/lb. The test specimens on which the experimental data were taken had calorimeters on the back surfaces. The calculations shown here do not include the effect of the calorimeter. However since this figure was made, the effect of the calorimeter has been included and the calculated curve for 3,000 Btu/lb shifted slightly to the right and slightly above the data curve shown here. The significant feature of this figure is the indication that it is possible to analytically predict the heating rate effect. If one can predict test results, one can extrapolate to conditions more severe than the test environment with much greater confidence.

Mechanical Erosion of Char

The next item to be discussed is the erosion of char by aerodynamic shear. This is a phenomenon that is not presently well understood but which can be demonstrated to be very significant. Manned vehicles experience long heating periods and in order to improve ablation material insulative qualities so as to provide protection for long heating times, there has been a trend toward decreasing material density. This has been shown to increase the effectiveness of the materials. However the chars which are produced by the low-density materials may be quite fragile. Even the low to moderate shear forces experienced in a manned entry may result in substantial erosion of the char and a drastic decrease in the material efficiency.

Figure 31 shows sectioned test specimens subjected to different shear levels. Two materials were tested, a molded phenolic-nylon and a glass reinforced epoxy resin. The phenolic material was 36 lb/ft^3 and the epoxy material was about 32 lb/ft^3. However there was a vast difference in char strength as is indicated here. The original specimen profiles are shown for reference purposes. At the low shear level, the phenolic material experienced no difficulty, whereas the epoxy material experienced significant erosion. At the high shear level, the difference in performance is greatly magnified - particularly when one notes that the phenolic material was exposed about four times as long.

The reason for pointing out these shear tests is that, in the past, experimenters have been obsessed with producing high enthalpy test devices. In many instances, the high enthalpy devices utilize very low mass flows and produce negligible shear on specimens. Phenomena such as shown here can be completely overlooked in such cases.

As a matter of fact, some thought is now being devoted to the consideration of duplication in terms of what the ablating surface feels rather than devoting so much attention to the simulation of free-stream parameters. Figure 32 shows some of the inputs to the surface of the material. The inputs are thermal, chemical, and mechanical. The thermal inputs shown here are the absorbed radiative heating and the net convective heating. The chemical input is the rate of diffusion of oxygen. The mechanical inputs are the pressure and the shear.

First-order approximations show that the inputs are related as shown. The denominators are the enthalpy, concentration, and velocity differences across the boundary layer.

Some preliminary testing has been done utilizing this approach. The results are shown in figure 33. A test was made in a high enthalpy facility which produced the test conditions shown here. Because the facility is newly installed and control equipment is presently lacking, the oxygen concentration was high. The test results obtained on a phenolic-nylon specimen were as shown. Calculations were made to determine what the test conditions, other than enthalpy, should be in order to produce similar results. A specimen tested under the calculated conditions in the low enthalpy facility produced the listed results which are quite similar to the high enthalpy results.

Figure 34 shows the sectioned test specimens to further demonstrate the similarity. Admittedly these are preliminary data, but it is believed that more attention should be devoted to this approach to simulation. It is quite possible that present facilities, limited as they are, can produce more meaningful test data.

FLIGHT TESTS OF ABLATIVE MATERIALS

Up to now, ground tests have been discussed exclusively. In spite of the vast number of ground tests, they are, at best, partial simulations of many effects. The final verification of a heat shield design, or of an analytical prediction, or a simulation technique, must be accomplished by flight tests. Flight tests provide the necessary confidence factor for the utilization of ground test results.

An example of the type of test of interest is the pending test of charring ablator in a high enthalpy reentry environment which cannot presently be simulated on the ground. The booster that is to be utilized in this test

is the four-stage Scout booster. A fifth stage, in the form of a spherical rocket, is added to the payload. Two rockets are fired to propel the payload upward to the desired position and the remaining three rockets drive the payload into the earth's atmosphere at a velocity of about 28,000 fps. ($\gamma \approx -7.5°$, $\frac{W}{C_D A} \approx 165$ psf.)

Figure 35 is a picture of the payload with the components separated. The 18-inch-diameter aft end of the payload is at the left of the photograph where interstage structure can be seen attached to the spherical motor. These components are separated before reentry. The instrumentation deck is to the right of the spherical motor. Next is the instrumentation deck housing. The white truncated cone is the payload afterbody which is constructed of magnesium covered with Teflon for thermal protection. The next component is the payload battery pack. The 11-inch-diameter payload nose cap at the extreme right is the primary experiment. A low-density charring ablator is bonded to a steel shell. The ablator is well instrumented with thermocouples and the previously described ablation sensors.

Considerable ground test data for the material were generated. In some of the tests, excessive char erosion was apparent. However, the actual failure mechanism could not be determined. Using available data, several organizations made predictions of how the material would perform in the flight test. The results were as shown in figure 36. The amount of heat shield material remaining is plotted against time, measured from the beginning of heating. The heating pulse is shown for reference purposes. The shaded band shows the range of predictions. At the top edge of the band where success is predicted, the prediction procedure was almost entirely empirical to the extent of employing an unrealistic ablation model with empirically determined characteristics. At the bottom edge of the band,

the heat shield is predicted to fail before peak heating. In this case, a more reasonable ablation model was utilized with correlated test data to prescribe char removal. The data however were taken at conditions somewhat different from the entry environment. Several other predictions fell between these two extremes but most of them predicted failure near the end of heating.

This is a very graphic example of the wide variation in results that are obtained when test data are extrapolated considerably beyond the range of parameters of the tests in which the data are taken. However, it should be pointed out that the performance of this material could not be characterized to the desired extent before the predictions were made.

CONCLUDING REMARKS

The effects of several environmental parameters on the behavior of ablation materials have been examined. Practically all the entry heating parameters such as enthalpy, pressure, heating rate, aerodynamic shear, and so forth, affect material performance. However, the significance of the effects depends to a large extent upon the type of material. Inasmuch as it is rarely possible to simulate several environment effects simultaneously, the primary inputs must be determined and the test simulation must account for the effects of these inputs. The particular materials of concern must be characterized by test and analysis to determine which of the many environmental inputs are the most significant.

It must also be evident that extrapolation of experimental data to an environment considerably more severe than the test environment can lead to erroneous conclusions. Admittedly at the present time, extrapolation must

generally be resorted to for the most advanced entry missions. However, by combining careful characterization of materials in less severe environments with analytical predictions of behavior in the flight environment, one may develop procedures that can result in adequate heat shield designs.

REFERENCES

1. Anderson, R. A.: Research, Design Considerations, and Technological Problems of Structures for Planetary Entry Vehicles. Proceedings of the NASA-University Conference on the Science and Technology of Space Exploration, Chicago, Illinois, Nov. 1-3, 1962, vol. 2, NASA SP-11, pp. 511-519.

2. Heldenfels, R. P.: Ground Facilities for Testing Reentry Structures and Materials. Proceedings of the Conference on Physics of the Solar System and Reentry Dynamics, Virginia Polytechnic Institute Engineering Bulletin No. 150, Aug. 1962, pp. 315-338.

3. Cann, G. L.; Teem, J. M.; Buhler, R. D.; and Branson, L. K.: Magnetogasdynamics Accelerator Techniques. Arnold Engineering Development Center, AEDC TR 62-145, July 1962.

4. Warren, W. R.: Laboratory Experimental Studies in Reentry Aerothermodynamics. General Electric Company, Missile and Space Vehicle Dept., Rept. TIS R59 SD 362, 1959.

5. Brooks, W. A.; Swann, R. T.; and Wadlin, K. L.: Thermal Protection for Spacecraft Entering at Escape Velocity. Society of Automotive Engineers Preprint 513 F, Apr. 1962.

6. Lundell, J. H.; Winovich, W.; and Wakefield, R.: Simulation of Convective and Radiative Entry Heating. Symposium on Hypervelocity Techniques, Denver, Colorado, Mar. 20-21, 1962.

7. Diaconis, N. S.; Weber, H. E.; and Warren, W. R.: Techniques for Severe Radiative and Convective Heating Environments for Materials Evaluation. General Electric Co., MSD TIS R64 SD 24, Mar. 1964.

8. Roberts, L.: Ablation Materials for Atmospheric Entry. Proceedings of the NASA-University Conference on the Science and Technology of Space Exploration, Chicago, Illinois, Nov. 1-3, NASA SP-11, vol. 2, pp. 461-467.

9. Dow, M. B.: Comparison of Measurements of Internal Temperatures in Ablation Material by Various Thermocouple Configurations, NASA TN D-2165, 1964.

10. Peters, R. W.; and Wilson, R. G.: Experimental Investigation of the Effect of Convective and Radiative Heat Loads on the Performance of Subliming and Charring Ablators. NASA TN D-1355, 1962.

11. Swann, R. T.: Effect of Thermal Radiation From a Hot Gas Layer on Heat of Ablation. Journal of Aerospace Sciences (Readers' Forum), vol. 25, no. 7, July 1961, pp. 582-583.

12. Dow, M. B.; and Swann, R. T.: Determination of Effects of Oxidation on Performance of Charring Ablators. NASA TR R-196, 1964.

13. Clark, R. K.: Effect of Environmental Parameters on the Performance of Low-Density Silicone-Resin and Phenolic-Nylon Ablation Materials. NASA TN D-2543, 1965.

14. Swann, R. T.; Dow, M. B.; and Tompkins, S. S.: Analysis of the Effects of Environmental Conditions on the Performance of Charring Ablators. Presented at the AIAA Entry Technology Conference, Williamsburg and Hampton, Virginia, Oct. 12-14. 1964.

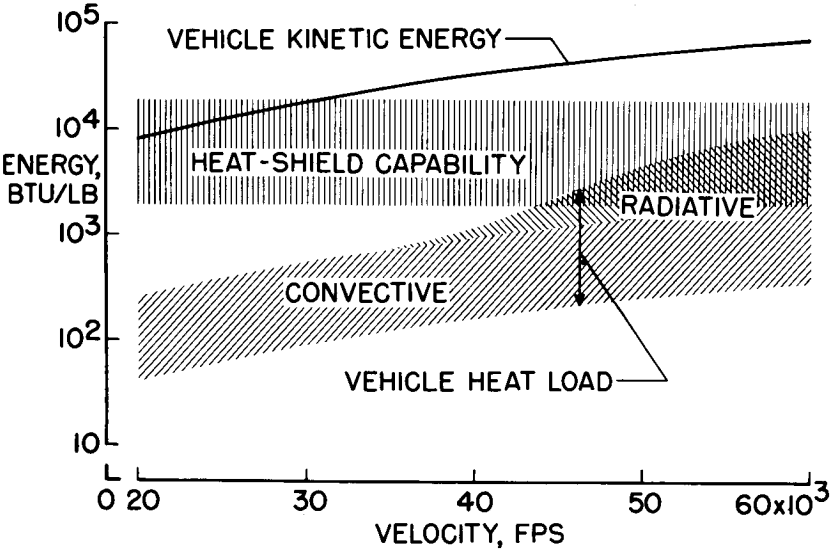

Figure 1.- Dissipation of the kinetic energy of entry vehicles.

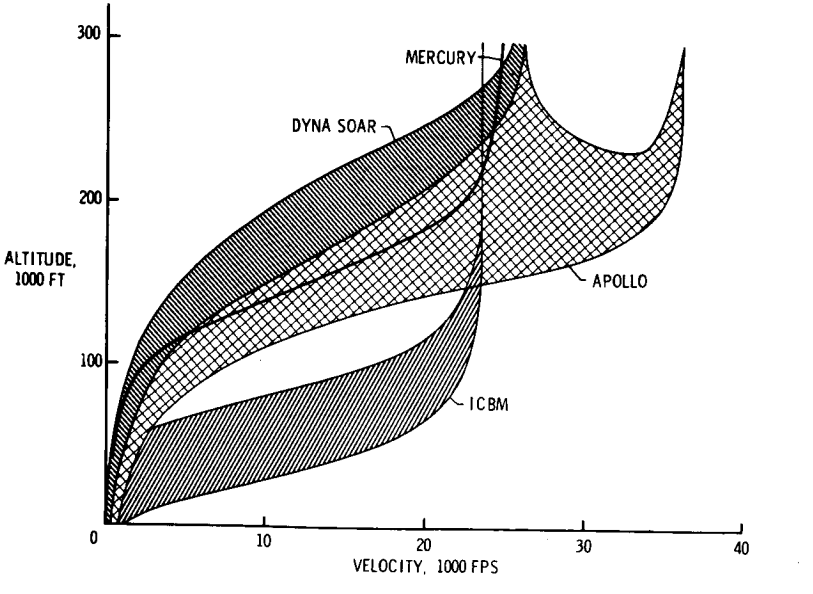

Figure 2.- Entry vehicle flight regions.

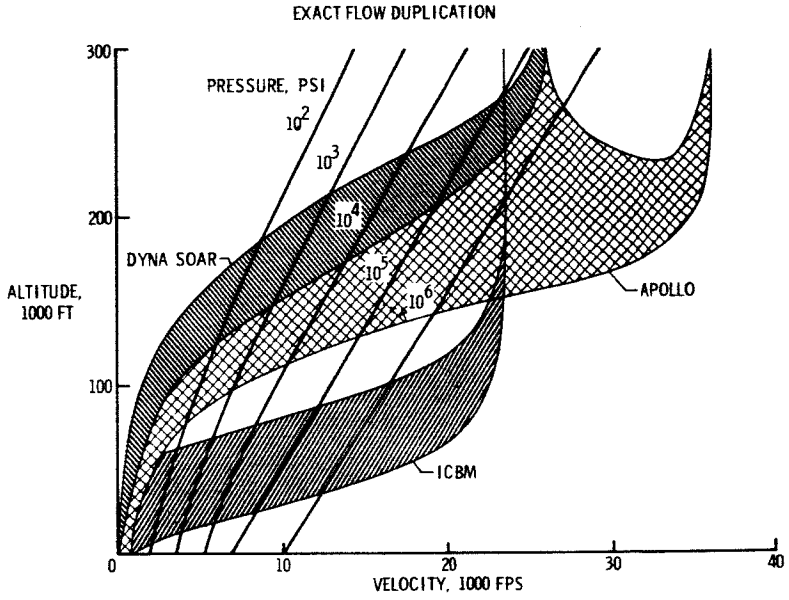

Figure 3.- Settling chamber pressure required for exact flow duplication.

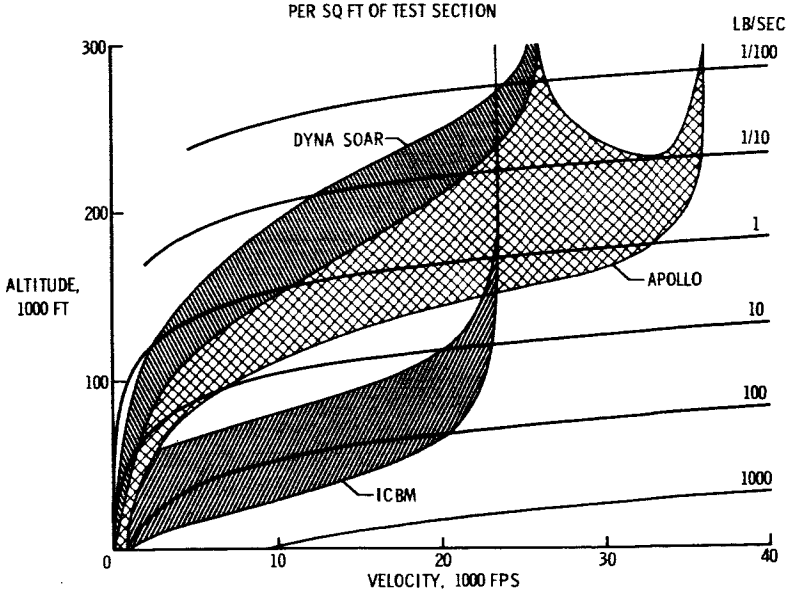

Figure 4.- Mass flow rate required for exact flow duplication.

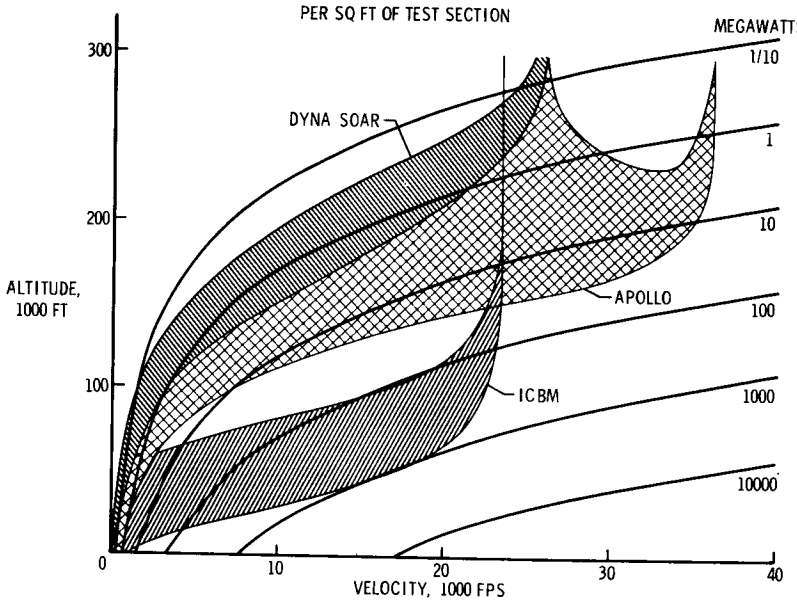

NASA

Figure 5.- Heat energy required for exact flow duplication.

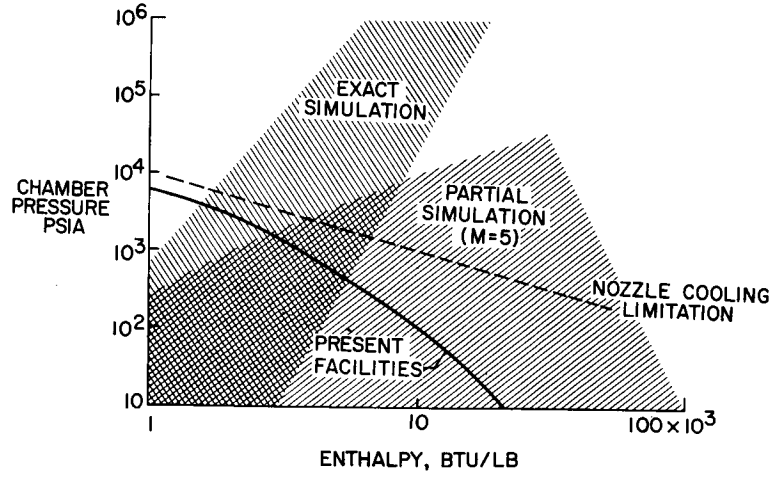

NASA

Figure 6.- Capabilities of present arc facilities.

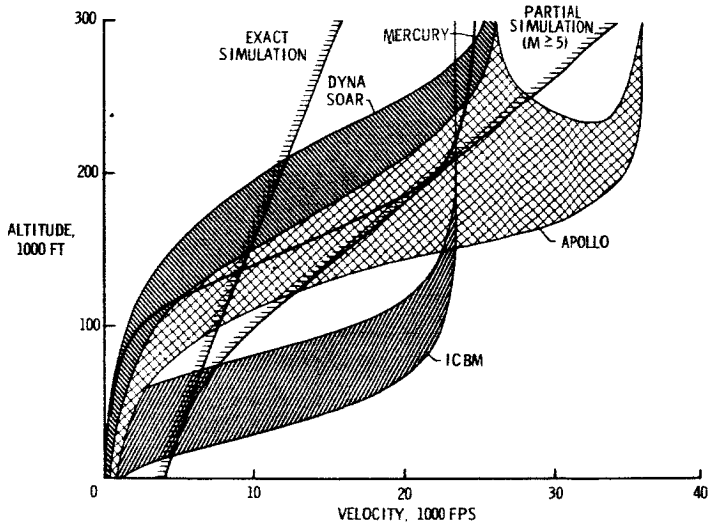

NASA

Figure 7.- Comparison of arc facilities simulation capabilities with entry flight regions.

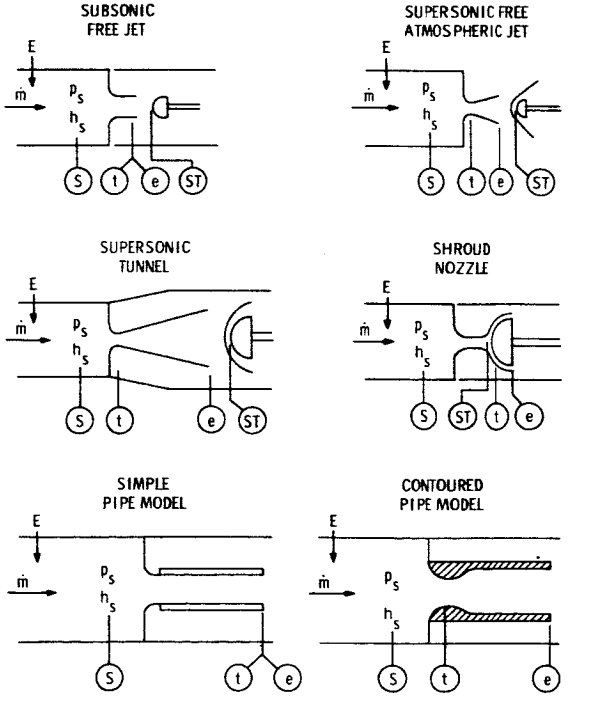

NASA

Figure 8.- Configurations of test streams produced by arc facilities.

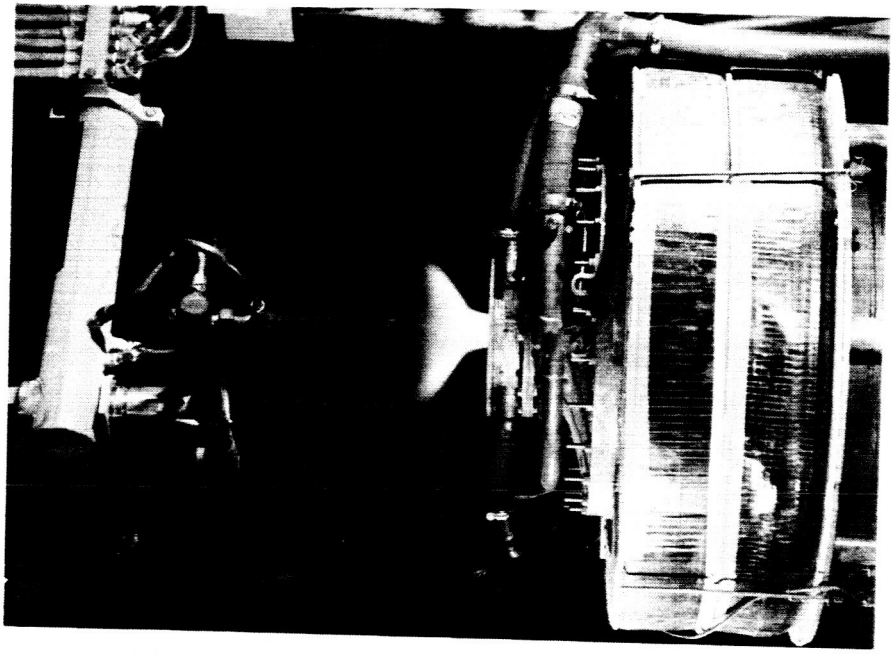

NASA

Figure 9.- A splash test in the Langley Research Center 2500-kilowatt arc jet.

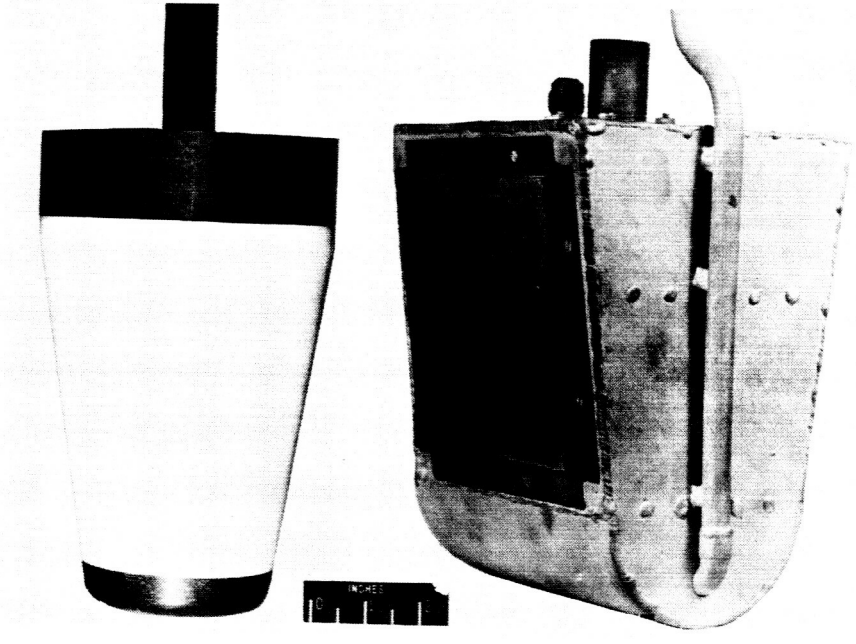

Figure 10.- Configuration of test specimens.

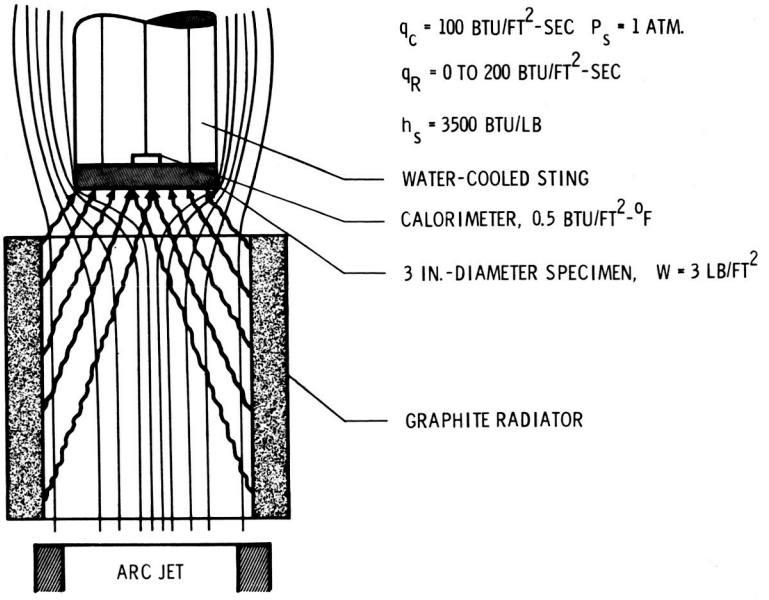

NASA

Figure 11.- Convective and radiative heating device used at Langley Research Center.

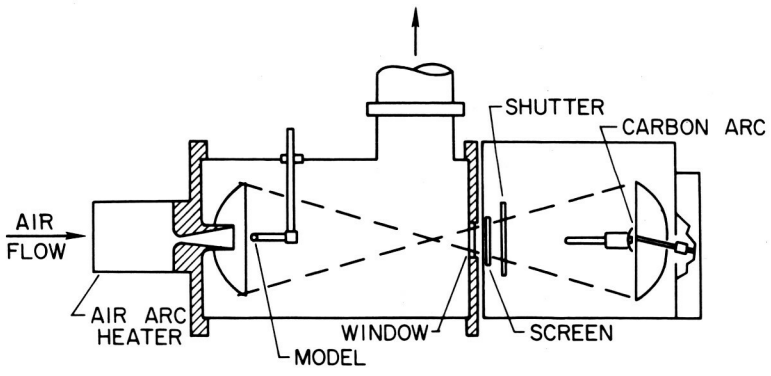

MODEL DIAMETER = 0.75 IN.
CONVECTIVE HEATING RATE = 600 BTU/FT^2-SEC
RADIATIVE HEATING RATE = 750 BTU/FT^2-SEC

NASA

Figure 12.- The Ames Research Center Entry Heating Simulator.

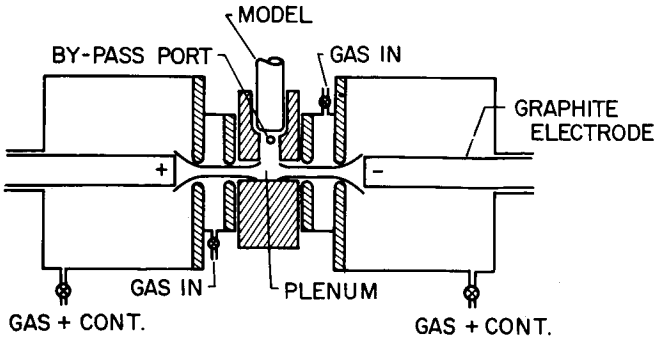

NASA

Figure 13.- General Electric Company's tandem Gerdien arc.

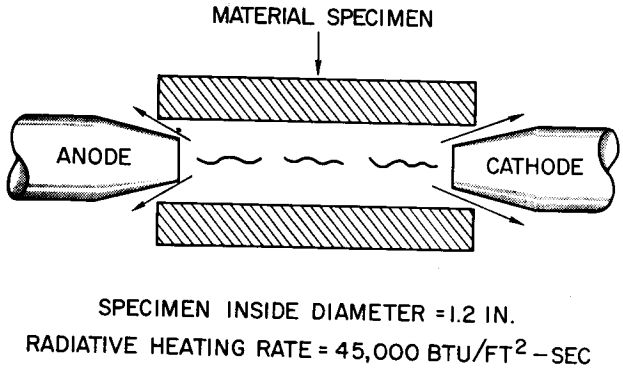

NASA

Figure 14.- A radiative heating device wherein the test material contains the electric arc.

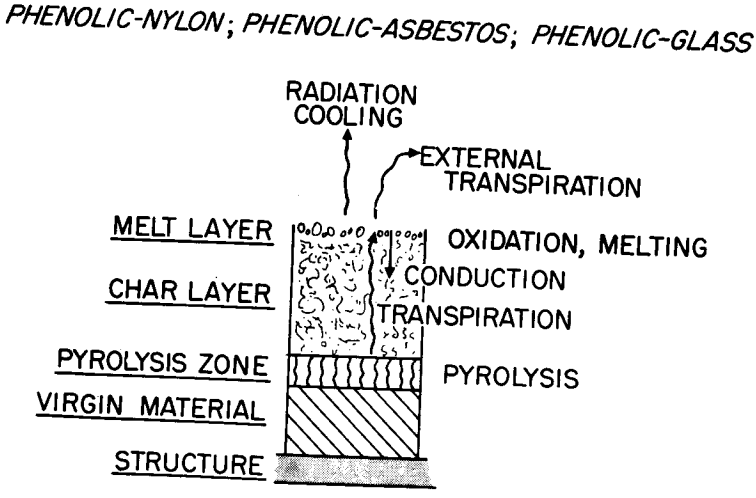

NASA

Figure 15.- The zones and functions of a charring ablator.

SURFACE ENERGY BALANCE:

$$q_c \left(1 - \frac{h_w}{h_e}\right) f\left[\left(\dot{m}_T \frac{h_e}{q_c}\right)\right] + \alpha q_R + \dot{m}_c \Delta h_c$$

NET CONVECTIVE HEATING — RADIATIVE HEATING — COMBUSTIVE HEATING

$$= \sigma \varepsilon_1 T_1^4 - k \frac{\partial T}{\partial x} + \dot{m}_c H_c$$

RERADIATION — CONDUCTION TO INTERIOR — HEAT OF SUBLIMATION

DEGRADING MATERIAL ENERGY BALANCE:

$$\frac{\partial}{\partial x}\left(k \frac{\partial T}{\partial x}\right) + \frac{\partial}{\partial x}\left[\sum \dot{m}_i h_i\right] = \frac{\partial}{\partial t}\left[\sum \rho_j h_j\right]$$

HEAT CONDUCTED — HEAT CONVECTED — HEAT ABSORBED

NASA

Figure 16.- The basic equations for ablation.

PHENOLIC-NYLON 76 LB/FT^3
PT-PT 13% RH TC, #24 AND #30
$\dot{q}$ = 90 BTU/FT^2-SEC, t = 135 SEC

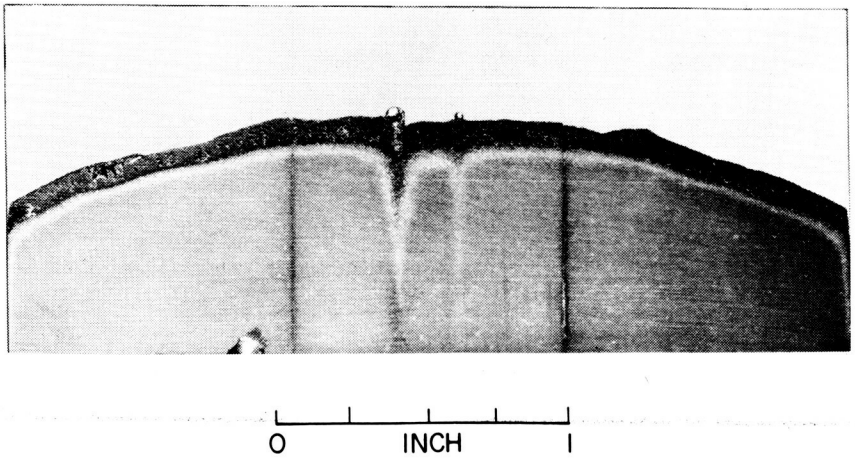

NASA

Figure 17.- The conduction of heat along thermocouple wire.

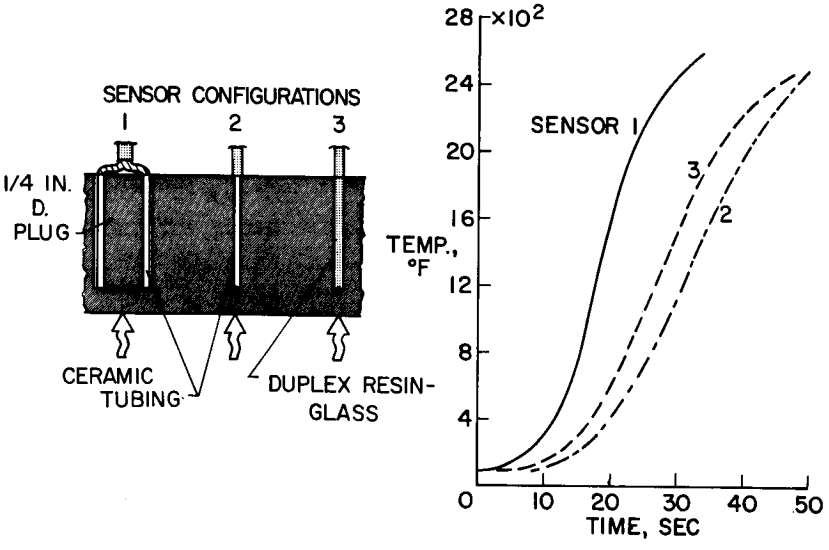

NASA

Figure 18.- The effect of thermocouple configuration on temperature measure.

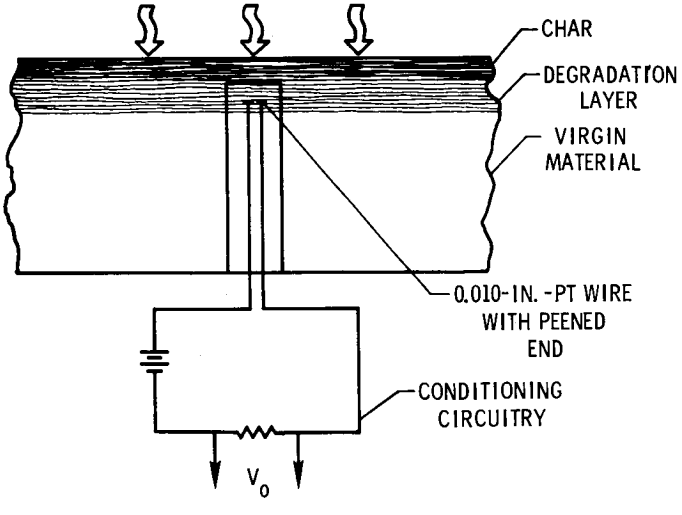

NASA

Figure 19.- The make-wire ablation sensor.

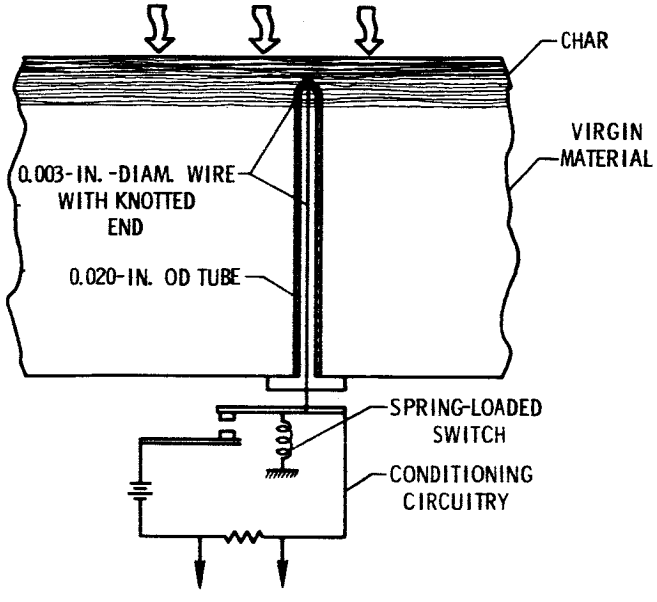

NASA

Figure 20.- The spring-wire ablation sensor.

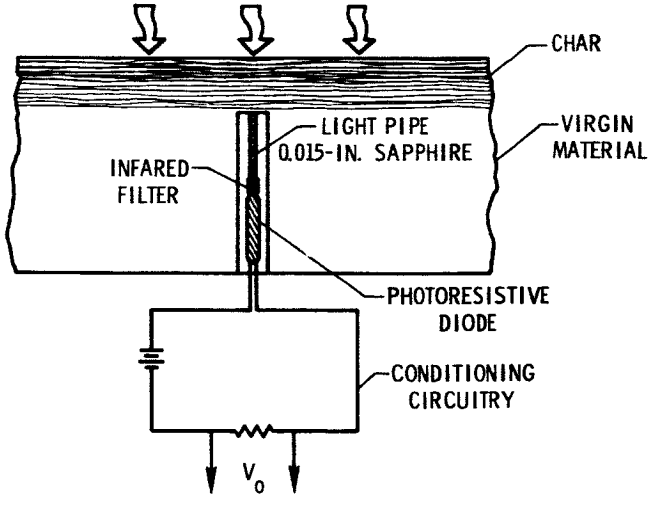

NASA

Figure 21.- The light-pipe ablation sensor.

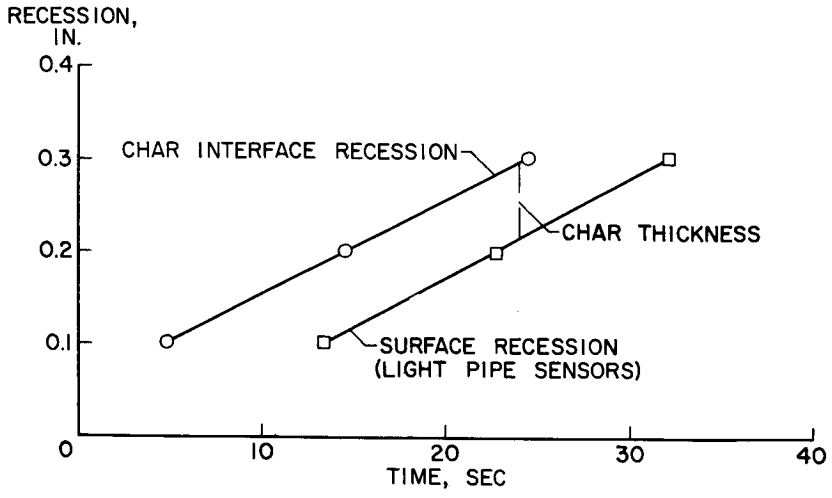

NASA

Figure 22.- Determination of char thickness with ablation sensors.

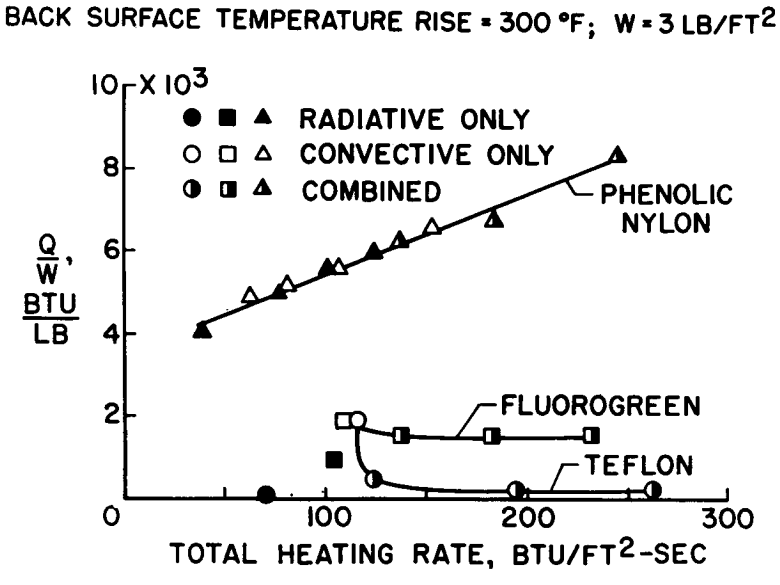

NASA

Figure 23.- The effect of radiative heating on ablation material performance.

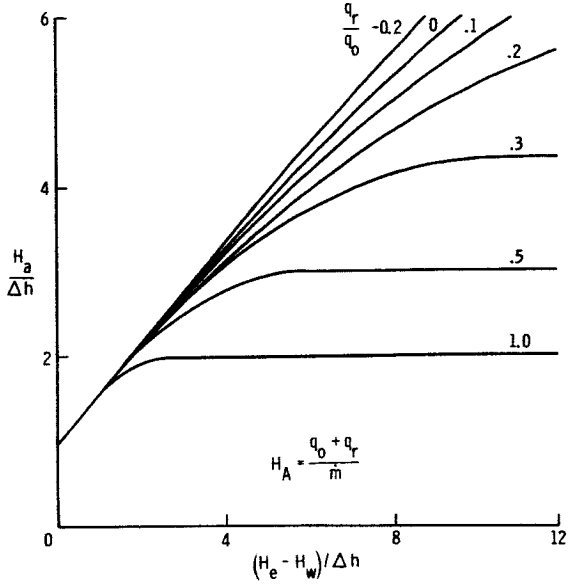

NASA

Figure 24.- Calculated ablation efficiency with radiative heating.

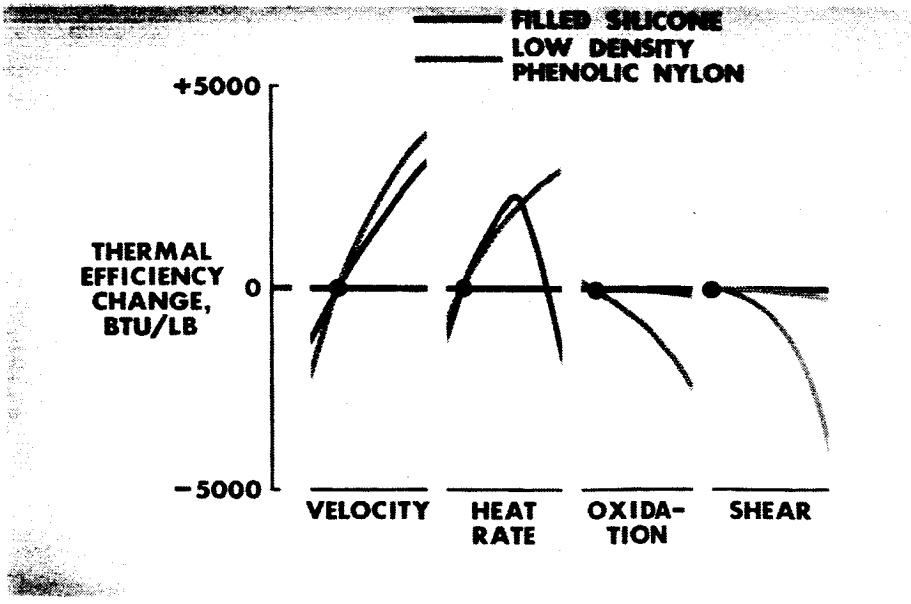

NASA

Figure 25.- The effect of environmental parameters on heat-shield efficiency.

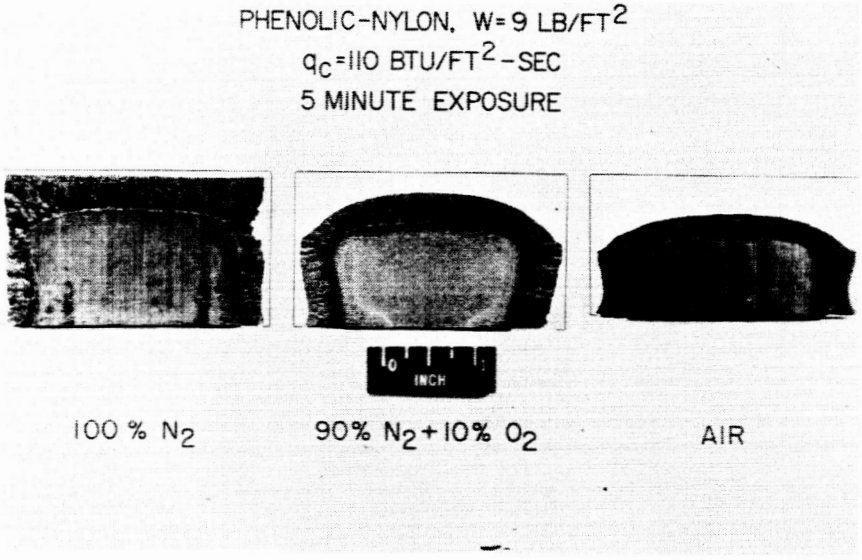

NASA

Figure 26.- The effect of oxygen on char erosion.

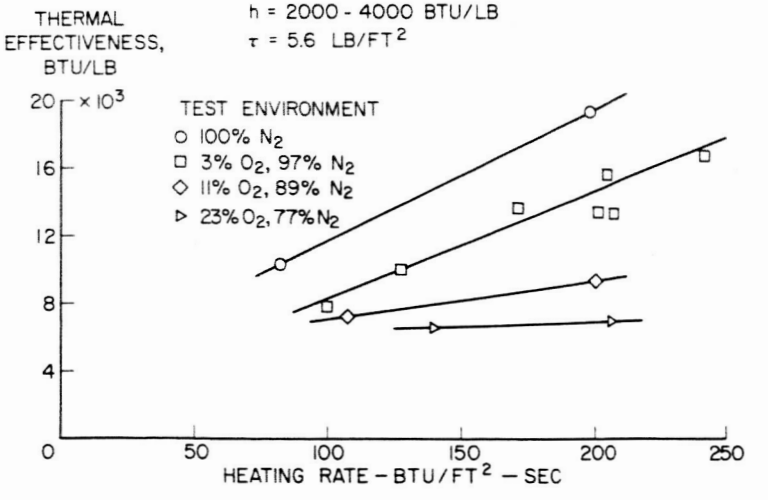

NASA

Figure 27.- The thermal effectiveness of low-density phenolic-nylon in various gas streams.

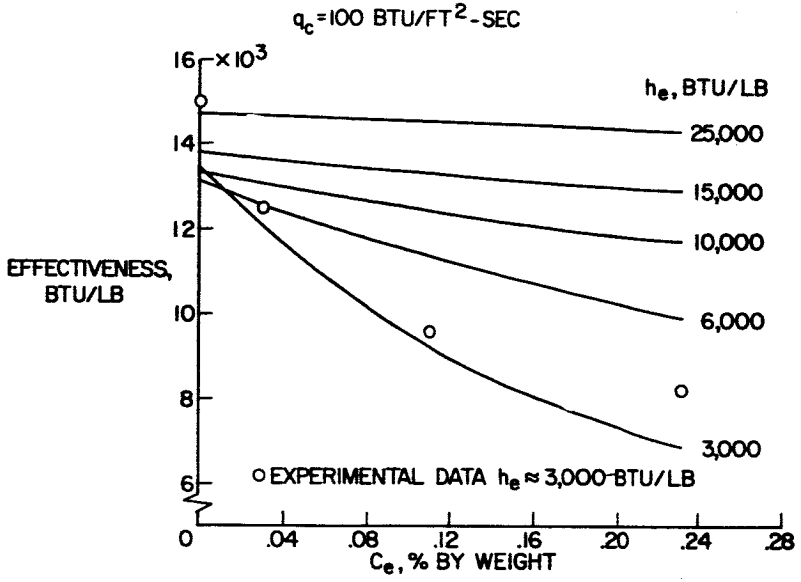

NASA

Figure 28.- The effect of oxidation on the efficiency of a charring ablator.

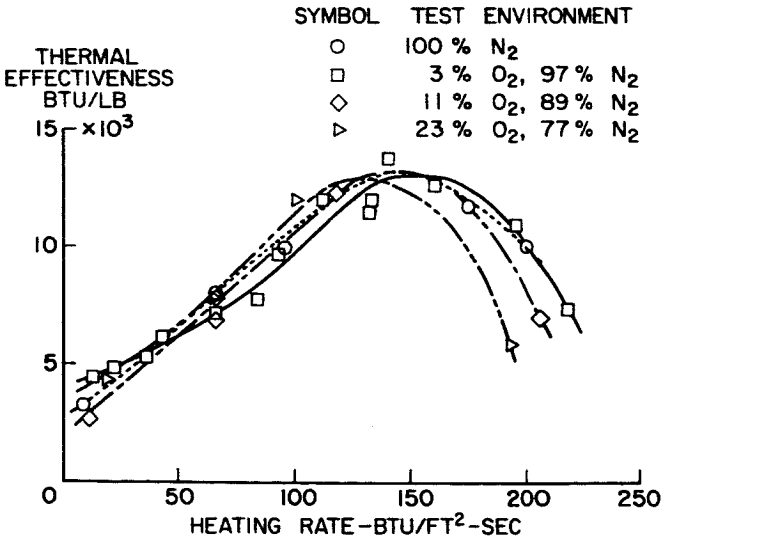

NASA

Figure 29.- The thermal effectiveness of a low-density silicone-resin ablator.

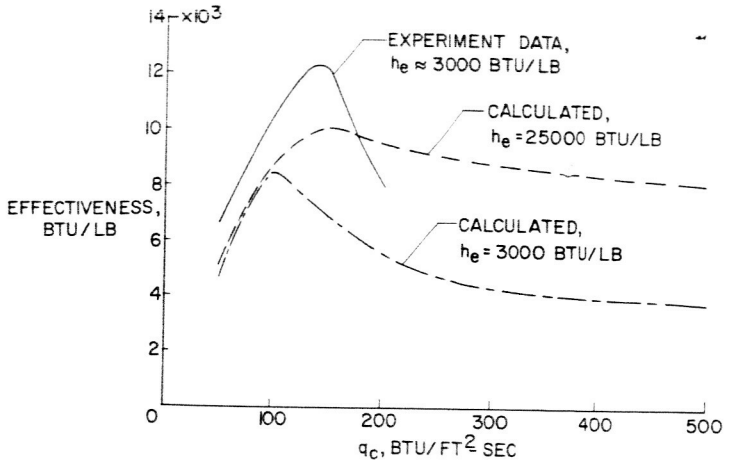

NASA

Figure 30.- The effect of heating rate on the performance of a silicone-resin ablator.

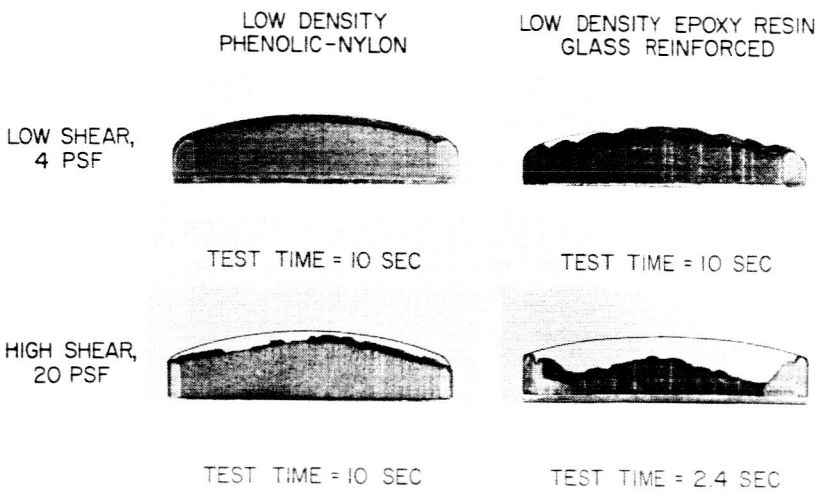

NASA

Figure 31.- An example of char removal by aerodynamic shear.

THERMAL INPUT:

$$\alpha q_R + q_{C,NET}$$

CHEMICAL INPUT:

$$\dot{m}(O_2)$$

MECHANICAL INPUT:

$$P_w \hat{n} + \tau_w \hat{\tau}$$

RELATIONS BETWEEN INPUTS:

$$\frac{q_{c,NET}}{h_e - h_w} \approx \frac{\dot{m}(O_2)}{C_e - C_w} \approx \frac{\tau_w}{u_e}$$

NASA

Figure 32.- The environmental inputs to an ablating surface.

	HIGH ENTHALPY	LOW ENTHALPY
CONDITIONS FOR SIMILARITY:		
ENTHALPY, BTU/LB	10,050	3600
HEATING RATE, BTU/FT^2-SEC	200	150
OXYGEN CONCENTRATION	0.380	0.116
TEST DURATION, SEC	20.6	27.4
TEST RESULTS:		
SURFACE RECESSION, IN.	0.03	0.03
CHAR THICKNESS, IN.	0.08	0.09
THICKNESS DEGRADED, IN.	0.11	0.12

NASA

Figure 33.- The production of similar ablation test results in dissimilar test environments.

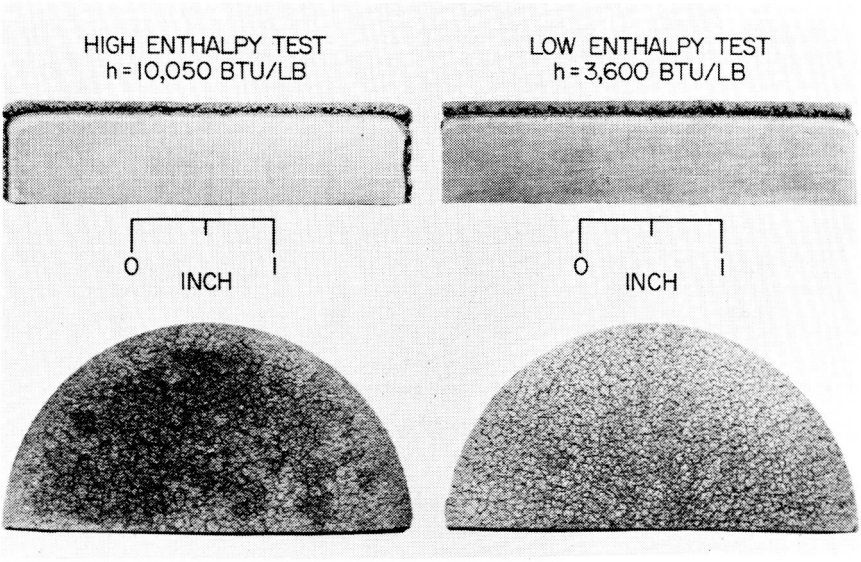

NASA

Figure 34.- Sectioned specimens showing similar results from dissimilar environments.

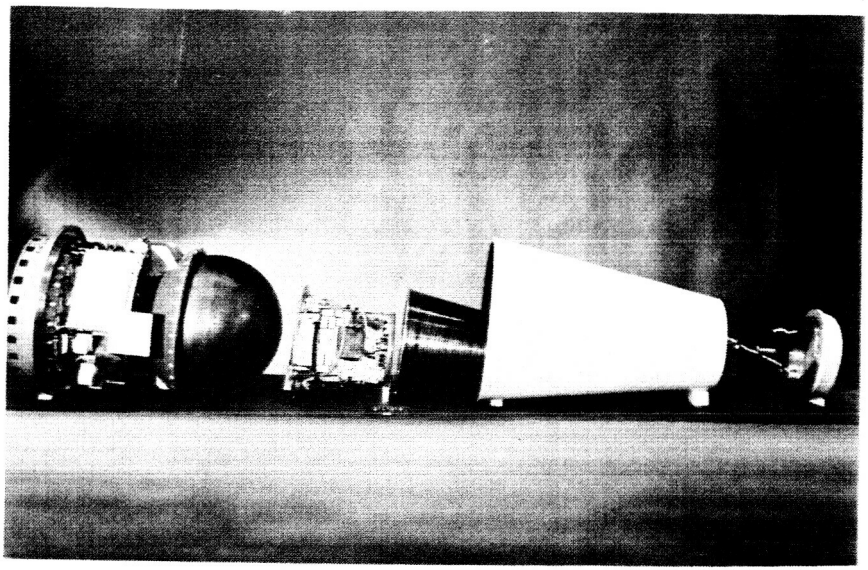

NASA

Figure 35.- Components of a Langley Research Center Scout Reentry Project payload.

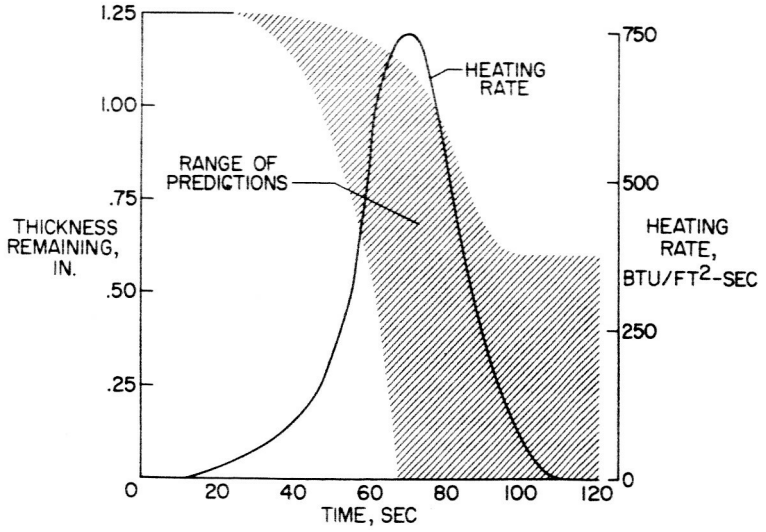

NASA

Figure 36.- Empirical predictions of a heat-shield performance for a Scout Reentry Project payload.

DETECTION OF, AND COMMUNICATION WITH SPACE VEHICLES DURING ATMOSPHERIC ENTRY; PROBLEMS IN SIMULATION

by

S. C. Lin*

Avco-Everett Research Laboratory

INTRODUCTION

In considering the problem of communicating with outer space and detection of spacecraft from the ground, one usually has to worry about only the propagation characteristics of electromagnetic waves of vacuum wavelength falling within either one of the two well known "atmospheric windows," namely; (1) the "optical window" extending from about 0.3 microns to a few microns, and (2) the "RF window" extending from a few millimeters to about 30 meters in the wavelength scale. However, during entry (or reentry) of a spacecraft into the earth's atmosphere, there exists two physical phenomena which tend to complicate the communication problem on the one hand, and to simplify the detection problem on the other hand.

To explain these phenomena, let us take a look at the hypersonic flow field around a typical vehicle depicted in Figure 1. This schematic drawing is reproduced from a paper published by Professor Lester Lees of California Institute of Technology in 1962 (Ref. 1). Even though a sphere is used here as an example for the sake of simplicity, the

---

* Now Professor of Engineering Physics, University of California, at San Diego, La Jolla, California.

general features of the flow field are quite characteristic of those of the hypersonic flow around a realistic spacecraft, such as the Mercury capsule and the planned Apollo re-entry vehicle. As noted by Professor Lees, one of the most striking features of the flow field around such a blunt object at hypersonic speed is the bow shock wave. This shock wave, nearly parabolic in shape, is first formed in front of the re-entering spacecraft at altitudes of the order of 300,000 to 400,000 ft, depending on the size of the spacecraft. The gas that traverses the strong, nearly normal portion of the bow shock wave, is compressed and heated irreversibly by the shock, and forms an outer wake behind the body. The temperature and density of the gas behind the apex of the bow shock wave, where the gas is practically stagnant, is illustrated in Fig. 2. This figure is reconstructed from a paper by B. Kivel, dated 1959.[2] The temperature and density shown here as functions of flight velocity and altitude were based on a local equilibrium adiabatic shock compression process. The dotted lines illustrated some typical velocity-altitude relationships for two typical spacecrafts during re-entry; namely, a Mars probe and a near-orbit earth satellite. It is seen that the gas temperature in the stagnation region, that is, the region behind the apex of the bow shock wave, is typically of the order of 6,000 to 15,000°K. After the shock compression, the gas re-expands as it accelerates around the side of the spacecraft so that the temperature in the other part of the flow field may be expected to be somewhat lower. However, even after isentropic expansion back to ambient pressure, which occur in a distance of about 50 to 100 diameters behind the spacecraft, the gas temperature would still remain at about 4500°K at satellite velocity and at about 7000°K at the Mars probe velocity. At these high

temperatures, air, which is normally transparent through the visible part of the spectrum, becomes highly dissociated, ionized and optically active. This is illustrated in Fig. 3 and 4, which depict the chemical composition of air behind the normal shock wave up to satellite velocity, and the spontaneous emission intensity up to 18,000°K temperature under the condition of thermodynamic equilibrium. Since this emitted radiation, which amounts to many kilowatts or even megawatts per liter of the high temperature air, is given out mostly in the visible part of the spectrum, it becomes a bothersome background noise when one tries to communicate with a spacecraft through the "optical window" of the atmosphere. On the other hand, this strong radiation also serves as a natural beacon announcing the arrival of the spacecraft as it enters the earth's atmosphere. An example of this phenomenon is illustrated in Fig. 5, which shows a ballistic camera trace of a missile nose cone as recorded by the Avco Everett Research Laboratory over the south Atlantic.[4] This photograph was taken with an open shutter camera in much the same way as in the recording of luminous meteor trails.

The second physical phenomenon which complicates the communication problem of hypersonic flight is the ionization phenomenon. At satellite velocity, the degree of ionization behind a normal shock under the conditions of thermodynamic equilibrium is about 0.1%. At higher velocities, the degree of ionization is correspondingly higher (see Fig. 6 and Ref. 5). Even at the degree of ionization of 0.1%, the high temperature air is already a better conductor of electricity than sea water by a factor of about 100. In terms of number of free electrons present, a 0.1% ionization corresponds to 5×10^{13} electrons per cubic centimeter behind a bow shock at an altitude of 40 miles. This is about 10^{8} times

greater than the maximum electron density found in the ionosphere. Thus, a re-entering satellite would soon find itself engulfed in a plasma sheet which is practically impenetrable to radio frequency electromagnetic radiation. This gives rise to the so-called "communication black-out" phenomenon, which normally occupies the essential part of the re-entry period.

Even though the thermal ionization phenomenon just mentioned does not make the gas emit strongly in the radio frequency part of the electromagnetic spectrum, it nevertheless manifests itself in the detection problem in another way; namely, as the ionized gas expands around the side of the spacecraft into the wake, the electrons that are produced by the bow shock wave do not disappear immediately. Instead, they recombine at a finite rate and hence persist over considerable distances behind the spacecraft. For spacecrafts of sufficiently large sizes, the wake flow often becomes turbulent even at relatively high altitudes (see Refs. 1 and 6). As the ionized gas produced by the bow shock wave is inhomogeneously mixed with the cold ambient air in the turbulent flow field, the resultant gas mixture becomes a very good scatterer of radio frequency electromagnetic radiation.[7] This is illustrated in Fig. 7, which shows the strong radio echoes observed by Lin, Goldberg, and Janney[8] during re-entry of the MA-6 Mercury capsule carrying Lt. Col. John Glenn in his first orbital flight on February 20, 1962. The radio frequency employed in this case was 30 Mc/S and the altitude of the Mercury capsule during the observation was about 230,000 ft. For several seconds before and after the Mercury capsule passed overhead the observation station, the equivalent back-scattering cross section of the turbulent wake of the Mercury capsule was found to be several

thousand times greater than the bare-body cross section of the Mercury capsule itself in free space.

COMMUNICATIONS THROUGH IONIZED SHOCK LAYERS AND WAKES

With the above introductory remarks, we shall now examine the fundamental problems related to the radiation and ionization phenomena. In particular, we shall try to identify the various physical quantities which govern the absolute intensities of these phenomena. In view of the fact that the problems of communication through the optical window and through the RF window of the atmosphere are somewhat different (even though the fundamental processes are somewhat related), we shall consider these two problems separately. Here we are using the word "communication" in a somewhat general sense to include both the problems of detection and of signal-sending.

Communication Through the Optical Window: The problem of communication through the optical window invariably involves the question of absolute spectral emissivity of the high temperature air produced in a hypersonic flow field. A typical set of emission spectra from shock-heated air, nitrogen and oxygen is illustrated in Fig. 8. It is seen that the spectra generally consist of intense molecular bands, atomic lines, and continua of various origins which spread over the major portion of the visible spectrum. In the problem of detection of spacecraft during re-entry, one is most interested in those parts of the spectrum where the emission is the strongest in order to select the most suitable optical sensor. On the contrary, in the signal-sending problem, one is

interested in the other parts of the spectrum where the emission is the weakest so that the background noise within the communication channel (e.g., a narrow-band laser beam) can be avoided as much as possible. In this latter problem, one is also interested in knowing the absorption coefficient of the high temperature gas in the same spectral region, so that the sending of optical signals through the shock layer can be made with a minimum amount of attenuation.

In order to determine the absolute spectral emissivity and absorbtivity in the various parts of the hypersonic flow field, it is necessary first of all to know the thermodynamic state of the gas in the various parts of the flow field. Secondly, one has to know all the chemical kinetic processes which determine the relative concentration of the different chemical species which participate in the emission and absorption processes. (This includes also the excitation and de-excitation mechanisms of the various energy states for each chemical species.) Finally, after knowing the relative population of the various energy states of the different chemical species, one needs to know further the absolute optical transition probabilities associated with various molecular bands and atomic lines.

Communication Through the RF Window: Due to the great disparity between the atomic length scale and the wavelength of radio frequency electromagnetic waves, the bound states of atoms and molecules generally do not absorb strongly in the radio frequency part of the electromagnetic spectrum. Therefore, the communication problem through the RF window essentially involves the presence of free electrons in the high temperature gas.

The problem of propagation of radio waves through an ionized medium

has been a subject of intense study at the turn of this century by physicists and geophysicists, such as Lorentz, Appleton, Chapman, Sellmeyer, Heavyside, Hartree and others.[10, 11] More recently, this has also been a subject of intense study by plasma physicists,[12, 13] but in this latter case the interest has mainly been centered around the problems of wave propagation and emission in a highly ionized gas in the presence of a strong magnetic field. In the present discussion, however, it suffices to go back to the classical dispersion formulae as derived by Lorentz and others to illustrate the point.

The propagation of a plane wave of amplitude $\underset{\rightarrow}{E}$ in a dispersive medium can in general be represented by the following equation:

$$\underset{\rightarrow}{E} = \underset{\rightarrow}{E}_o \exp[i(\omega t - \gamma \frac{z}{\lambda_o})] \tag{1}$$

where

$$\gamma = n - ik = (\varepsilon - i \frac{4\pi\sigma}{\omega})^{1/2} \tag{2}$$

in the complex propagation constant; ω is the angular frequency; and $\lambda_o = C/\omega$ is the free-space wavelength dived by 2π. The real part of the propagation constant n, known as the "refractive index." determines the velocity of propagation; while the imaginary part k, known as the "extinction coefficient," determines the rate at which the amplitude of the electromagnetic wave attenuates with distance along the direction of propagation z. The refractive index n and the extinction coefficient k are in turn related to the dielectric constant ε and the electrical conductivity σ through the second half of Eq. (2). For an ionized gas in the absence of a strong magnetic field, the dielectric constant and the electrical conductivity are respectively given

by (according to Lorentz, as modified by Sellmeyer, see Ref. 9)

$$\varepsilon = 1 - \frac{\omega_p^2}{\omega^2 + \nu^2} \tag{3}$$

$$4\pi\sigma = \frac{\omega_p^2 \gamma}{\omega^2 + \nu^2} \tag{4}$$

In the above expression, ω_p is the angular plasma frequency, which is linearly proportional to the square root of the number density of free electrons n_e, such that (e being the electron charge, and m_e being the electron mass)

$$\omega_p^2 = \frac{4\pi e^2}{m_e} n_e \tag{5}$$

The quantity ν , known as the electron collision frequency, on the other hand, is a complicated averaged quantity which measures the rate of damping of the organized electron motion due to collisions with the gas molecules, atoms and positive ions.[11] However, in a dilute ionized gas, one may write as an approximation

$$\nu = \bar{C}_e \sum_j n_j \bar{Q}_j \tag{6}$$

where $\bar{C}_e$ is the mean thermal velocity of the electrons, n_j and $\bar{Q}_j$ are respectively the number density and velocity-averaged momentum transfer cross section for collision between an electron and the type-j particle in the ionized gas. The summation sign is to extend over all particles except the electrons.

From the above expressions, it is seen that the rate of attenuation of electromagnetic waves generally increases with the electron number density and with the gas density.

In 1956, the author has made some rough estimates of the amount of attenuation of radio frequency electromagnetic waves to be expected through the shock layer and through the wake,[14] using the above dispersion formulea and the then incomplete information concerning the properties of the hypersonic flow field. The results are reproduced here in Figs. 9, 10(a) and (b). The surprising conclusion was that even at re-entry velocity corresponding to that of long range missiles (i.e., somewhat below the satellite velocity), it appeared very difficult to overcome the"communication blackout" phenomenon during re-entry, except perhaps through the use of extremely-low or extremely-high radio frequencies. However, the basic information concerning the atomic and molecular properties of high temperature air as well as the hypersonic flow field was too incomplete and uncertain at that time to allow one to consider such estimates very quantitative. To obtain quantitative information, one needs to know again the precise thermodynamic state of the gas in the various parts of the flow field; the chemical kinetic processes which govern the rates of production and of disappearance of free electrons; the momentum transfer cross sections of the various chemical species in much the same order as in the optical communication problem.

THE PROBLEM OF SIMULATION

From the foregoing discussion it is quite clear that the problem

of communication with a spacecraft during a re-entry crosses many fields. Its solution requires a simultaneous treatment of the fluid dynamics problem, the chemical kinetics problem, and the problem of propagation of electromagnetic waves in an inhomogeneous hypersonic flow field. Because of the complexity of the problem, there naturally arises the question of whether one can obtain an analogue-type solution to the overall problem through the use of properly constructed scale model in the laboratory without going into the intermediate steps of understanding the various processes. In other words, there is a question of whether the re-entry communication problem can be easily simulated. Unfortunately, the answer seems to be discouragingly negative as far as direct simulation is concerned. The reasons are many. For one thing, the chemical kinetic processes which govern the thermodynamic and chemical properties of the flow field do not have a simple density dependence. For example, the endothermic processes which govern the dissociation and ionization rates of air in the shock compression region mainly involve binary collisions, whereas the exothermic processes which govern the atomic recombination rate and the electron attachment rate in the expansion region mostly involve ternary collisions. For binary reactions, the instantaneous rates depend on the square of the local gas density; while for termary reactions, the instantaneous rates depend on the cube of the local gas density. This is illustrated by Fig. 11, which shows the various regions in the model size versus gas density plot in which the scaling of the chemical reaction rates in the hypersonic wake is either binary, ternary, or a combination of both.[15] For another thing, in the propagation problem, the refractive index n and the extinction coefficient κ not have a simple density and wavelength dependence (see Eqs.

1 through 6). Therefore, in order to obtain full simulation of all the phenomena, one must duplicate the physical dimension of the spacecraft, the free stream conditions, and the electromagnetic wavelength at the same time.

While the problem of full simulation appears very difficult, if not impossible, it is fortunate that there is a natural separation between the dynamics aspect of the hypersonic flow problem and the chemical physics aspect of the hypersonic flow problem, in the sense that the pressure and velocity distributions are relatively insensitive to the equation of state of the gas. Similarly, there also exists a natural separation between the fluid dynamics problem and the electromagnetic problem of propagation, to the extent that within limits of the electromagnetic wave power density there is very little interaction between the two phenomena. This, in effect, allows one to treat the three aspects of the problem quite separately and to carry out partial simulation whenever appropriate. Final answer to the overall problem can then be obtained through synthesis. We shall now illustrate how this can be done:

Referring again to the schematic drawing of the hypersonic flow field shown in Fig. 1, the pressure field is mostly controlled by the shape of the bow shock (see Ref. 1). Due to continuous decrease in strength of the bow shock wave away from the apex, the chemical reaction and excitation processes occur mostly in those parts of the fluid which are closest to the flight axis of the re-entering spacecraft (that is, the high enthalpy gas that has been processed by the nearly normal portion of the bow shock wave). Since the total mass of this gas is small compared with the total mass of air engulfed by

the bow shock wave, it has relatively little effect on the overall pressure field of the hypersonic flow. On the other hand, the bulk of the gas which passed through the outer and relative weak part of the bow shock wave experiences little temperature change and hence has little chemical activity. Thus, the pressure distribution throughout the hypersonic flow field can be determined quite reliably through the application of hypersonic flow theories that have been developed for perfect gases of constant specific heats.[16] From the pressure field so determined, the velocity field for the high enthalpy flow near the flight axis can in turn be determined from the (nearly one-dimensional) equation of motion. From the known pressure and velocity fields, the time history of chemical reactions following each fluid element can then be determined if all the chemical kinetic and excitation rate constants were known.[11] Knowing the distribution of chemical species in the high enthalpy flow, the electromagnetic properties of the hypersonic flow field can in turn be calculated from the atomic and molecular properties of the various chemical species. From the known distribution of electrical properties of the flow field, a final simulation of the electromagnetic propagation can be made through the use of models made of suitable dielectric or diamagnetic material which duplicate the distribution of the complex propagation constant of the flow field.

What we just proposed is in effect to subdivide the entire simulation problem into three separate parts; namely, (i) an aerodynamic simulation to determine the pressure and velocity field, using hypersonic wind tunnel or ballistic range facilities which simulate the flight Mach number and Reynolds number but not necessarily the stagnation

Galilean transformation in the direction tangential to the shock surface.) The operating principle of a shock tube has been adequately described in previous literatures.[18] As illustrated in Fig. 12, the basic elements of this apparatus consist of just a high pressure chamber and a low pressure chamber connected by a suitable diaphragm. When the diaphragm is ruptured, a shock wave is formed and propagates down the low pressure chamber during the early transient of the pressure equilization process. Observations can then be made of the various physical phenomena at the downstream end of the low pressure chamber through the use of suitably fast detectors. By simple variation of geometry, the shock tube can be adapted to perform quantitative experiments over wide ranges of temperature, density and chemical composition of the gas samples. With proper care, it is also possible to reduce all the undesirable effects, such as wall contamination, flow inhomogeneity, etc., to the level of small perturbations. Thus, the resultant shock-heated gas sample (that is, the region between the shock surface and the contact discontinuity in Fig. 12(b)) approaches that of an idealized one-dimensional flow behind a plane shock wave. Figure 13 shows an actual photograph of a relatively large diameter shock tube which has been constructed some time ago at the Avco-Everett Research Laboratory for chemical kinetic studies.

For simulation of the chemical kinetic processes behind a bow shock wave in flight, it is now only necessary to duplicate the shock velocity and ambient air pressure in the laboratory. Figure 14 shows the shock velocity and initial pressure ranges which are accessible to shock tubes of various types.[20] This may be compared with the velocity-density regime of interest to the flight case shown in Fig. 2. Typical

enthalpy corresponding to the flight condition. In this connection, existing hypersonic theories based on non-reacting perfect gases may well be utilized;[16] (ii) a chemical kinetics and atomic physics simulation, using high temperatures shock tubes or molecular beams to determine the fundamental rate constants, excitation cross sections, and other atomic and molecular properties of interest. Here, one may, of course, enlist the help of existing chemical kinetics and atomic theories whenever appropriate; (iii) an electromagnetic simulation using dielectric or diamagnetic models to study the antenna pattern if existing propagation theories prove to be inadequate.

Of the above three items, (i) is already adequately covered by Mr. Potter earlier in this session;[17] (ii) is a topic which I would like to elaborate on in a few moments; (iii) is a topic quite outside the scope of the present session.

CHEMICAL KINETICS AND ATOMIC PHYSICS SIMULATION

Within the remaining time available, I would like to view briefly the problem of chemical kinetics and atomic physics simulation. In particular, I would like to highlight some of the significant results which have been obtained from recent high temperature shock tube studies in connection with the problem under consideration.

Considering the shock compression process across the bow shock wave as a locally one-dimensional phenomenon, one can quite readily reproduce all the chemical kinetic processes in the laboratory using a high temperature shock tube. (Note that the flow across a plane oblique shock wave is equivalent to the flow across a normal shock wave with a simple

results showing the equilibrium spectral radiation intensity behind the shock wave; the ratio between the peak nonequilibrium radiation to the equilibrium radiation; the electrical conductivity of shock-heated air; some of the momentum transfer cross sections between electron and neutral atoms; the electron density distribution behind a normal shock; the peak nonequilibrium electron density; and the characteristic ionization distance behind the shock are illustrated respectively in Figs. 15 through 21. For detailed information concerning the individual experiments leading to the results just presented, the readers are referred to the referenced literature indicated in the respective figure captions.

Finally, to illustrate how the chemical kinetics information may be utilized to determine the electromagnetic property of the hypersonic flow field from a synthesis of the aerodynamics and chemical kinetics simulation, a typical plot of the free electron number density distribution in the wake of a sphere at hypersonic speed, and the absolute root-mean-square electron density flucutation in the wake, are illustrated respectively in Figs. 22 and 23. Detailed descriptions of how such synthesis was carried out may be found in Refs.15 and 23.

REFERENCES

1. L. Lees and L. Hromas, "Turbulent Diffusion in the Wake of a Blunt-Nosed Body at Hypersonic Speeds, J. Aerospace Sciences, 29, 976 (1962).

2. B. Kivel, "Radiation from Hot Air and Stagnation Heating," J. Aerospace Sciences, 28, 96 (1961).

3. L. Lamb and S. C. Lin, "Electrical Conductivity of Thermally Ionized Air Produced in a Shock Tube," J. Appl. Phys., 28, 754 (1957).

4. C. C. Petty, "Semi-Automated Reduction of Photograph in Data for Missile Re-entry," Avco-Everett Research Laboratory, AMP 138, June, 1964; also Proceedings of the Photo-Optical Data Reduction Seminar of the Society of Photo-optical Instrumentation Engineers, St. Louis, Mo., March 2-3, 1964.

5. J. D. Teare, "Ionization Behind Shock Waves," p. 217, Progress in Astronautics and Aeronautics, Vol. 12 (Ed. K. E. Shuler and J. B. Fenn), Academic Press, New York (1963).

6. L. Lees, "Hypersonic Wakes and Trails," AIAA Journal, 2, 417 (1964).

7. E. E. Salpeter and S. B. Treiman, "Backscatter of Electromagnetic Radiation from a Turbulent Plasma," J. Geophys. Res., 69, 869 (1964).

8. S. C. Lin, W. P. Goldberg, and R. B. Janney, "Radio Echoes from the Ionized Trails Generated by a Manned Satellite During Re-entry," Avco-Everett Research Laboratory, Research Report 127, April, 1962; also J. Geophys. Res., 67, 3851 (1962).

9. J. C. Keck, J. C. Camm, B. Kevel and T. Wentink, Jr., "Radiation from Hot Air, Part II," Annals of Physics, 7, 1 (1959).

10. S. K. Mitra, "The Upper Atmosphere," 2nd Ed., Chapter VI, Asiatic Society, Calcutta (1952).

11. H. Margenau, "Conduction and Dispersion of Ionized Gases at High Frequencies," Phys. Rev., 69, 508 (1946).

12. W. P. Allis and S. J. Buchsbaum, "Waves in Anisotropic Plasmas," Massachusetts Inst. of Technology Press, Cambridge (1963).

13. T. H. Dupree, "Theory of Radiation Emission and Absorption in Plasma," Phys. of Fluids, 7, 923 (1964).

14. S. C. Lin, "A Rough Estimate of the Attenuation of Telemetering Signals through the Ionized Gas Envelope around a Typical Re-entry Missile," Avco-Everett Research Laboratory, Research Report 74, February, 1956.

15. S. C. Lin and J. E. Hayes," A Quasi One-Dimensional Model for Chemically Reacting Turbulent Wakes of Hypersonic Objects," Avco-Everett Research Laboratory, Research Report 157, July 1963.

16. W. D. Hayes, and R. F. Probstein, "Hypersonic Flow Theory," Academic Press, New York (1959).

17. J. L. Potter, "Flow Fields, Pressures, Forces, Moments and Motions," Conference on the Role of Simulation in Space Technology, Virginia Polytechnic Institute, Blacksburg, Virginia, August 17-21, 1964.

18. E. L. Resler, S. C. Lin, and A. R. Kantrowitz, "The Production of High Temperature Gases in Shock Tubes," J. Appl. Phys., 23, 1390 (1952).

19. S. C. Lin, and W. I. Fyfe, "Low-Density Shock Tube for Chemical Kinetics Studies," Phys. of Fluids, 4, 238 (1961).

20. J. C. Camm and P. H. Rose, "Electric Shock Tube for High Velocity Simulation," Phys. of Fluids, 6, 663 (1963).

21. R. A. Allen, P. H. Rose, and J. C. Camm, "Nonequilibrium and Equilibrium Radiation at Super-Satellite Re-entry Velocities," Avco-Everett Research Laboratory, Research Report 156, September, 1962; also Institute of Aerospace Sciences, Preprint 63-77, (1963).

22. S. C. Lin and J. D. Teare, "Rate of Ionization Behind Shock Waves in Air, II, Theoretical Interpretation," Phys. of Fluids, 6, 355 (1963).

23. S. C. Lin, "A Partial-Dissipation Approximation for Chemical Reactions in Heterogeneous Turbulent Flows," Avco-Everett Research Laboratory, Research Report 180, April, 1964.

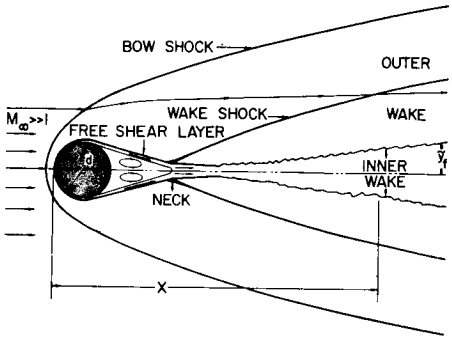

Figure 1: Wake behind blunt body at hypersonic speeds (after Lees, Ref. 1).

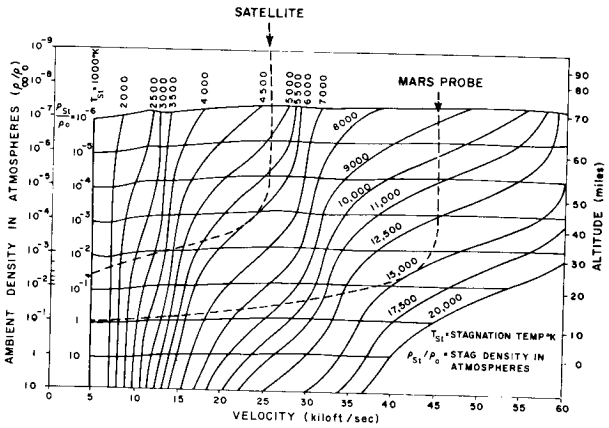

Figure 2: Stagnation temperature and density values as a function of ambient density and flight velocity.

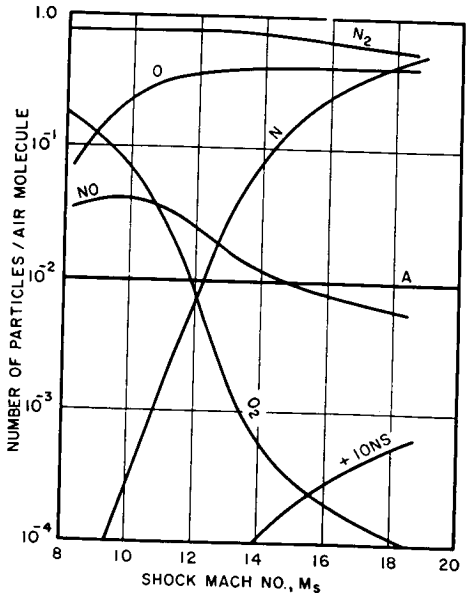

Figure 3: Composition of air behind moving shock wave as a function of shock Mach number. Initial temperature of undisturbed gas, T_1 = 293°K; initial pressure p_1 = 1 mm Hg.

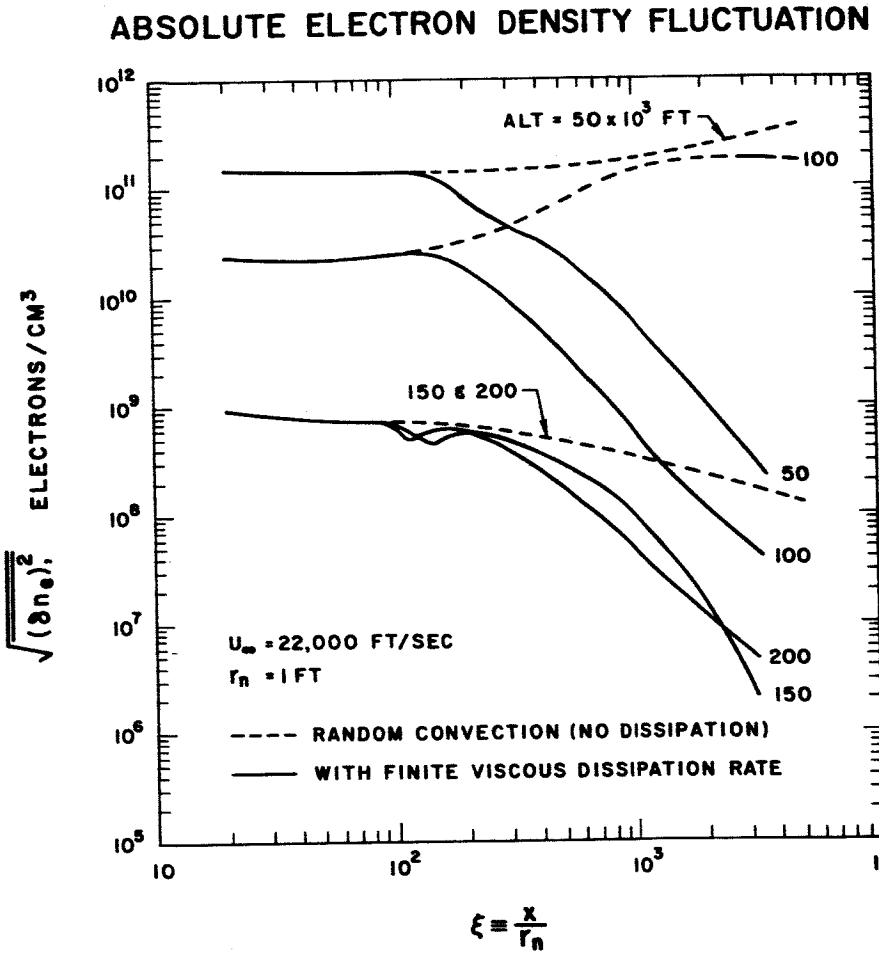

Figure 23: Absolute root-mean-square electron density fluctuation in a quasi one-dimensional turbulent wake behind a hypersonic sphere (see Ref. 23).

CALCULATED AND OBSERVED IONIZATION RISE DISTANCE

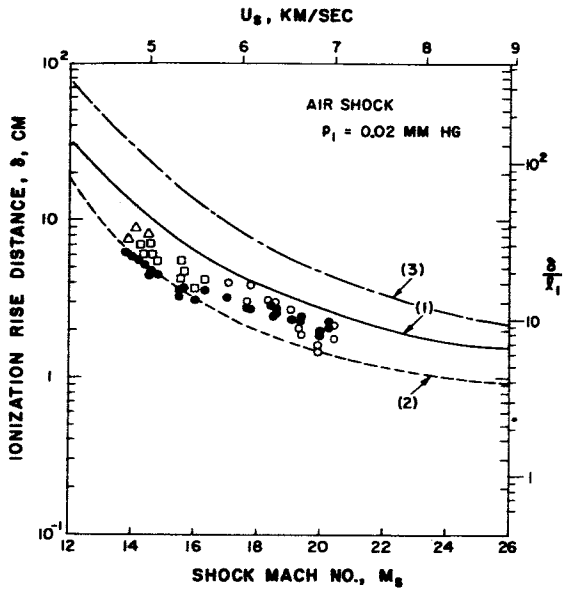

Figure 21: Comparison between calculated and observed ionization rise distance behind the shock as a function of shock velocity at P_1 = 0.02 mm Hg (see Ref. 22).

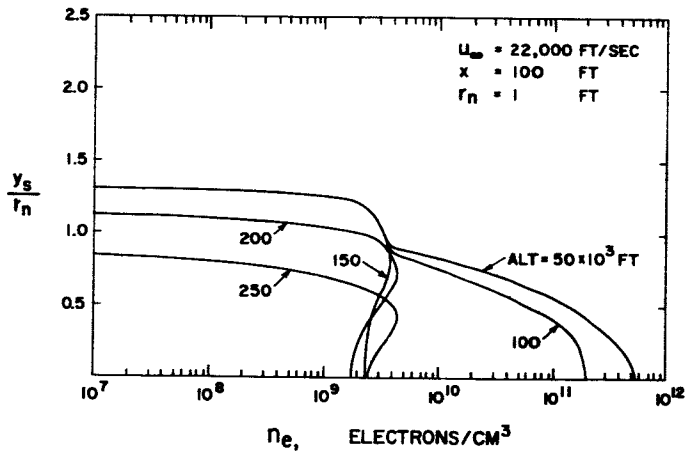

Figure 22: Radical distribution of electron density in a hypothetical axisymmetric, laminar, inviscid, but chemically reacting hypersonic wake behind a sphere of 1 ft. radius at 22,000 ft/sec velocity and at ambient density corresponding to the various indicated altitudes (see Ref. 15).

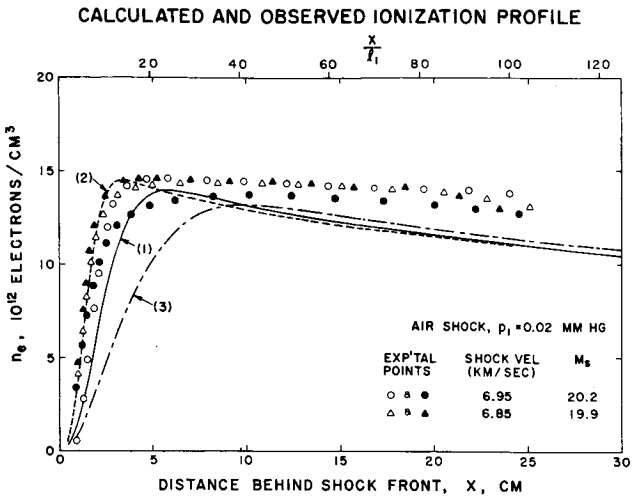

Figure 19: Comparison between calculated and observed electron density distributions behind the shock for the case $U_s = 6.9 \pm 0.05$ km/sec and $P_1 = 0.02$ mm Hg. (See Ref. 22).

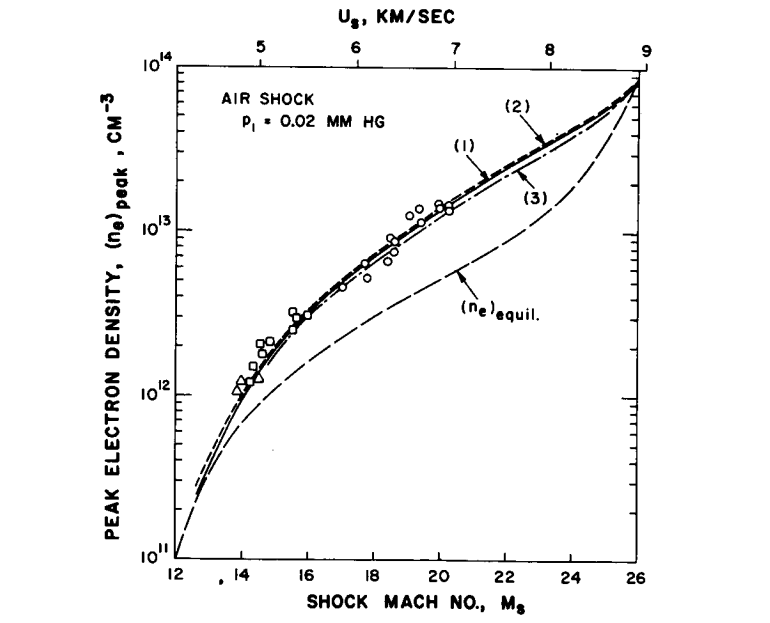

Figure 20: Comparison between calculated and observed peak electron density behind the shock as a function of shock velocity at $P_1 = 0.02$ mm Hg (see Ref. 22.).

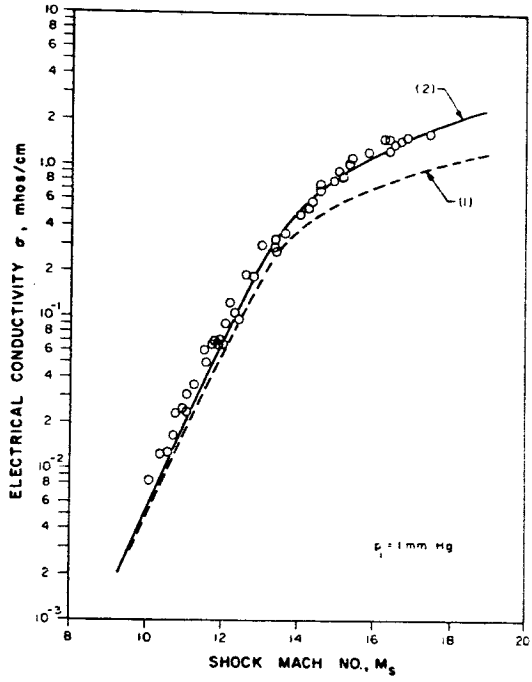

Figure 17: Comparison between experimental and theoretical electrical conductivity of air behind normal shock wave (see Ref. 3).

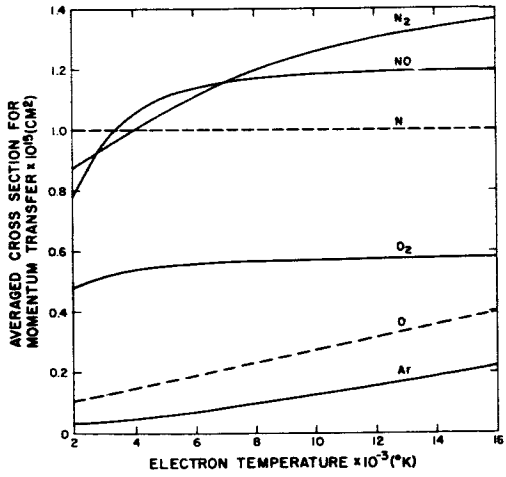

Figure 18: Velocity-averaged cross sections for momentum transfer between electrons and the various neutral components of high temperature air, as functions of electron temperature (see Ref. 5).

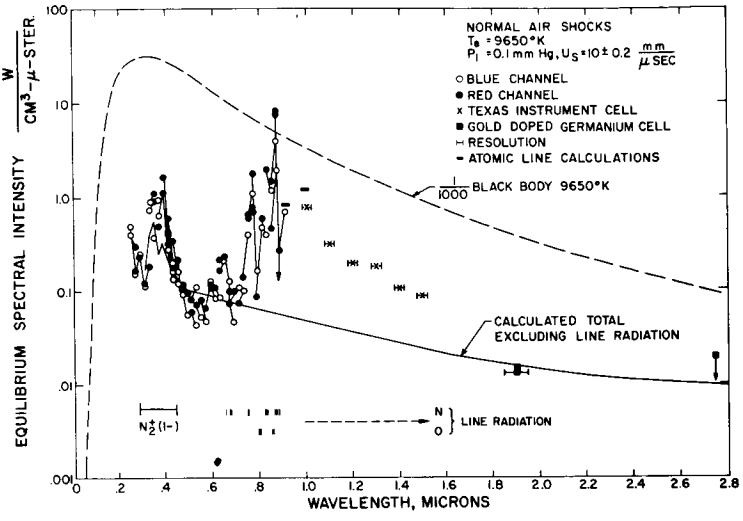

Figure 15: Equilibrium radiation data obtained by photomultipliers and infrared gauges versus wavelength obtained on incident air shocks U_s = 10 mm/μsec, P_1 = 0.1 mm Hg. The degree of ionization is about 10% (after Allen, Rose and Camm, Ref. 21).

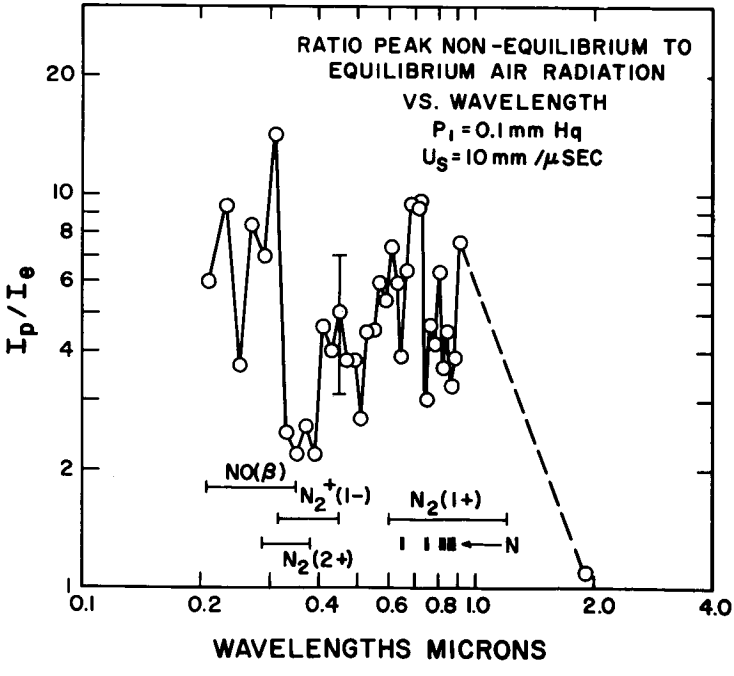

Figure 16: Ratio of peak non-equilibrium radiation to equilibrium radiation versus wavelength at super-satellite velocity according to Allen, Rose and Camm (Ref. 21).

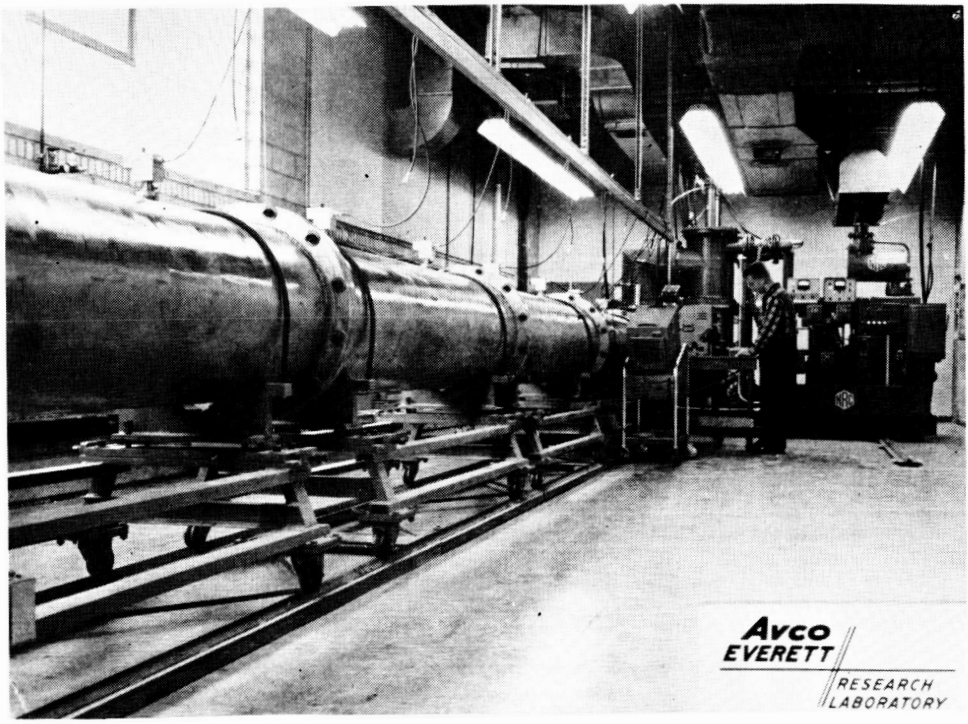

Figure 13: Photograph of a 24" diameter shock tube at the Avco-Everett Research Laboratory (see Ref. 19).

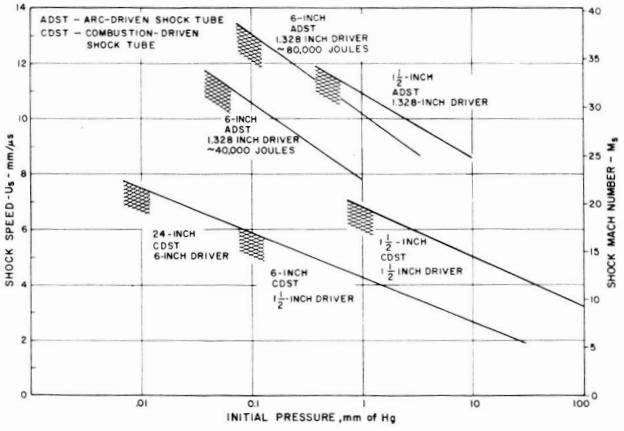

Figure 14: Approximate performance limits experienced for shock tubes presently in use. The combustion-driven shock tubes (CDST) are limited by a 10,000 psi driver pressure, and low density test time limitation depending on diameter. The arc-driven shock tubes (ADST) are limited by the energy density available in the driver, the expansion ratio between the driver and driven sections, and the test time limitation (after Camm and Rose, Ref. 20).

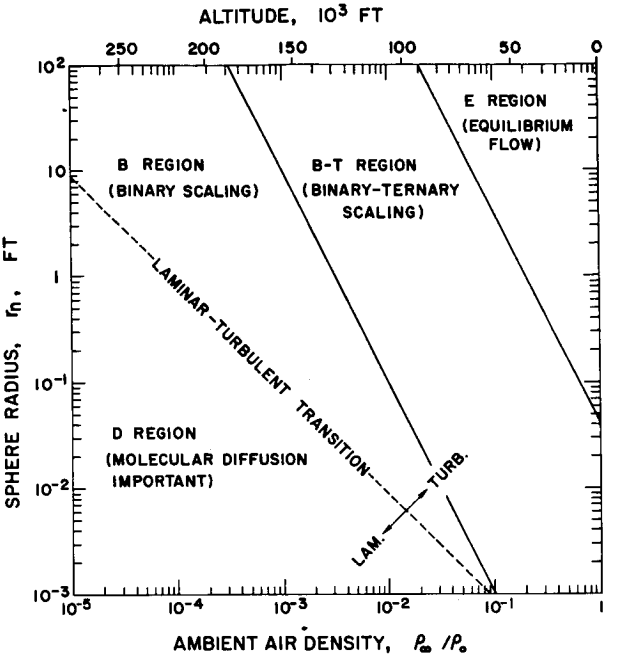

Figure 11: Approximate boundaries for scaling of chemically reacting hypersonic flow field behind spheres at 22,000 Ft/sec velocity in air (See Ref. 15).

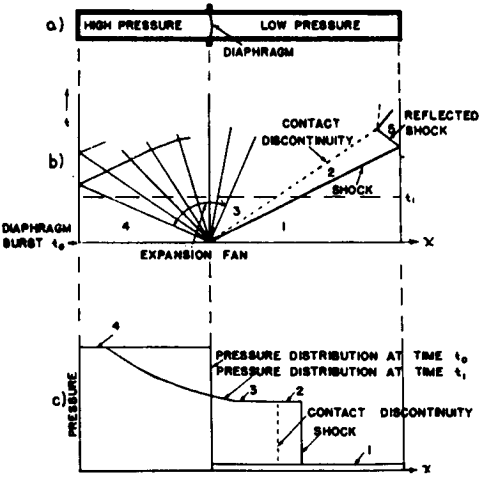

Figure 12(a): Schematic drawing of a conventional shock tube
(b): x-t diagram showing the progress of shock and expansion waves following the diaphragm burst. The gases which were originally in the high and low pressure portions of the shock tube are separated by the contact discontinuity.
(c): The pressure distribution along the shock tube at times t_0 and t_1.

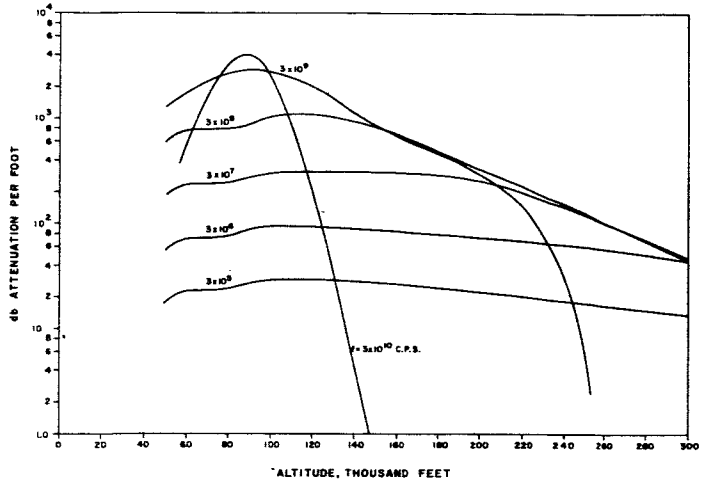

Figure 10(a): Attenuation of plane electromagnetic waves through the wake of a blunt body during re-entry for equilibrium ionization (Ref. 14).

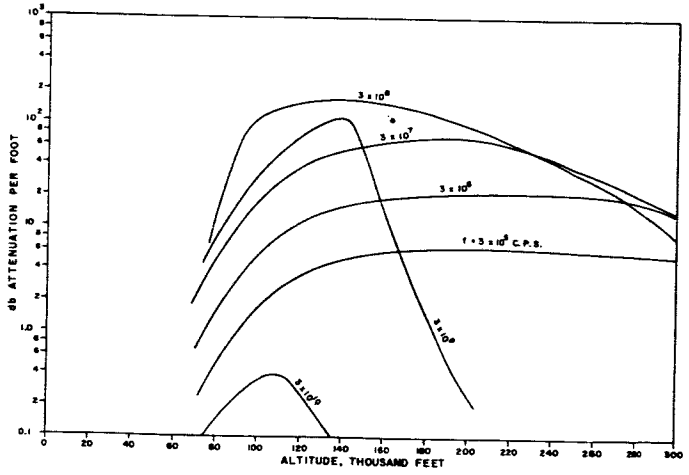

Figure 10(b): Attenuation of plane electromagnetic waves through the wake of a blunt body during re-entry for frozen ionization (Ref. 14).

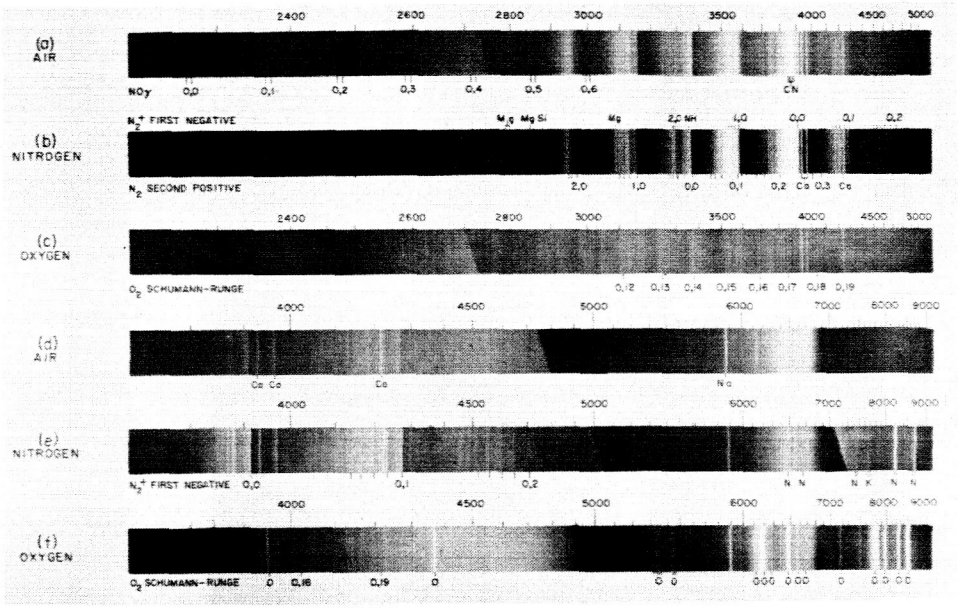

Figure 8: Shock tube spectra of high temperature air, nitrogen, and oxygen obtained by Keck, Camm, Kivel and Wentink (Ref. 9).

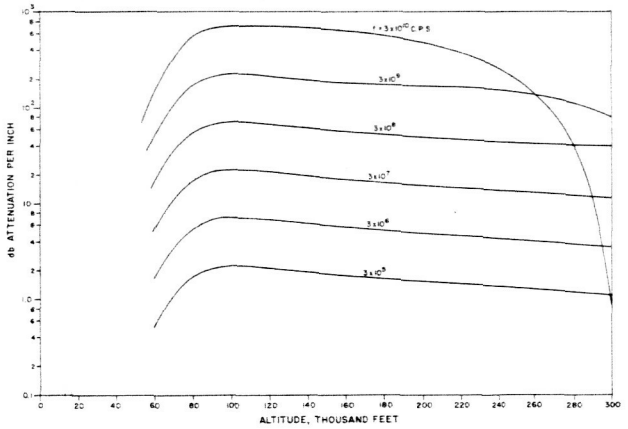

Figure 9: Attenuation of plane electromagnetic waves through the bow shock layer of a blunt body during re-entry (Ref. 14).

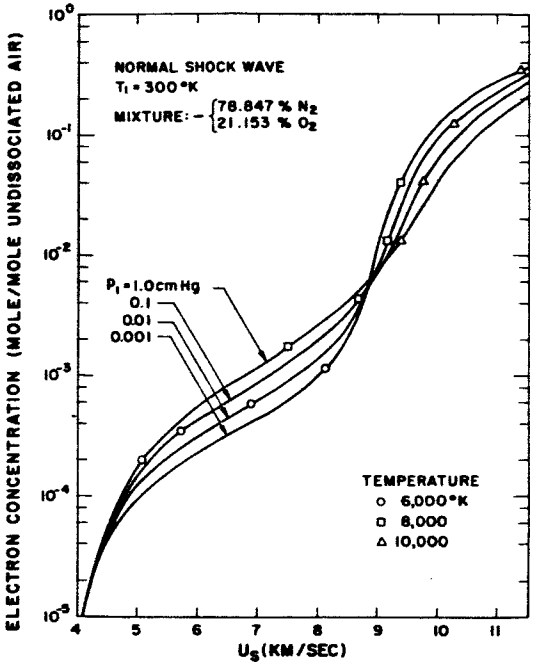

Figure 6: Equilibrium degree of ionization behind a normal shock wave in argon-free air as a function of shock velocity for a range of values of initial pressure, p_1, in the undisturbed gas. The variation of equilibrium temperature with shock speed is also shown (see Ref. 5).

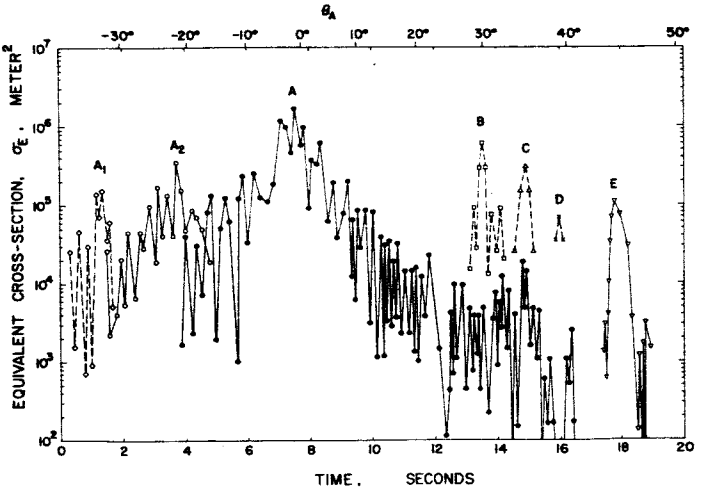

Figure 7: Back-scatter cross section of MA-6 Mercury capsule during re-entry observed by Lin, Goldberg and Janney(Ref. 8).

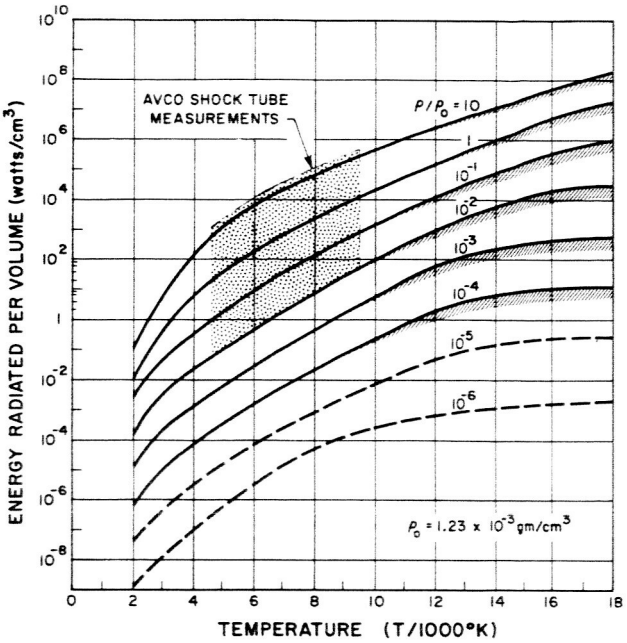

Figure 4:
Total emitted radiation energy per unit volume of high temperature air in full equilibrium as a function of temperature for constant values of the density. (see Ref. 2).

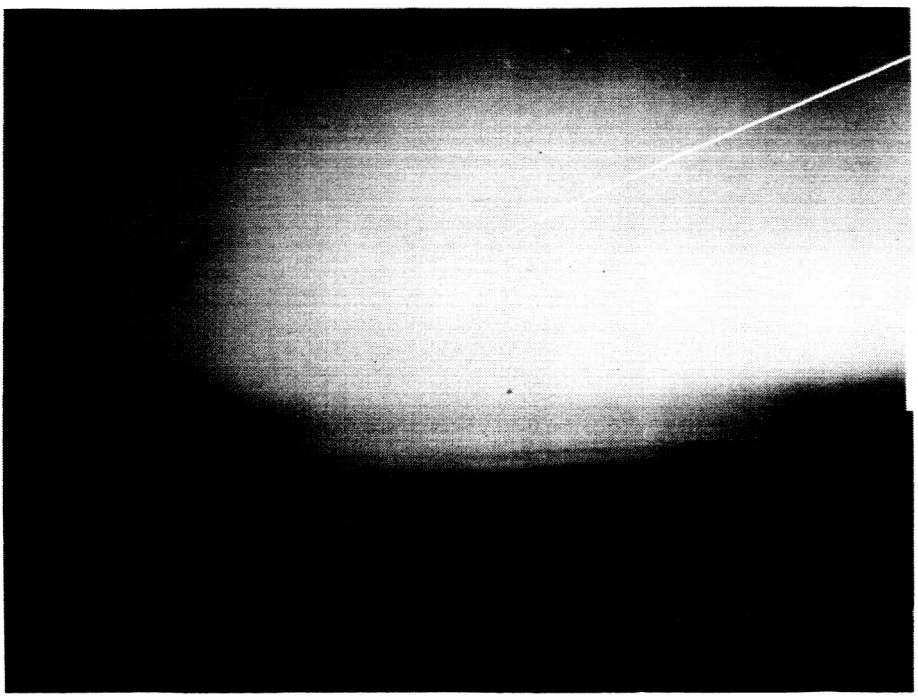

Figure 5: Ballistic camera photo of ICBM nose cone re-entry over the South Atlantic, taken by the Avco-Everett Research Laboratory Re-entry Experiments Operation (Ref. 4).

FLIGHT REENTRY EXPERIMENTS

by

Herbert A. Wilson, Jr.

and

Robert L. Wright

NASA - Langley Research Center

INTRODUCTION

Reentry technology has long depended on the simulation provided by wind tunnels, shock tubes, arc jets, and a variety of other ground facilities to advance the experimental verification of the results predicted from theory or postulated empirically from previous tests. As the application of information thus obtained approaches the point of application to the design of flight systems, the question of the extent to which the information can be applied with confidence inevitably arises. Sources of uncertainty are the assumptions necessary to obtain theoretical solutions, the inadequacy with which the complex reentry environment can be totally simulated on the ground, and the question of how well the ground facility results have been validated by flight comparisons. Thus the value of flight reentry testing is greatest when the tests either explore the nature of a phenomenon, difficult or impossible to simulate on the ground, or provide the validation for use of a system or concept developed from ground-based research.

The discussion presented outlines the current activity in flight reentry research at the Langley Research Center in terms of the techniques being used in a number of flight projects to investigate reentry environment, radio attenuation, materials behavior, and observable phenomena.

Several of the other papers given in these proceedings have highlighted some of the difficulties of simulating flight reentry phenomena in ground facilities. These center mainly on the size of the model that can be tested, the duration of the test, and the level of the variables determining heating rate. Virtually all ground facilities make compromises in at least one of these significant variables. The nature of these compromises is defined in figures 1, 2, and 3. Typical Mach number-altitude corridors for ballistic and lifting reentry bodies currently of interest are shown in figure 1. In figure 2, the capabilities of the so-called "cold" hypersonic facilities are superimposed on the reentry corridors. These facilities (most notably the 22-inch helium tunnel) cannot match the stream enthalpy, therefore are limited as to heating input, but can provide high Mach number basic fluid dynamics data. Capabilities of the "hot" hypersonic facilities are shown overlaid on the same reentry corridors in figure 3. These facilities give a reasonable simulation at low velocity, but for increasing flow velocity, they generally tend to fall off in their simulation of the heating. One exception is the expansion tube which suffers the characteristic difficulty of shock-type facilities in that the experiment time is small, that is, milliseconds or microseconds instead of minutes.

FLIGHT-TEST IMPLEMENTATION

A reentering body, generally speaking, first meets the atmosphere at a high altitude and a high velocity and slows down as it penetrates the atmosphere. Typical flight-test trajectories and the atmospheric environment they traverse are shown in figure 4. The trajectories shown are the Scout R-4 and ST-8 reentries. The hashed area indicates a proposed materials test at 40,000 fps. All of the vehicles to be discussed later fly trajectories similar to these, with the exception of the RAM (Radio Attenuation Measurements) vehicle, which flies a straightaway trajectory (not shown) with all data obtained on ascent.

This figure also indicates several conditions, such as oxygen dissociation, nitrogen dissociation, and ionization which characterize the environment in different regimes and account for a variety of different aerodynamic and flow-field effects. The region of the flight environment of greatest concern at the present is indicated as the Apollo Reentry Envelope and the current programs for obtaining data in this envelope will be discussed later.

Launch Vehicles

Flight programs are often identified in terms of the launch vehicle which may be misleading. Actually, the vehicles exist to support the program, and not vice versa, but vehicle nomenclature does in many cases provide a convenient reference to the program. The launch vehicles currently being used are shown in figure 5. The four-stage Pacemaker vehicle is a low-cost vehicle capable of speeds of the order of 14,000 to 16,000 feet per second. Its use enables low-cost flights for preliminary exploratory work, and for flights providing some overlap with ground facilities.

The payload capability of the Pacemaker is approximately 40 pounds. The RAM B vehicle is capable of boosting 200 pounds on a straightaway, ascending trajectory to a velocity of approximately 18,000 feet per second. The Trailblazer vehicle, used mainly in the field of reentry observables, imparts extremely high velocities (34,000 feet per second) to payloads on the order of 5 grams when equipped with a shaped-charge gun as a last stage.

The workhorse for our heavily instrumental payloads is the Scout vehicle which is used in both the four-and five-stage configurations. Reentry velocities and payload weights of 26,000 feet per second and 200 pounds, respectively, have been attained with the four-stage configuration and 28,000 feet per second and 150 pounds in the five-stage configuration. A photograph of the five-stage Scout vehicle in the launch tower is shown in figure 6. It should be noted that everything forward of the third stage is covered with a heat shield. Figure 7 shows a typical five-stage Scout reentry, in this case the ST-8 heating and environmental test which will be discussed in detail later. Launched from Wallops Island, the flight plan called for two stages firing upward and three downward or reentry-firing stages. A peak velocity of 22,500 feet per second was achieved with impact southeast of Bermuda.

A recent development is the Project Fire vehicle which consists of the Atlas-D boosting a second-stage X-259 motor equipped with a guidance and control system and a 200-pound spacecraft (fig. 5). The second-stage rocket and the guidance and control systems are adapted from the Scout vehicle. The Fire vehicle is capable of a reentry velocity of approximately 38,000 feet per second.

Data Acquisition

The spacecraft used with the launch vehicles just described are

tailored to the particular program requirements. A key factor in each spacecraft is the selection of the sensors, transducers, and other data acquisition system components. A summary of the measurements and sensor selection for the Fire Project Reentry spacecraft is shown in figure 8. Figure 9 shows a block diagram of the instrumentation for a typical spacecraft for monitoring and transmitting the transducer data. Such data as temperature measurements are usually commutated, while pressures and accelerations are measured continuously. The telemetry system provides for broadcasting data in real time through one transmitter and antenna system. Inasmuch as the reentering spacecraft experience communications blackout, it is necessary to circumvent this problem with a delay train. A delayed tape unit with a delay long enough to last through the blackout period stores these data until the vehicle has slowed to less than 10,000 feet per second. At this time, all of the measurements that occurred during reentry are rebroadcast until impact. This technique has been very useful and is used on all of the five-stage Scout reentry shots and the Fire Project.

With a recoverable system, an onboard recoverable recorder will provide additional redundancy. On the Pacemaker vehicle, a recovery system was developed, consisting of a sequence of drogue-chutes and parachutes to provide a gradual descent into the ocean. Beacons provide locations aids for rapid recovery and all the data are obtained from the onboard recorder. This recovery technique system is indicated in figure 10.

FLIGHT-TEST PROGRAMS

The preceding sections have reviewed the test conditions that can

be simulated by ground facilities and flight tests, and outlined flight-test implementation in terms of available launch vehicles and methods of data acquisition. With this material as a background, the role of simulation in flight reentry experiments can be determined by looking at the details of some specific flight programs. The flight programs to be discussed deal with investigations of one or more of the following problem areas:

(1) Environmental (heating);

(2) Materials response;

(3) Communications problems; and

(4) Observables.

These categories are essentially areas of interest which will provide basic data for determining design parameters and trade-offs in the design of a full-scale spacecraft that must reenter the earth's atmosphere, such as Apollo or future interplanetary exploration vehicles.

Environmental

The first environmental spacecraft to be discussed is the Scout ST-8 reentry package. A photograph of the spacecraft is shown in figure 11. Spacecraft components and pertinent dimensions are presented in figure 12. The chief feature of the environmental payload is the inconel nose cap calorimeter, whose purpose was to provide quantitative total heat-transfer information during the first 15 seconds of reentry. Beneath the inconel nose cap was a teflon nose cap to protect the spacecraft and instrumentation package. Ablation sensors were mounted on the front of the nose cap to provide further information on the heating during the later part of the reentry. A canister contained the instrumentation, including the delay train system described earlier, with the actual structure of the vehicle afterbody serving as the antenna.

The sequence of events during reentry is indicated on the velocity-altitude diagram in figure 13. Low-level calorimeter heating data were obtained above 300,000 feet. The prime heating data occurred as the spacecraft descended from 300,000 to 200,000 feet, where the inconel cap melted. After the inconel nose cap melted, the ablation sensors in the teflon nose cap provided overall measurements of the ablation recession due to total heat input. A typical temperature history obtained during the prime heating period is shown in figure 14 to indicate the good quality of the data obtained from the flight.

A further step in investigation of hypervelocity environment has been undertaken by the Fire Project which has primary emphasis on the heat-transfer process at lunar return velocity of about 38,000 feet per second. Figure 15 is a representation of the total heat pulse and radiative heat pulse that would occur for a reentry at 37,000 to 38,000 feet per second. At this velocity, the total heat is predominately convective, but the speed is sufficiently high for the radiative heating to become appreciable. At the outset of the Fire Project, there was considerable speculation on whether or not this radiative heating had a large input due to nonequilibrium. A primary part of the Fire objective was to evaluate the nonequilibrium radiation. Since then, however, estimates of nonequilibrium heating indicate the problem to be considerably less serious than expected. Nevertheless, a major objective of the Fire Project was the determination of the total heating at high speeds and, in particular, the division of the total heating between radiation and convection.

To facilitate this objective, total heat transfer was measured by means of a rather complex succession of metal calorimeters on the front of the spacecraft using thermocouples as sensors. Hot gas radiation was

measured through windows in the stagnation region, at the shoulder of the body, and in the afterbody. Spectral measurements were made at the stagnation location and total radiometers were provided at all three windows. Materials response (regression rates) and radio attenuation information was also obtained.

The Project Fire reentry package and its supporting structure (the conical adaptor on top of the last-stage motor) can be seen in figure 16. The reentry package, similar in shape to the Apollo, had three calorimeters which were designed to be effective at different times during the flight. The reason for using three calorimeters is illustrated in figure 17. It is obvious that a single calorimeter could not be designed to survive the entire flight. The total heat pulse curve shows that portion of the heat pulse for which each of the three calorimeters would provide data. An ablation material was placed between the calorimeters to protect the subsequent calorimeter until exposure. Therefore, with this sequence of calorimeters, enough of the total heating pulse curve could be obtained so that, with the aid of theory, the entire heat pulse curve could be determined. Figure 18 presents the mission profile and the major sequence of events in the Project Fire trajectory. Reentry at a velocity of 37,800 feet per second occurred in the vicinity of Ascension Island, 4500 miles downrange from Cape Kennedy, the launch site.

Figure 19 presents a summary of flight-test data available from aerodynamic heating environmental experiments. Most of the data have been obtained from blunt-nosed configurations. The Fire Spacecraft which was Apollo shaped and the other heating projects were mainly blunt nosed. However, many of the spacecraft that will fly in the future will not necessarily

be blunt-nosed bodies by any means. An experiment on which preliminary work is currently being performed, utilizes the long, slender and relatively sharp cone shown in figure 20. The objectives of the experiment are to determine turbulent heat-transfer results at a velocity of approximately 20,000 feet per second (approximately twice the speed for which any similar data are available). These results are important not only for long conical bodies, but for vehicles such as the space plane or any type of glide reentry vehicle which operates at a relatively high Reynolds number and depends on radiation heat transfer to dissipate some of its heat. Thus, this vehicle must be long (10 feet) and flown at relatively low altitudes for at least a portion of its trajectory to assure turbulent flow over the last part of the cone.

Materials Reponse

In the materials response area, as discussed earlier by Mr. Brooks, there have been diverse predictions made from the available ground test data. Flight tests therefore are useful for determining which predictions are most reliable. A sectioned view of a 3-inch-diameter specimen tested in an arc-heated facility is shown in figure 21. A section of a heat shield of the same material from a flight model which experienced a similar total heating history is seen in figure 22. It is evident that the char layer from the flight test is much thinner than that from the ground test.

In other cases, phenomena difficult to test on the ground can be investigated. Figures 23 and 24 show the results of a flight test to determine possible effects on heat shield behavior of meteorite damage before reentry. The flat-faced model, roughly 6 inches in diameter, is shown in figure 23 before flight. Three ablation sensors were mounted

across the front face and a 1/4-inch-diameter hemispherical crater was located approximately 1 1/2 inches from the stagnation point. A second indentation, simulating meteorite damage, is seen on the cylindrical portion of the spacecraft. The spacecraft was test flown on the Pacemaker vehicle and recovered. Figure 24 shows the damage resulting from the change in the flow field caused by the simulated meteorite damage.

The prime objective of the Scout R-4 experiment, flown August 18, 1964, was to provide a real environment test of a candidate material for the Apollo heat shield to verify test work done in ground facilities. As the spacecraft and experiment were discussed fully in the presentation by Mr. Brooks, no further discussion is considered necessary.

Communication Problems

The communications blackout or attenuation of radio signals due to the ionizing sheath around a spacecraft during reentry is currently being investigated by the RAM (Radio Attenuation Measurements) program. Figure 25 indicates the velocity regimes for various ionization reactions, including molecular, atomic, photo and electron-impact ionization. Also noted in the figure are the regimes investigated by the RAM flight tests. RAM A and B flights have produced good measurements of the attenuation for VHF C-band and X-band frequencies in the molecular ionization range with straightaway or ascending flights. A considerable amount of work has also been done in this regime with ICBM tests. Proposed RAM C flights will investigate the velocity band where atomic ionization is fully developed. Future tests will measure the blackout region for flight velocities above 30,000 feet per second.

A diagram of the RAM C spacecraft is shown in figure 26. The spacecraft is 20 inches in diameter at the base, 38 inches long, and weighs

several hundred pounds. The important things to note on the diagram are the VHF, C-band, and X-band antenna systems with the associated telemetry equipment.

Figure 27 presents the C-band and VHF blackout regions. The boundaries were established with a combination of the theory and flight tests. RAM and Mercury trajectories from which some of these data were obtained are indicated on the figure as is the proposed Apollo trajectory.

Observables

NASA and the Smithsonian Astronomical Observatory are currently engaged in a joint project whose purpose is to create artificial meteors. The objectives of this project are found in figure 28.

Trailblazer I and II vehicles were used to impart reentry velocities of approximately 34,000 feet per second to a simulated meteor. A 5-inch-diameter rocket motor was mounted atop the four-stage vehicle. A shaped-charge accelerator was connected to the fifth-stage spherical motor as shown in figure 29. After burnout of the fifth stage, the shaped charge is detonated, compressing the spit-back tube into a pellet which is propelled through the inhibitor as an artificial metoer at extremely high velocity. The velocity, deceleration, light intensity, and spectra of the simulated meteor can be measured. Also, with the aid of ground test firings, pellets can be recovered and the mass and shape determined.

Thus, by injecting an artificial meteor of approximately known mass at a known velocity and at a location where observation stations have been placed, it is possible to calibrate observables for natural meteors to determine more accurately the luminous and ionization efficiency.

A typical meteor reentry flight profile is shown in figure 30. The first two stages fire upward to attain an altitude of about a million feet

and the last three stages and shaped-charge accelerator fire downward to impart the needed reentry velocity. Launched from Wallops Island, the pellet impacts some 100 nautical miles downrange, making the east coast from Wallops to Hatteras available for setting up optical and radar observation sites. Other meteor simulation tests, using two-stage Nike-Cajun vehicles with the shaped-charge accelerator, have produced reentry at lower velocities to provide luminous efficiency data over a range of reentry velocities. Figure 31 shows some results of the Meteor Simulation Project. The theory of Öpik, developed in 1958, for the luminous efficiency of meteors is indicated for a range of reentry velocities.

CONCLUDING REMARKS

The foregoing discussion has shown the way in which flight testing supplements, extends, and reinforces the usefulness of data from ground test facilities. Flight tests can provide an anchor point in evaluating ground test data. Although flight tests can avoid some of the inherent problems of ground facilities, they are expensive, putting a premium on each test to provide the most data that can be acquired.

The portions of the reentry flight spectrum which can be simulated by "hot" and "cold" ground facilities are reviewed and some of the current flight programs for obtaining data in the Apollo Reentry Envelope are discussed. The programs are categorized as to (1) environment (heating), (2) materials response, (3) communication problems, and (4) observables. A discussion of the launch vehicles, unknown parameters, and methods of data acquisition for each program is presented.

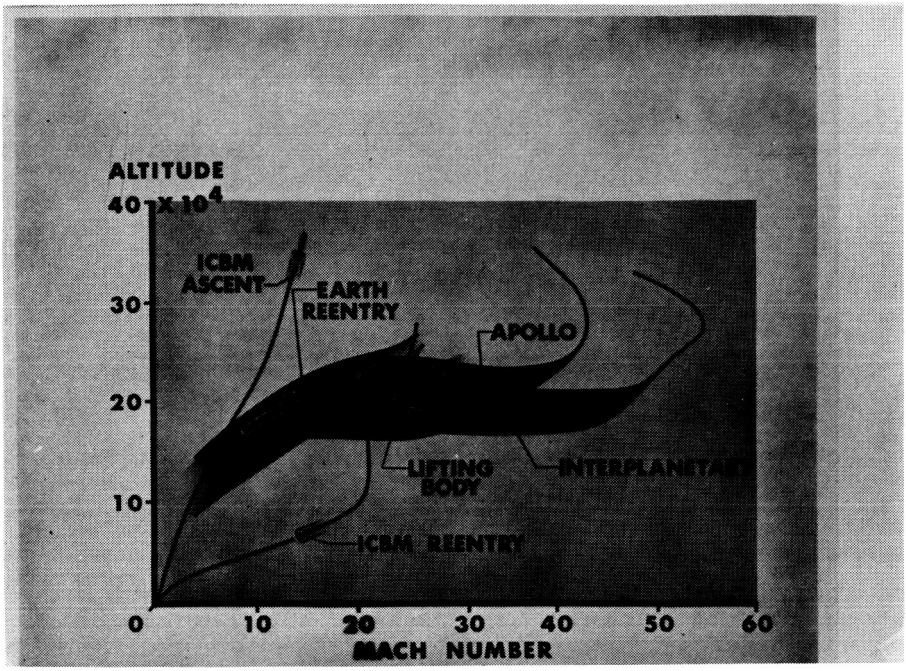

NASA

Figure 1 Typical reentry corridors

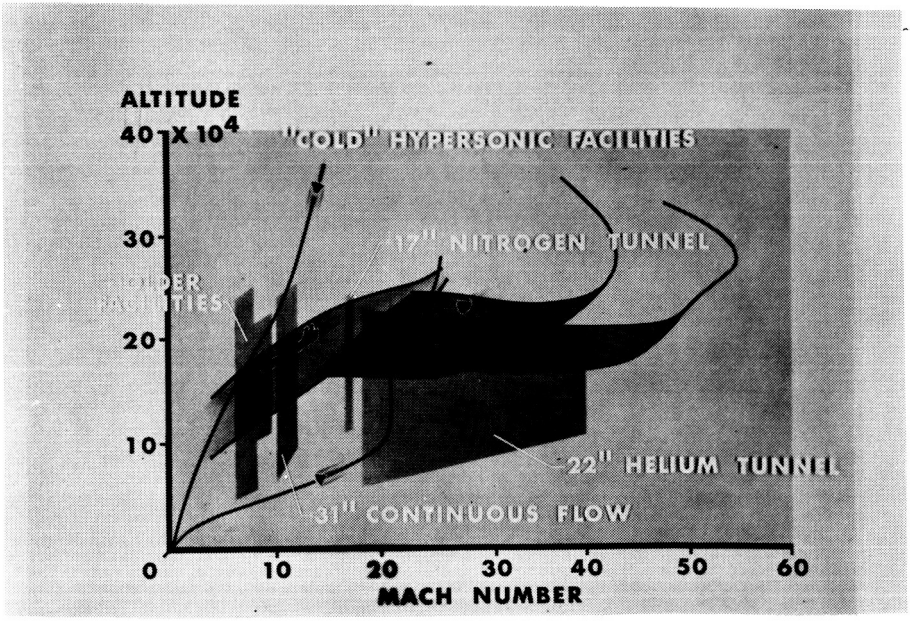

NASA

Figure 2 Capabilities of "cold" hypersonic ground-test facilities

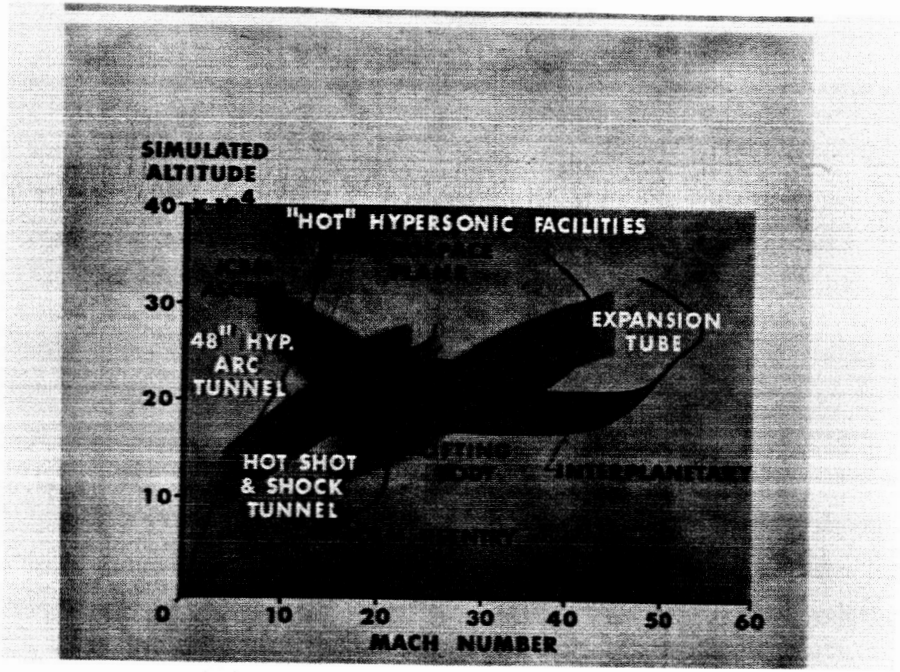

NASA

Figure 3 Capabilities of "hot" hypersonic ground-test facilities

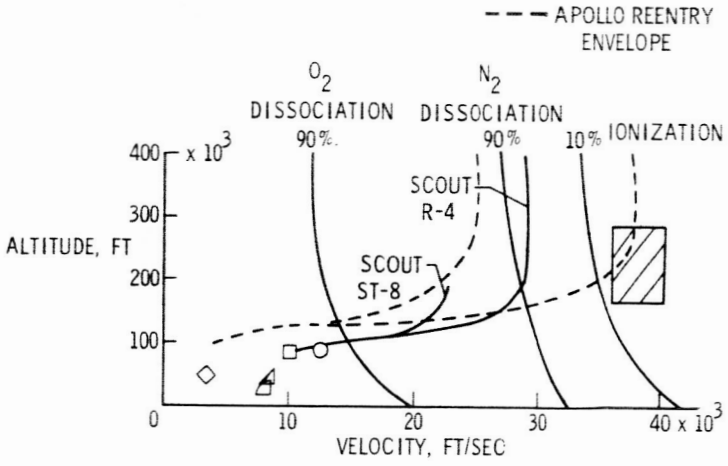

NASA

Figure 4 Typical flight-test trajectories and environment

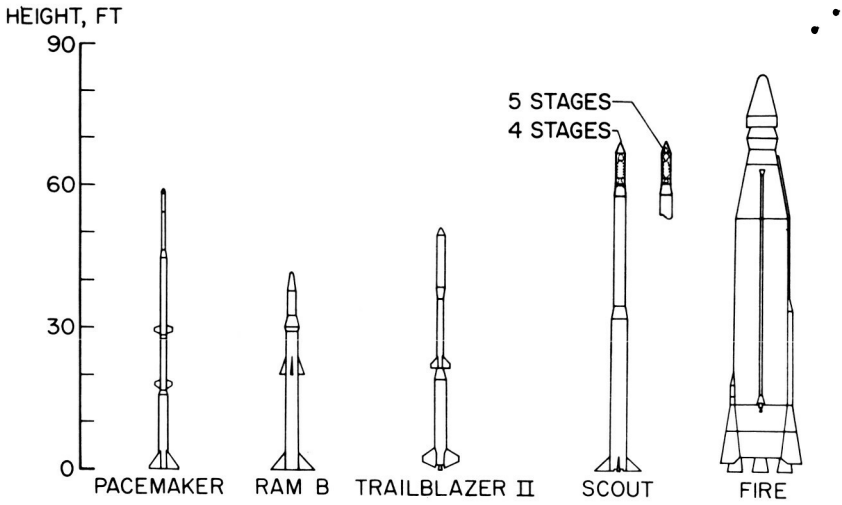

NASA

Figure 5 Reentry launch vehicles

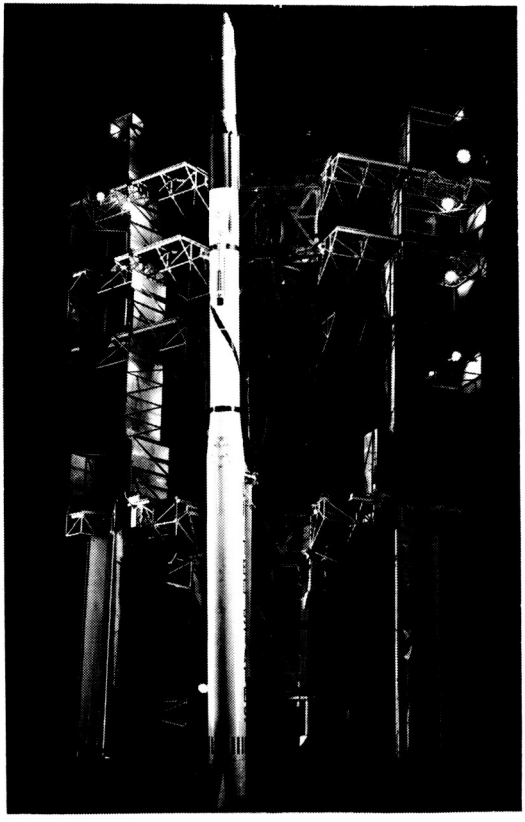

NASA

Figure 6 Five-stage Scout vehicle in launch tower

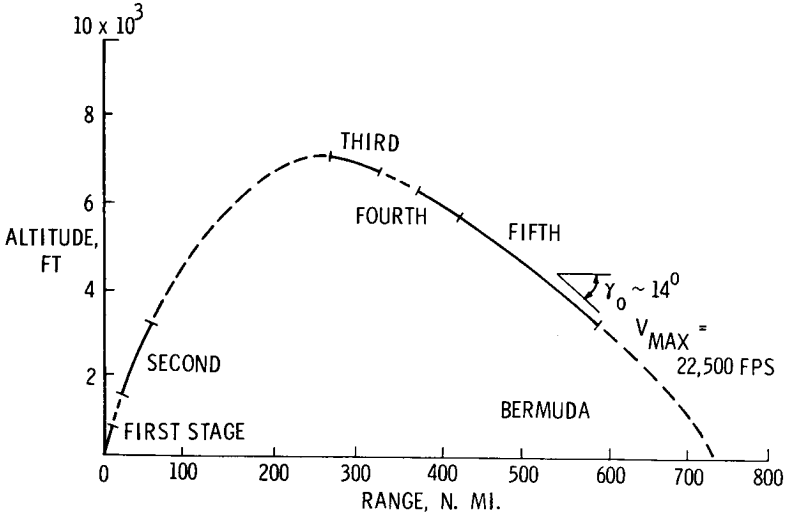

Figure 7 Typical Scout reentry trajectory

RESEARCH MEASUREMENTS

MEASUREMENT	METHOD	SENSOR
TOTAL HEAT TRANSFER	METAL CALORIMETERS	THERMOCOUPLES
HOT GAS RADIATION	WINDOW AND RADIATION SENSOR	TOTAL AND SPECTRAL RADIOMETERS
MATERIALS RESPONSE	REGRESSION RATE	THERMOCOUPLES STEPPED IN DEPTH
RADIO ATTENUATION	ANTENNA CHARACTERISTICS	VSWR, IMPEDANCE, AND SIGNAL RECEPTION

Figure 8 Research measurements and sensors

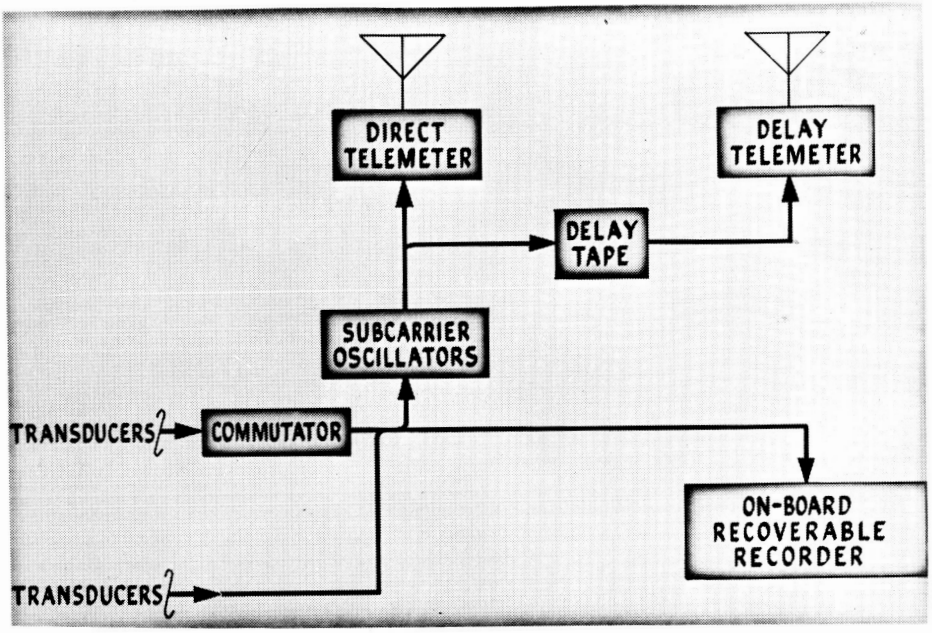

NASA

Figure 9 Data acquisition instrumentation

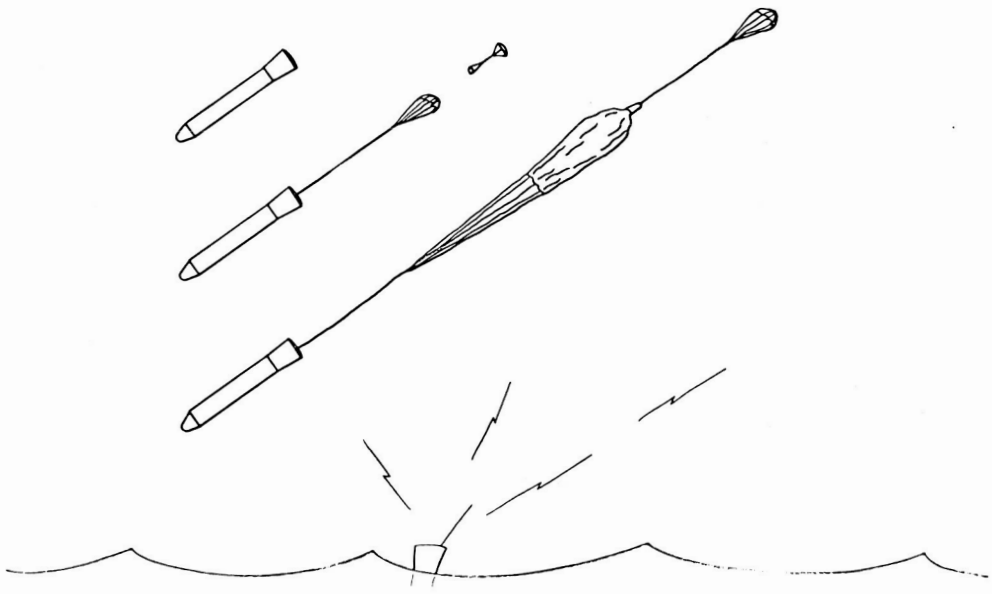

NASA

Figure 10 Spacecraft recovery system

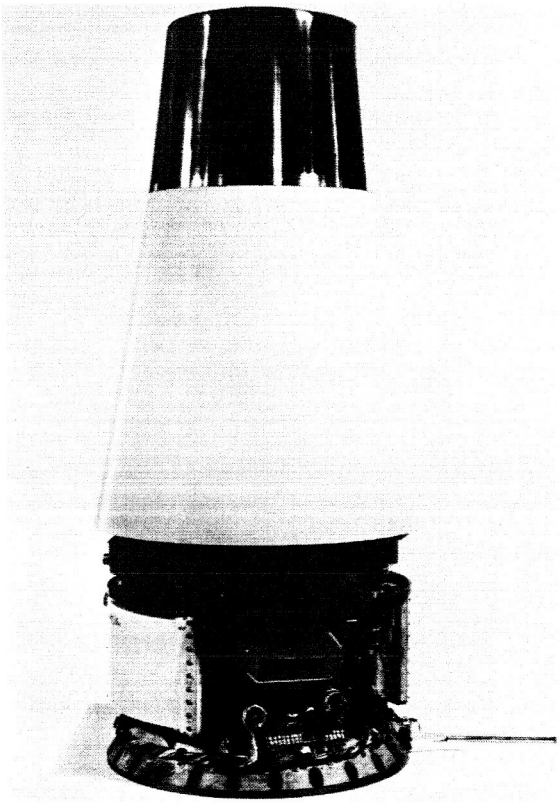

Figure 11 Scout ST-8 reentry package

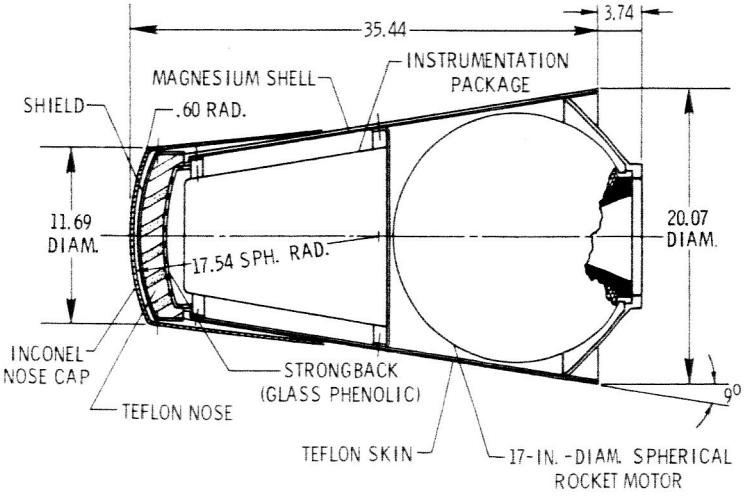

Figure 12 Scout ST-8 components

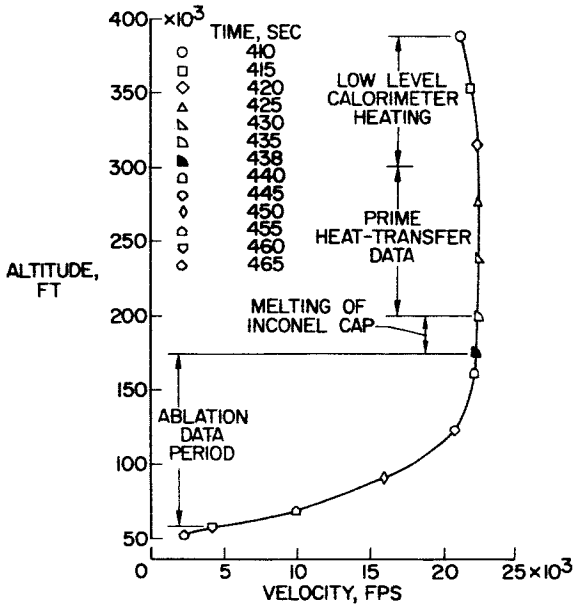

Figure 13 Sequence of events during ST-8 reentry

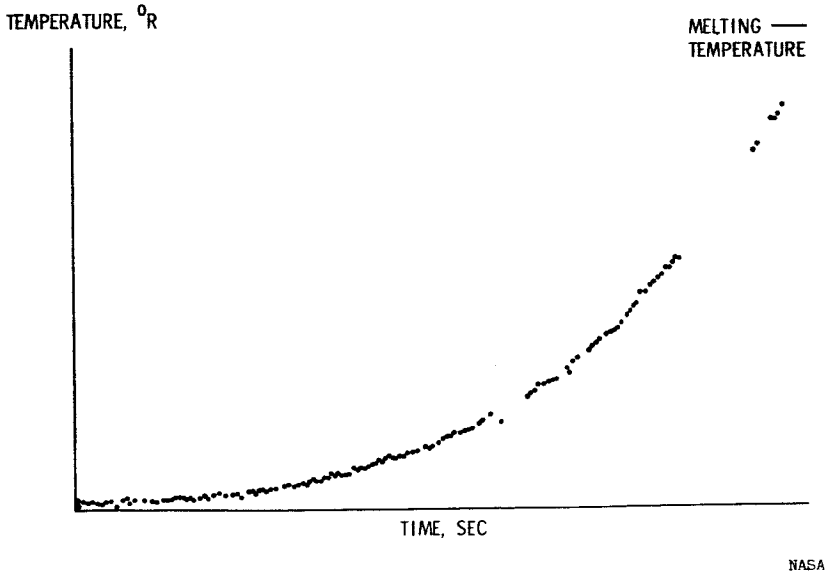

Figure 14 Typical temperature history during prime heating period

SCHEMATIC HEATING TIME HISTORIES

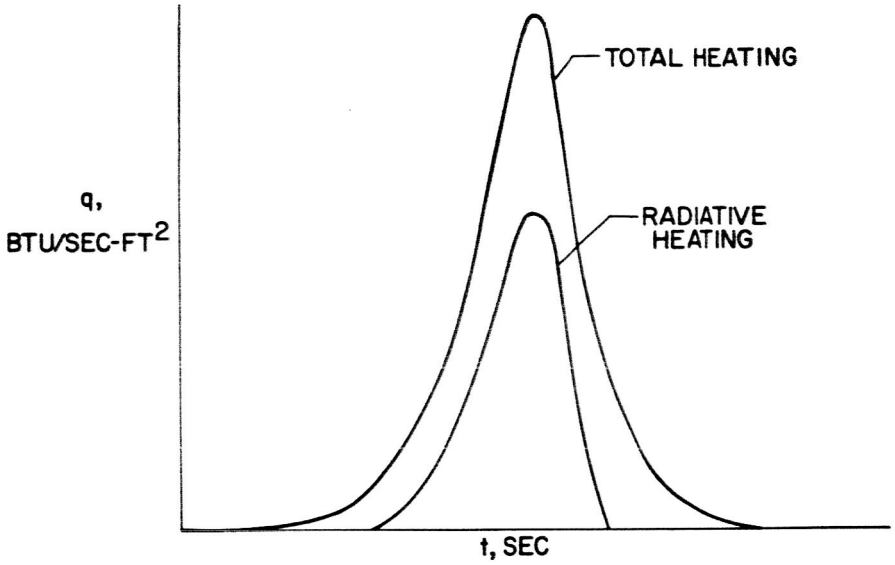

Figure 15 Approximate total and radiative heat pulses for a 38,000 fps reentry

PROJECT FIRE REENTRY PACKAGE

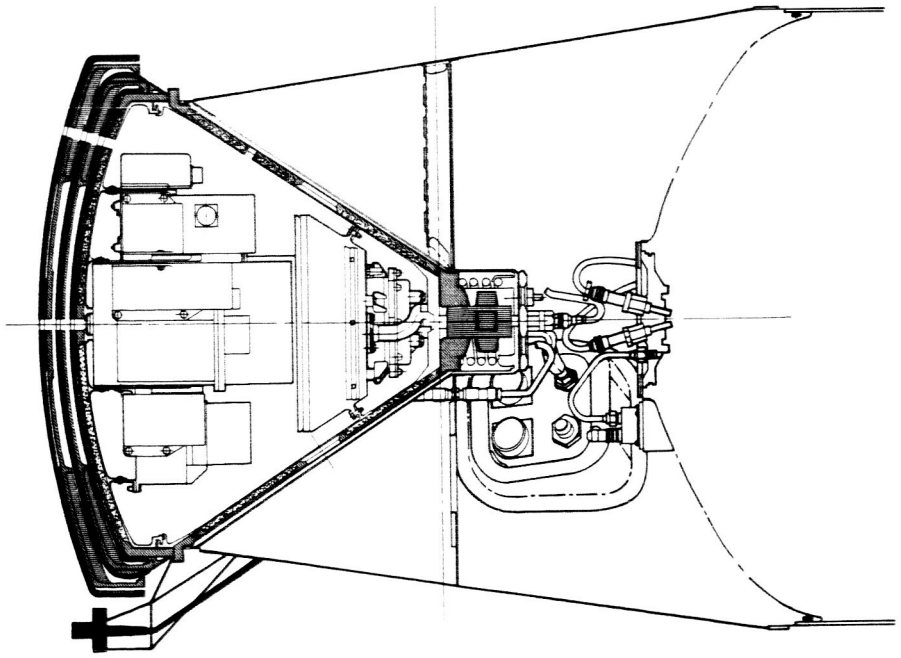

Figure 16 Project Fire reentry package and supporting structure

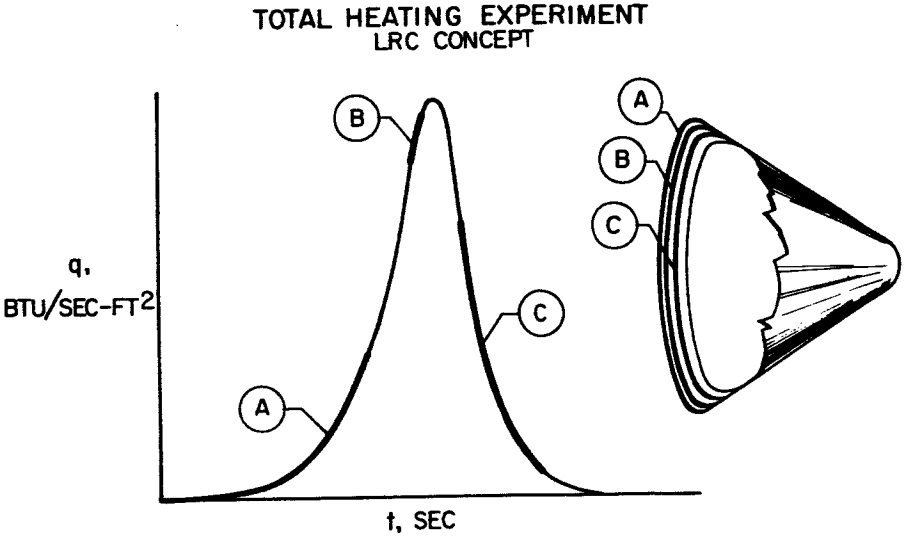

Figure 17 Portions of the heat pulse for which each calorimeter provided data

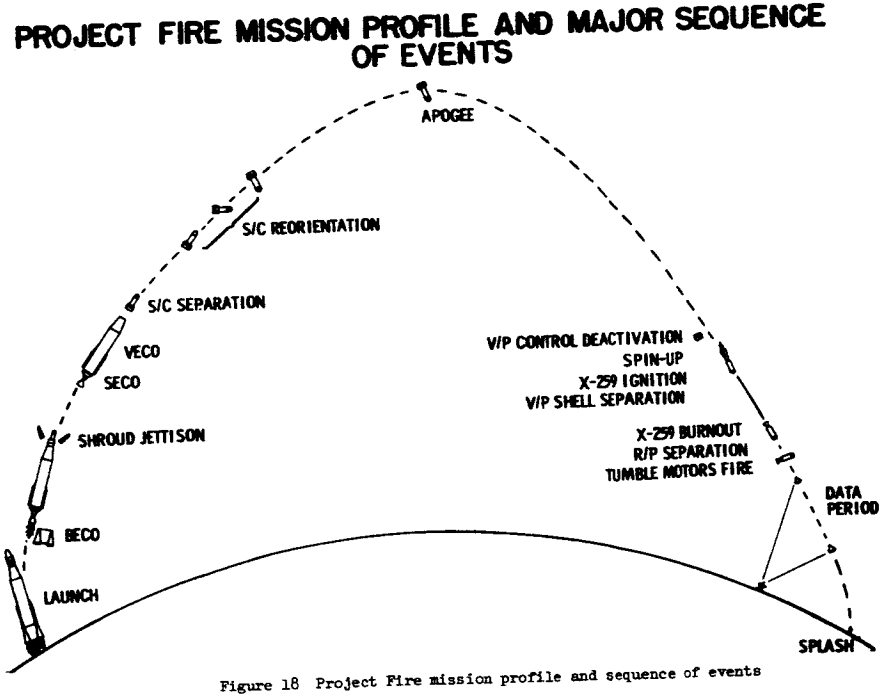

Figure 18 Project Fire mission profile and sequence of events

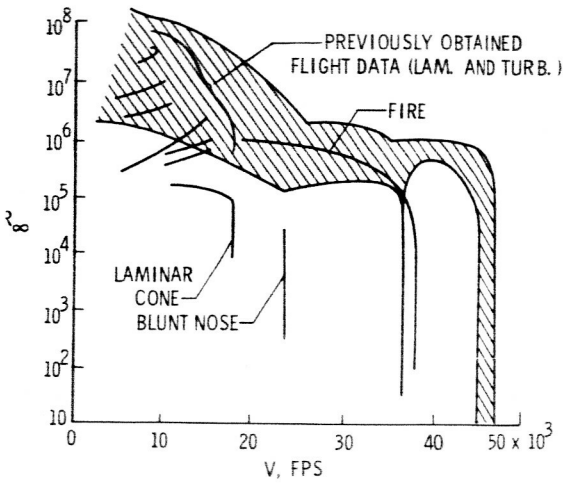

NASA

Figure 19 Summary of flight-test testing data

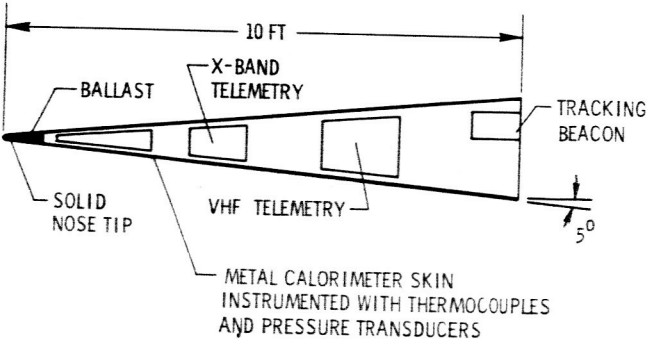

NASA

Figure 20 Turbulent heat-transfer experiment spacecraft

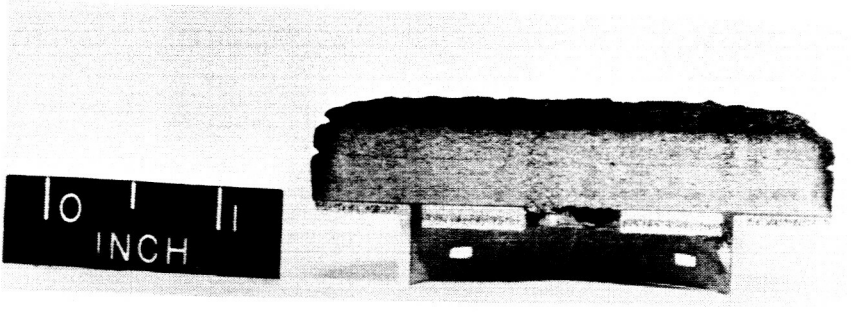

NASA

Figure 21 Ground-test ablation simulation specimen

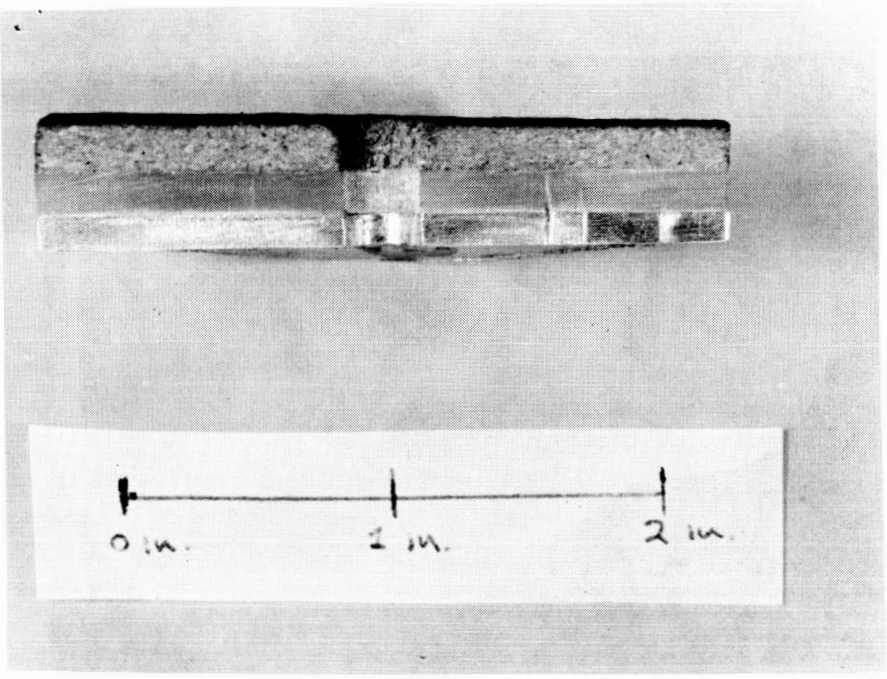

NASA

Figure 22 Flight-test ablation simulation specimen

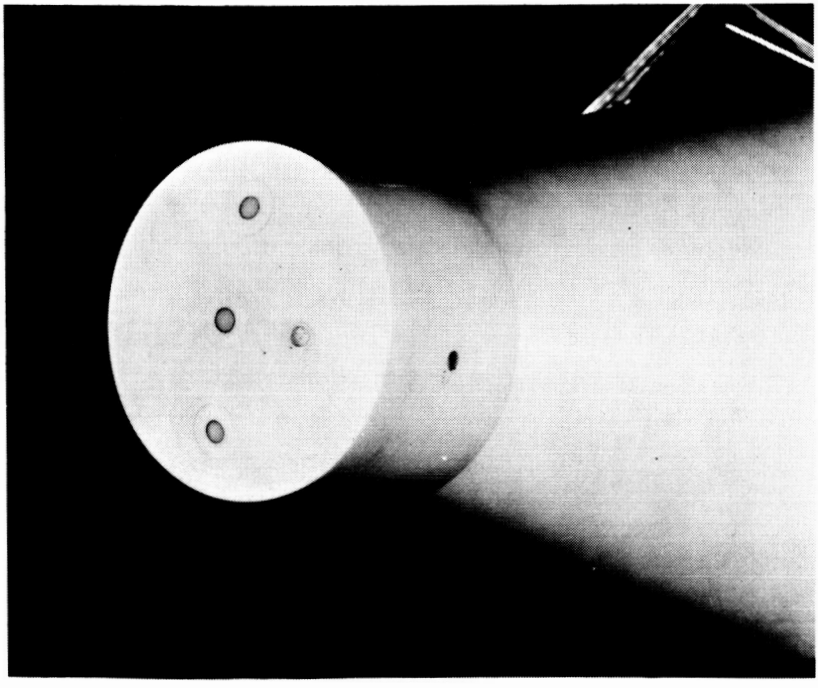

NASA

Figure 23 Meteorite damage ablation model before flight

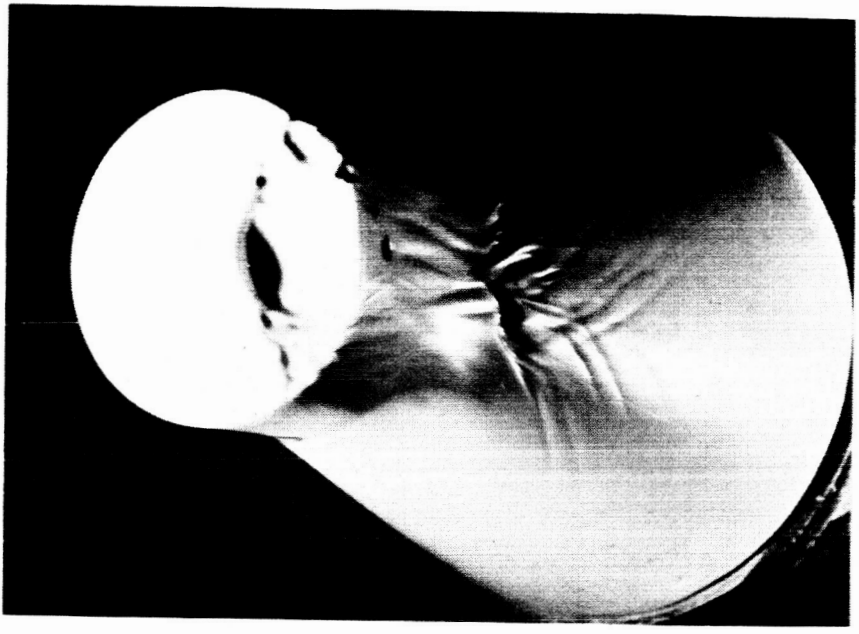

NASA

Figure 24 Meteorite damage ablation model after flight

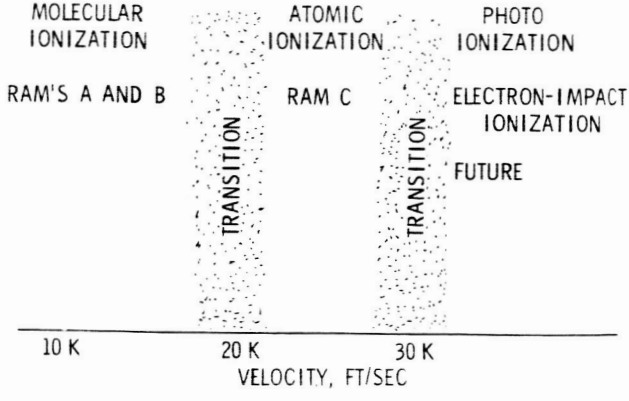

NASA

Figure 25 Velocity regimes for ionization reactions

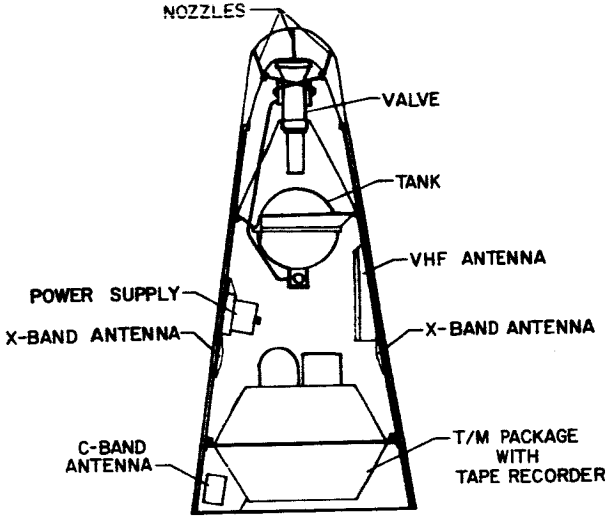

NASA

Figure 26 RAM spacecraft

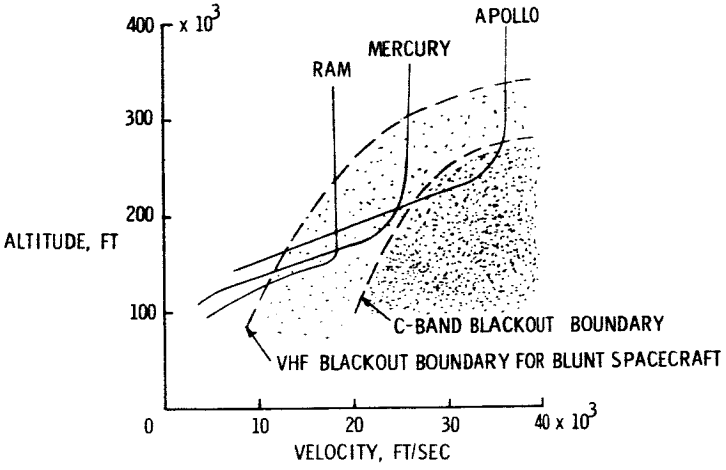

NASA

Figure 27 VHF and C-band blackout regions

OBJECTIVES:

1. CALIBRATE THE OBSERVABLES FOR NATURAL METEORS
   (a) BY OPTICAL MEASUREMENTS
   (b) BY RADAR MEASUREMENTS
2. DETERMINE TWO KEY COEFFICIENTS IN THE PHYSICAL THEORY OF METEORS FOR EACH OF THE PREDOMINANT METALS FOUND IN NATURAL METEORS
   (a) LUMINOUS EFFICIENCY, $\tau = \frac{\text{LIGHT ENERGY}}{\text{KINETIC ENERGY}}$
   (b) IONIZATION EFFICIENCY, $\tau_q = \frac{\text{IONIZATION ENERGY}}{\text{KINETIC ENERGY}}$
3. REENTER PURE METALS AT 10 TO 25 KM/SEC
   (a) ROCKET VEHICLES
   (b) SHAPED CHARGES

NASA

Figure 28 Meteor simulation project objectives

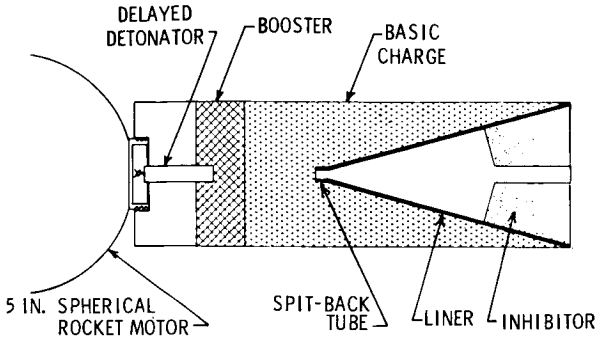

NASA

Figure 29 Shaped-charge accelerator

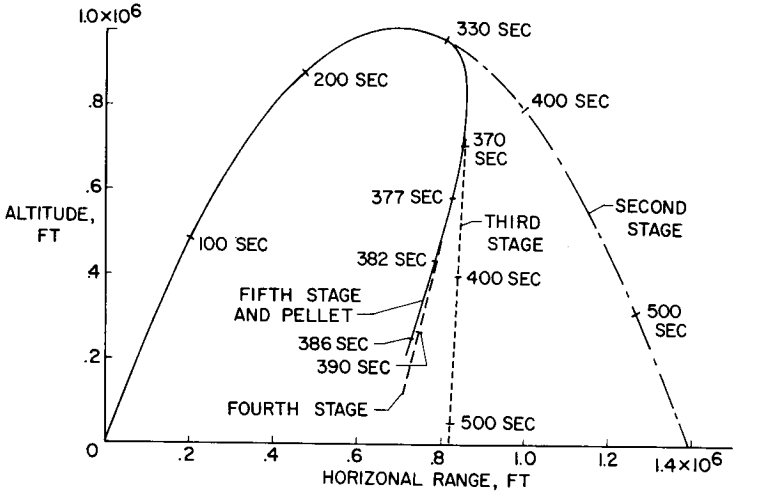

NASA

Figure 30 Typical simulated meteor reentry flight profile

LUMINOUS EFFICIENCY

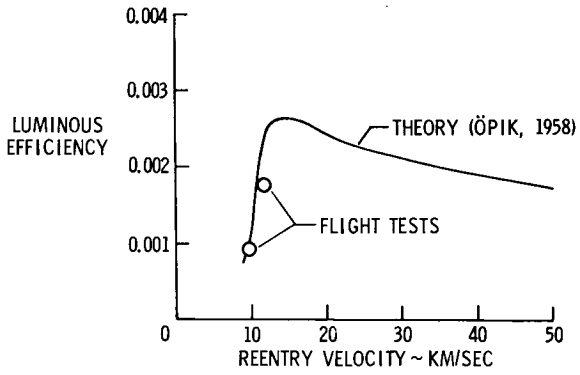

Figure 31 Luminous efficiency results

BACKGROUND OF PILOTED SIMULATOR DEVELOPMENT

by

C. B. Westbrook

Wright-Patterson AFB

ABSTRACT

In this paper a review is made of the piloted simulation facilities commonly used in the United States. An attempt is made to classify these facilities and to understand how and why these facilities are needed and came into being and how they are used. Some thoughts on the philosophy of use of simulation are offered and conclusions presented.

INTRODUCTION

In recent years the use of piloted simulators has become more and more widespread in the research and development process. In this paper a review is made of the simulation facilities in use in the aerospace industry and related organizations. An attempt is made to classify these facilities and to understand how and why these facilities are needed and came into being, and how they are used. It is hoped that this collection of information, the codifications, and the conclusions may be of benefit to those who use and are planning to use simulation facilities.

Before proceeding further, it is desirable to discuss the definition of

the word simulator. As commonly used by various individuals of differing interests, it has a rather widely varying definition. Simulators can be considered in the most broad sense as facilities which will allow an analog representation of a particular control element, combination of control elements or the complete flight control - airframe - pilot system. This would include simulators to obtain data on control hardware, the human pilot and his display, the airframe with elasticity, and the complete system. This paper is particularly directed at piloted simulators, those in which a human operator performs a control task; however, it is felt that consideration of the wide spectrum of simulators under this broad definition is useful in giving a perspective view of the subject.

CATEGORIZATION AND DESCRIPTION OF SIMULATORS

There are numerous ways in which simulators can be classified or grouped. Several ways will be discussed briefly. First there is the hazy concept of computation as differentiated from simulation. Another way of looking at simulators is by the phase of research and development in which they are commonly used. It will be observed that this division does not occur very neatly. Finally, simulators can be categorized relative to the element or elements of the flight control system that they are intended to obtain information on.

First, let us look at the area of simulators versus computation, for a moment. In 1935, Mueller at Massachusetts Institute of Technology devised an electrical device for solving the longitudinal stability equations. In Reference 1.35 in addition to reporting the result of his work, he predicts the possibilities of extending his device to real time and even to use of

hand controls and perhaps investigation of pilot training. During World War II and the years immediately following, rapid progress was made in development and application of differential analyzers. By 1948, electronic analog computers of significance were beginning to be available. The availability of these computers made possible the development of flight control system simulators as we know them today. All major aircraft companies in the United States have large general purpose analog computer facilities, ranging in size from 200 to 600 operational amplifiers or even larger. While simulators themselves, in a sense, these analog computers are used both for general computational purposes and also for connection with a cockpit and/or equipment to form a simulator.

While not a simulator by any stretch of the word, digital computers are making spectacular progress and have made improvement possible in scientific and engineering computations. A number of advanced operational flight simulators already use digital computers. It is undoubtedly true that the availability of these powerful tools will make possible further drastic improvements in simulation as they have done already in computation.

The phase of research and development of aerospace vehicles that you are concerned with influences considerably your choice of and use of simulators. These phases can be listed as (1) research, (2) preliminary design, (3) development, (4) flight test and (5) training and operational use. First is the research phase in which knowledge is gathered on various subjects of interest. Upon initiation of a program to design and build a vehicle, the preliminary design phase is encountered followed by detailed development of the vehicle and all of its components. The flight testing phase has its special needs for simulation. Finally, the phase is reached where the vehicles are in production and use and the operational commands are faced with

training and maintaining the proficiency of their crews.

Those using research and development simulators can thank the training simulator people for providing the motivation for and the development of many of the techniques and equipments necessary for what is used. Much of the literature on simulation in past years now relates to this area. During the early years, World War II and somewhat before, various techniques and devices called trainers were developed to meet the vast training problems. Hundreds of millions of dollars were spent on trainers during World War II in the United States alone. Expert opinion is that this expenditure saved much over actual flight, in fact, that training in flight would have been impossible. With the availability of analog computers in the late forties, modern training simulators became a possibility. Also a factor was the development and availability of improved concepts and knowledge about servo systems and components developed in World War II, especially in Germany. Modern operational training simulators are large expensive devices carefully designed to simulate as nearly as possible the actual cockpit environment and the characteristics of the production vehicle. As a matter of fact, however, numerous analyses have shown that these trainers can quickly save far more than they cost in reducing expensive flight time needed to maintain pilot proficiency particularly in such areas as instrument flight and simulated emergencies.

There is no sharp line between the first four phases in the kind of simulators used as will be apparent in later discussions. The operational trainer because of the special needs and the special economic factors involved has been essentially a clearly separated category. In view of the very limited production of future vehicles and their highly specialized and complicated nature this sharp line of demarcation may not remain.

Simulators do group themselves, to a degree, with regard to the element or elements of the flight control system that they are to provide information about. To illustrate my definition of the flight control system consider Figure 1. This block diagram has a block representing the human pilot, a block representing the control equipment needed inside the vehicle, and a block representing the dynamic characteristics of the airframe. Simulators as used with respect to each of these system elements will be discussed.

Finally and most important of all to the system engineer, simulators to examine and evaluate the total flight control system consisting of all these elements will be discussed.

Assemblies of the various components of, for example, the hydraulic or electrical systems are often made. In some cases, these assemblies and the test performed tend to become complex and to verge on what could be called simulation. In general, however, the inclination is to call these bench or laboratory tests unless combined with the airframe dynamics and a pilot.

And now for a few words on the block representing the human pilot. A great variety of simulators have been and are being used to determine man's tolerance to one or more of the environmental conditions that he may encounter. There are centrifuges and various other devices to subject men to accelerations, air bearing platforms and water tanks to attempt to simulate zero g, and airplanes to actually demonstrate zero g. Chambers exist to subject men to intolerable noise and chambers to impose absolute quiet. Men have been exposed to extreme cold and roasted to high temperatures in other tests. Confinement capsules resembling cockpits and space cabins are being utilized. Simulators have been and are being used to determine the dynamic characteristics of the human pilot as a servo element.

These simulators have been of the simple fixed base type and will be discussed a little later when considering simulators to examine the complete flight control system.

To a great extent, the discussion to this point has been in the nature of giving perspective to the subject of simulation. This is important, it is believed, in understanding each other, understanding how the trend to simulation came about, and making determinations of future trends. At this point, simulators of the complete flight control system will be discussed. These, no doubt, are what many first think of when simulation is mentioned.

A bewildering variety of simulators is being used to analyze the flight control system as a whole. Figure 2 is an attempt to break these facilities down in some logical grouping. The first natural grouping is between ground based and flight.

Figure 2 divides the ground based simulators into groups as to the motions that can be imparted to the pilot; no motion, rotations, translations, and combinations of rotation and translation. In Appendix I are listed various flight control system simulators that are available. This listing is undoubtedly not complete. The class of simple cockpit - analog computer simulator that is so common in the industry and the various research organizations has been excluded.

The majority of the fixed base, and the motion simulators as well, use instrument displays, these range from simple scope or dial instrument displays to elaborate display simulators. External display simulators are becoming more common, usually for approach and landing studies, VTOL investigations, and to simulate the space environment. The complete mission of an orbital vehicle can be simulated at a number of facilities.

In a few cases, an attempt to simulate accelerations has been made by pulling on the shoulder straps or exerting pressure on the seat cushions. This is indicated by the "pseudo G" block of Figure 2. The worth of this feature in improving correlation of data with actual flight is not known.

It has become standard practice in aircraft and missile development to make use of a category of simulator that is called the "iron bird" or the "iron monster". This category is of great importance in the design and development process. The first step in the development of an "iron bird" is normally the use of a simple cockpit - analog computer simulator. Simulators such as this can be quickly built up and adapted to the problems of the particular mission and configuration by connection with the analog computer facilities that are available in all companies.

As the design of the vehicle progresses and components of the control system are designed and begin to be available, the "iron bird" simulator is built. Normally, these simulators go through a continuous refinement process all through the years of development starting with little actual equipment, then insertion of early components and then the production hardware. The cockpit also normally shows such a growth starting with simple controls and presentation and finally, in some cases, a very complete mock up. In some cases where it is felt necessary, structural elasticity effects are included to provide adequate simulation. The simulation of the aerodynamic characteristics also undergoes continuous revision as knowledge of the airplane grows with analyses and wind tunnel tests performed.

In certain cases of extremely complex systems, a second partial "iron bird" may be built to obtain reliability and qualification information on the system and the components in addition to the system performance information normally sought on the "iron bird".

In some cases a final stage of simulation would be to connect the actual airpalne system with analog computers to prove the performance.

Referring back to Figure 2, let us pass on to a brief discussion of the various motion simulators in use. Very few, if any, simulators are now available with only one rotational degree of freedom. Depending on the intended function of the simulator, two or three rotational degrees of freedom will normally be incorporated. An example of two rotations is the pitch roll chair used in past years at NASA. A number of three rotational degree of freedom simulators have recently come into being, motivated basicially by interest in space vehicles, VTOL configurations, and reaction controls. Many of these devices utilize air bearings and in some cases they are quite elaborate. NASA - Lewis has a four gimbal type simulator in which high spin rates are possible.

The rotation simulators of the Link trainer type have limitations on the rotational travel. By incorporating initial motion into the simulator and then "washing out" the motion in actuality but continuing it on the instruments, what is said to be a very effective simulation of continuous motion is obtained. This capability is incorporated in the Air Force general purpose simulator and is referred to in Figure 2 as "pseudo motion".

Centrifuges, as is known, have been used to produce steady g forces on pilots to determine their tolerance and capabilities while enduring these forces. At the Naval Air Development Center at Johnsville, Pennsylvania, a facility is available which combines a centrifuge with a piloted capsule with two rotational degrees of freedom. Much interesting work was done on this facility with respect to the X-15 program.

An interesting facility to simulate zero g was investigated by Lockheed, Marietta, Georgia. This facility simulates zero g by spinning a man submerged

in water about his longitudinal axis.

The only simulator that the author knows of that has just one translational degree of freedom and no rotational freedom is the g seat at G/D, designed to study turbulence at low altitudes. Normally if translational degrees of freedom are included some rotational degrees are also included such as on the pitch - heaving g seats available at NASA - Langley and North American, Columbus.

Grumman has a unique facility which incorporates pitch, roll, and heave. It has both external and internal display and incorporates "wash out" to simulate large motions. It is especially useful for VTOL, low altitude flight, and approach and landing studies.

A large simulator is available at Bell-Dallas to study VTOL problems. This simulator has a three degree of freedom cabin mounted on a strut. This strut can be moved up and down to provide heaving to the cabin and also can be moved in the other two directions to provide a corrected vertical acceleration as the cabin is rotated.

NASA - Ames has a six degree of freedom simulator which has a three rotation cabin able to translate to a limited degree in all three axes. This would be intended for V/STOL and approach and landing studies.

Another impressive facility is the NASA - Ames facility having a three rotational degree of freedom cabin able to translate vertically, mounted on a centrifuge.

A number of very elaborate and expensive simulators have been built or are in construction to simulate various space missions, rendezvous, docking, lunar approach, and lunar landing. Expecially worthy of mention are the several simulators at NASA - Langley, LOLA and the Lunar Landing Facility.

To provide the various motions to the simulators as discussed, results

in additional complexity and cost so that, in general, as we move from left to right on Figure 2 the problems of constructing and operating the simulators are increased.

The purpose in adding these motions to the simulators, of course, is to add fidelity to the simulation, improving the correlation with actual flight. Unfortunately, this correlation is in a very imperfect stage and the answer to what is the minimum motion to provide acceptable fidelity of simulation is not available.

It is quite possible for motion of one sort or another introduced into a simulator, while being impressive to see, to do more harm than good as far as giving results comparable to the flight situation.

About fifteen years ago as a result of the newly developed knowledge and ability in artificial stability and computation, an idea was born of a flight research facility which has been called the variable stability airplane. At the present stage of advanced concepts, a better name might be in-flight simulation. The latest versions do much more than vary the stability. In Appendix II of this paper are listed all of the variable stability aircraft of which the author has knowledge, in more or less chronological order. The development of the concept and the increasing complexity and also capability of these aircraft can be followed by reading through this listing and the descriptions. The listing starts with the Cornell-Navy F4U-5 and has reached its high point with the Air Force-Cornell T-33. The Air Force-Cornell T-33 has the features of variable stability, control, feel, display and L/D. It has the capability to vary stability and control characteristics with time such as occurs in a re-entry. It does not as yet have the ability to vary C_{L_α} without varying other derivatives. This would be a desirable addition. The T-33 can also be used as a fixed base ground simulator by connecting it to an analog computer in its hanger.

In the area of V/STOL variable stability aircraft, NASA - Ames has a limited variable stability installation in an X-14 aircraft and NASA - Langley has an installation in a helicopter. Coming in the future is a new aircraft, the X-22, which is designed from the beginning as a variable stability machine.

Being such a realistic simulator when properly done, the variable stability aircraft is a most valuable research tool. It is also valuable in evaluation of preliminary design concepts and in training and indoctrinating flight test pilots. The concept has been proposed for use in operational trainers. Enthusiasts have even proposed a universal trainer using variable stability ideas. Such thinking does not recognize the practical limitations and difficulties that exist. There may be certain possibilities in this idea for the future, however.

Experience has shown that, in common with most flight tests, use of these airplanes for research and development is expensive and time consuming for each data point obtained. In the opinion of the author the most suitable usage of these airplanes is to make final checks and correlations of data points that have been explored as well as possible in ground simulators. See Appendix III for extensive references to variable stability aircraft.

TYPICAL USE OF SIMULATION IN RESEARCH AND DEVELOPMENT

At this point it may be interesting to indicate what would be typical use of simulators during the research and development cycle.

Figure 3 shows the various phases of this cycee. Relatively simple fixed base simulators are widely used in research programs involving the human pilot. For research purposes, this simplicity is not necessarily a

handicap. It is more important to carefully control the experiment and specify the controlled element precisely than to come to as exact similitude as possible.

There are many basic studies yet to be performed on the pilot-vehicle combination for which extremely simple simulation is entirely adequate. For example, use is still being made of Dr. Elkind's data, obtained at MIT many years ago, following a target on a scope with an electronic pointer. These basic studies and the associated simple simulators are particularly suitable for the university environment. One university, Princeton, has a variable stability aircraft, a Navion. It has a simple installation, however, it is a very effective tool for demonstrations and research studies either by thesis students or the faculty. Government facilities, as has been shown, have and operate many elaborate simulators for research purposes. There is tendency for these studies to become oriented to some system under study or development such as Apollo, SST, CX-HLS, C-142, etc. These studies then tend to be related to one later phase of the research and development process.

The three phases of primary importance to an aircraft company are shown in the center of Figure 3. During the preliminary design extensive use of the simple cockpit simulator would be made to firm up design requirements and to give information on specific problem areas not sufficiently covered by general research programs. Considerable variation in the extent of these programs would be caused by the mission and configuration. For instance, at the present time this phase of simulation would be considerably higher if a VTOL fighter were under consideration than if a more conventional fighter were in design. As is no doubt obvious both the kinds of simulators used and the types of programs conducted are very similar to those in the research phase.

Variable stability aircraft can and have been of use in examining particular problem areas of specific designs not sufficiently understood.

In the detailed development phase, heavy emphasis is laid on the "iron bird" simulator. In a not too sophisticated system most of the effort may be placed on the equipment development and proof testing. Preliminary exposure of the flight test group to the characteristics of the system will be provided in order to allow proper planning of the flight test program.

In view of the elaborateness of the "iron bird" simulator, considerable expense is involved in both constructing and operating it. However, its use is universally endorsed by the industry, with no exceptions to the knowledge of the author, as a time and money saver. Basically its use is a function of the complexity of the design, the degree to which the design is pushing the state of the art, and, related to the first two, the dollar cost of the system. With the tremendous cost of bringing a design to the flight test stage, the fantastic cost of flight test time, and the horrendous economic waste caused by mistakes, miscalculations, and redesign, the "iron bird" is felt by all to be an essential.

As the aircraft progresses into the flight test stage, increased emphasis may again be placed on the cockpit simulator. The dust may be brushed off the simple simulator and it may be improved to demonstrate dangerous conditions to the pilots and to guide the test program. The "iron bird" is utilized in evaluating the final equipment to be used in the production aircraft.

If the particular design is conventional both in aerodynamic configuration and its control system and is of relatively low performance, simulators may not be used. A judgment that they are not needed would be based on the economic factors referred to previously and to what could be called a

"confidence factor". This "confidence factor" is a function of how sure the engineers are of their knowledge and theoretical calculations. Such cases with a high "confidence factor" will be very few in the future.

On the other extreme are the designs which push the state of the art to the extreme such as Dyna Soar, and certainly Apollo. In these cases research type information is needed and will be gathered through all the phases indicated. Extremely complex simulation can be easily justified on the basis of the high cost of the total system. Much of the equipment is necessarily of high performance or of new design and consequently needs much simulator evaluation. Pilot training needs are much greater than normal. In view of the research nature of many such vehicles, the operational use phase merges into the normal flight test phase with resulting readjustments in the consideration of flight test and operational training simulators.

Users of aircraft, the operational commands of the services and the airlines, are most concerned with the operational use phase. As has been discussed, very elaborate operational trainers have become very common. The accent has been on procedural training. Exact matching of the dynamic behavior has not been an essential objective and only recently have any motion cues been considered worthy of providing. There is now interest in the Air Force in providing motion cues to simulate various maneuvers and emergency conditions. Even the airlines have become interested as a result of the recent series of incidents and accidents of jet transports caused by turbulence initiated maneuvers. There has been considerable interest by the airlines and FAA in use of a variable stability aircraft as a final operational trainer for SST operation.

NEED FOR AND PHILOSOPHY OF USE OF SIMULATION

In the main, the discussion to this point has been concerned with "what" simulators are available and in use. Some of the discussion has been concerned with "where" these simulators are used. Some comments have been made as to "how" this trend became possible, basically the availability of computation equipment and servo system knowledge and capability. It may be interesting to examine briefly some of the underlying reasons "why" this trend has become established and is expanding.

Fundamentally, simulators are used where basic knowledge is weak, complex interrelationships are not fully understood and calculations, estimates, or judgments are not trusted. In other words the confidence factor, referred to previously, is low. Also involved are the economic factors. With a modern complex weapon system, the costs of carrying a design through the flight test phase may be a billion dollars or more. Shown on Figure 4 are some facts on system costs. If we were to include systems such as Apollo, or beyond, on the chart the costs would really go to an asymptote. When we examine the configuration, the speed regimes to be traversed, and the complexity of the vehicle to perform its mission, the reasons for differences in cost between the Wright Flyer and the F-111 become apparent. These economic "facts of life" underlie any discussion of the trend to simulation.

Another factor to be considered is the fact that for modern systems there may be no extensive production, as such, to eliminate "bugs". Under such conditions major errors or deficiencies in the design are intolerable.

The use of simulation is affected by the philosophy of development of new aircraft in a country. Rapid exploitation of the state of the art invites

the "cut and try" approach. Such a philosophy has been followed in the United States, exemplified by the research series of aircraft. If the development of new types of aircraft proceeded at a slow steady pace, research would normally be properly accomplished prior to initiation of the design and a designer would not have the compulsion to use such extensive simulation. This rapid pace of development application of knowledge, however, has become a way of life and it is not believed that it will change under present conditions.

From the above factors a continual and increasing trend toward complex simulation can be predicted. There is a very real danger involved, however. Simulators are not only costly in dollars to build and operate but more importantly they are costly in technical talent to operate. Technical talent of high grade is not plentiful and if too much is tied up in work related to simulation, to the detriment of analytical studies and planning, the consequences can be serious. Most serious of all is the type of attitude that sometimes develops, to simulate without thinking. This is deadly. It results in blind repetitive programs of little real worth.

This is not to imply opposition to simulation, to the contrary. Rather it is a plea for their intelligent use.

Another thought related to the above is with regard to the organization of simulator groups. It is the author's feeling that simulator groups many times tend to look on the simulator facility as their goal and try to continually develop and improve it whether it is needed or not. It appears much preferable for an organization to be problem oriented, having and using simulators as necessary to solve their problems.

CONCLUSIONS

In the preceding discussion an attempt has been made to give some perspective to the subject by classification of simulators in various ways, a review of various facilities available in the United States and some historical background given. Discussed in more detail were flight control system simulators, particularly the "iron bird" type used extensively in development. An indication of the typical use of simulators in research and development was made. Finally some notes on the need for any philosophy of use of simulators were made.

In closing, it can be stated that simulation is a tool, use it as such and do not let it use you.

The assistance of R. Sickeler, P. Pietrzak and F/L Harris, RCAF in preparing the Appendices following is acknowledged.

BIBLIOGRAPHY

1. Simulation Facilities and Computers

1.1 Balsink, Edward B., & Sovine, Donald M., "Analogue Computer Mechanization of a Tilt-Wing VTOL Aircraft", WADD TN 59-344, July 1960

1.2 Beecham, L. J., Walters, U. L., & Partridge, D. W., "Proposals for an Integrated Wind Tunnel-Flight Dynamics Simulator System", Royal Aircraft Establishment, Nov. 1962

1.3 Binder, H. S., & Mayer, G. F., "Salient Features of Recent Dynamic Simulators", Grumman Aircraft Engineering Corp., 1961

1.4 Bisplinghoff, R. L.; Ashley, Holt; and Halfman, R., "Aeroelasticity", Addison-Wesley Publishing Company, Inc. 1955

1.5 Blaschke, A. C., "Solution of Differential Equations by Mechanical and Electromechanical Means", AAF MR TSEPE 673-93A, 17 January 1946

1.6 Bonalie, A. F., "Safety and Economic Aspects of Flight Simulators", IAS Preprint #606, January 1956

1.7 Brice, David, "The Simulated Aeroplane:, Aeronautics, December 1954

1.8 Carmody, Edmund O., "The Role to be Played by Training Devices in the Training of Aviation Personnel:, Aeronautical Engineering Review, May 1954

1.9 Connelly, Mark E., "Simulation of Aircraft", Servomechanisms Laboratory M.I.T., Cambridge, Report Nr 7591-R-1, Feb. 1958

1.10 Connelly, Mark E., "Computers for Aircraft Simulation", Electronic Systems Laboratory, M.I.T., Dec 15, 1959

1.11 Cooper, G. E., "The Use of Piloted Flight Simulators in Take-Off and Landing Rsch", Ames Rsch Center, AGARD, Jan. 1964

1.12 Davis, Leroy, "Trainer Delivery Procedure, Special Store Eclipse-Pioneer Type 48T14 AF Type AF/E 37A-T-1 (Weapon Delivery Simulator)", WADC TR 57-83, November 1957

1.13 deFlorez, Luis, "Synthetic Aircraft", Aeronautical Engineering Review, April 1949

1.14 deFlorez, Luis & Smith, E. K., "Helicopter Flight Trainer", Aeronautical Engineering Review, Fol. 15 #5, May 1956

1.15 Denniston, J. L., "NAA Dynamic Flight Simulator", North American Aviation, June 1961

1.31 Mazelsky, Bernard; Amey, H. G., Jr., "On the Simulation of Random Excitations for Airplane Response Investigations on Analog Computers", Journal of the Aeronautical Sciences, Vol. 24 #9, September 1957

1.32 McCann, "Direct Analogy Electric Analog Computer", Instrument Society of America Journal, April 1956

1.33 Meissinger, Hans F., The New Cyclone Simulation Laboratory, "A Discussion of the Simulator Design and the Solution of a Three-Dimensional Guidance Problem", Reeves Instrument Corp., May 1953 (Title Unclassified) (Report Confidential)

1.34 Mitchell, Thorpe, "The Case for the Differential Analyzer for Lateral Response Investigation", RAE TN 1203, June 1943

1.35 Mueller, R. R., "An Electrical Device for Solving the Equations of Longitudinal Motions , Journal of Aeronautical Sciences, March 1936

1.36 Mulher, J. J., "The Physical and Functional Characteristics of Flight Control Systems Simulators", NADC-ED-5913, 28 April 1959 (Naval Air Development Center)

1.37 Murphy, G., "Similitude in Engineering", New York, The Ronald Press Co. 1950

1.38 Neice, Stanford E.; Carson, James A.; & Cunningham, Bernard E., "Experimental Investigation of the Simulation of Atmosphereic Entry of Ballistic Missiles", NACA RM A57126, December 1957

1.39 Newell, Allen, "New Areas of Application of Computers", Rand Report P-2142, 1960

1.40 Nixon, F. E., "What Can Electronic Simulators Do for the Missile Designer?", IAS 528, January 1955

1.41 Notess, C. B., "Simulation of the Effects of Winds and Turbulence Upon Longitudinal Motions of an Aircraft Flying at Low Altitudes and High Speed", Cornell Aeronautical Lab., FDM 309, June 1960

1.42 Osborne, S. P.; Smith, S. G., "An Improved Flight Instrument Simulator", Royal Aircraft Establishment, Technical Note NR IAP 1086, Dec. 1958

1.43 Outman, V., "Vehicle Design Needed: Idea Exchange on Testing by Simulation", Aerospace Engineering, Vol. 22, No. 1, January 1963

1.44 Pecoraro, Joseph N., "The Use of an Operational Flight Trainer as a Research Tool for Aircraft Instrumentation and Cockpit Re-arrangement", Aeronautical Engineering Review, May 1954

1.16 Eggers, A. J., "A Method for Simulating the Atmospheric Entry of Long-Range Ballistic Missiles", NACA RM A55115, December 1955

1.17 Fox, Paul L., "Design Study for Trainer, Visual Flight Attachment for Aircraft Flight Simulator", WADC TR 57-137 Part 2, September 1958

1.18 Gait, J. J., "A Study of the Massachusetts Institute of Technology Flight Simulator", Royal Aircraft Establishment, Technical Note Nr GW357, (Title Unclassified) (Report Confidential) February 1955

1.19 Hardy, James D. & Clark, Carl C., "The Development of Dynamic Flight Simulation", Aero/Space Engineering, June 1959

1.20 Harnett, R. T.; Robinson, A. C., "Role of Computers in the Engineering of Air Weapons Systems", Paper presented at the 8 August 1960 Meeting of the Mid-western Simulation Council

1.21 Harper, R. P., Jr., "Simulation and the Pilot", AIAA Paper, Aug. 1963

1.22 Howe, R. M., "Flight Simulator Theory Study", WADC TR 58-456, Dec. 57

1.23 Howe, R.; Lemm, R. G., "A Standardized Computer for Solving the Three-Dimensional Flight Equations", WADC TN 59-283, May 1959

1.24 Hudson, E. M., "An Adaptive Tracking Simulator", Otis Elevator Co., May 1962

1.25 Isakson, G.; Buning H., "A Study of Problems in the Flight Simulation of VTOL Aircraft", WADC TN 59-305, February 1960

1.26 Johnson, H. I., "Simulation and Training Facilities", Astronautics and Aerospace Engineering, Vol. 1, No. 1, February 1963

1.27 Lathian, G. B., "Simulated Flight Training, Its Uses and Limitations", IAS 755, October 1957

1.28 Lowrey, R. O., Space Flight Simulators, "Design Requirements and Concepts," IAS 60-61, July 1960

1.29 MacGowan, Roger; Whigham, Wilton, Army Ballistic Missile Agency Report, RE-TR-1-61, 16 January 1961, "General Purpose Digital Computers for Engineering and Scientific Applications"

1.30 Marx, M. F., "Computers in Flight Control System Development", Quarterly Electronics Digest, Third Quarter 1960, Vol. 1, Nr. 3, published by Light Military Electronics Dept of General Electric, Utica, New York

1.60 General Electric, "Physical Simulation Engineering", 1962

1.61 Helicopter Flight Simulators, Flight, December 24, 1954, pp. 908-910

1.62 Staff of the NASA, "Compilation of Papers Summarizing Some Recent NASA Research on Manned Military Aircraft", NASA TM X-240, October 1960 (Title Unclassified) (Report Confidential)

1.63 Space Technology Laboratories, "New Manned Spacecraft Simulator at STL", April 1963

1.64 Various Authors, "Dynamic System Studies:, WADC TN 54-250, Parts 1 through 16, 1954 - 1956 (Parts 3, 9, 11, Confidential) (Parts 12 and 15 secret)

1.45 Pietsch, Roy; Yound, James M., "The Simulation of a High Speed Aircraft with the New Texas Tester", Military Physics Research Lab., U. of Texas, Austin, September 1953

1.46 Rathert, G. A. Jr; Creer, B. Y.; & Sadoff, M., "The Use of Piloted Flight Simulators in General Research, NASA, April 1961

1.47 Ringham, G. B.; Cutler, A. E., "Flight Simulators", Royal Aeronautical Society Journal, March 1954, pp. 153-170

1.48 Ryder, Frederick L., "Energy Versus Compatibility Analogs in Electrical Simulators of Structures", Journal of the Aero/Space Sciences, Vol. 26 #2, February 1959

1.49 Schelhorn, A. E., "A Study of the Dynamic Response Characteristics of Flight Simulators", WADC TR 59-98, April 1959

1.50 Schwarm, Edward G., "Electronic Simulation for the Jet Age", Aero/Space Engineering, May 1958

1.51 Sedov, "Similarity and Dimensional Methods in Mechanics", Academic Press 1959

1.52 Shirley, R. C., "Development of Assault Drone Simulator", Naval Air Development Center Report Nr EL-5328, April 1953 (Title Unclassified) (Report Confidential)

1.53 Smith, F.; Hicks, W. D. T., "The R.A.E. Electronic Simulator for Flutter Investigations in Six Degrees of Freedom or Less", Report Nr Structures 152, Dec 3, 1953 (Title Unclassified) (Report Confidential)

1.54 Stedber, Joseph A., "A Simple Visual Display Projector Useful for VTOL Simulation", Grumman Aircraft Eng. Corp., Jan 1961

1.55 Sullivan, Douglas R., "An Aircraft Dynamics Simulator", Instrumentation Lab., Mass. Inst. of Tech, Report Nr E-499, September 1955

1.56 Warner, Edward, Chairman, "Symposium - Electronic Control and Stabilization of Aircraft", Aeronautical Engineering Review Vol. 12 #5, May 1953

1.57 Westbrook, C. B., "Simulation in Modern Aero-Space Vehicle Design", AGARD 366, 1961

1.58 Wycharski, H. J., "Reproduction of Aircraft Dynamic Response in Real-Time by a Digital Computer System", Aerospace Engineering, Vol. 20 No. 5, May 1961

1.59 Anon., "The Design of a Rigid Frame Fixture for the Application of Simulated Aerodynamic Forces and Effects to Missile Body Structures", Army Missile Test Center, White Sands, N. Mexico, Special Report Nr 35, April 1960

2. Variable Stability, Control and Feel Aircraft

2.1 Milliken Jr., William F. (Cornell Aeronautical Laboratory) "Progress in Dynamic Stability and Control Research", IAS Paper Jan 29, 1947

2.2 Graham, Dunstan (Cornell) "Automatic Control and the Lateral Oscillatory Motion", TB-574-F-1, 1 April 49

2.3 Campbell, Graham and Bull, Gifford, (Cornell) "Determination of the Longitudinal Stall Dynamics of the PT-26 Airplane", TB-498-F-2, 24 Feb 50

2.4 Graham, Dunstan and James, Clarence (Cornell), "A Flight Investigation of Minimum Acceptable Lateral Dynamic Stability" TB-574-F-3, 30 April 60

2.5 Segel, L. (Cornell), "Investigation of Devices for Modifying the Phugoid Oscillation of Aircraft", TE-665-F-2, 17 Aug 50

2.6 Milliken Jr., W. F. (Cornell), "Dynamic Stability and Control Research" CAL-39, Presented at the Third International Joint Conference of the R. Ae. S. - IAS, Brighton, England, Sept 3-14, 1951

2.7 Kidd, Edwin A. and Notess, Charles B. (Cornell), "Theoretical Investigation of Methods for Artificially Stabilizing the Modes of Motion of the C-45 Aircraft, TB-754-F-1, 1 Oct 51

2.8 Lathrop, Richard C. and Graham, Dunstan, "Flight Research On Force Wheel Control", WADC TN WCT 52-39, October 1952

2.9 Kidd, Edwin A. and Gould, Arthur (Cornell), "Artificial Stability Installation in C-45 Airplane", WADC TR 53-432, July 53

2.10 McNeill, Walther E., Drinkwater III, Fred J. and VanDyke Jr., Randolph D. (NACA-Ames), "A Flight Study of the Effects on Tracking Performance of Changes in the Lateral-Oscillatory Characteristics of a Fighter Airplane", RM A53H10, 22 Sept 53

2.11 Bull, Gifford (Cornell), "Investigation of Lateral Stability at Stall," WADC TR 54-498, Feb 1954

2.12 Moore, Norton B. (McDonnell Aircraft Corp), "Artificial Stability Flight Tests of the XF-88A Airplane", WADC TR 52-298, July 1954

2.13 Kidd, Edwin A. (Cornell), "Artificial Stability Installations in B-26 and F-94 Aircraft", WADC TR 54-441, Sept 1954

2.14 Newell, Fred and Campbell, Graham (Cornell), "Evaluations of Elevator Force Gradients and Types of Force Feel in a B-26", WADC TR 54-442, Nov. 1954

2.15 Newell, Fred and Campbell, Graham (Cornell), "Flight Evaluation of Variable Short Period and Phugoid Characteristics in a B-26", WADC TR 54-594, Dec 1954.

2.16 Ball, J. N. (Cornell), "Preliminary Report on T-33 Variable Stability and Control Project", FRM 219, 27 Jaunary 1955

2.17 Bull, Gifford and Kidd, Edwin A. (Cornell), "Air to Air Tracking with Linear and Non-Linear Yaw Damping", (Unclassified Title) WADC TR 55-223 (Report Confidential) June 55

2.18 Sjoberg, S. A. (NACA-Langley), "A Flight Investigation of the Handling Characteristics of a Fighter Airplane Controlled Through Automatic-Pilot Control Systems", RM L55F01b, 1 Sept 1955

2.19 Whitten, James B.; Reeder, John P.; and Crim, Abner D. (NACA-Langley), "Helicopter Instrument Flight and Precision Maneuvers as Affected by Changes in Damping in Roll, Pitch and Yaw", NACA TN 3537, Nov. 1955

2.20 McNeill, Walter E. and Creer, Brent Y. (NACA-Ames), "A Summary of Results Obtained During Flight Simulation of Several Aircraft Prototypes with Variable Stability Airplanes", RM a56C08, 25 May 1956

2.21 Ball, J. N. (Cornell), "Installation of an Automatic Control System in a T-33 Airplane for Variable Stability Flight Research (Part 1 - Preliminary Investigation and Design Studies)", WADC TR 55-156 (AD 97136) July 1956

2.22 Newell, Fred and Rhoads, Donald W. (Cornell), "Flight Evaluations of the Effect of Variable Phugoid Damping in a B-26 Airplane", WADC TR 56-223 (AD 118103) December 1956

2.23 Beilman, J. L. and Harper Jr., R. P. (Cornell), "Installation of an Automatic Control System in the T-33 Airplane for Variable Stability Flight Research (Part 3 - Ground and Flight Checkout)", WADC TR 55-156 Part 3, Cornell Report TB-936-F-3, August 1957

2.24 Anon (Cornell), "Flight Evaluation of the Effect of Variable Spiral Damping in a JTB-26B Airplane", TB-1094-F-1, 19 Oct 57

2.25 Newell, Fred (Cornell), "Effects of Breakout Force on Longitudinal Handling Qualities", WADC TR 57-155, AD 142306, December 1957

2.26 Newell, Fred (Cornell), "Evaluations of Some Breakout Forces at Several Short Period Dynamics in a Variable Stability JTB-26", WADC TR 57-155, 1957

2.39 Faber, Stanley and Crane, Harold L. (NASA-Langley), "A Longitudinal Control Feel System for In-Flight Research on Response Feel", NASA TN D-632, Jan 1961

2.40 Breuhaus, W. O., "Flight Research Utilizing Variable Stability Aircraft", IAS Preprint #541, Jan 1955

2.41 Tapscott, R. J., "Criteria for Control and Response Characteristics of Helicopters and VTOL Aircraft in Hovering and Low-Speed Flight", (Released for presentation at IAS 1960 Annual Meeting, New York City.)

2.42 Sjoberg, S. A., Russell, Walter R. and Alford, William L., "A Flight Investigation of the Handling Characteristics of a Fighter Airplane Controlled through an Attitude Type of Automatic Pilot", NACA RM L56A12, April 10, 1956

2.43 Reeder, John P., and Whitten, James B., "Some Effects of Varying the Damping in Pitch and Roll on the Flying Qualities of a Small Single-Rotor Helicopter", NACA TN 2459, 1952

2.44 Russell, Walter R., Sjoberg, S. A., and Alford, William L., "Flight Investigations of Automatic Stabilization of an Airplane Having Static Longitudinal Instability", NASA TN D-173, Dec 1959

2.45 Russell, Walter R., and Alford, William L., "Flight Investigation of a Centrally Located Rigid Force Control Stick Used with Electronic Control System in a Fighter Airplane", NASA TN D-102, Sept 1959

2.46 Sjoberg, Sigurd A., Russell, Walter R., and Alford, William L., "Flight Investigation of a Normal-Acceleration Automatic Longitudinal Control System in a Fighter Airplane", NASA Memo 10-26-58L, 1958

2.47 Goldberg, J. H., "Effects of Spring and Inertia Devices on the Longitudinal Stability of Aircraft", WADC TR 53-350, July 1953

2.48 Newell, F.; Schelhorn, A.; and Dolbin, B. (Cornell), "Development and Flight Calibration of a Variable Drag Device on a Variable Stability T-33 Airplane", ASD TDR-62-910, August 1963

2.49 Chalk, C. (Cornell), "Additional Flight Evaluations of Various Longitudinal Handling Qualities in a Variable Stability Jet Fighter", WADC TR 57-719 (Part 1), January 1958

2.50 Chalk, C. (Cornell), "Additional Flight Evaluations of Various Longitudinal Handling Qualities in a Variable Stability Jet Fighter", WACD TR 57-719 (Part 2), July 1958

2.51 Flt. Research Dept. (Cornell), "Installation of an Automatic Control System in a T-33 Airplane for Variable Stability Flight Research", (Part 2 - Detail Design, Fabrication and Installation) WADC 55-156, September 1956

2.27 Kuehnel, Helmut A., Beckhardt, Arnold R. and Champine, Robert A. (NACA-Langley), "A Flight Investigation of the Effects of Varied Lateral Damping on the Effectiveness of a Fighter Airplane as a Gun Platform", NACA TN 4199, January 1958

2.28 Chalk, Charles R. (Cornell), "Additional Flight Evaluations of Various Longitudinal Handling Qualities in a Variable-Stability Jet Fighter", WADC TR 57-719 Part I (AD 142184) January 1958

2.29 McFadden, Norman M.; Pauli, Frank A. and Heinle, Donovan R. (NACA-Ames), "A Flight Study of Longitudinal-Control-Systems Dynamic Characteristics by the Use of a Variable Control-System Airplane" (Title Unclassified) NACA RM A57L10, Report Confidential. 3 March 1958

2.30 McNeill, Walther E. and Vomaski, Richard F. (NASA-Ames) "A Flight Investigation to Determine the Lateral Oscillatory Damping Acceptable for an Airplane in the Landing Approach", NASA Memo 12-10-58A, Feb 1959

2.31 Schuler, John M. (Cornell) "Flight Evaluation of an Automatic Control System for Stabilizing the Large Uncontrolled Motions of Airplanes in Stalled Flight", TB-1132-F-2, Oct 1959

2.32 Salmirs, Seymour and Tapscott, Robert J. (NASA-Langley) "The Effects of Various Combinations of Damping and Control Power on Helicopter Handling Qualities During Both Instrument and Visual Flight", NASA TN D-58, Oct 1959

2.33 Goldberg, Joseph H. and Gangwish, Robert C. (Princeton University) "Required Lateral Handling Qualities for Helicopters in Low-Speed Instrument Flight", Report NR 496, Feb 1960

2.34 Brissenden, Roy F.; Alford, William L. and Mallick, Donald L. "Flight Investigation of Pilot's Ability to Control an Airplane Having Positive and Negative Static Longitudinal Stability Coupled with Various Effective Lift-Curve Slopes", NASA TN D-211, Feb 1960

2.35 Infanti, N. L. and Harper Jr., Robert P. (Cornell), "NT-33 Variable Stability Airplane Demonstration Program", FDM NR 311, 15 June 1960

2.36 Harper Jr., Robert P. (Cornell) "In-Flight Simulation of Re-entry Vehicle Handling Qualities", presented at the IAS National Summer Meeting, Los Angeles, Calif. IAS Paper 60-93, June 28 - July 1, 1960

2.37 Newell, Fred (Cornell), "Feasibility Study of Thrust Reversers and Spoilers for L/D Control on a T-33 Airplane", FDM NR 312, 9 Sept 60

2.38 Infanti, N. L. (Cornell), "Augmented Capabilities of the Variable Stability T-33 Airplane for Ground and Flight Handling Qualities Evaluations", Report NR TE-1234-F-1, Nov 1960

2.52 Harper, R. P., Jr. (Cornell), "In-Flight Simulation of the Lateral-Directional Handling Qualities of Entry Vehicles", WADC TR-147, February 1961

2.53 Harper, R. P., Jr. (Cornell), "Flight Evaluations in Variable Stability Airplanes of Elevator Control Motion Gradients for High-Speed Bombers", WADC TR 56-258, November 1956

2.54 Breuhaus, W. O. (Cornell), "Dry Run in the 'X-15'", Research Trends, Vol. IX, Fall 1961

2.55 Kidd, E. A. and Bull, G. (Cornell), "Handling Qualities Requirements as Influenced by Pilot Evaluation Time and Sample Size", Report No. TB-1444-F-1, February 1962

2.56 Bull, G. (Cornell), "Minimum Flyable Longitudinal Handling Qualities of Airplanes", Report No. TB-1313-F-1, December 1959

2.57 Kidd, E. A. and Harper, R. P., Jr. (Cornell), "Fixed Base and In-Flight Simulation of Longitudinal and Lateral-Directional Handling Qualities for Piloted Re-Entry Vehicles", ASD TDR-61-362, February 1964

2.58 Chalk, C. R. (Cornell), "Fixed-Base Simulator Investigation of the Effects of L and True Speed on Pilot Opinion of Longitudinal Flying Qualities", ASD TDR-63-399, November 1963

2.59 Chalk, C. R. (Cornell), "Flight Evaluation of Various Short Period Dynamics at Four Drag Configurations for the Landing Approach Task", RTD-TDR-64-60, March 1964

2.60 Newell, F. D. (Cornell), "Simulator Evaluation of Airplane Longitudinal Responses for the Instrument-Landing Approach", RTD TDR-64-84, March 1964

2.61 Newell, F. D. (Cornell), "Date for 96 Touchdowns made by Three Pilots in an Airplane with Slow Longitudinal Response Dynamics For Comparison with NASA Simulator Data", Report No.TM -1755-F-1, September 1963

2.62 Infanti, Nello L, (Cornell), "Variable Stability Demonstrations to the USAF Aerospace Research Pilot School", Report No. TE-1864-F-1, Sept. 1963

2.63 Berry, D. T. (AFFTC), "An Evaluation of a Variable Stability Airplane Simulation of the X-15", AFFTC TR-61-42, September 1961

2.64 Roll, L. S. and Drinkwater, F. J. III, "A Flight Determination of the Attitude Control Power and Damping Requirements for a Visual Hovering Task in the Variable Stability and Control X-14A Research Vehicle", NASA TN D-1328, May 1962

2.65 Salmirs, S. and Tapscott, R. J., "Instrument Flight Trials with a Helicopter Stabilized in Attitude About Each Axis Individually", NACA TN 3947, 1957

2.66 Garren, J. F., Jr., "Effects of Gyroscopic Cross Coupling Between Pitch and Roll on the Handling Qualities of VTOL Aircraft", NASA TN D-812, April 1961

2.67 Garren, J. F., Jr., "Effects of Gyroscopic Cross Coupling Between Pitch and Yaw on the Handling Qualities of VTOL Aircraft", NASA TN D-973, November 1961

2.68 McGregor, D. M., "An Investigation of the Effects of Lateral-Directional Control Cross-Coupling on Flying Qualities Using a V/STOL Airborne Simulator", NRC of Canada, Aeronautical Report LR-390, December 1963

2.69 Daw, D. and McGregor, D. M., "Development of a Model-Controlled V/STOL Airborne Simulator", NRC of Canada, Aeronautical Report LR-352, August 1962

2.70 Cornell, "Specification Variable Stability System X-22A VTOL Research Aircraft", Report No. 2127-947024, Part I-November 1963, Part II-April 1964

2.71 Cornell"Composite Specification Demonstration Requirements for Model X-22A Tri-Service VTOL Research Aircraft", Report No. 2127-947028, Jan. 1964

2.72 Peterson, F. S., USN, Redress, H. A., and Weil, J., "Lateral-Directional Control Characteristics of the X-15 Airplane", NASA TM X-726, March 1962

2.73 Berry, Donald T., "An Evaluation of a Variable Stability Airplane Simulation of the X-15", AFFTC-TR-61-42, Sept. 1961

2.74 Brenhaus, W. O., (Cornell), "Simulation of the X-15 Using the T-33 Variable Stability Airplane"

2.75 Garren, J. F., Jr., and Kelly, J. R. "Description of An Analog Computer Approach to V/STOL Simulation Employing a Variable Stability Helicopter", NASA TN D-1970, Jan. 1964

2.76 Kidd, E. A.; Bull, Gifford; Harper, Robert P., Jr., "In-Flight Simulation Theory and Application", Apr. 61

2.77 Breuhaus, W. O., Cornell Aero Lab. "Airborne Simulator for the SST" March 63

2.78 Harper, R. P., Jr., "In Flight Simulation of the Lateral Directional Handling Qualities of Entry Vehicles," WADD TR 61-147, Nov. 1961

3. Handling Qualities and Piloted Simulator Studies

3.1 A'Harrah, R., "Low Altitude High Speed Handling & Riding Qualities", AIAA Journal of Aircraft, January 1964

3.2 Andrews, William H.; Holleman, Euclid C., "Experience with a Three-Axis Side Located Controller During a Static and Centrifuge Simulation of the Piloted Launch of a Manned Multistage Vehicle", NASA TN D-546, Nov. 1960

3.3 Ashkenas, Irving L.; McRuer, Duane T., "The Determination of Lateral Handling Qualities Requirements from Airframe Human Pilot Systems Studies", WADC TR 59-135, June 1959

3.4 Assadourian, Arthur; Cheatham, Donald C., "Longitudinal Range Control During the Atmospheric Phase of a Manned Satellite Re-entry", NASA TN D-253, May 1960

3.5 Banks, William B.; Spangenberg, Donald N., "Responses of the Human Pilot in a Simulated Day Superiority Type Fighter", (Title Unclassified) Flight Control Lab., M. I. T., Report Nr FCL-7010-T20, May 1955 (Report Confidential)

3.6 Beasley, G. P., "Pilot-Controlled Simulation of Rendezvous Between a Spacecraft and a Commanded Module Having Low Thrust", NASA TND-1613, March 1963

3.7 Bird, D., (Boeing), "Flight Control Studies in the Small Stick Deflection Area, AIAA Journal of Aircraft, May-June 1964

3.8 Bowman, D. R.; Mathews, R. H., "A Moving Base Flight Simulator Evaluation of Model F4H-1 Longitudinal Control Characteristics and Flying Qualities", McDonnell Aircraft Corp., Sept. 1961 (Report Confidential)

3.9 Brown, B. Porter; Johnson, Harold I.; & Mungall, Robert G.; "Simulator Motion Effects on a Pilot's Ability to Perform a Precise Longitudinal Flying Task", NASA TN D-367, May 1960

3.10 Brown, B. Porter & Johnson, H. I., "Moving Cockpit Simulation Investigation of the Minimum Tolerable Longitudinal Maneuvering Stability", NASA TN D-26, September 1959

3.11 Burton, B. B.; Kurbjun, M. C.; Brissenden, E. C.; & Foudriat, E. C., "Pilot Control of Rendezvous", NASA-Langley, Jan. 1961

3.12 Burton, B. B.; Brissenden, R. F.; Foudriat, E. C.; & Whitten, J. B., "Analog Simulation of a Pilot-Controlled Rendezvous", NASA TN D-747, April 1961

3.13 Carpenter, D. & Jenny, R., (McDonnell), "Statistical Approach to Low Speed Control Criteria for V/STOL Aircraft", AIAA Paper 64-286

3.14 Chalk, C. R., "Fixed-Base Simulator Investigation of the Effects of L and True Speed on Pilot Opinion of Longitudinal Flying Qualities", ASD TDR 63-399, Nov. 1963

3.15 Chambers, Randall M. & Eggleston, John M., "Pilot Performance During Centrifuge Simulated Boost and Reentry of Proposed Space Vehicles", AGARD Paper presented Athens, Greece, May 11-15, 1959

3.16 Cheatham, Donald C., "A Study of the Characteristics of Human-Pilot Control Response to Simulated Aircraft Lateral Motions", NACA RM L52C17, 1952

3.17 Cooper, George E., "Understanding and Interpreting Pilot Opinion", Aeronautical Engineering Review, Vol. 16 #3, March 1957, pp. 47-52

3.18 Cooper, N. R., "X-15 Flight Simulation Program", Aerospace Engineering, Vol. 20, Nr 11, Nov. 61

3.19 Creer, B. Y.; Heinle, D. R. & Wingrove, R. C., "Study of Stability and Control Characteristics of Atomosphere Entry Type Aircraft Through Use of Piloted Flight Simulators", IAS 59-129, 1959

3.20 Creer, Brent Y.; Steward, John D.; Merrick, Robert B.; and Drinkwater, Fred J. III; "A Pilot's Opinion Study of Lateral Control Requirements for Fighter-Type Aircraft", NASA Memo 1-29-59A, 1959

3.21 Creer, Brent Y.; Smedal, Harald A.; Wingrove, Rodney C.; "Centrifuge Study of Pilot Tolerance to Acceleration and the Effects of Acceleration on Pilot Performance", NASA TN D-337, November 1960

3.22 Crone, R. M. & A'Harrah, R. C., "Development of Lateral-Directional Flying Qualities for Supersonic Vehicles Based on a Stationary Flight Simulator Study", IAS 60-18, January 1960

3.23 Davidson, Roger M.; Cheatham, Donald C., & Kaylor, Jack T., "Manual Control Simulation Study of a Non-Lifting Vehicle During Orbit Retro-Rocket Firing, and Re-entry Into the Earth's Atmosphere", (Title Unclassified) NASA TM X-359, Sept. 1960, (Report Confidential)

3.24 Doennebrink, F. A.; Biggers, J. V.; Sherman, H.; & Speiser, K. "Manual Control of Re-entries at Superorbital Velocities Using Simplified Centrifugal Force Rate Equations", IAS Paper 62-89, June 1962

3.25 Donnebrink, F. A.; Biggers, J. V.; Spiegler, S.; & Vandenberg, "A Simulation Study of Manual Control of Re-entry at Hyperbolic Velocities", Grumman Rpt. Nr ADR 09-01-61.4, Dec. 1961

3.26 Douvillier, Joseph G. Jr.; Turner, Howard L.; McLean, John D.; & Heinle, Donovan R., "Effects of Flight Simulator Motion on Pilot's Performance of Tracking Tasks", NASA TN D-143, Feb 1960

3.27 Eggleston, John M.; Baron, Sheldon; & Cheatham, Donald C., "Fixed Base Simulation Study of a Pilot's Ability to Control a Winged-Satellite Vehicle During High-Drag Variable-Lift Entries", NASA TN D-228, April 1960

3.28 Faber, Stanley, "Ground-Simulator Study of the Effects of Stick Force and Displacement on Tracking Performance", NACA TN 3428, Apr 55

3.29 Faber, Stanley, "Qualitative Simulator Study of Longitudinal Stick Forces and Displacements Desirable During Tracking", NACA TN 4202, Feb 1958

3.30 Faye, A. E., "Attitude Control Requirements for Hovering Determined Through the Use of a Piloted Flight Simulator", NASA TN D-792, April 1961

3.31 Fletcher, Dorothy E.; Collins, Carter C.; & Brown, John Lott; "The Effects of Positive Acceleration Upon the Performance of an Air-to-Air Tracking Task", U. S. Naval Air Development Center, NADA-MA-5807, 2 June 1958

3.32 Foss, F. & Magruder, "Low Speed Aerodynamic Characteristics of the Double Delta Supersonic Transport", AIAA Preprint 64-591

3.33 Garren, J. F., Jr. & Assadourian, A., "VTOL Height-Control Requirements in Hovering as Determined from Motion Simulator Study", NASA TN D-1488 October 1962

3.34 Gerdes, R. M., & Weick, R. F., "A Preliminary Piloted Simulator and Flight Study of Height Control Requirements for VTOL Aircraft", NASA TN D-1201, Feb. 1962

3.35 Hall, A. W., & Harris, J. E., "A Simulator Study of the Effectiveness of a Pilot's Indicator Which Combined Angle of Attach and Rate of Change of Total Pressure as Applied to the Take-Off Rotation and Climbout of a Supersonic Transport", NASA TN D-948, Sept 1961

3.36 Hall, S. D., "A Simulator Assessment of an Integrated Control System for a Fighter Aircraft", Royal Aircraft Establishment TN ARM 591, Nove. 1956

3.37 Harter, George A. & Fitts, Paul M., "The Functional Simulation of Complex Systems by Means of an Analog Computer, with the F-86D, E-4 System as a Specific Example", Part 1, AFPTRC TN 56-133 Part 1, December 1956

3.38 Higgins, H., & Slomber, H., "The Effects of Variable Sweep on Supersonic Transport Handling Qualities", Boeing Company, AIAA Preprint 64-603

3.39 Holleman, Euclid C., & Boslaugh, David L, "A Simulator Investigation of Factors Affecting the Design and Utilization of a Stick Pusher for the Prevention of Airplane Pitch-Up", NACA RM H57J30, 1958 (Title Unclassified) (Report Confidential)

3.40 Holleman, Euclid C., & Stillwell, Wendell H., "Simulator Investigation of Command Reaction Controls", NACA RM H58D22, (Title Unclassified) (Report Confidential) July 1958

3.41 Holzhauser, C.; Deckert, W.; Wuigley, H.; & Kelley, M., "Design and Operating Considerations of Commercial STOL Transports", AIAA Paper 64-285 (NASA)

3.42 James, Harry A.; Wingrove, Rodney C.; Holzhauser, Curt A.; & Drinkwater, Fred J. III, "Wind-Tunnel and Piloted Flight Simulator Investigation of a Deflected-Slipstream VTOL Airplane, The Ryan VZ-3RY", NASA TN D-89, November 1959

3.43 Kelley, H. J., "Flight Simulator Investigation of F-11-F-1 High Speed Longitudinal Stability & Control Characteristics", Grumman Aircraft Engineering Corporation, January 1956 (Grumman Report RE-72)

3.44 Klinar, W. J., and Craig, S. J., "Study of VTOL Control Requirements During Hovering and Low-Speed Flight Under IFR Conditions", IAS Paper 61-60, January 1961

3.45 Kuehnel, H. A., "Human Pilot's Dynamic-Response Characteristics Measured in Flight and on a Non-moving Simulator", NASA TN D-1229, March 1962

3.46 Lineberry, E. C., Jr.; Brissenden, R. F.; & Kurbjun, M. C., "Analytical and Preliminary Simulation Study of a Pilot's Ability to Control the Terminal Phase of a Rendezvous with Simple Optical Devices and a Timer", NASA TN D-965, October 1961

3.47 Matrange, G. J.' Washington, H. P.; Chenoweth, P. L.; & Young, W. R., "Handling Qualities & Trajectory Requirements for Terminal Lunar Landing, As Determined from Analog Simulation", NASA TN D-1921, Aug 63

3.48 Matthews, Howard F. & Merrick, Robert B., "A Simulator Study of Some Longitudinal Stability and Control Problems of a Piloted Aircraft in Flights to Extreme Altitude and High Speed", (Title Unclassified) NACA RM A56F07, Sept 1956 (Report Confidential)

3.49 McKee, John W., "Single-Degree-of-Freedom Simulator Investigation of Effects of Summing Display-Instrument Signals on Man-Machine Control", NASA TN D-148, December 1959

3.50 McNeill, W. E., "A Piloted Simulator Study of the Loss of Altitude by a Jet Transport in a Go-Around from an Instrument-Landing Approach", NASA TN D-2060, Sept 1963

3.51 McRuer, Duane T.; Ashkenas, Irving L & Guerre, C. L., "A Systems Analysis View of Longitudinal Flying Qualities", WADD TR 60-43, Jan 1960

3.52 Morris, W.; McCornick, R & Sinccori, J. (Northrop), "Moving Base Simulator of an All Mechanical Control System for VTOL Aircraft", AIAA Journal of Aircraft, Jan 1964

3.53 Muler, David; & Clark, James, "Research on Methods for Presenting VTOL Aircraft Handling Qualities Criteria", United Aircraft Corp., AIAA Preprint 64-618

3.54 Naish, J. M., "Simulation of Visual Flight, With Particular Reference to the Study of Flight Instruments", BRCP 488, 1960

3.55 Palmer, W. E., "A Flight Simulator Study of the Lateral-Directional Stability Requirements of Piloted Air Vehicles", North American Aviation, Inc., March 1961

3.56 Patierno, J. & Isca, J. A., "Instrument Flight Simulator Study of the VTOL Controllability-Control Power Relationship", IAS Paper 61-118-1812, June 61

3.57 Phillips, William H. & Cheatham, Donald C., "Ability of Pilots to Control Simulated Short-Period Yawing Oscillations", NACA RM L50D06, November 1950

3.58 Quigley, H. C., & Lawson, H. F., "Simulator Study of the Lateral-Directional Handling Qualities of a Large Four-Propellered STOL Transport Airplane", NASA TN D-1773, May 1963

3.59 Queijo, M. J.; Miller, G. K., Jr.; & Fletcher, H. S., "Fixed-Base-Simulator Study of the Ability of a Pilot to Perform Soft Lunar Landings", NASA TN D-1484, Oct. 1962

3.60 Queijo, M. J.; Riley, D. K.; & Miller, G. K. "A Fixed-Base-Simulator Study of the Ability of a Pilot to Establish Close Orbits Around the Moon and to Perform Soft Lunar Landings", IAS Paper 62-13, Jan 1962

3.61 Queijo, M. J. & Riley, D. R., "A Fixed-Base-Simulator Study of the Ability of a Pilot to Establish Close Orbits Around the Moon", NASA TN D-917, June 1961

3.62 Rathert, George A. Jr.; Creer, Brent Y.; & Douvillier, Joseph G. Jr., "Use of Flight Simulators for Pilot-Control Problems", NASA Memo 3-6-59A, February 1959

3.63 Reeder, J. P., "Handling Qualities Experience with Several VTOL Research Aircraft", NASA TN D-735, March 61

3.64 Riley, D. R. & Suit, W. T., "A Fixed-Base Visual-Simulator Study of Pilot Control of Orbital Docking of Attitude-Stabilized Vehicles", NASA TN D-2036, Jan 1964

3.65 Sadoff, M., "Simulated Stability Augmentation System Failures", NASA TND-1552, Nov. 1962

3.66 Sadoff, Melvin; McFadden, Norman M.; & Heinle, Donovan R.; "A Study of Longitudinal Control Problems at Low and Negative Damping and Stability with Emphasis on Effects of Motion Cues", NASA TN D-348, Jan 1961

3.67 Sadoff, Melvin, "The Effects of Longitudinal Control-System Dynamics on Pilot Opinion and Response Characteristics as Determined from Flight Tests and from Ground Simulator Studies", (Title Unclassified) NASA Memo 10-1-58A, October 1958 (Report Confidential)

3.68 Sadoff, M., & Harper, C. W., "Piloted Flight-Simulator Research--A Criticial review", Aerospace Engineering, Vol. 21 Nr 9, Sept 1962

3.69 Semple, C. A. & Brown, J. E., "A Simulator Study of a Three-Axis Attitude Controller for Use in Space Vehicles: The Relationship of Gains to Performance", IEEE Paper, May 1963

3.70 Sherman, Windsor L.; Faber, Stanley; & Whitten, James B., "Study of Exist Phase of Flight on a Very High Altitude Hypersonic Airplane by Means of a Pilot-Controlled Analog Computer" (Title Unclassified) NACA RM L57K21 (Report Confidential) January 1958

3.71 Smedal, Harald A.; Greer, Brent Y.; & Wingrove, Rodney C.; "Physiological Effects of Acceleration Observed During a Centrifuge Study of Pilot Performance", NASA TN D-345, Dec 1960

3.72 Smedal, Harald A.; Holden, George R.; and Smith, Joseph R. Jr., "A Flight Evaluation of an Airborne Physiological Instrumentation System, Including Preliminary Results under Conditions of Varying Accelerations", NASA TN D351, December 1960

3.73 Stillwell, Wendell H. & Drake, Rubert M., "Simulator Studies of Jet Reaction Controls for Use at High Altitude" (Title Unclassified) NACA RM H58G18a, Sept 1958, (Report Confidential)

3.74 Silliman, W. B., & Cooper, N., "Manual Control Studies Under Transverse Acceleration", North American Aviation, Inc. Feb 1960, Rpt NA-60-291

3.75 Taylor, L. W., Jr., & Day, R. E., "Flight Controllability Limits and Related Human Transfer Functions as Determined from Simulator and Flight Tests", NASA TN D-746, May 1961

3.76 Taylor, L. W. Jr., Samuels, J. L,; & Smith, J. W., "Simulator Investigation of the Control Requirements of a Typical Hypersonic Glider", NASA TM X-635 March 1962 (Confidential)

3.77 Weil, Joseph & Day, Richard E., "An Analog Study of the Relative Importance of Various Factors Affecting Roll Coupling", NACA RM H56A06, April 1956

3.78 Westbrook, C. B. & McRuer, D. T., "Handling Qualities and Pilot Dynamics", Aero/Space Engineering, May 1959

3.79 Westbrook, C. B. & McRuer, D. T., "Aircraft Handling Qualities and Pilot Response Characteristics", AGARD Report 125, 1957

3.80 White, Maurice L. & Drinkwater, Fred J. III, "A Comparison of Carrier Approach Speeds as Determined from Flight Tests and from Pilot-Operated Simulator Studies", NACA RM A57D30, June 1957

3.81 White, M. D.; Sadoff, M.; Bray, R. S.; & Cooper, G. E., "Assessment of Critical Problem Areas of the Supersonic Transport by Means of Piloted Simulators", Aerospace Engineering, Vol. 21, Nr 5, May 1962

3.82 White, M. D.; Vomaske, R. F.; McNeill, W. E.; & Cooper, G. E., "A Preliminary Study of Handling-Qualities Requirements of Supersonic Transports in High-Speed Cruising Flight Using Piloted Simulators", NASA TN D-1888, May 1963

3.83 White, M. D., Sadoff, M.; Bray, R. S. & Cooper, G. E., "Assessment of Critical Problem Areas of the Supersonic Transport by Means of Piloted Simulators", IAS Paper 62-20, Jan 1962

3.84 Wingrove, R. C. & Coate, R. E., "Piloted Simulator Tests of a Guidance System Which Can Continuously Predict Landing Point of a Low L/D Vehicle During Atmosphere Re-entry", NASA TN D-787, March 1961

3.85 Wingrove, R. C. & Coate, R. E., "Piloted Simulation Studies of Re-entry Guidance and Control at Parabolic Velocities", IAS Paper 61-195-1889, June 1961

3.86 Wolowicz, Chester H.; Drake, Hubert M. & Videan, Edward N., "Simulator Investigation of Controls and Display Required for Terminal Phase of Co-planar Orbital Rendezvous:, NASA TN D-511, Oct 1960

3.87 Woodling, C. H. & Clark, C. C., "Studies on Pilot Control During Launching and Reentry of Space Vehicles, Utilizing the Human Centrifuge", IAS 59-39, January 1959

3.88 Young, J. W. & Basher, Lawrence E. Jr., "Moving-Cockpit-Simulator Study of Piloted Entries into the Earth's Atmosphere for a Capsule-Type Vehicle at Parabolic Velocity", NASA TN S-1797, May 1963

3.89 Young, J. W. & Russel, W. R., "Fixed-Base-Simulator Study of Piloted Entries into the Earth's Atmosphere for a Capsule-Type Vehicle at Parabolic Velocity", NASA TN D-1497, Oct 1962

3.90 Vomaske, R. F; Sadoff, M. & Drinkwater, F. J. III, "The Effect of Lateral-Directional Control Coupling on Pilot Control of An Airplane as Determined in Flight and in a Fixed-Base Flight Simulator", NASA TN D-1141, Nov 1961

3.91 "AIAA Simulation for Aerospace Flight Conference", presented Aug 26-28 1963, Columbus, Ohio

3.92 "Simulator Assessment of Take-Off and Landing", English Electric, Jan 1963

3.93 "Simulator Study to Determine Handling Qualities Criteria for VTOL Aircraft", Grumman Aircraft Corp., Oct 1960

3.94 "Preliminary Evaluation of Two Jet-Transport Simulators for the Investigation of Landing-Contact Conditions", NASA TN D-1495, Nov 1960

4. Flight Control System Studies

4.1 Adams, James J., "An Analog Study of an Airborne Automatic Landing-Approach System", NASA TN D-105, December 1959

4.2 Assadourian, Arthur, "Operating Characteristics of an Acceleration Restrictor as Determined by Means of a Simulator", NACA TN 3319, Dec 1954

4.3 Anon., "XSM-64A Simulator", Autonetics Report Nr EM-1369, October 1958

4.4 Blanton, H. E., "Use of Flight Simulators in the Design of Aircraft Control Systems", Aeronautical Engineering Review, February 1954

4.5 Bollay, William, "Aerodynamic Stability and Automatic Control", Fourteenth Wright Brothers Lecture, Journal of the Aeronautical Sciences, Sept 1951

4.6 Bond, Robert W., "Flight Simulation of the X-10 Missile" North American Aviation Report Nr EM-444, October 1953 (Title Unclassified) (Report Confidential)

4.7 Brown, E. Porter, "Ground Simulator Studies of the Effects of Valve Friction, Stick Friction, Flexibility, and Backlash on Power Control System Quality", NACA Report 1348, 1958

4.8 Cooper, N. R., "X-15 Flight Simulation program", NARS, NIAS Joint Meeting.

4.9 Crane, Harold L., "Analog-Computer Investigation of Effects of Friction and Preload on the Dynamic Longitudinal Characteristics of a Pilot-Airplane Combination", NACA RM L57118, Nov 1957 (Title Unclassified) (Report Confidentail)

4.10 Creer, Brent Y., "An Analog Computer Study of Several Stability Augmentation Schemes Designed to Alleviate Roll-Induced Instability", NACA RM A56H30, February 1957 (Title Unclassified) (Report Confidential)

4.11 Dawson, John W. & Pantazelos, Peter G., "Simulated Dynamic Response of the F-100A in a Large-Scale Rolling Maneuver", Dynamic Analysis & Control Lab., Mass. Inst. of Tech. Report Nr 95. September 1955 (Title Unclassified) (Report Confidential)

4.12 Early, James W. & Doody, Bernard J., "Application of an Adaptive Control System to an Aircraft with a Fixed-gain Autopilot", WADC TN 56-334, August 1956

4.13 Early, James W. & Sovine, Donald M., "A Preliminary Investigation of Automatic Recovery from Unusual Attitudes", WADC TN 56-390, September 1956

4.14 Farr, J. E.; Hoffman, D. P.; Cooper N. R.; "Evaluation of the General Electric Self-Adaptive Control System on the X-15 Flight Control Simulator", ASD TR 61-81, Aug 61

4.15 Gautraud, John A. & Flanders, James H., "Design of Flight Control Systems for Cross-Coupled Aircraft", Instrumentation Lab., Mass. Inst. of Tech., Report Nr E-525, February 1956 (Title Unclassified) (Report Confidential)

4.16 Gillis, Clarence L., "A Brief Analog Investigation of Inertia Coupling in Rolling Maneuvers of an Airplane Configuration Using A Variable-Incidence Wing as the Longitudinal Control", NACA RM L57F18, August 1957, (Title Unclassified) (Report Confidential)

4.17 Godde, Harry H., "Simulation-Its Place in System Design", IRE Proceedings Vol. 39 #12, December 1951

4.18 Henschke, Ulrich K. & Mauch, Hans A., "Control Action Simulator," USAF AMC Memo Report Nr MCREXD-696-110D July 1949

4.19 Hollingsworth, R. E.; Roberts, H. E.; Schellhase, M. W. "Techniques for Flight Simulator Evaluation of the E-4 Fire Control System with the Texas Tester", University of Texas Report Nr MPRL-373, February 1958

4.20 Imai, O. & Koener, W. G., "Fundamentals of Design of Piloted Aircraft Flight Control Systems", Vol. V, "The Artificial Feel System", BuAer Report AE-61-4-V, May 1953

4.21 Jones, Arthur L. & White, John S., "Analogue-Computer Simulation of an Autopilot Servo System Having Nonlinear Response Characteristics", NACA TN 2707 June 1952

4.22 Jones, Walter G. & Kirlin, William F., "An Analog Computer Study of the Effects of Jet Aircraft Artificial Damping Caused by Rate Gyro Non-Linearities", AFIT Report Nr. GSC 55-6, March 55 (Title Unclassified) (Report Confidential)

4.23 Lear, William P., "Trends in Autopilot Developments", Aeronautical Engineering Review, Vol 15 #1, January 1956

4.24 Lessing, Henry C. & Reese, David E. Jr., "A Simulation Study of a Wingless Missile", NACA RM A55L06, February 1956

4.25 Mathews, Charles W., "Analog Study of the Effects of Various Types of Control of a Pilot-Airplane Combination", NACA TM L55F01a, August 1955

4.26 Monroe, W. R., "Application of Electronic Simulation Techniques to the Development of Airplane Flight Control Systems", Aeronautical Engineering Review, Vol. 14 #5, May 1955

4.27 Passera, Anthony L. & Garner, Douglas G., "Simulator Studies of a Simple Homing System", NACA RM L55G06, Oct. 1955

4.28 Phillips, William H., Brown, B. Porter, and Matthews, James T. "Review and Investigation of Unsatisfactory Control Characteristics Involving Instability of Pilot-Airplane Combination and Methods for Predicting These Difficulties from Ground Test", (Supersedes RML53F17a) NACA TN 4064, August 1957

4.29 Porter, Richard F., "An Analog Computer Study of a Stability Augmentation System for F-86E Aircraft", WCT TN 54-104

4.30 Porter, Richard F., "Analog Computer Study of the Automatic Flare-Out Landing of a C-54 Aircraft with an E-4 Automatic Pilot", WCT 52-53, Dec 1953

4.31 Richardson, J. D. and A'Harrah, R. C., "The Application of Flight Simulators to the Development of the A-5A Vigilante" AIAA Paper, August 1963

4.32 Robinson, Alfred C.; Early, James W.; & Doody, Bernard J.; "Simulation Study of Control of an Aircraft at or Near the Absolute Ceiling", WADC TR 56-39, March 1956

4.33 Shih, S. L., "Pilot-Airplane Link System Utilizing Inverse, Aerodynamic, and Damper Gain Changes", General Electric Rpt. Nr R56APS167, Feb 1957

4.34 Smith, Earl F., "Use of Angular Accelerometer to Improve Aircraft Stability", Instrumentation Lab., M. I. T., 1950 Rpt Nr 6445-T-28

4.35 Statler, I. C. & Beilman, J. L., "Dynamic Lateral Stability Through Non-Linear Automatic Control", Cornell Report Nr TB-697-F-1, January 1952 (Report Confidential) (Title Unclassified)

4.36 Stone, C. R., "A Study to Determine an Automatic Flight Control Configuration to Provide a Stability Augmentation Capability for a High Performance Supersonic Aircraft", WADC TR 57-349, May 58

4.37 Willis, J. M., "Results of Engineering Test Made on the Franklin Institute Dynamic Flight Simulator", Bell Helicopter Report Nr D228-370-001, April 1960

BLOCK DIAGRAM - FLIGHT CONTROL SYSTEM

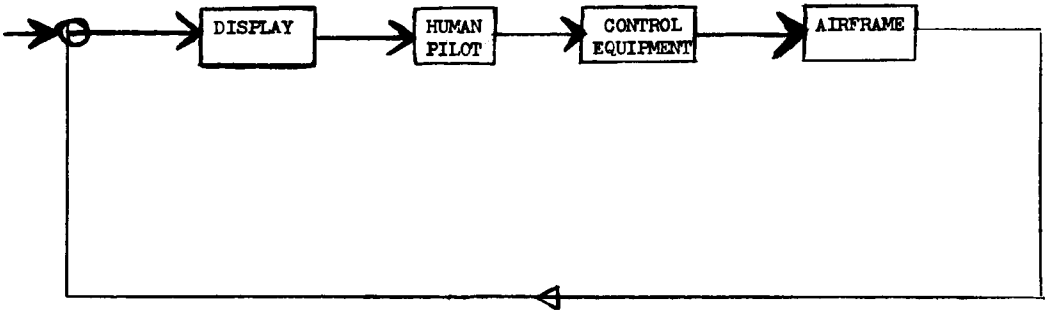

Figure 1

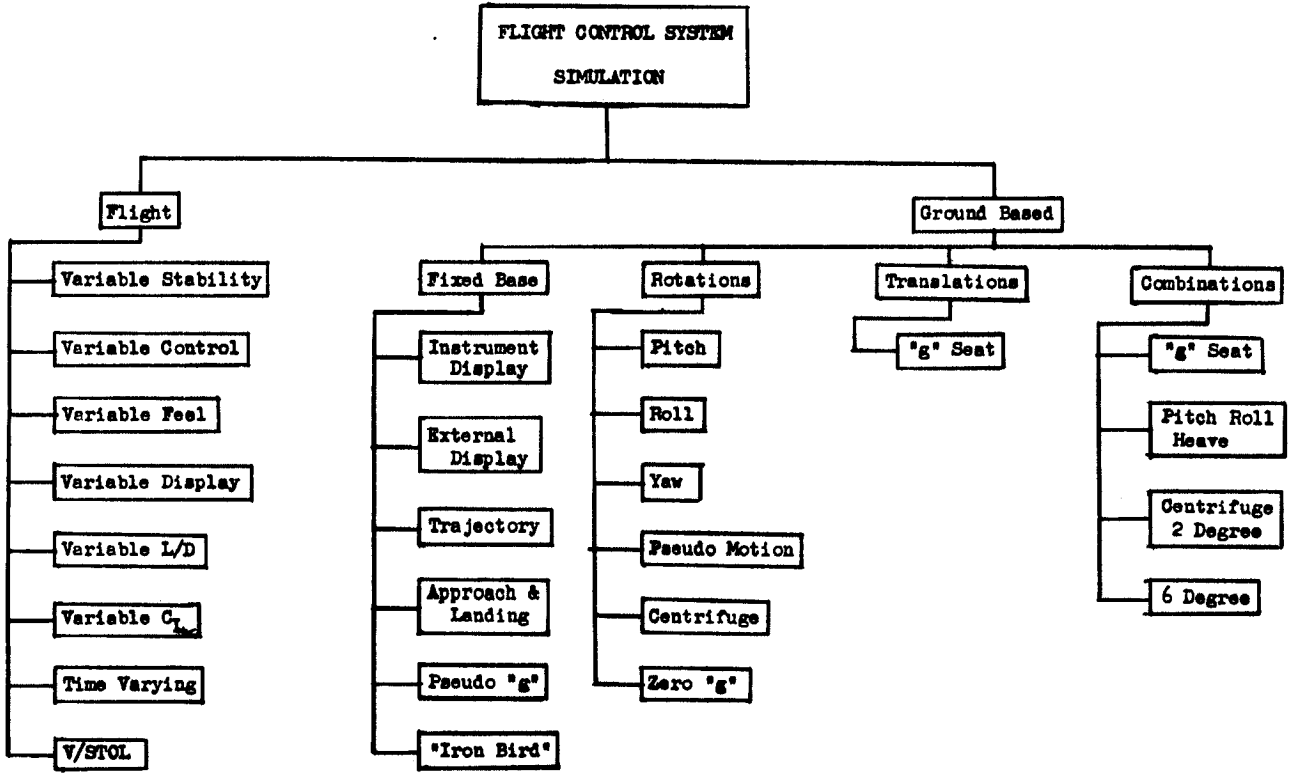
FLIGHT CONTROL SYSTEM SIMULATION
Flight
Variable Stability
Variable Control
Variable Feel
Variable Display
Variable L/D
Variable $C_{L_{max}}$
Time Varying
V/STOL
Ground Based
Fixed Base
Instrument Display
External Display
Trajectory
Approach & Landing
Pseudo "g"
"Iron Bird"
Rotations
Pitch
Roll
Yaw
Pseudo Motion
Centrifuge
Zero "g"
Translations
"g" Seat
Combinations
"g" Seat
Pitch Roll Heave
Centrifuge 2 Degree
6 Degree

Figure 2

FLIGHT CONTROL SIMULATOR USE

IN DESIGN CYCLE

	Design Requirements Data on Specific Problems	Final Design Requirements Proof of Design Acceptability Equipment Development Pilot Training	Pilot Training Pilot proficiency Dangerous Regimes Resolution of Problems	Crew Training Procedural Training Navigation All Weather Operation
RESEARCH	PRELIMINARY DESIGN	DETAILED DEVELOPMENT	FLIGHT TEST	OPERATIONAL USE

TIME →

Figure 3

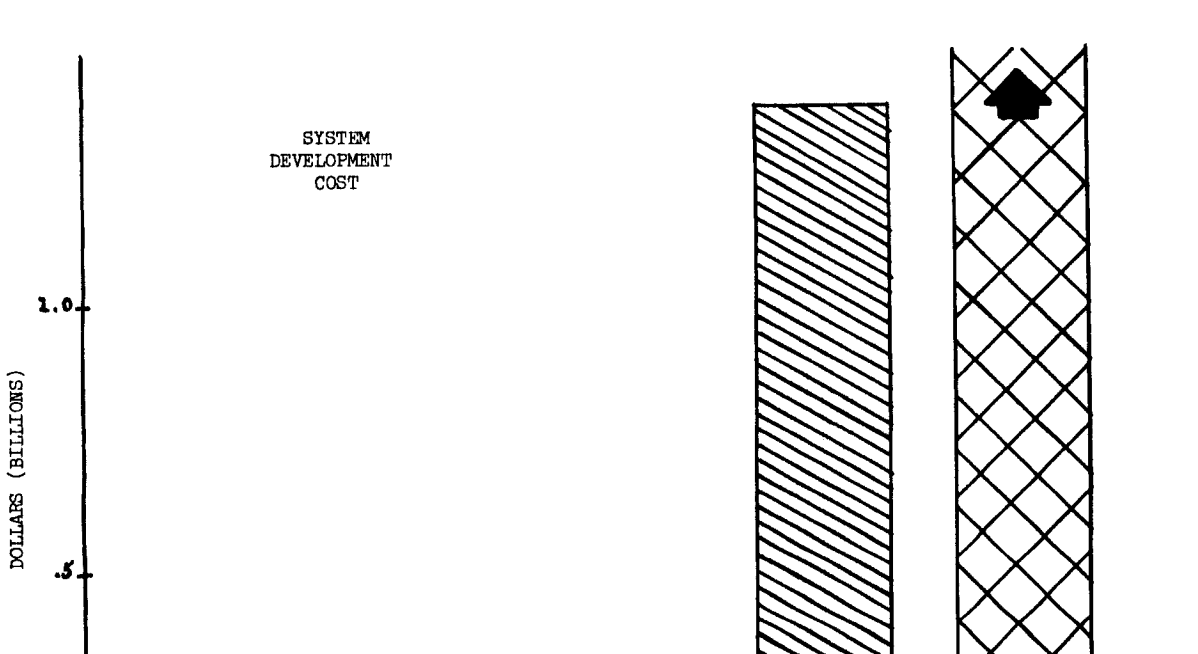
SYSTEM
DEVELOPMENT
COST
DOLLARS (BILLIONS)
1.0
.5
WRIGHT
FLYER
P-47
B-52
B-70

Figure 4

Appendix I

F/C SYSTEM GROUND SIMULATORS

TITLE	LOCATION	DESCRIPTION	REFERENCE OR REPORTS	COMMENTS
General Purpose Hypersonic Simulator	Air Force WPAFB Ohio	Fixed base simulator to evaluate new display and instrument concepts in the hypersonic flight regime. Primarily used in re-entry studies.		
T-37 General Purpose F/C Simulator	Air Force WPAFB Ohio	Modified T-37 moving base simulator used for instrument and flight control-display concept research. Has force wheel steering split axis auto-pilot, and electronically generated visual runway presentation.		
Night Sky Simulator	Air Force WPAFB Ohio	A small fixed base simulator enclosed in a dynamic star field to study the inter-relationship between the external visual motion cues and the symbolic cockpit displays.		
Flight Control Integrated Systems Facility	Air Force WPAFB Ohio	Hybrid, 6 degree (plus) of freedom simulation facility for use in design and evaluation of all aspects of flight control systems. Can tie in airborne electronics and fixed base fully instrumented cockpits		This facility is essentially composed of analog and digital computers plus the X-20 Guidance and Control Dynamics Model.
Six mode Simulator	Air Force WPAFB Ohio	6-Degree of freedom simulator. Hydraulic shakers will actuate pushrods and universal joints to vibrate a magnesium test platform. Will accommodate 2,000 lb. load and induce vibrations up to 30 cps and g-loads as high as 20.		To be built by MB Electronics

TITLE	LOCATION	DESCRIPTION	REFERENCE OR REPORTS	COMMENTS
Dynamic Escape Simulator	Air Force WPAFB, Ohio	450 ton simulator to study performance of pilots under stresses of simultaneous tumbling, spinning, oscillation, vibration and rapid acceleration during launch, flight and re-entry phases.		Being built by Franklin Institute
Aerospace Simulator	AFMTC Cape Canaveral, Fla.	Aerospace profile simulator for pilot training and integration of pilot with ground crew.		
Rotation Simulator	AF School of Aviation Medicine	3 degrees of freedom, roll, pitch, yaw. 10 ft sphere on air bearing. Pilot can operate jets or reaction wheels. Pilot display, perturbations, can be introduced. Pressure can be simulated 50 rpm in one axis, 70 rpm resultant.		
Spin Chair	AF School of Aviation Medicine Brooks AFB, Tex.	Rotatable chair electronically controlled for study of pilot reactions and disorientation.		
Ballistic Control Simulator	Edwards AFB (Air Force)	Simulator floated on air bearing and driven by reaction jets powered by high pressure nitrogen in spheres.		Used by AF in training future space pilots.
Flight Acceleration Simulator	Naval Air Development Center Johnsville, Pa.	Centrifuge combined with piloted capsule with two degrees of freedom.		
Photo-reconnaisance Plane Simulator	Navy	Free to move in 4 directions, gives pilot-student realistic over-the-ground moving image of his camera targets. Supplements existing Chance Vought F8U-1P Crusader photo-plane cockpit and camera trainers.		To be delivered by Chance Vought

TITLE	LOCATION	DESCRIPTION	REFERENCE OR REPORTS	COMMENTS
SST Cruise Simulator	NASA-Ames	Cruising flight stability and control qualities simulated dynamically. 4 degrees-of-freedom-pitch, roll, yaw, and lateral acceleration.		
SST Approach and Landing Simulator	NASA-Ames	Stationary cockpit with flight simulated by servo-driven instruments and a closed-circuit television display projected onto a screen.		
3 Degree of Freedom	NASA-Ames	Gas bearing, 360 rotation possible in 3 axes provided with cockpit and controls.		
V/STOL Landing Simulator	NASA-Ames	Landing Approach Simulator having 120 ft of vertical travel, constructed on outside of 40 x 80' wind tunnel.		
Visual Projection Facility	NASA-Ames	Projection facility to simulate horizon stars or landing approach situation. Can be used with other simulators		
5 Degree Simulator	NASA-Ames	Roll-pitch-yaw carriage free to heave, installed on a centrifuge.		
Apollo Mid Course	NASA-Ames	Air supported table for investigation of space control systems.		
6 Degree Simulator	NASA-Ames	6 degree of freedom simulator having limited travel for V/STOL and transport landing studies.		
Lunar Landing Test Vehicle	NASA-FRC	Manned jet lift vehicle for investigating lunar landing.		

TITLE	LOCATION	DESCRIPTION	REFERENCE OR REPORTS	COMMENTS
"Iron" Cross Control Simulator	NASA, HSFS Edwards, AFB, Cal.	Three degrees of freedom, roll pitch and yaw. Used to investigate pilot control with jet reaction devices.		
General Purpose Simulator	NASA Edwards AFB	Fixed Base, cockpit simulator, contact analog display in color.		
LOLA Lunar Orbit & Landing Approach Simulator	NASA Langley	Four maps of moon will be photographed by television and projected inside a dome. Display will simulate view from 200 miles to 0.75 miles.		
Lunar Landing Research Facility	NASA Langley	Steel Framework 400 ft long by 250 high and 50' wide. 11,000 # lunar landing vehicle suspended so that 5/6 of weight is carried by cables		
Visual Docking Simulator	NASA Langley	Fixed base with television display projected from moveable mirror 20' diameter spherical projection screen.	AIAA 64-334	
Planetarium Simulator	NASA Langley	Fixed base simulator using 55' inflated radome as planetarium		
Lunar Gravity Simulator	NASA Langley	200 ft. long oval track on its side with cable suspension. Cable supports to pilots head, body, and legs.		
Rotating Space Station Simulator	NASA Langley	Similar to above, except that a totating drum is incorporated instead of a stationary wall.		To be built
"g" Seat	NASA Langley	Vertical translation and pitching degrees of freedom. For evaluation of low altitude flight characteristics.	NASA TM X-420	

TITLE	LOCATION	DESCRIPTION	REFERENCE OR REPORTS	COMMENTS
SST Simulator	NASA Langley	Fixed base, cockpit display-Simulated air traffic control		
Space Rendezvous Docking Simulator	NASA Langley	Large 6 degree-of-freedom simulator installed in a hangar on overhead truck and dolly	AIAA 64-334	
MASTIF Multiple Axis Test Inertia Facility	NASA-Lewis	Four gimbals to simulate yaw, roll and pitch angles. Installed in altitude wind tunnel--altitude and temperature factors of space flight can be simulated. High spin rates possible.		Used for reaction control and Mercury Capsule studies.
Apollo Mission Simulator	NASA-Lewis	Simulator will duplicate what crew will see and hear during prelaunch, launch, parking and earth orbit, escape injection, coast, circumlunar pass, circular lunar orbit, lunar excursion module separation and rendezvous, injection into trans-earth trajectory, coast, re-entry and landing.		Being built by Fink Div. of GPI.
Lunar Landing Module Simulator	NASA	Simulator to practice rendezvous and docking for Apollo. Can move 25° around each axes.		Being built by Martin
Control Simulator	Bell Helicopter Dallas, Texas	6 degrees of freedom simulator - load capacity of 1000 lbs. 5 cycles/second in pitch, roll and yaw.		Particularly useful for helicopter and V/STOL studies.
STOL Control Simulator	Boeing Witchita, Kansas	A six degree of freedom STOL flight simulator to examine handling qualities, flight control and display.		

TITLE	LOCATION	DESCRIPTION	REFERENCE OR REPORTS	COMMENTS
Vibration Study Effects	Boeing Wichita	Vibrations between 1-30 cps with amplitude of 20 inches at lowest frequency up to 1/64 inches at highest frequency are produced by a hydraulic cylinder actuating a platform holding in aircraft seat. Checks pilot's ability to read instruments and actuate controls under vibration.		
Multiple Stress Chamber	Boeing Seattle	Pilot subjected to vibrations and enviromental conditions of boost. Pilot performs tracking task.		
Space Flight Simulator	Boeing Seattle	Rendezvous Docking simulator-fixed base with large circular screen-6 degree of freedom space display also includes a full scale moving cockpit docking simulator.		
VTOL and Terrain Simulator	Boeing Seattle	Fixed base-6 degree of freedom point legal source display projected on quarter flight sphere-allows flight over terrain 15 by 1.1 inches		
Control Systems Simulator	Vought Dallas, Texas	Structure supported by air bearing. Reaction controls inertia wheels - will accommodate a pilot.		
Fixed Base Orbital Flight Simulator	Vought Dallas, Texas	Fixed base, elaborate cockpit with 560 amplifier analog computer puls digital computer to simulate six degree of freedom flight mechanics and equations for orbital and space navigation.	Vought Report ADB 1-4	Particularly useful for orbital flight, rendezvous and re-entry studies.
V/STOL Simulator	Vought Dallas, Texas	Fixed base - hydraulic stick & rudder feel-extensive display.	IAS Paper 6-60	

TITLE	LOCATION	DESCRIPTION	REFERENCE OR REPORTS	COMMENTS
Space Flight Simulator	Vought Dallas, Texas	3 axis motion compartment. External display on 20 ft sphere surrounding cockpit, enclosed in space environmental conditions simulator, heat, noise, vibrations, pressure, temperatures, radiation & meteoritic impact. Digital computer used to simulate flight mechanics equations.	Vought Report ADB 1-4	
T-33 Ground Simulator	Cornell Aero Lab., Buffalo New York	T-33 Variable Stability Airplane used as fixed base ground simulator by use of computer to simulate dynamic equations.		
Carrier Landing Simulator	Douglas	Fixed base simulating mirror landing approach system.		
ANIP Simulator	Douglas, EL Segundo, Calif.	Fixed base - investigation of advanced display concepts.		
General Purpose Flight Simulator	G/D Ft. Worth,	Fixed base, instrument display plus projection, external viewing.		Particularly useful for low altitude flight simulation
"g" Seat	G/D Ft Worth Texas	Simple simulator used to simulate jolting ride at low altitude, scope display.		Low altitude flight studies
Air Bearing Simulator	GD/Astronautics Point Loma	For testing and product improvement of contour stage control system during coast phase. Consists of pedestal, 30" sphere and two 25' boom and relate response of control jets to autopilots commands.		

TITLE	LOCATION	DESCRIPTION	REFERENCE OR REPORTS	COMMENTS
Space Vehicle Pilot Simulator	General Electric Missile & Space Vehicle Dept.	9' x 12' room accoustically insulated bordered by large computer-programmer observation area. Vehicle characteristics simulated. Simple seat-control-display setup used.	WADD TR 60-695 Part I and Part II	
Motion Simulator	GE/Missile & Space Vehicle Division	Air bearing supported simulator for testing Numbus control system-360° in pitch, 160° yaw, 120° roll.		
Docking Simulator	GE M&SVD	Cold gas altitude and translation controls in 5 degrees of freedom. Target assembly moves for 6th degree motion on 2 axis.		
Motion Simulator	Grumman Aircraft Eng. Co.	Free in roll, pitch and heave-3 "g" acceleration limit, instrument display and also provided with external display for VTOL and approach and landing simulation.	Grumman Reports	Particularly useful for approach and low altitude studies.
Lunar Landing Simulator	Grumman	Simulator utilized for control system parameter studies and for evaluation of lunar landing techniques. Controlled by analog computers. Comprises 2 degree-of freedom motion seat and a 4 degree-of-freedom visual display.		
Mark IV Space Cabin Simulator	Lear Grand Rapids, Michigan	Fixed base, elaborate display, space cabin simulator.		
Null Gravity Simulator	Lockheed Marietta	Simulates zero g's by placing in center of spinning tank of fluid.		Not completed
"Humming Bird" VTOL Simulator	Lockheed Marietta, Ga.	VTOL tethered rig using jet engines to evaluate VTOL handling qualities and flight control.		Other tethered rigs have been used (X-13, Avro machine, etc.) to check specific designs

TITLE	LOCATION	DESCRIPTION	REFERENCE OR REPORTS	COMMENTS
Lifting Body Simulator	Martin/ Baltimore	Will simulate entire flight of orbital lifting, body vehicle--100,000' to touch-down, 6 degree-of-freedom projection of approach area displayed on 16' x 20' wall.		
Gemini Simulator	McDonnell	Will be used to simulate last 100' of flight and docking with Lockheed Agena stage. Crew station located on Gimbal and translation structure. Agena is on target structure.		
Simulator	Norair	6 degrees of freedom, moving base. Peak vertical g of 15. Cockpit instrument display		
Visual Flight Simulator	North American Aviation Columbus, Ohio	Fixed base, V/STOL Simulator with television presentation free in 6 degrees of freedom projecting terrain picture.	IAS Crone & O'Harrah	Used for V/STOL studies
"g" Seat	North American Aviation Columbus, Ohio	Subjects pilot to variable vertical acceleration similar to ride through turbulence. Vertical translation and pitching degrees of freedom. Similar to NASA-Langley "g" seat.		
SST Simulator	North American Aviation Los Angeles Boeing, Seattle	Boeing 707 cockpit-pitch and vertical translation analog computation with digital time varying input. Display derived from moving belt projected on screen.		
Flight Simulator	Ryan	Realistic visual-display for optimization of aircraft systems designs-moving terrain type-stationary cockpit located near projected center of wrap-around screen. Controls in 2 place simulator are for pilot only and include collective for lift control, stick for pitch and roll, rudder for yaw, and throttle for forward speed control.		

TITLE	LOCATION	DESCRIPTION	REFERENCE OR REPORTS	COMMENTS
Rotating Station Simulator	North American	Will study effects of prolonged artificial-g on four-man orbital lab modules at each end of 150" center beam.		Being built
V/STOL Flight Simulator	UAC/Sikorsky	Capable of representing helicopters, compound helicopters, tilt wing, fan-in-wing and lift-engine or deflected exhaust VTOL aircraft.		

NOTE: The above listing does not include the class of fixed base simple cockpit-computer simulator. There are literally scores of these simulators of varying degrees of simplicity in government and industry. Also not included is the class of fixed base simulators used in the development of the flight control system of a given vehicle, the "iron bird" simulators. It is quite probable that there are simulators in existence or planned that should be added.

Appendix II

IN FLIGHT SIMULATORS

TYPE AIRCRAFT	DATE	SYSTEM DESCRIPTION	PROJECT-PURPOSE	ACCOMPLISHMENTS
F4U-5 (Navy-Cornell)	1948-49	Servomechanism system of the autopilot, fed with electrical signals from sideslip and yawing velocity pickups, deflected auxiliary rudder. Simulated changes in directional stability & damping in yaw. Periods from 1.5 to 5.5 sec. Ref. 2.2 and 2.4	Obtain pilots comments on a large range of aircraft dutch roll frequencies and damping in order to justify or revise many handling qualities requirements.	A proposal for Navy handling qualities requirements as a result of these tests was "The Lateral-Directional Oscillation shall always lose at least 40% of its amplitude during each cycle following a disturbance."
PT-26 (Air Force Cornell)	1949-50	Stabilizer incidence adjustable in flight to large negative values. Airplane would maintain steady state glides at angles of attack as high as 28 degrees. Angle of attack at the peak of the lift curve peak 15 deg. Manual means used to prevent wing roll off. In later tests an autopilot used. Ref. 2.3 & 2.11	Project purpose was to obtain both static and dynamic data pertaining to the longitudinal motions of an airplane at angles of attack covering both stalled and unstalled flight.	Static data obtained in trimmed power-off glides Qualities determined were pitch angle, angle of attack, normal acceleration, longitudinal acceleration.
B-17 (Air Force)	1951-52	Conventional autopilot was connected to a force wheel. This wheel fed in a signal to the autopilot through strain gages on the spokes of the wheel, and on the pedals. Final arrangement was such that a small force commanded bank angle while a force over 3 pounds commanded aileron displacement (or roll rate). Ref. 2.8	Purpose of this work was to investigate the possibility of the pilot controlling the autopilot rather than the aircraft direct. Provided better stability characteristics and smoother control without adding additional force.	Use of force wheel control, in conjunction with inboard stabilization of airframe dynamics, made simultaneous flight path stability and control realizable.

TYPE AIRCRAFT	DATE	SYSTEM DESCRIPTION	PROJECT-PURPOSE	ACCOMPLISHMENTS
C-45F (Air Force Cornell)	1951-53	Provided continuously variable artificial inputs proportional to yaw velocity sideslip, rate of change of sideslip and yaw acceleration to the rudders; yaw velocity and roll acceleration to the ailerons; and rate of change of airspeed to the elevator. Artificial force feel on all three controls is provided with continuously variable force gradients. Ref. 2.5, 2.7, and 2.9	Purpose was to make all the nature modes of the airplane's motion non-oscillatory and convergent. Automatic turn coordination within a practical degree of accuracy was to be provided.	Essentially dead beat Dutch roll and phugoid were accomplished. (Limited pilot evaluation)
B-26B (Air Force Cornell)	1951-present	An Artificial longitudinal stability & control system was installed to provide extreme variations in the following parameters; short period mode frequency and damping, phugoid mode period and damping, and control force and position needed to trim and maneuver. Short period f = .2 to .6 CPS, I = .15 to 1.2; Phugoid I = .15 to +.60, f = .01 to 0.5 CPS. In 1962, a second B-26 was given similar variable stability capabilities in both longitudinal and lateral directional modes. This second aircraft is used primarily for demonstration flights Ref. 2.13, 2.14, 2.15 and 2.22	Purpose of this program was to determine in flight the optimum & minimum flyable characteristics of bomber type aircraft. The program was later extended to investigate handling quality characteristics of other large aircraft and to train test pilots at locations such as the USAF & Navy Test Pilot Schools	Consistent pilot ratings of various values of short period frequency & damping ratios were obtained. Accomplishments include: 1) Investigation of the effects of various short period & phugoid dynamics, elevator force gradients & types of force feel on handling quality characteristics of bomber type aircraft. 2) A study of SST longitudinal stability & control characteristics during the approach & landing maneuver. 3) Approach to over 230 Air Force, Navy, FAA, and manufacturers' pilots in stability and control evaluation techniques.

TYPE AIRCRAFT	DATE	SYSTEM DESCRIPTION	PROJECT-PURPOSE	ACCOMPLISHMENTS
Navy T-33 (NASA-Langley)	1952-53	Variable damping in yaw was obtained by a flap-type control surface fitted to a fixed fin called a nose fin located on the forward part of the airplane. Ref. 2.27	Flight investigation of the effects of varied lateral damping on the effectiveness of a typical high speed fighter airplane as a gun platform.	Results of simulated strafing runs indicate that the gun-line dispersion could be expected to be decreased about 7% by increased lateral damping and to be increased about 85% by decreased damping.
F86A (NASA-Ames)	1952-54	This variable-stability servomechanism operated in essentially the same manner as the F6F-3 equipment except the rudder & rudder tab were driven automatically & the primary power used was hydraulic rather than electric. Range of the stability derivatives were: C_{n_β} .50 to 0; C_{n_r} .38 to -1.6; C_{n_p} .34 to -1.0; C_{l_β} .074 (normal); C_{l_p} .385 (normal); $C_{n_{\delta a}}$ -.016 to .104; $C_{l_{\delta r}}$ .0155 (normal) Ref. 2.20	Same as F6F-3 but higher speed range.	Simulation of higher performance prototype aircraft. Periods appear to have run from 1.0 to 1.6

TYPE AIRCRAFT	DATE	SYSTEM DESCRIPTION	PROJECT-PURPOSE	ACCOMPLISHMENTS
F6F-3 (NASA-Ames)	1952-56	Variation of the stability derivatives through servo actuation of the ailerons and rudder were obtained. The stability derivatives ranges were as follows: C_{n_β} .079 to -.002 C_{n_r} .143 to -.306 C_{n_p} .250 to -.151 C_{l_p} .125 to -1.02 C_{l_β} .048 to -.350 $C_{l_{\delta_r}}$ .118 to 0 $C_{n_{\delta a}}$ .007 (normal) Ref. 2.10 & 2.20	Simulation of prototype aircraft in order to define the ranges of acceptable characteristics which could be used as design criteria. Pilot opinion of lateral oscillatory characteristics relative to current flying qualities were considered.	Flight experience was obtained which in most cases directly applied to particular flying qualities problems associated with individual prototype development programs. Aircraft also used in simulating tracking in rough air.
F94A (Air Force Cornell)	1952-58	Artificial longitudinal stability & control systems were installed to provide extreme variations in 1. Short period mode frequency and damping. 2. Phugoid mode period & damping. 3. Control forces & position needed to maneuver & to trim. 4. Control breakout forces. Short period f = .7 to 1.15 CPS I = .25 to 1.75 Ref. 2.13, 2.26, & 2.28	Purpose of this program was to determine in flight the optimum and minimum acceptable characteristics of a fighter aircraft. (Associated with B-26 work	Similar to B-26

TYPE AIRCRAFT	DATE	SYSTEM DESCRIPTION	PROJECT-PURPOSE	ACCOMPLISHMENTS
H-5 Helicopter (NASA-Langley)	1952-58	A single rotor helicopter was outfitted so that the damping in roll, yaw & pitch could be varied by means of electrical components. The components were actuated by the rear cyclic stick or rudder pedals as well as by signals proportional to rate of roll, yaw or pitch (signals proportional to helicopter attitude were also available but were not used in the tests.) Ref. 2.19 and 2.32	An investigation of helicopter damping as it effects flying qualities.	Variations of flying qualities with increased damping in roll yaw, roll and pitch. Results indicate that increased damping can improve the accuracy of maneuvers and reduce the effort required of the pilot.
Navion (Air Force Princeton)	1952-present	Bob weights and springs, etc. to vary longitudinal dynamics. Ref. 2.47 Variable stability equipment has been subsequently added.	Investigate effects of these devices on longitudinal dynamics.	Demonstrated flight characteristics involving degeneration of short period & phugoid into other dynamic modes.
XF88A (Air Force McDonnell)	1954	The variable-stability system basically consisted of aileron & rudder servos actuated by sideslip, yaw and roll rate inputs. Dutch roll oscillations were induced by rudder kicks in straight and level flight. Ref. 2.12	To fulfill the need of improved specifications on rolling motion. Examples - amplitude ratio of roll angles to yaw angle or roll angle to sideslip etc. Establish a tolerable intolerable boundary surface, for flight with auxiliary equipment inoperative.	Periods from 1.00 to 2.555 were accomplished.

TYPE AIRCRAFT	DATE	SYSTEM DESCRIPTION	PROJECT-PURPOSE	ACCOMPLISHMENTS
F86E (Air Force Cornell)	1954-55	A non-linear yaw damper was added to the rudder with the servo driving the rudder direct. An artificial rudder feel system using dynamic pressure and a spring was used to simulate the normal airplane feel. The yaw damper was set so that sensitivity was left high for small sideslip angles around zero. Ref. 2.17	To make the rudder motion not only proportional to yaw rate but also to yaw rate as it varies with sideslip. With this equipment it was hoped that in a dutch roll oscillation, the aircraft would return to center swiftly but be damped well near center.	Tracking aim errors with this system were reduced to about two-thirds the value experienced with the normal airplane with damping of the dutch roll to around 70% of critical (I = .7).
F9F-2 (NASA)	1954-55	Two types of automatic pilots were used; one of these was of the attitude type and the other was of the rate type. With the attitude automatic pilot control system, two-types of stick force feel were used, spring feel and damper feel. Motion of the stick generated an electrical signal proportional to its deflection. Ref. 2.18, 2.44, 2.45 & 2.46	A flight investigation to obtain experimental information on the handling qualities of a fighter airplane controlled through an automatic pilot control system.	The pilot liked the characteristics provided by the damper force feel system much better than those provided by the spring feel system. The flying qualities of the airplane with the rate sutomatic pilot control system was very good.
T-33 (Air Force Cornell)	1954-present	Irreversible hydraulic power controls are used to drive the control surfaces. This system is also designed for research in the field of design of cockpit controls. The basic system which was limited to steady state or quasi-steady state flight conditions has	This aircraft was initiated in order to increase the effectiveness of research work on the problems that are continually arising in the field of airplane stability & control (handling qualities).	Continual development and revision over a period of several years of this aircraft has brought about a flying simulator which can duplicate the characteristics of almost any aircraft under any conditions. Accomplishments include:

TYPE AIRCRAFT	DATE	SYSTEM DESCRIPTION	PROJECT-PURPOSE	ACCOMPLISHMENTS
T-33 Cont'd		been supplemented by a device which permits changing of stability derivatives as a function of time for a predetermined flight path. Installation of drag petals has added a variable L/D capability which permits simulation of low L/D lifting bodies and of vehicles operating on the back side of the thrust required curve. Also, it is possible to link the airplane to a computer to convert it to a ground simulator. ω_{n_d} = (less than 0) to 1.5 cps I_{n_ϕ} = (less than 0) to 0.6 $\omega_{n_{s.p.}}$ = (less than 0) to 1.5 cps $I_{n_{s.p.}}$ = -0.1 I 1.5 Phugoid period 25-200 sec I_p = -0.20 to 0.60 (Refs. 2.16, 2.21, 2.23, 2.35, 2.36, 2.37 and 2.38).	One of the revised purposes of this aircraft is for carrying out a systematic investigation of the re-entry task & handling qualities problems associated with advanced vehicles.	1. Pilot training for the X-15 program. 2. Investigation of lateral-directional handling quality parameters to assist in the development of the TSR-2. 3. Investigation of the effects of L and true speed on longitudinal handling qualities. 4. A study of longitudinal and lateral-directional handling qualities for piloted reentry vehicles. 5. Determination of the significance of certain longitudinal and lateral-directional flight parameters in limiting minimum approach & landing speeds. 6. Determination of handling quality characteristics of advanced vehicles possessing unusual dynamics such as a coupled roll-spiral mode. 7. Accumulation of a large amount of handling qualities data for conventional aircraft upon which to base improvements of present design requirements. 8. Verification and evaluation of the importance of new handling quality parameters such as M_u, X_u, $1/T_{h1}$, $[(\frac{\omega\phi}{\omega d})^2 - \|]/\| \phi/\beta \|$ associated with advanced vehicles.

TYPE AIRCRAFT	DATE	SYSTEM DESCRIPTION	PROJECT-PURPOSE	ACCOMPLISHMENTS
YF86D (NASA-Ames)	1956-58	By use of a control system stabilizer, position was commanded thru a servo system by stick force. The breakout force, system time constant, and system gain (i.e. stabilizer angle per unit stick force) could be varied over a wide range. Aircraft dynamics were varied over a wide range. tude and speed. short period f = .63 & .57 CPS I = .21 & .36 breakout force 0 to 25 lb time constant 0 to 4 sec static force gain 1 deg/lb to .04 deg per pound. Ref. 2.29	Obtain pilots comments on: 1. Breakout forces large enough to be objectionable & to make small precise control application difficult 2. sensitivity which makes it difficult to avoid persistent amplitude oscillations. 3. Pilot-induced oscillations of a divergent nature.	In an examination of the over-all system response in the two test flight conditions, the dynamic normal acceleration response of the airplane to stick force appeared to be the critical factor in the pilot's choice of control system dynamics.
F86E (NASA-Ames)	1957-59	Servo actuation of the ailerons & the rudder provided artificial variation of some of the lateral and directional aerodynamic stability parameters. Three modes of aileron & stabilizer system operation were available to the pilot: 1. normal control, 2. position servo (fly by wire), 3. variable stability. Stability derivatives ranges were as follows:	Basically this aircraft was used to determine the acceptable lateral oscillatory damping in the landing approach with emphasis on the emergency condition of damper failure	Three regions of lateral oscillation characteristics were defined and investigated: 1. long period $3.11 \leq P \leq 4.32$ sec and moderate-roll-yaw coupling $0.49 \leq \lvert\phi/v_e\rvert \leq 0.70$ 2. long period $2.75 \leq P \leq 6.9$ sec and high roll-yaw coupling $0.93 \leq \lvert\phi/v_e\rvert \leq 1.65$ 3. short period $1.54 \leq P \leq 2.38$ sec and moderate roll-yaw coupling $0.45 \leq \lvert\phi/v_e\rvert \leq 0.63$.

TYPE AIRCRAFT	DATE	SYSTEM DESCRIPTION	PROJECT-PURPOSE	ACCOMPLISHMENTS
F86E Cont'd		C_{n_β} .510 to -.305 C_{n_r} 1.15 to -1.53 C_{n_p} .121 to -.200 $C_{n_{\delta_a}}$ .180 to -.142 C_{l_β} .430 to -.625 C_{l_p} .22 to -1.10 $C_{l_{\delta r}}$ .176 to -.152 Ref. 2.30		
F10.A (NASA-Langley Air Force)	1957-60	This vehicle was to provide the test engineer with the flexible features of a general purpose computer, coupled with those of a variable stability airplane. The airborne analog computing equipment was to be used in flight research programs to solve in real time certain sets of differential equations to provide control information to the aircraft. Inputs to the computer system as a whole were to come from the airplane motion and flight sensors, from the problem input equipment and from the pilot.	Some of the planned uses for this aircraft were roll requirements for blast escape and tracking, artificial stability for roll coupling, roll limiting & "G" limiting schemes, control stick steering, adaptive servo and other new techniques, study of negative stability augmenters, problems of unconventional bombing techniques and studying problems of advanced vehicles along portions of their trajectories.	Not flown

TYPE AIRCRAFT	DATE	SYSTEM DESCRIPTION	PROJECT-PURPOSE	ACCOMPLISHMENTS
F-100C Cont'd		Estimates based on perfect servos indicate the following characteristics will be available at 15,000 ft.		

Mode	Char	Max	Norm	Min	Mach
Lateral	ω_d	.95CPS	.59CPS	0CPS	.9
	I_d	1.0	0.13	-.80	.65
	$\lvert\phi/\beta\rvert$	24.0	2.00	.40	.80
Longitudinal	ω_{sp}	2.5CPS	1.5CPS	0CPS	1.1
	$I_{s.p.}$	.85	.30	-2.0	1.1

D-18 (NASA)	1959-60	The control surface modifications consisted of a main trailing-edge flap which was connected to the aileron for maximum lift-changing capability, a short auxiliary portion of the elevator to counteract the wing pitching moment caused by deflection of the main wing flap.	To provide an automatic control system capable of varying static longitudinal stability and lift curve slope. An investigation of positive and negative static longitudinal stability coupled with various effective lift-curve slopes.	Pilot opinions and flight results of an investigation at relatively low values of normal acceleration per degree change in angle of attack indicate that the upper tolerance limit of unstable static atability of the airplane (C_{m_α}) is between 0.10 and 0.16. Flight tests indicate that: (1) at the frequency of the short period mode, large amounts of normal-acceleration feel cause the control system to oscillate and excite the airplane short period mode at the same frequency. (2) The pitching acceleration component of feel is almost equivalent to viscous damping on the stick. A large
F11F-1-F (NASA)	1960-61	An adjustable feel system connected to the longitudinal control system of a transonic fighter airplane. Variable control feel including response feel is provided from the following five sources: control position, control rate, normal acceleration, pitching velocity, and pitching acceleration. Ref. 2.39	Provide a means whereby a through study could be made of the effects of large amounts of response feel and the stability of airplane and control system response modes.	

TYPE AIRCRAFT	DATE	SYSTEM DESCRIPTION	PROJECT-PURPOSE	ACCOMPLISHMENTS
FTU-3 (Navy-Cornell)	1958-59	A large vertical canard control surface was used to generate the required yawing moment to prevent the uncontrolled motions experienced at high angles of attack in the region of reduced stability, a $\dot{\beta}$ feedback loop was used to control this surface. Ref. 2.31	Determine a means of preventing large uncontrolled motions using automatic control.	In symmetrical stalls the motions were very mild; when large aileron and rudder deflections were applied at the stall, the airplane did little more than roll.
HUP-1 (Princeton)	1958-60	A standard Minneapolis-Honeywell E-12 autopilot was installed in this helicopter to provide for variation of dihedral effect, static directional stability, roll damping and yaw damping. The rolling convergence root held approximately constant at a value $\lambda_2 = -6.68$ Spiral mode damping varied from +.15 to -.85 and the Dutch roll damping (1/C 1/2) varied from .5 to 7.8. Ref. 2.33	Conduct a pilot evaluation of carefully selected stability configurations to provide pertinent commentary and numerical ratings which could be related to known dynamic characteristics.	Analysis of test results indicated a number of areas of importance in helicopter lateral handling qualities. Specifically it was found that the Dutch roll oscillation should be well damped; positive spiral damping is desirable, and, in fact, is light; steady state control deflections should not be required to make turns after completion of the entering transients.
F-100C (NASA-Ames)	1958-present	The following derivatives can be varied: Longitudinal-Directional-Lateral C_{m_α} C_{n_β} C_{l_β} C_{m_q} C_{n_r} C_{l_r} $C_{m_{\delta_s}}$ C_{n_p} C_{l_p} $\delta Fs/\delta f_s$ $C_{n_{\delta a}}$ $C_{l_{\delta a}}$ $C_{n_{\delta_r}}$ $C_{l_{\delta_r}}$	Used as a backup for ground simulators to pick up points where it is felt that motion cues are important. Has recently been transferred from FRC to Ames	Has been used to investigate X-15 controllability problems with roll damper off and to study SST handling quality characteristics.

TYPE AIRCRAFT	DATE	SYSTEM DESCRIPTION	PROJECT-PURPOSE	ACCOMPLISHMENTS
F11F-1-F Cont'd				pitching acceleration component excites an oscillation of the control system.
X-14 (NASA-Ames)	Sept 60-present	The Bell X-14 aircraft has been modified with the addition of a more powerful engine and a secondary automatically controlled jet control arrangement to permit its use as a variable stability airplane. The following moments can be obtained:	The purpose of this aircraft is to investigate hovering and transition, etc. for VTOL work.	Determination of the attitude control power and damping requirements for a visual hovering task.

ESTIMATED MAXIMUM EFFECTIVENESS

	Axis		Manual		Augmented
Roll	L_δ	$\frac{\text{rad.}}{\text{sec.}}$	1.9	+	1.72
Pitch	M_δ	$\frac{\text{rad}}{\text{sec.}}$	.95	±	.86
Yaw	N_δ	$\frac{\text{rad}}{\text{sec.}}$	.54	+	.48

TYPE AIRCRAFT	DATE	SYSTEM DESCRIPTION	PROJECT-PURPOSE	ACCOMPLISHMENTS
Bell 47G (NRC of Canada	1961 present	The vehicle has been modified so that stability and gust sensitivity can be varied about all three axes. Another similar vehicle that will be able to vary stability in the vertical plane as well, is presently entering service.	Obtain VTOL handling qualities under motion stimulus.	Have carried out investigations on the effects of lateral-directional cross-coupling on flying qualities and on the effect of weather-cock stability on the amount of directional control sensitivity and damping required.
YHC-1A (NASA)	1961	This new type helicopter which has sufficient space for an adequate payload is being fitted with improved variable stability equipment which will permit simulation not only of control power and angular velocity damping but also variations of static stability. During initial use additional equipment will be installed when feasible. This could include items such as methods of providing time lag in controls. Ref. 2.41	Stability and control and handling qualities tests of VTOL aircraft	
NC-130B (NASA-Ames)	1961 present	The aircraft has been equipped with blowing-type boundary layer control trailing edge flaps and a stability augmentation system which operates on signals associated with side force characteristics of the aircraft.	To investigate problem areas associated with the operation of large STOL aircraft at low forward speeds.	Speeds down to 68 knots have been achieved and investigations of low speed lateral-directional control problems have been conducted.

TYPE AIRCRAFT	DATE	SYSTEM DESCRIPTION	PROJECT-PURPOSE	ACCOMPLISHMENTS
X-22A (BuWeps Bell-	1962 present	Designed from the beginning to incorporate a variable stability & control system, the vehicle will be able to investigate the following parameters: 1) control power 2) control feel, 3) angular rate damping, 4) weight damping, 5) thrust response, 6) attitude stabilization, 7) stability derivatives The vehicle will be able to vary its characteristics continuously throughout transition.	To provide a versatile research vehicle for VTOL handling qualities research. Will investigate the vertical take-off and transition flight regimes in order to define future V/STOL design and specification criteria	None - System under development.
JETSTAR (NASA-FRC)	1963 present	Based on the model following principle, this aircraft will possess variable stability about all three axes. Forces along the longitudinal axis will be modified by thrust control.	To provide the capability of simulating the stability, control and certain performance characteristics of a variety of advanced airplanes (such as the SST) and aerospacecraft.	None - System under development.
367-80 (Boeing-NASA-Langley	Future	The aircraft has been equipped with boundary layer control high-lift flaps and is to be given a variable stability capability. Moments will be varied by servo actuation of the elevator, ailerons and rudder, lift will be varied by servo actuation of the speed brakes, and drag will be varied by thrust modulation.	To be used for in-flight simulation of supersonic transport configurations in the approach and landing phase and for slow speed flight research	Has demonstrated lift coefficients of 3.0 and speeds as slow as 65 knots. Variable stability modifications not yet incorporated.

TYPE AIRCRAFT	DATE	SYSTEM DESCRIPTION	PROJECT-PURPOSE	ACCOMPLISHMENTS
C-131	Future	This aircraft, which employs the concept of total in-flight simulation (TIFS), will be able to vary forces along and moments about all axes. TIFS will provide: 1) actual flight simulation, 2) fully representative test cockpit, 3) correct external visibility, 4) servo-driven displays to properly present simulated flight variables to the pilot, 5) cockpit controls with correct feel characteristics, 6) control of the test cockpit's linear and angular accelerations and motions to duplicate those of the simulated vehicle.	To provide a facility to assist in the development of advanced manned vehicles. The probable great size and weight of some of these vehicles combined with their tremendous range of performance create handling quality questions which at present are beyond our ability to answer. By defining and solving anticipated flight control problems associated with these vehicles, TIFS should supply the answers which at present can be obtained in no other way.	None - TIFS under development.
Dynamic Lunar Landing Simulator (NASA - FRC)	Future	18' high, four truss-type legs with shock struts attached. Pilot will ride in an encapsulated cockpit in a zero-altitude, zero-velocity ejection seat facing a display panel. GE CF-700 turbofan engine provides thrust equal to 83% of vehicle weight-simulating moons gravity (12% of earths).	Typical moon landings will be simulated by starting a descent from 5000' altitude. Thrust of engine will cause descent velocity to approximate that which would be experienced on moon. Pilot will control simulator's attitude through control system linked with 4 hydrogen peroxide attitude control jets on each of 4 landing legs. Deceleration rockets will be used to brake rate of descent at proper time.	None as yet.

TYPE AIRCRAFT	DATE	SYSTEMS DESCRIPTION	PROJECT-PURPOSE	ACCOMPLISHMENTS
VTOL Test Rig - (Lockheed)	1964	Free flight piloted vehicle powered by six jet engines.	To develop techniques for multiple jet lift engines, obtain control criteria and handling qualities data and demonstrate multiple engine jet lift capability.	None

VIRGINIA ENGINEERING EXPERIMENT STATION

DIRECTOR	583
Aerospace Engineering	255
Architecture (School)	243
Business (School)	440
Ceramic Engineering	548
Chemical Engineering	248
Chemistry	258
Civil Engineering	281
Electrical Engineering	409
Engineering Mechanics	245
Geological Sciences	279
Industrial Engineering	285
Mathematics	252
Mechanical Engineering	206
Metallurgical Engineering	382
Mining Engineering	380
Physics	295
Wood Construction	488

VIRGINIA POLYTECHNIC INSTITUTE ENGINEERING EXTENSION SERIES CIRCULAR NO. 4